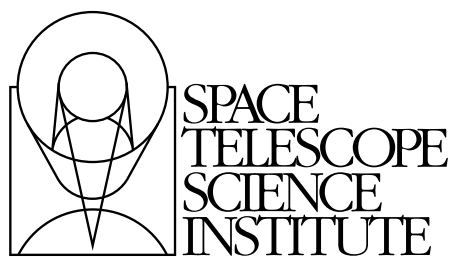


---

Version 3.0  
October 2002

# Advanced Camera for Surveys Instrument Handbook for Cycle 12



Space Telescope Science Institute  
3700 San Martin Drive  
Baltimore, Maryland 21218  
[help@stsci.edu](mailto:help@stsci.edu)

## User Support

For prompt answers to any question, please contact the Science and Instrument Support Department Help Desk.

- **E-mail:** [help@stsci.edu](mailto:help@stsci.edu)
- **Phone:** (410) 338-1082  
(800) 544-8125 (U.S., toll free)

## World Wide Web

Information and other resources are available on the ACS World Wide Web site:

- **URL:** <http://www.stsci.edu/hst/acs>

## Revision History

Version	Date	Editors
3.0	October 2002	Pavlovsky, C.M., Gilliland, R., Bohlin, R., Clampin, M., Cox, C., De Marchi, G., Hack, W., Hartig, G., Jogee, S., Krist, J., Mack, J., Mutchler, M., Riess, A., Sparks, W., Van der Marel, R., Van Orsow, D., Welty, A., Ford, H., Illingworth, G., Blakeslee, J., Martel, A., Meurer, G., Sirianni, M., Tsvetanov, Z., Walsh, J., Pasquali, A., Prizkal, N.
2.1	July 2001	Pavlovsky, C.M., et al.
2.0	June 2001	Suchkov, A., et al.
1.0	June 2000	Jedrzejewski, R., et al.

## Citation

In publications, refer to this document as:

Pavlovsky, C., et al. 2002, "ACS Instrument Handbook", Version 3.0, (Baltimore: STScI).

Send comments or corrections to:  
Space Telescope Science Institute  
3700 San Martin Drive  
Baltimore, Maryland 21218  
E-mail:[help@stsci.edu](mailto:help@stsci.edu)

# Acknowledgments

The technical and operational information contained in this Handbook is the summary of the experience gained both by members of the STSci ACS group, the ST-ECF and by the ACS IDT (P.I.: Holland Ford, Johns Hopkins University). The ACS IDT is Holland Ford (PI), Garth Illingworth (Deputy PI), George Hartig, Mark Rafal, Frank Bartko, Tom Broadhurst, Bob Brown, Chris Burrows, Ed Cheng, Mark Clampin, Jim Crocker, Paul Feldman, Marijn Franx, David Golimowski, Randy Kimble, Tom La Jeunesse, Mike Lesser, Doug Leviton, George Miley, Marc Postman, Piero Rosati, Bill Sparks, Pam Sullivan, Zlatan Tsvetanov, Paul Volmer, Rick White, Bob Woodruff, Narciso Benitez, John Blakeslee, Caryl Gronwall, André Martel, Gerhardt Meurer and Marco Sirianni. The contributions of Alan Welty and Susan Rose are also greatly appreciated.

## ACS Instrument Team at STSci

Name	Title	Phone	e-mail
Mark Clampin	Group Lead	(410) 338-4711	clampin@stsci.edu
Ralph Bohlin	Instrument Scientist	(410) 338-4804	bohlin@stsci.edu
Ron Gilliland	Instrument Scientist	(410)338-4366	gillil@stsci.edu
George Hartig	Instrument Scientist	(410) 338-4966	hartig@stsci.edu
Guido De Marchi	Instrument Scientist	(410) 338-4810	demarchi@stsci.edu
Shardha Jogee	Instrument Scientist	(410) 338-4349	jogee@stsci.edu
Adam Riess	Instrument Scientist	(410) 338-4509	ariess@stsci.edu
Bill Sparks	Instrument Scientist	(410) 338-4843	sparks@stsci.edu
Roeland Van der Marel	Instrument Scientist	(410)338-4931	marel@stsci.edu
Colin Cox	Systems Analyst	(410) 338-4792	cox@stsci.edu
John Krist	Optical Analyst	(410) 338-4901	krist@stsci.edu
Jennifer Mack	Data Analyst	(410)338-4565	mack@stsci.edu
Max Mutchler	Data Analyst	(410) 338-1321	mutchler@stsci.edu
Cheryl Pavlovsky	Data Analyst	(410) 338-4339	cheryl@stsci.edu
Doug van Orsow	Data Analyst	(410) 338-4568	vanorsow@stsci.edu



# Table of Contents

<b>Acknowledgments</b> .....	iii
ACS Instrument Team at STScI .....	iii

---

<b>Part I: Introduction</b> .....	1
-----------------------------------	---

<b>Chapter 1: Introduction</b> .....	3
1.1 Purpose .....	4
1.1.1 Document Conventions .....	4
1.1.2 Examples Used in this Handbook .....	4
1.2 Handbook Layout .....	5
1.3 Preparing an Observing Proposal with ACS .....	8
1.4 The Help Desk at STScI .....	8
1.5 The ACS Instrument Team at STScI .....	9
1.6 The ACS Web Site and Supporting Information .....	9

<b>Chapter 2: Special Considerations for Cycle 12</b> .....	11
2.1 ACS is a Recent Instrument .....	12
2.2 SBC Scheduling Policies .....	12
2.3 Prime and Parallel Observing with the SBC .....	13
2.4 Policy for Auto-Parallel Observations .....	14
2.5 Use of Available-but-Unsupported Capabilities .....	15
2.6 Data Volume Constraints .....	16
2.7 Charge Transfer Efficiency .....	16

---

**Part II: User's Guide** ..... 19**Chapter 3: Introduction to ACS** ..... 21

3.1 Instrument Capabilities .....	21
3.2 Instrument Design .....	22
3.2.1 Detectors .....	23
3.2.2 ACS Optical Design .....	24
3.3 Basic Instrument Operations .....	28
3.3.1 Target Acquisitions .....	28
3.3.2 Typical ACS Observing Sequence .....	28
3.3.3 Data Storage and Transfer .....	28
3.3.4 Parallel Operations .....	29
3.4 Designing an ACS Observing Proposal .....	29
3.4.1 Identify Science Requirements and Define ACS Configuration .....	32
3.4.2 Determine Exposure Time and Check Feasibility .....	33
3.4.3 Identify Need for Additional Exposures .....	34
3.4.4 Determine Total Orbit Request .....	34

**Chapter 4: Imaging** ..... 37

4.1 Imaging Overview .....	37
4.2 Which instrument to use? .....	43
4.2.1 Comparison of ACS and WFPC-2 .....	44
4.2.2 Comparison of ACS and NICMOS .....	45
4.2.3 Comparison of ACS and STIS .....	46
4.3 Caveats for ACS Imaging .....	48
4.3.1 Throughputs and Limiting Magnitudes .....	49
4.3.2 Limiting Magnitudes .....	50
4.3.3 Signal-To-Noise Ratios .....	50
4.3.4 Saturation .....	50
4.4 Wide Field Optical CCD Imaging .....	51
4.4.1 Filter Set .....	51
4.4.2 Long wavelength halo fix .....	52
4.5 High-Resolution Optical and UV Imaging .....	53
4.5.1 Filter set .....	53
4.5.2 Multiple electron events .....	54
4.5.3 Red leaks .....	54

4.6 Ultraviolet Imaging with the SBC.....	55
4.6.1 Filter Set .....	55
4.6.2 Bright-Object Limits .....	55
4.6.3 Optical Performance .....	55
4.6.4 Red-leaks.....	55
4.7 ACS Point Spread Functions .....	56
4.7.1 CCD pixel response function .....	56
4.7.2 Model PSFs .....	57
4.7.3 Encircled Energy.....	58
4.7.4 Geometric Distortions .....	60
4.7.5 PSF at Extreme Red Wavelengths and the UV .....	60
4.7.6 Residual Aberrations .....	61

## **Chapter 5: Polarimetry, Coronagraphy and Prism/Grism Spectroscopy.....**

5.1 Polarimetry.....	63
5.2 Coronagraphy .....	68
5.2.1 Coronagraph Design .....	69
5.2.2 Acquisition procedure and pointing accuracy .....	71
5.2.3 Vignetting and flat fields .....	72
5.2.4 Coronagraphic Performance .....	74
5.2.5 Residual light subtraction .....	76
5.2.6 The Off-Spot PSF .....	81
5.2.7 Planning ACS Coronagraphic Observations .....	83
5.2.8 “Campaign” Mode .....	85
5.3 Grism/Prism Spectroscopy .....	86
5.3.1 WFC G800L.....	87
5.3.2 HRC G800L .....	88
5.3.3 HRC PR200L .....	89
5.3.4 SBC PR110L .....	90
5.3.5 SBC PR130L .....	91
5.3.6 Observation Strategy .....	92
5.3.7 Extraction and Calibration of Spectra .....	95

## **Chapter 6: Exposure-Time Calculations.....**

6.1 Overview .....	97
6.1.1 The ACS Exposure Time Calculator.....	97
6.2 Determining Count Rates from Sensitivities.....	98
6.2.1 Imaging .....	101

6.2.2 Spectroscopy .....	103
6.3 Computing Exposure Times .....	104
6.3.1 Calculating Exposure Times for a Given Signal-to-Noise .....	104
6.4 Detector and Sky Backgrounds .....	105
6.4.1 Detector Backgrounds .....	106
6.4.2 Sky Background .....	106
6.5 Extinction Correction .....	111
6.6 Exposure-Time Examples .....	112
6.6.1 Example 1: WFC imaging a faint point source .....	112
6.6.2 Example 2: SBC Objective prism spectrum of a UV spectrophotometric standard star .....	113
6.6.3 Example 3: WFC VIS Polarimetry of the jet of M87 .....	114
6.6.4 Example 4: SBC imaging of Jupiter's aurora at Lyman-alpha .....	114
6.6.5 Example 5: Coronagraphic imaging of the Beta-Pictoris disk .....	115
6.7 Tabular Sky Backgrounds .....	116

## **Chapter 7: Feasibility and Detector Performance .....**

7.1 The CCDs .....	119
7.1.1 Detector Properties .....	119
7.1.2 CCD Spectral Response .....	121
7.1.3 Quantum Efficiency Hysteresis .....	121
7.1.4 CCD Long-Wavelength Fringing .....	121
7.1.5 Optical Performance .....	121
7.1.6 Readout Format .....	122
7.1.7 Analog-To-Digital Conversion .....	122
7.1.8 Flat Fields .....	123
7.2 CCD Operations and Limitations .....	126
7.2.1 CCD Saturation: the CCD Full Well .....	126
7.2.2 CCD Shutter Effects .....	126
7.2.3 Cosmic Rays .....	126
7.2.4 Hot Pixels .....	128
7.2.5 Charge Transfer Efficiency .....	130
7.2.6 UV Light and the HRC CCD .....	131



7.3 The SBC MAMA .....	131
7.3.1 MAMA Properties.....	131
7.3.2 SBC Spectral Response .....	133
7.3.3 Optical Performance .....	134
7.4 SBC Operations and Limitations .....	134
7.4.1 MAMA Overflowing the 16 Bit Buffer .....	134
7.4.2 MAMA Darks.....	135
7.4.3 SBC Signal-to-Noise Ratio Limitations .....	136
7.4.4 SBC Flatfield.....	137
7.4.5 SBC Nonlinearity .....	138
7.5 SBC Bright-Object Limits.....	138
7.5.1 Overview.....	138
7.5.2 Observational Limits .....	139
7.5.3 How Do You Determine if You Violate a Bright Object Limit? .....	140
7.5.4 Policy and Observers' Responsibility in Phase I and Phase II .....	141
7.5.5 What To Do If Your Source is Too Bright for Your Chosen Configuration? .....	143
7.5.6 Bright-Object Protection for Solar System Observations .....	143
<b>Chapter 8: Observing Techniques .....</b>	<b>145</b>
8.1 Operating Modes.....	145
8.1.1 WFC ACCUM Mode .....	146
8.1.2 HRC ACCUM Mode.....	148
8.1.3 SBC ACCUM Mode .....	148
8.1.4 HRC ACQ Mode .....	149
8.2 Patterns and Dithering .....	149
8.2.1 How to obtain dithered data.....	150
8.2.2 Supported Patterns.....	151
8.2.3 How to combine dithered observations .....	151
8.2.4 How to determine the offsets .....	152
8.3 A Road Map for Optimizing Observations.....	152
8.4 CCD Gain Selection .....	155
8.4.1 WFC Gain .....	155
8.4.2 HRC Gain .....	156

8.5 ACS Apertures .....	156
8.5.1 WFC Apertures .....	156
8.5.2 Ramp filter apertures .....	158
8.5.3 The Small Filter Apertures .....	159
8.5.4 Polarizer Apertures .....	160
8.5.5 HRC Apertures .....	161
8.5.6 SBC Apertures .....	161
8.6 Fixing Orientation on the Sky .....	163
8.7 Parallel Observations .....	166
8.7.1 Parallel Observing .....	166

<b>Chapter 9: Overheads and Orbit-Time Determination .....</b>	<b>173</b>
9.1 Overview .....	173
9.2 ACS Exposure Overheads .....	174
9.3 Orbit Use Determination Examples .....	177
9.3.1 Sample Orbit Calculation 1: .....	177
9.3.2 Sample Orbit Calculation 2 .....	178
9.3.3 Sample Orbit Calculation 3: .....	179
9.3.4 Sample Orbit Calculation 4: .....	180
9.3.5 Sample Orbit Calculation 5: .....	181

---

## **Part III: Supporting Material .....**

<b>Chapter 10: Imaging Reference Material .....</b>	<b>185</b>
10.1 Introduction .....	186
10.2 Using the Information in this Chapter .....	186
10.2.1 Sensitivity Units and Conversions .....	186
10.2.2 Signal-To-Noise .....	187
10.2.3 Point Spread Functions .....	188
10.3 Distortion in the ACS .....	234
10.3.1 WFC .....	235
10.3.2 HRC .....	237
10.3.3 SBC .....	238
10.3.4 Summary .....	239

---

<b>Part IV: Calibration</b> .....	241
<b>Chapter 11: Pipeline Calibration</b> .....	243
11.1 Overview and New Features.....	243
11.1.1 On The Fly Reprocessing (OTFR).....	243
11.1.2 Post Flash Calibration .....	246
11.1.3 Distortion Correction and Dither Combining .....	246
11.2 ACS Pipeline.....	248
11.3 ACS Data Products .....	251
11.3.1 Storage Requirements for ACS Data .....	253
11.3.2 Speed of Pipeline Processing.....	254
<b>Chapter 12: Calibration Accuracies</b> .....	257
12.1 Summary of Accuracies .....	257
<b>Chapter 13: Calibration Plans</b> .....	261
13.1 Ground Testing and Calibration .....	262
13.2 SMOV Testing and Calibration .....	262
13.3 Cycle 11 Calibration .....	264
13.3.1 Calibration Priorities.....	264
13.4 Cycle 12 Calibration .....	266
<b>Glossary</b> .....	269
<b>Index</b> .....	273





PART I:

# Introduction

---

The Chapters in this Part explain how to use this Handbook, where to go for help, and special considerations for using ACS in Cycle 12.





## CHAPTER 1:

# Introduction

### In this chapter. . .

1.1 Purpose / 4
1.2 Handbook Layout / 5
1.3 Preparing an Observing Proposal with ACS / 8
1.4 The Help Desk at STScI / 8
1.5 The ACS Instrument Team at STScI / 9
1.6 The ACS Web Site and Supporting Information / 9

The Advanced Camera for Surveys (ACS) is a third-generation instrument that was installed in the Hubble Space Telescope during Servicing Mission 3B, March 7, 2002. Its primary purpose is to increase the discovery efficiency of imaging with HST by providing a combination of detector area and quantum efficiency that surpasses that available from previous instruments by a factor of 10 or so. It consists of three independent cameras that provide wide-field, high resolution and ultraviolet imaging capability respectively, with a broad assortment of filters designed to address a large range of scientific goals. Additional coronagraphic, polarimetric and grism capabilities make this a versatile and powerful instrument. This Handbook provides instrument-specific information you need to propose for ACS observations (Phase I), design accepted programs (Phase II), and understand ACS in detail.

This Chapter explains the layout of the Handbook and describes how to use the Help Desk at STScI and the STScI ACS World Wide Web (WWW) pages to get help and further information. Instrument and operating updates will be posted on the ACS web pages.

## 1.1 Purpose

The *ACS Instrument Handbook* is the basic reference manual for the Advanced Camera for Surveys, and describes the instrument's properties, performance, operations and calibration. The Handbook is maintained by scientists at STScI. Additional information has been provided by the Investigation Definition Team, led by Dr. Holland Ford of Johns Hopkins University, and by the principal contractors, Ball Aerospace.

We have designed the document to serve three purposes:

- To provide instrument-specific information for preparing Cycle 12 Phase I observing proposals using ACS.
- To provide instrument-specific information to support the design of Phase II proposals for accepted ACS programs, in conjunction with the Phase II Proposal Instructions.
- To provide technical information about the operation and expected performance of the instrument, which can help in the understanding of problems and in the interpretation of data acquired with ACS.

### 1.1.1 Document Conventions

This document follows the usual STScI convention in which terms, words and phrases which are to be entered by the user in a literal way on an HST proposal are shown in a typewriter font (e.g., `ACS/WFC`, `F814W`). Names of software packages or commands are given in bold type (e.g., **calacs**).

Wavelength units in this Handbook are in Angstroms ( $\text{\AA}$ ), and fluxes are generally given in  $\text{erg cm}^{-2}\text{s}^{-1}\text{\AA}^{-1}$ .

### 1.1.2 Examples Used in this Handbook

To illustrate the use of ACS, we have devised a set of representative programs that cover a range of its capabilities. We hope that they will prove helpful to users both in determining the capabilities of the instrument and in writing a proposal to request HST time. The examples are:

1. Wide Field Channel imaging of a faint point source.
2. Solar Blind Channel (SBC) prism spectroscopy of a faint standard star.
3. Polarimetry of the jet of M87.
4. SBC imaging of Jupiter's aurora.
5. Coronagraphy of the circumstellar disk of  $\beta$  Pic.



---

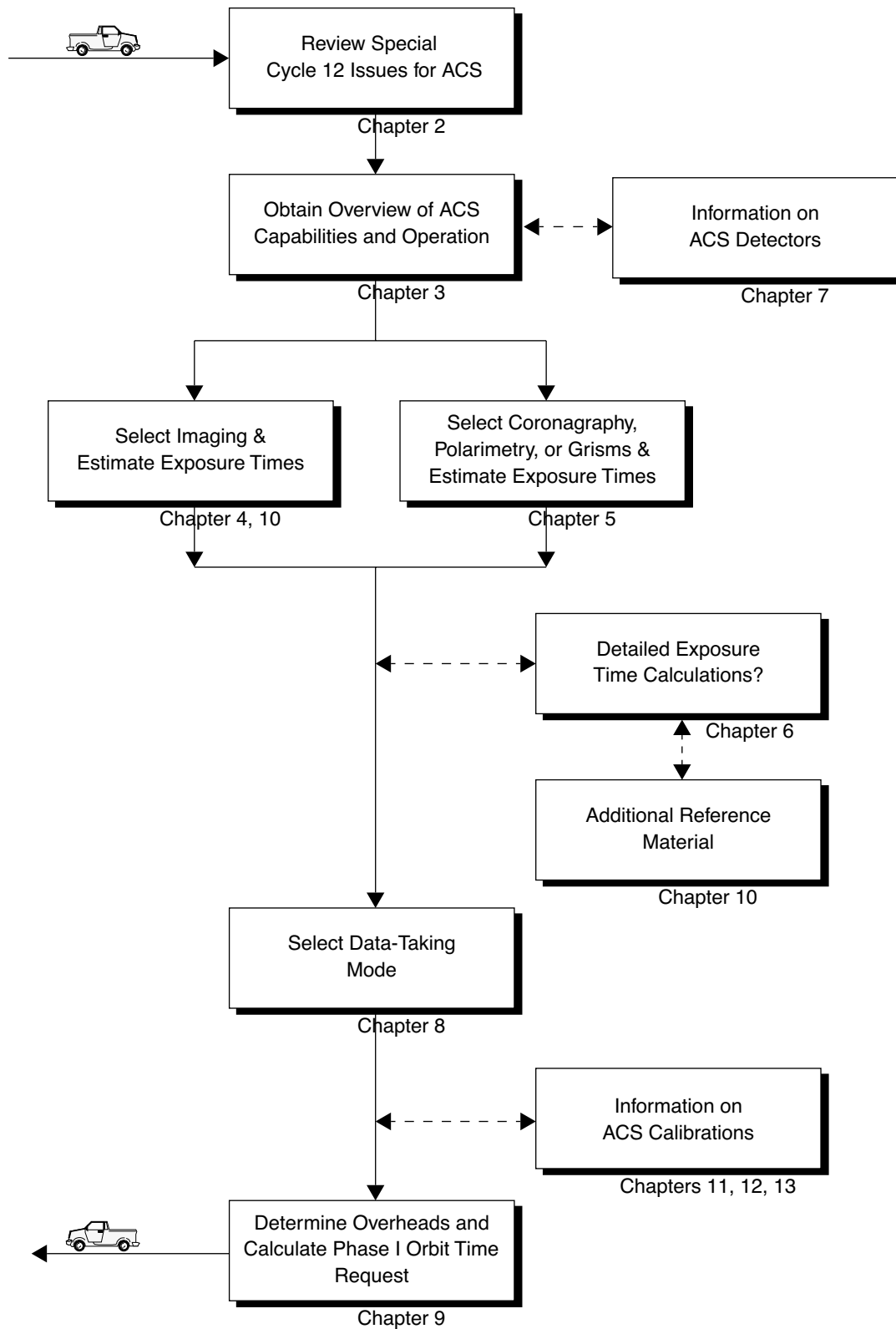
## 1.2 Handbook Layout

To guide you through ACS's capabilities and help optimize your scientific use of the instrument we have divided this handbook into four parts:

- Part I - Introduction
- Part II - User's Guide
- Part III - Supporting Material
- Part IV - Calibration

Figure 1.1 provides a roadmap to navigating this Handbook.

Figure 1.1: ACS Handbook Roadmap for Proposal Preparation



The chapters of this Handbook are as follows:

- Part I - Introduction
  - Chapter 1 - *Introduction*, includes information about getting help.
  - Chapter 2 - *Special Considerations for Cycle 12*, describes special policy considerations for using ACS during Cycle 12.
- Part II - User's Guide
  - Chapter 3 - *Introduction to ACS*, provides an introduction to ACS's capabilities. A discussion is provided to help guide you through the technical details you need to consider in choosing the optimum ACS configuration and in determining the number of orbits to request.
  - Chapter 4 - *Imaging*, provides a description of ACS's imaging capabilities, including camera resolutions and sensitivities.
  - Chapter 5 - *Polarimetry, Coronagraphy and Prism/Grism Spectroscopy*, provides detailed information on these specialized observation modes.
  - Chapter 6 - *Exposure Time Calculations*, describes how to perform signal-to-noise calculations, either by using pencil and paper, or by using software tools that are provided on the World Wide Web.
  - Chapter 7 - *Feasibility and Detector Performance*, provides a description of the three detectors and their physical characteristics, capabilities and limitations, including saturation, linearity and bright object limits.
  - Chapter 8 - *Observing Techniques*, describes some methods that can be used to obtain the best science from ACS, including dithering and the use of pre-defined patterns that mitigate the effects of detector imperfections.
  - Chapter 9 - *Overheads and Orbit Time Determination*, provides information to convert from a series of planned science exposures to an estimate of the number of orbits, including spacecraft and ACS overheads. This chapter applies principally to the planning of Phase I proposals.
- Part III - Supporting Material
  - Chapter 10 - *Imaging Reference Material*, provides summary information and filter transmission curves for each imaging filter.
- Part IV - Calibration
  - Chapter 11 - *Pipeline Calibration*, briefly describes the processing of ACS data by the STScI pipeline and the products that are sent to observers.

- Chapter 12 - *Expected Calibration Accuracies*, summarizes the accuracies expected for ACS data calibrated by the STScI pipeline.
- Chapter 13 - *Calibration Plans*, provides an overview of the current state of ACS calibration and how that has changed as a result of plans for Servicing Mission Observatory Verification (SMOV) and Cycle 11 and Cycle 12 calibration.

---

## 1.3 Preparing an Observing Proposal with ACS

Use the *ACS Instrument Handbook* together with the *Hubble Space Telescope Call for Proposals for Cycle 12* (CP) when assembling your ACS Phase I proposal. In addition the *HST Primer* provides a basic introduction to the technical aspects of HST and its instruments, and explains how to calculate the appropriate number of orbits for your Phase I observing time requests. The CP provides policy and instructions for proposing; the *ACS Instrument Handbook* contains detailed technical information about ACS, describing its expected performance, and presenting suggestions for use. The next Chapter in the Handbook describes special considerations for Cycle 12.

If your Phase I proposal is accepted, you will be asked to submit a Phase II proposal in which you specify the exact configurations, exposure times and sequences of observations that ACS and the telescope should perform. To assemble your Phase II proposal, you should use the *ACS Instrument Handbook* in conjunction with the *Phase II Proposal Instructions*. The Instructions describe the exact rules and syntax that apply to the planning and scheduling of ACS observations and provide relevant observatory information.

---

## 1.4 The Help Desk at STScI

STScI maintains a Help Desk, the staff of which quickly provide answers on any HST-related topic, including questions regarding ACS and the proposal process. The Help Desk staff have access to all of the resources available at the Institute, and they maintain a database of answers so that frequently asked questions can be immediately answered. The Help Desk staff also provide STScI documentation, in either hardcopy or electronic form, including *Instrument Science Reports* and *Instrument Handbooks*. Questions sent to the Help Desk are answered within two working days. Usually, the Help Desk staff will reply with the answer to a question, but occasionally they will need more time to investigate the

answer. In these cases, they will reply with an estimate of the time needed to reply with the full answer.

We ask that you please send *all* initial inquiries to the Help Desk. If your question requires an ACS Instrument Scientist to answer it, the Help Desk staff will put one in contact with you. By sending your request to the Help Desk, you are guaranteed that someone will provide you a timely response. To contact the Help Desk at STScI:

- **Send E-mail:** [help@stsci.edu](mailto:help@stsci.edu) (preferred)
- **Phone:** 1-410-338-1082  
Toll-free in the U.S.: 1-800-544-8125

The Space Telescope European Coordinating Facility (ST-ECF) also maintains a Help Desk. European users should generally contact the (ST-ECF) for help; all other users should contact STScI. To contact the ST-ECF Help Desk:

- **Send E-mail:** [stdesk@eso.org](mailto:stdesk@eso.org)

---

## 1.5 The ACS Instrument Team at STScI

STScI maintains a team of Instrument Scientists, Scientific Programmers, and Data Analysts who support the development, operation and calibration of ACS. The team is also responsible for supporting ACS users. The current membership of the ACS team can be found on the ACS WWW pages under “Help”.

---

## 1.6 The ACS Web Site and Supporting Information

The ACS group at STScI maintains a World Wide Web (WWW) site, as part of STScI’s web service. The address for the STScI ACS page is:

<http://www.stsci.edu/hst/acs>


The STScI ACS pages include sections that fall into the following categories:

- **Late Breaking News:** This is where new and important information is posted.
- **Document Archive:** Electronic versions of this Handbook will be maintained on the WWW site. In addition, more detailed technical information concerning the development, performance, testing, operation and calibration of ACS are contained in a series of ACS Instru-

ment Science Reports (ISRs) and STScI Analysis Newsletters (STANs). These reports can be downloaded from the WWW pages or paper copies can be requested from the Help Desk.

- **Software Tools:** This section includes the Exposure Time Calculator (ETC), which can be used to predict exposure times for ACS observations.
- **Data Analysis:** Includes links to the locations of reference files and the CALACS tutorial.
- **Performance:** Information on the status of ACS and discussion of calibration strategies.
- **FAQs:** This section contains answers to the most Frequently Asked Questions.
- **Help:** This section tells you whom to contact when you need help.

Other information, not specific to ACS, can generally be accessed through the top-level STScI web page: <http://www.stsci.edu/>



## CHAPTER 2:

# Special Considerations for Cycle 12

**In this chapter . . .**

2.1 ACS is a Recent Instrument / 12
2.2 SBC Scheduling Policies / 12
2.3 Prime and Parallel Observing with the SBC / 13
2.4 Policy for Auto-Parallel Observations / 14
2.5 Use of Available-but-Unsupported Capabilities / 15
2.6 Data Volume Constraints / 16
2.7 Charge Transfer Efficiency / 16

ACS was installed in HST as part of Servicing Mission 3B, on March 7, 2002. During the same mission, the NICMOS Cooling System (NCS) was installed, returning the Near Infrared Camera and Multi-Object Spectrometer (NICMOS) to scientific operation. In addition, the Solar Arrays were replaced with smaller, rigid arrays and a Power Control Unit was changed out. As with earlier servicing missions, observers must appreciate that it will take time for us to understand, calibrate and optimize the use of these new capabilities. The servicing mission orbital verification has confirmed that instrument performance is fully consistent with prelaunch expectations.

## 2.1 ACS is a Recent Instrument

While planning your Cycle 12 observations, keep in mind that ACS is still a relatively new addition to HST. Sensitivities, brightness limits, optical performance, software and hardware execution times, and other characteristics contained in this handbook represent our best estimates at this time.

As this Handbook is being revised for Cycle 12 the final SMOV programs are executing. However, results for primary on-orbit calibrations such as geometric distortion quantification, establishment of absolute sensitivity response for all filters, and adjustment of flat fields are substantially finished and analyzed. The instrument optics have been aligned to optimize the PSF for all three cameras, and key performance elements are verified. Many important calibrations, however, are still being worked on.

As we learn more information about ACS it will be posted on our WWW site (see Section 1.6) and published in the STANS.

The calibration state of the ACS will continue to evolve rapidly in the period prior to Cycle 12, but should be well established by the start of Cycle 12. The performance criteria quoted in Chapter 12, Calibration Accuracies, remain for this Handbook at pre-launch quotes. Early calibrations with data taken on-orbit show that the listed accuracies will in general be met, although some may well change in detail as relevant calibrations are analyzed and reference files or tables are updated. We will endeavor to keep users informed as to the accuracies attainable with the current calibration files through information on the ACS WWW site.

---

## 2.2 SBC Scheduling Policies

The STIS MAMA control electronics were found in orbit to be subject to resets due to cosmic-ray upsets, therefore STIS MAMAs are operated only during the contiguous orbits of each day which are free of the South Atlantic Anomaly (SAA). Even though the design of the ACS MAMA control electronics in the SBC was modified so that it would not be susceptible to cosmic-ray hits, the background count rate still exceeds the bright object limits for the SBC during SAA passage. Consequently, the SBC will in general only be scheduled for use during SAA-free orbits. As we expect the SBC usage to be relatively low compared to the CCD cameras, we do not expect this to pose a problem to users.



## 2.3 Prime and Parallel Observing with the SBC

As explained in greater detail in Section 7.5, the MAMA detector that ACS uses in the ultraviolet is subject to damage at high illumination rates. To protect the instrument, we have established limits on the maximum count rate at which the detector may be illuminated. These count-rate limits translate into a set of configuration-dependent bright-object screening magnitudes. These are summarized in Table 7.7.

STScI will perform screening of all SBC exposures prior to scheduling. Targets not established as safe for the configuration in which they are being observed will not be scheduled. Observations that pass screening but are lost in orbit due to a bright-object violation will not be rescheduled. Observers are responsible for assuring that their observations do not violate the SBC count-rate limits. A detailed description of the SBC bright-object limits and the observers' responsibility is presented in Section 7.5.

To assure that STScI can adequately screen observations, special constraints are imposed on parallel observing with the SBC. More:

- No pure parallels are allowed using the SBC.
- Coordinated parallels are allowed with the SBC only if an exact spacecraft orientation (**ORIENT**) is requested and the RA and Dec. of the parallel field determined. Note that the specification of an exact **ORIENT** usually limits the scheduling of observations to a ~4–6 week period each year. The observer is responsible for assuring that observations do not violate the SBC count rate limits both for coordinated parallel SBC observations and for primes.
- **SNAPSHOT** observations with the SBC will not be allowed for Cycle 12.

Table 2.1 below summarizes the policy with respect to SBC observing in Cycle 12.

Table 2.1: Bright-Object Protection Policy for SBC Observations

Type of Observing	Policy
Prime	Allowed if target passes screening
Snapshots	Not allowed
Coordinated parallel	Allowed only if <b>ORIENT</b> is exactly specified and field passes screening
Pure parallel	Not allowed

Targets that are one magnitude or more fainter than the magnitude limits in the screening tables generally automatically pass screening. For a target that is within one magnitude of the screening limits, observers must provide a calibrated spectrum of the source at the intended observing

wavelength. If such a spectrum is not available, the prospective GO must request an orbit in Phase I for a pre-qualification exposure, during which the target spectrum must be determined by observation in an allowed configuration (see Section 7.5 for more details).

Please also note that if you are proposing SBC target-of-opportunity observations, we ask you to provide an explanation in your Phase I proposal of how you will ensure that your target can be safely observed.

---

## 2.4 Policy for Auto-Parallel Observations

As described in Section 8.7, ACS is able to make simultaneous observations using the Wide-Field Channel and the High Resolution Channel. Such observations are added automatically by the scheduling system if doing so does not impact the primary exposures. However, since the WFC and HRC share the same filter wheel, the filter used in the “parallel” channel is determined by that selected for the “prime” detector; the observer does not have the capability to select the parallel filter independently. This means that the possibility and character of these “Auto-Parallel” observations are purely a result of the choices made by the proposer of the prime program. For this reason, the following policies will be in effect for Auto-Parallel observations:

- Auto-Parallel observations are the property of the PI of the program using the prime ACS detector.
- Auto-Parallel observations are not available for independent scheduling.
- There are some fairly severe timing constraints under which Auto-Parallel observations may be added. The scheduling system will add parallels if it can do so without affecting the prime science.
- If WFC data are taken in parallel with prime HRC observations, the `GAIN` setting will be 2 (see Section 4.3), also for HRC parallels added to prime WFC exposures, the `GAIN` will be 2.
- WFC Auto-parallel observations are subject to compression at a level that can occasionally result in some data loss. Such observations will not be repeated.

## 2.5 Use of Available-but-Unsupported Capabilities

We have established a set of core scientific capabilities for ACS which will be supported for Cycle 12 and are described fully in this Handbook. In addition there are a few capabilities with ACS, some of which are mentioned in this Handbook, for which limited access is available. These capabilities are "available-but-unsupported," and in consultation with an ACS Instrument Scientist can be requested. These include a few apertures, limited interest optional parameters, some GAIN options, and filterless (CLEAR) operation. If you find that your science cannot be obtained using fully supported modes, or that it would be much better with use of these special cases, then you may wish to consider use of an unsupported mode.

Use of unsupported modes comes at a price, and they should be used only if the technical requirement and scientific justification are particularly compelling. The following caveats apply:

- Calibrations for available-but-unsupported modes will not be provided by STScI, it will be the observer's responsibility to obtain such as needed.
- STScI adopts a policy of shared risk with the observer for the use of these modes. Requests to repeat failed observations taken with unsupported capabilities will not be honored if the failure is related to use of this capability.
- User support from STScI will be more limited.

Cycle 12 Phase I proposals that include use of unsupported ACS capabilities must include the following:

- Justification of why supported modes don't suffice;
- A request for any observing time needed to calibrate;
- Justification for added risk of use in terms of scientific payback;
- Demonstration that the observers are able to analyze such data.

During the Phase II proposal submission process, the ACS group lead must formally approve use of available-but-unsupported modes. This ensures that all technical problems have been accounted for; we will ask that you summarize the above four points in a brief email message requesting approval for available-but-unsupported modes.

Archival research may also be hindered by use of these modes. As a result, requests for use of unsupported modes which do not adequately address the above four points, or which will result in only marginal improvements in the quality of the data obtained, may be denied by the ACS group lead, even if the request was properly included in your Phase I proposal.

The current list of available-but-unsupported items are:

- Apertures: WFC RAMPs, WFC2-2K
- Optional parameters: SIZEAXIS1, CENTERAXIS1, CENTERAXIS2, COMPRESSION, AUTOIMAGE, PAREXP, WFC: GAIN=4,8, HRC: GAIN=1,8
- Spectral elements: CLEAR (both WFC and HRC)
- ACQ mode: optional parameter GAIN

---

## 2.6 Data Volume Constraints

If ACS data are taken at the highest possible rate for more than a few orbits or in the CVZ, it is possible to accumulate data faster than it can be transmitted to the ground. High data volume proposals will be reviewed and on some occasions, users may be requested to break the proposal into different visits, consider using sub-arrays, or taking other steps to reduce data volume.

---

## 2.7 Charge Transfer Efficiency

Both the STIS and WFPC2 CCDs have shown a significant degradation in charge transfer efficiency (CTE) performance since their installation. The degradation is due to radiation damage of the silicon inducing the creation of traps that impede the clocking of the charge on the CCD. Since reading out the ACS WFC requires 2048 parallel transfers and 2048 serial transfers, it is expected that CTE effects will begin to manifest themselves in the first few years of ACS operation. For this reason, it is likely that some types of science, particularly those in which the sky background in each image is expected to be low ( $<20$  electrons/pixel), will be most effectively performed during the first two years of ACS operation.

As a conservative benchmark, we expect that after 1 year of operation there will be a loss of approximately 10% in the counts from a star with between 50 and 150 total counts placed at row 1024 in one of the WFC chips. For a similar target placed at the WFC reference point, the corresponding loss will be about 17%. These predictions are based on the results obtained from analysis of STIS CCD data. Early calibration results after only a few months since installation of ACS are encouraging in that CTE losses remain low, but only with the passage of more time will the actual CTE effects for ACS be quantified.

As CTE effects worsen, users will most likely want to use the post-flash capability to add a background level to their images. This causes the Poisson noise from the background to increase, but improves the CTE performance of the detector. We do not plan to offer the use of the post-flash capability during Cycle 12, but users will need to consider these trades in later Cycles. Please refer to Section 7.2.5 for more information on this topic.





PART II:

# User's Guide

---

The Chapters in this Part describe the basics of observing with ACS. Included are a description of the instrumental layout and basic operations, the imaging, spectroscopic, polarimetric and coronagraphic capabilities of ACS, the performance and limitations of its detectors, exposure-time calculations, and overhead and orbit-request determinations.

This part of the Handbook is all you need to plan your Phase I ACS Proposal.





# Introduction to ACS

In this chapter . . .

3.1 Instrument Capabilities / 21
3.2 Instrument Design / 22
3.3 Basic Instrument Operations / 28
3.4 Designing an ACS Observing Proposal / 29

In this Chapter we provide an overview of the capabilities and scientific applications of ACS. We describe the optical design and basic operation of the instrument, and provide a flow chart and discussion to help you design a technically feasible and scientifically optimized ACS observing proposal.

## 3.1 Instrument Capabilities

The ACS is a camera designed to provide HST with a deep, wide-field survey capability from the visible to near-IR, imaging from the near-UV to the near-IR with the PSF critically sampled at 6300 Å, and solar blind far-UV imaging. The primary design goal, now verified, of the ACS Wide-Field Channel is to achieve a factor of 10 improvement in discovery efficiency, compared to WFPC2, where discovery efficiency is defined as the product of imaging area and instrument throughput.

ACS has three channels, each optimized for a specific goal:

- Wide field channel (WFC): 202 × 202 arcsecond field of view from 3700–11,000 Å, and peak efficiency of 48% (including the OTA). The plate scale of 0.05 arcsecond/pixel provides critical sampling at 11,600 Å.

- High resolution channel (HRC):  $29 \times 26$  arcsecond field of view from 2000–11,000 Å, and peak efficiency of 29%. The plate scale of 0.027 arcsecond/pixel provides critical sampling at 6300 Å.
- Solar Blind Channel (SBC):  $35 \times 31$  arcsecond field of view from 1150–1700 Å, and peak efficiency of 7.5%. The plate scale of 0.032 arcsecond/pixel provides a good compromise between resolution and field of view.

In addition to these three prime capabilities, ACS also provides:

- Grism spectroscopy: Low resolution ( $R \sim 100$ ) wide field spectroscopy from 5500–11,000 Å available in both the WFC and the HRC.
- Objective prism spectroscopy: Low resolution ( $R \sim 100$  @ 2000 Å) near-UV spectroscopy from 2000–4000 Å available in the HRC.
- Objective prism spectroscopy: Low resolution ( $R \sim 100$  @ 1216 Å) far-UV spectroscopy from 1150–1700 Å available in the SBC.
- Coronagraphy: Aberrated beam coronagraphy in the HRC from 2000–11,000 Å with 1.8 arcsecond and 3.0 arcsecond diameter occulting spots.
- Imaging Polarimetry: Polarimetric imaging in the HRC and WFC with relative polarization angles of  $0^\circ$ ,  $60^\circ$  and  $120^\circ$ .

Table 4.1, 4.2, and 4.3 provide a full list of filters and spectroscopic elements for each imaging channel.

ACS is a versatile instrument that can be applied to a broad range of scientific programs. The high sensitivity and wide field of the WFC in the visible and near-infrared will make it the instrument of choice for deep imaging programs in this wavelength region. The HRC, with its excellent spatial resolution, provides full sampling of the HST PSF at  $\lambda > 6000$  Å and can be used for high precision photometry in stellar population programs. The HRC coronagraph can be used for the detection of circumstellar disks and QSO host galaxies.

---

## 3.2 Instrument Design

In this section, we provide a high-level summary of the basic design and operation of ACS, concentrating on the information most relevant to the design of your HST observing proposal. Subsequent chapters provide more detailed information on specific aspects of the instrument's performance and the design of proposals.

### 3.2.1 Detectors

ACS uses one or more large-format detectors in each channel:

- The WFC detector, called **ACS/WFC**, employs a mosaic of two  $2048 \times 4096$  Scientific Imaging Technologies (SITe) CCDs, with  $\sim 0.05$  arcsecond pixels, covering a nominal  $202 \times 202$  arcsecond field of view (FOV), and a spectral response from  $\sim 3700$  to  $11,000 \text{ \AA}$ .
- The HRC detector, called **ACS/HRC**, is a  $1024 \times 1024$  SITe CCD, with  $\sim 0.028 \times 0.025$  arcsecond pixels, covering a nominal  $29 \times 26$  arcsecond field of view, and spectral response from  $\sim 2000$  to  $11,000 \text{ \AA}$ .
- The SBC detector, called the **ACS/SBC**, is a solar-blind CsI Multi-Anode Microchannel Array (MAMA), with  $1024 \times 1024$   $\sim 0.034 \times 0.030$  arcsecond pixels, and a nominal  $35 \times 31$  arcsecond FOV, with far-UV spectral response from  $1150$  to  $1700 \text{ \AA}$ .

#### The WFC & HRC CCDs

The ACS CCDs are thinned, backside-illuminated devices cooled by thermo-electric cooler (TEC) stacks and housed in sealed, evacuated dewars with fused silica windows. The spectral response of the WFC CCDs is optimized for imaging at visible to near-IR wavelengths, while the spectral response of the HRC CCD is optimized specifically for the near-UV. Both CCD cameras produce a time-integrated image in the ACCUM data-taking mode. As with all CCD detectors, there is noise (*readout noise*) and time (*read time*) associated with reading out the detector following an exposure. The minimum exposure time is 0.1 sec for HRC, and 0.5 sec for WFC, and the minimum time between successive identical exposures is 45s (HRC) or 135s (WFC) for full-frame and can be reduced to  $\sim 36$ s for subarray readouts. The dynamic range for a single exposure is ultimately limited by the depth of the CCD full well ( $\sim 85,000 \text{ e}^-$  for the WFC and  $155,000 \text{ e}^-$  for the HRC), which determines the total amount of charge that can accumulate in any one pixel during an exposure without saturation. Cosmic rays will affect all CCD exposures: CCD observations should be broken into multiple exposures whenever possible, to allow removal of cosmic rays in post-observation data processing; during Phase II you can use the **CR-SPLIT** optional parameter to do this (See Section 7.2.3).

#### The SBC MAMA

The SBC MAMA is a *photon-counting* detector which provides a two-dimensional ultraviolet capability. It can only be operated in ACCUM mode. The ACS MAMA detector is subject to both *scientific* and *absolute* brightness limits. At high local ( $\geq 50 \text{ counts sec}^{-1} \text{ pixel}^{-1}$ ) and global ( $> 285,000 \text{ counts sec}^{-1}$ ) illumination rates, counting becomes nonlinear in a way that is not correctable. At only slightly higher illumination rates, the

MAMA detectors are subject to damage. We have therefore defined absolute local and global count-rate limits, which translate to a set of configuration-dependent bright-object screening limits. Sources which violate the absolute count rate limits in a given configuration *cannot be observed in those configurations*, as discussed under Section 7.5.

### 3.2.2 ACS Optical Design

The ACS design incorporates two main optical channels: one for the WFC and one which is shared by the HRC and SBC. Each channel has independent corrective optics to compensate for HST's spherical aberration. The WFC has three optical elements, coated with silver, to optimize instrument throughput in the visible. The silver coatings cut off at wavelengths shortward of 3700 Å. The WFC has two filter wheels which it shares with the HRC, offering the possibility of internal WFC/HRC parallel observing for some filter combinations (Section 8.7). The optical design of the WFC is shown schematically in Figure 3.1. The HRC/SBC optical chain comprises three aluminized mirrors, overcoated with MgF<sub>2</sub> and is shown schematically in Figure 3.2. The HRC or SBC channels are selected by means of a plane fold mirror (M3 in Figure 3.3). The HRC is selected by inserting the fold mirror into the optical chain so that the beam is imaged onto the HRC detector through the WFC/HRC filter wheels. The SBC channel is selected by moving the fold mirror out of the beam to yield a two mirror optical chain which images through the SBC filter wheel onto the SBC detector. The aberrated beam coronagraph is accessed by inserting a mechanism into the HRC optical chain. This mechanism positions a substrate with two occulting spots at the aberrated telescope focal plane and an apodizer at the re-imaged exit pupil.

While there is no mechanical reason why the coronagraph could not be used with the SBC, for health and safety reasons **use of the coronagraph is forbidden with the SBC.**

Figure 3.1: ACS Optical Design: Wide Field Channel

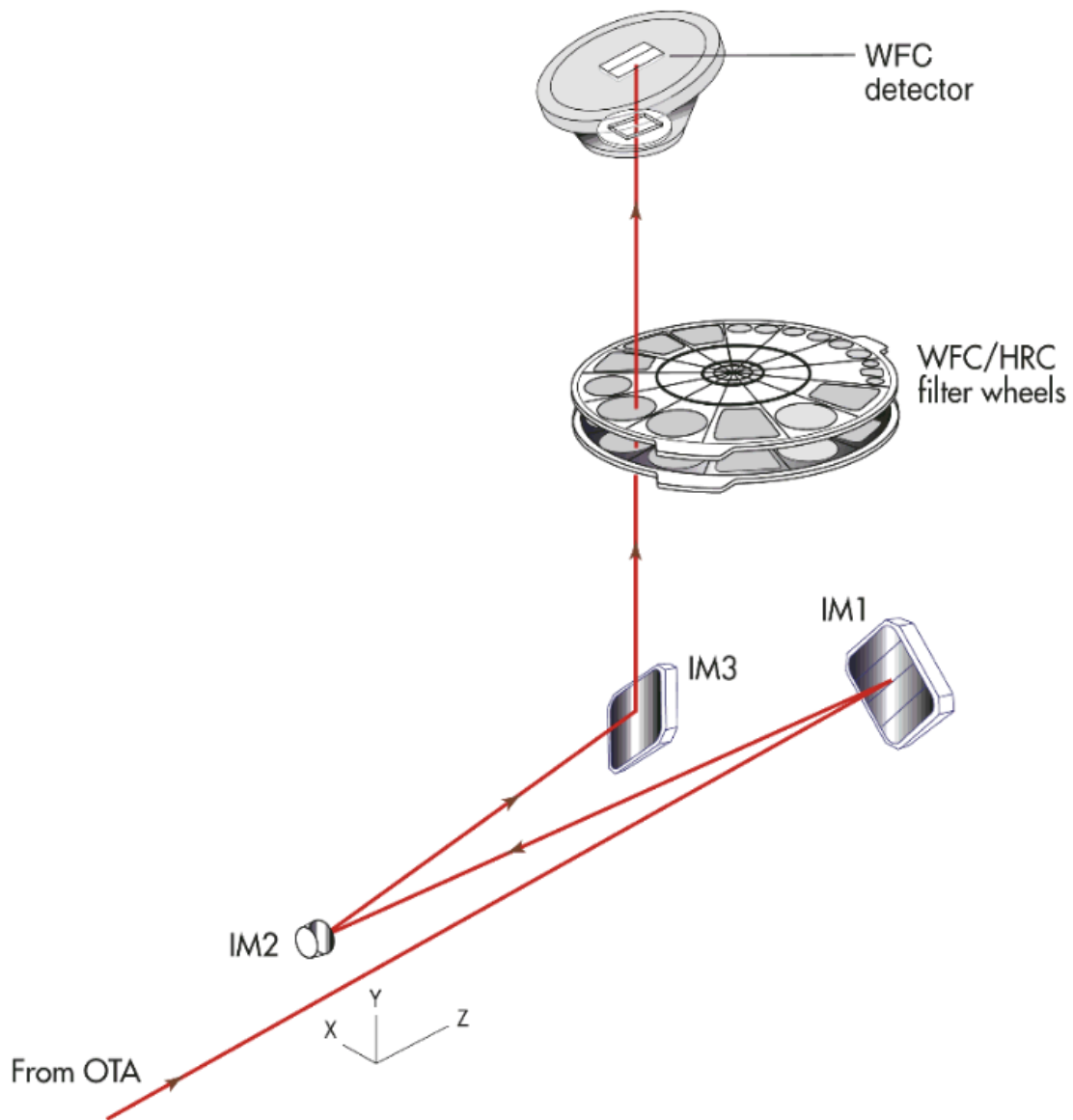
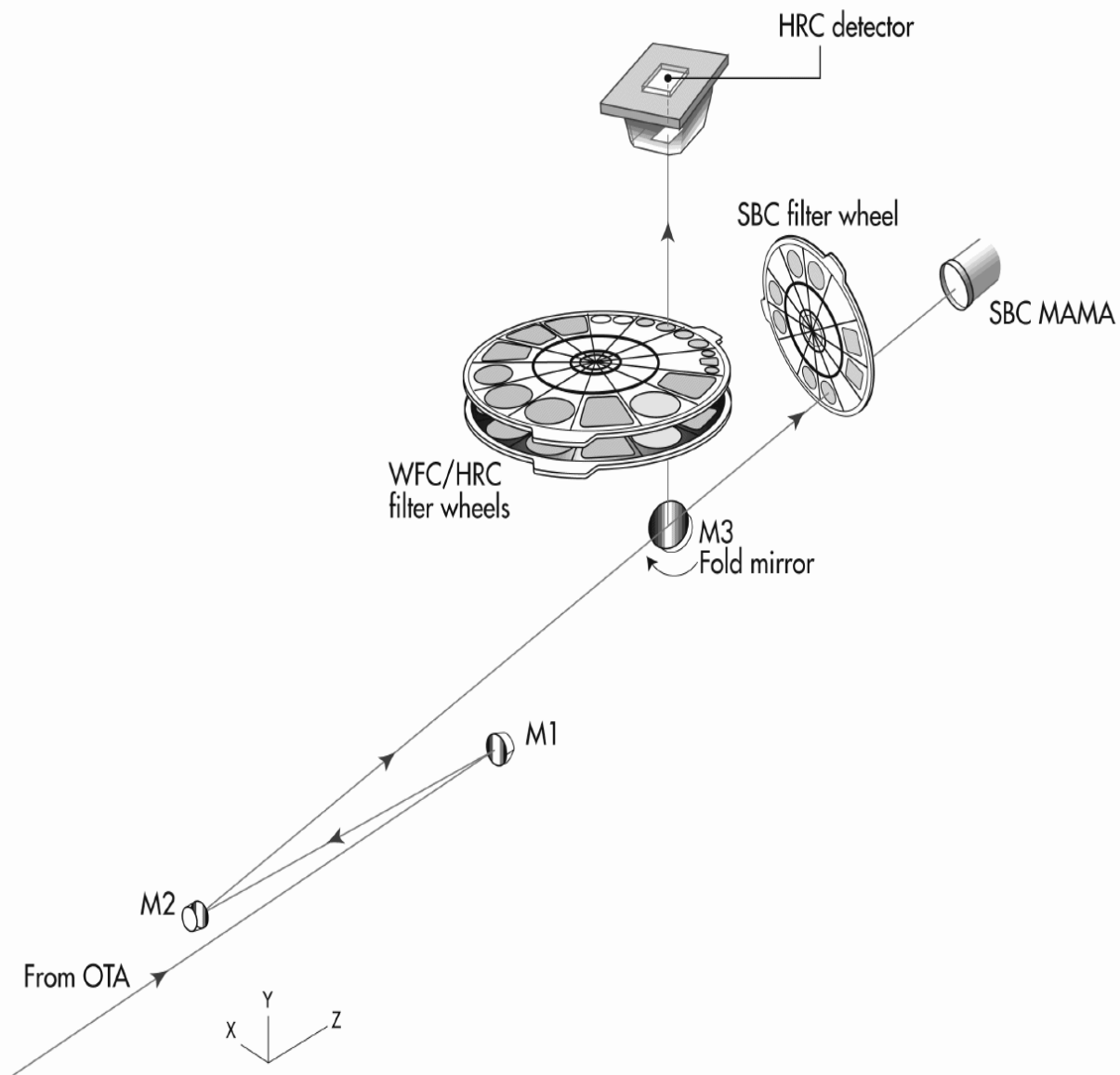


Figure 3.2: ACS Optical design: High Resolution/Solar Blind Channels



### Filter Wheels

ACS has three filter wheels: two shared by the WFC and HRC, and a separate wheel dedicated to the SBC. The WFC/HRC filter wheels contain the major filter sets summarized in Table 3.1. Each wheel also contains one clear WFC aperture and one clear HRC aperture (see Chapter 4). Parallel WFC and HRC observations are possible for some filter combinations and these are automatically added by APT, unless the user disables this option or if adding the parallel observations cannot be done due to timing

considerations. Note that since the filter wheels are shared it is not possible to independently select the filter for WFC and HRC parallel observations.

Table 3.1: ACS CCD Filters

Filter Type	Filter Description	Camera
Broadband	Sloan Digital Sky Survey (SDSS) B, V, Wide V, R, I Near-UV	WFC/HRC WFC/HRC HRC
Narrowband	H $\alpha$ (2%), [OIII] (2%), [NII] (1%) NeV (3440 Å) Methane (8920 Å)	WFC/HRC HRC HRC/[WFC <sup>1</sup> ]
Ramp filters	2% bandpass (3700-10700 Å) 9% bandpass (3700-10700 Å)	WFC/HRC WFC/HRC
Spectroscopic	Grism Prism	WFC/HRC HRC
Polarizers	Visible (0°, 60°, 120°) Near-UV (0°, 60°, 120°)	HRC/[WFC <sup>1</sup> ] HRC/[WFC <sup>1</sup> ]

1. Limited field of view (72" x 72") for these filters using WFC

The SBC filters are shown in Table 3.2.

Table 3.2: SBC Filters

Filter Type	Filter Description
Medium Band	Lyman-Alpha
Long pass	MgF <sub>2</sub> , CaF <sub>2</sub> , BaF <sub>2</sub> , Quartz, Fused Silica
Objective Prisms	LiF, CaF <sub>2</sub>

### Calibration-Lamp Systems

ACS has a calibration subsystem, consisting of tungsten lamps and a deuterium lamp for internally flat fielding each of the optical chains. The calibration subsystem illuminates a diffuser on the rear surface of the ACS aperture door, which must be closed for calibration exposures. Under normal circumstances, users are not allowed to use the internal calibration lamps.

In addition, a post-flash capability was added to the instrument to provide the means of mitigating the effects of Charge Transfer Efficiency (CTE) degradation. We do not expect to use this facility much in Cycle 12, but in later years, as radiation damage of the CCDs causes the CTE to degrade, it is likely that more users will want to avail themselves of this facility.

---

## 3.3 Basic Instrument Operations

### 3.3.1 Target Acquisitions

For the majority of ACS observations target acquisition is simply a matter of defining the appropriate aperture for the observation. Once the telescope acquires its guide stars, your target will be within  $\sim 1$ – $2$  arcseconds of the specified pointing. For observations with the ramp filters, one must specify the desired central wavelength for the observation. For the special case of coronagraphic observations, an onboard target acquisition will need to be specified. The nominal accuracy of the onboard target acquisition process is expected to be  $\sim 7$  mas, comparable to that achieved by STIS.

### 3.3.2 Typical ACS Observing Sequence

ACS is expected to be used primarily for deep, wide-field survey imaging. The important issues for observers to consider will be the “packaging” of their observations, i.e. how observations are **CR-SPLIT** to mitigate the impact of cosmic rays, whether sub-stepping or “dithering” of images is required, and how, if necessary, to construct a mosaic pattern to map the target. HRC observations and narrowband observations with the WFC are more likely to be read-noise limited, requiring consideration of the optimum **CR-SPLIT** times. Observations with the MAMA detectors do not suffer from cosmic rays or read noise, but long integration times will often be needed to obtain sufficient signal-to-noise in the photon-starved ultraviolet.

A typical ACS observing sequence is expected to consist of a series of **CR-SPLIT** and dithered  $\sim 10$ – $20$  minute exposures for each program filter. Coronagraphic observations will require an initial target acquisition observation to permit centering of the target under the occulting mask. Observers will generally not take their own calibration exposures. See Chapter 8 for more details of observing strategies.

### 3.3.3 Data Storage and Transfer

At the conclusion of each exposure, the science data is read out from the detector and placed in ACS’s internal buffer memory, where it is stored until it can be transferred to the HST solid state data recorder (and thereafter to the ground). The internal buffer memory is large enough to hold one WFC image, or sixteen HRC or SBC images, and so the buffer will typically need to be dumped during the following WFC exposure. If



the following exposure is longer than ~338 seconds, then the buffer dump from the proceeding exposure will be performed during integration (see Section 9.2 for a more complete discussion).

ACS's internal buffer stores the data in a 16 bit-per-pixel format. This structure imposes a maximum of 65,535 counts per pixel. For the MAMA detectors this maximum is equivalent to a limit on the total number of detected photons per pixel which can be accumulated in a single exposure. For the WFC and HRC, the 16 bit buffer format (and not the full well) limits the photons per pixel which can be accumulated without saturating in a single exposure when  $GAIN = 1$  for WFC, and  $GAIN \leq 2$  for the HRC is selected. See Chapters 7 and 8 for a detailed description of ACS instrument operations.

### 3.3.4 Parallel Operations

Parallel observations with the WFC and HRC are possible with ACS for certain filter combinations (See Section 8.7).

ACS can be used in parallel with any of the other science instruments on HST, within certain restrictions. Figure 3.3 shows the HST field of view following SM3B with ACS installed. Dimensions in this figure are approximate; accurate aperture positions can be found on STScI's Observatory web page under "Pointing"<sup>1</sup> or by using the Visual Target Tuner (VTT). The ACS grism and prism dispersion directions are approximately along the V2 axis. The policy for applying for parallel observing time is described in the Call for Proposals. We provide suggestions for designing parallel observations with ACS in Section 8.7. While the ACS CCDs can be used in parallel with another instrument on HST, subject to certain restrictions described in Section 8.7, there are significant restrictions on the use of the MAMA detectors in parallel – see Chapter 2.

---

## 3.4 Designing an ACS Observing Proposal

In this section, we describe the sequence of steps you will need to take when designing your ACS observing proposal. The process is an iterative one, as trade-offs are made between signal-to-noise ratio and the limitations of the instrument itself. The basic sequence of steps in defining an ACS observation are:

---

1. Pointing web page: <http://www.stsci.edu/instruments/observatory/taps.html>

- Identify science requirements and select the basic ACS configuration to support those requirements.
- Estimate exposure time to achieve the required signal-to-noise ratio, determine GAIN selection, CR-SPLIT, dithering and mosaic strategy and check feasibility, including saturation and bright-object limits.
- Identify any additional target acquisition (coronagraph), and calibration exposures needed.
- Calculate the total number of orbits required, taking into account the overheads.

Figure 3.3: HST Field of View Following SM3B

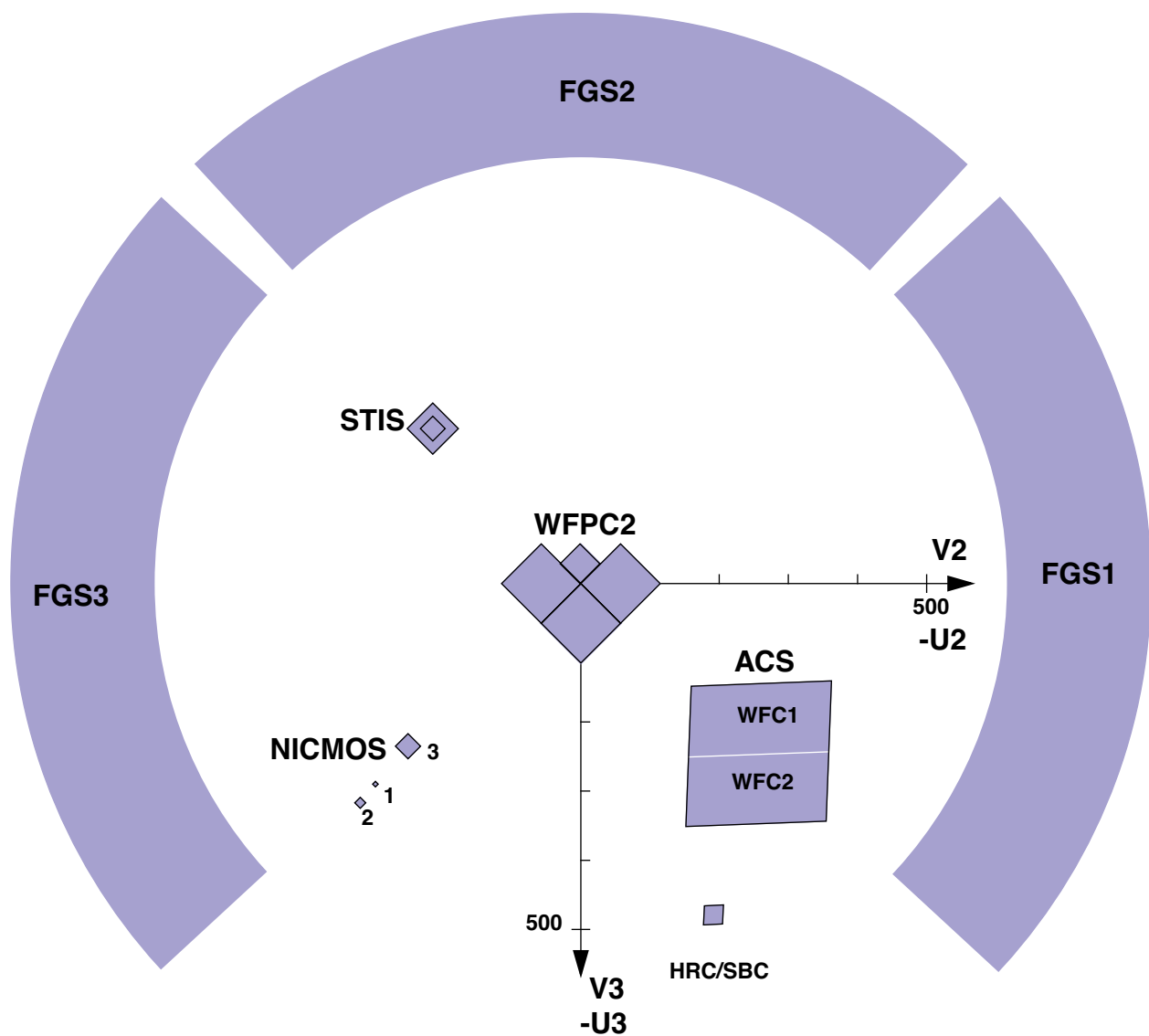
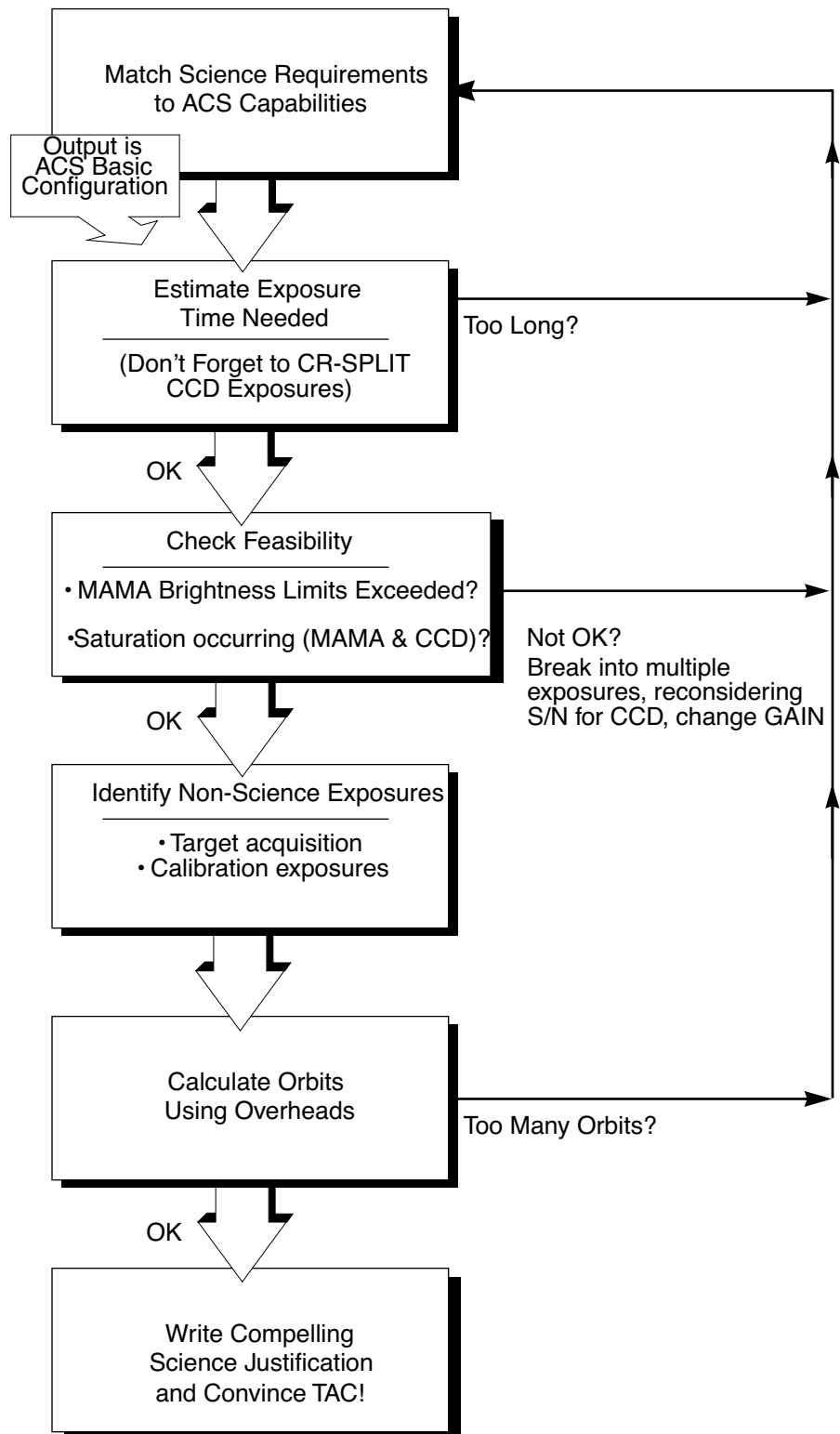


Figure 3.4: Defining an ACS Observation



### 3.4.1 Identify Science Requirements and Define ACS Configuration

First and foremost, of course, you must identify the science you wish to achieve with ACS. Basic decisions you will need to make are:

- Filter selection
- Nature of target

As you choose your science requirements and work to match them to the instrument's capabilities, keep in mind that those capabilities differ greatly depending on whether you are observing in the optical or near-UV with the CCD, or in the far-UV using the MAMA detector. Tradeoffs are described in Table 3.3.

Table 3.3: Science Decision Guide

Decision	Affects	Tradeoffs
Field of view	Camera Filter selection	WFC: 202 x 202 arcseconds HRC: 29 x 26 arcseconds SBC: 35 x 31 arcseconds
Spectral response	Camera Filter selection	WFC: 3700-11,000 Å HRC: 2000-11,000 Å SBC: 1150-1700 Å
Spatial Resolution	Camera	WFC: ~50 milliarcsecond pixels HRC: ~27 milliarcsecond pixels SBC: ~32 milliarcsecond pixels
Filter Selection	Camera	WFC: broad, medium & narrow band ramps HRC: Visible, UV, ramp middle sections
Spectroscopy	Camera Spatial resolution Field of View Wavelength range	Grism (G800L): WFC and HRC Prism (PR200L): HRC Prism (PR110L, PR130L): SBC
Polarimetry	Filters	UV polarizers combine with Wheel 2 filters VIS polarizers combine with Wheel 1 filters
Coronagraphy	Filter selection	Coronagraphic imaging available with HRC only

#### Imaging

For imaging observations, the base configuration is detector (Configuration), operating mode (MODE=ACCUM), and filter. Chapter 4 presents detailed information about each of ACS's imaging modes.

#### Special Uses

We refer you to Chapter 5 if you are interested in any of the following special uses of ACS: slitless spectroscopy, polarimetry and coronagraphy.

### 3.4.2 Determine Exposure Time and Check Feasibility

Once you have selected your basic ACS configuration, the next steps are to:

- Estimate the exposure time needed to achieve your required signal-to-noise ratio, given your source brightness. (You can use the ACS Exposure-Time Calculator for this, see also Chapter 6 and the plots in Chapter 10).
- For observations using the CCD detectors, assure that for pixels of interest, you do not exceed the per pixel saturation count limit of the CCD full well or the 16 bit pixel word size at the **GAIN** setting you choose.
- For observations using the MAMA detector, assure that your observations do not exceed brightness (count-rate) limits.
- For observations using the MAMA detector, assure that for pixels of interest, your observations do not exceed the limit of 65,535 accumulated counts per pixel per exposure imposed by the ACS 16 bit buffer.

To determine your exposure-time requirements consult Chapter 6 where an explanation of how to calculate signal-to-noise and a description of the sky backgrounds are provided. To assess whether you are close to the brightness, signal-to-noise, and dynamic-range limitations of the detectors, refer to Chapter 7. For a consideration of observation strategies and calibration exposures, consult Chapter 8.

If you find that the exposure time needed to meet your signal-to-noise requirements is too great, or that you are constrained by the detector's brightness or dynamic-range limitations, you will need to adjust your base ACS configuration. Table 3.4 summarizes the options available to you and steps you may wish to take as you iterate to select an ACS configuration which is both suited to your science and is technically feasible.

Table 3.4: Science Feasibility Guide

Action	Outcome	Recourse
Estimate exposure time	If too long -> re-evaluate instrument configuration.	Consider use of an alternative filter.
Check full-well limit for CCD observations	If full well exceeded and you wish to avoid saturation-> reduce time per exposure.	Divide total exposure time into multiple, short exposures. <sup>1</sup> Consider use of different Gain.
Check bright-object limits for MAMA observations	If source is too bright -> re-evaluate instrument configuration.	Consider the use of an alternative filter or change detectors and wavelength regime.
Check 65,535 counts-per-pixel limit for MAMA observations	If limit exceeded -> reduce time per exposure.	Divide total exposure time into multiple, short exposures

1. Splitting CCD exposures affects the exposure time needed to achieve a given signal-to-noise ratio because of the read noise.

### 3.4.3 Identify Need for Additional Exposures

Having identified your desired sequence of *science* exposures, you need to determine what additional exposures you may require to achieve your scientific goals. Specifically:

- For coronagraphy, determine what target-acquisition exposure will be needed to center your target under the selected occulting mask.
- If the success of your science program requires calibration to a higher level of precision than is provided by STScI's calibration data, and if you are able to justify your ability to reach this level of calibration accuracy yourself, you will need to include the necessary calibration exposures in your program, including the orbits required for calibration in your total orbit request.

### 3.4.4 Determine Total Orbit Request

In this, the final step, you place all your exposures (science and non-science, alike) into orbits, including tabulated overheads, and determine the total number of orbits you require. Refer to Chapter 9 when performing this step. If you are observing a small target and find your total time request is significantly affected by data-transfer overheads (which will be the case *only* if you are taking many separate exposures under 338 seconds with the WFC), you can consider the use of CCD subarrays to lessen the data volume. Subarrays are described in Chapter 8 in sections “WFC CCD Subarrays” on page 147 and “HRC CCD Subarrays” on page 148.

At this point, if you are happy with the total number of orbits required, you're done! If you are unhappy with the total number of orbits required, you can, of course, iterate, adjusting your instrument configuration, lessening your acquisition requirements, changing your target signal-to-noise or wavelength requirements, until you find a combination which allows you to achieve your science goals with ACS. Good luck!





# CHAPTER 4: Imaging

**In this chapter . . .**

4.1 Imaging Overview / 37
4.2 Which instrument to use? / 43
4.3 Caveats for ACS Imaging / 48
4.4 Wide Field Optical CCD Imaging / 51
4.5 High-Resolution Optical and UV Imaging / 53
4.6 Ultraviolet Imaging with the SBC / 55
4.7 ACS Point Spread Functions / 56

In this Chapter we focus on the imaging capabilities of ACS. Each imaging mode is described in detail. Plots of throughput and comparisons to the capabilities of WFPC2 and STIS are also provided. Curves of sensitivity and exposure time to achieve a given signal-to-noise as a function of source luminosity or surface brightness are referenced in this chapter, but presented in Chapter 10. We note the existence of bright-object observing limits for SBC channel imaging; these are described in detail in Chapter 7, including tables of the SBC bright-object screening magnitudes as a function of mode and spectral type.

---

## 4.1 Imaging Overview

ACS can be used to obtain images through a variety of optical and ultraviolet filters. When the selected ACS camera is the WFC or the HRC, the appropriate filter in one of the two filter wheels is rotated into position and a clear aperture is automatically selected on the other filter wheel. For SBC imaging the single filter wheel is rotated to the required position. A

number of apertures are defined for each ACS camera. In general, these refer to different target positions on the detector.

Table 4.1 and Table 4.2 provide a complete summary of the filters available for imaging with each detector. Figures 4.1 through 4.5 show the filter transmission curves. In Figure 4.9 we show the integrated system throughputs.

The CCD filter wheels contain filters with two different sizes. Some filters (F435W, F475W, F502N, F550M, F555W, F606W, F625W, F658N, F660N, F775W, F814W, F850LP and G800L) are full-sized filters that can be used with both WFC and HRC. Others (F220W, F250W, F330W, F344N, F892N, POL0UV, POL60UV, POL120UV, POL0V, POL60V, POL120V, PR200L) are smaller, giving a full unvignetted field of view when used with the HRC, but a vignetted field of view of only 72"×72" when used with the WFC. Use of the small UV filters is not supported with the WFC due to the unpredictable behavior of the silver coatings shortward of 4000Å.

The Ramp Filters are designed to allow narrow or medium band imaging centered at an arbitrary wavelength. Each ramp filter is divided into three segments, of which only the middle segment may be used with the HRC. See "Ramp filters" on page 52 for more details on these filters.

Note that although the CLEAR filters are specified in the filter wheel tables, users do not need to specify these filters in their HST proposals; they are added automatically in conjunction with the desired filter in the complementary wheel. In the SBC filter wheel, every third slot (#1, 4, 7, 10) is blocked off, so that in the case of a bright object limit violation, it is only necessary to rotate the filter wheel to an adjacent slot to block the incoming light.

With either the WFC and HRC it is possible to select a filterless observation by specifying CLEAR (this is an "available-but-unsupported" filter) as the filter name, although the image will be of degraded quality. Rough wavelengths and widths when used with the WFC or HRC are listed in Table 4.1 under CLEAR entries. Use of CLEAR will provide slightly degraded PSFs with the HRC and seriously degraded PSFs for the WFC. Applications are expected to be rare, but a valid use could be astrometry of extremely faint targets with the HRC when color information is not required.

Table 4.1: ACS WFC/HRC Filters in Filter Wheel #1

Filter Name	Central Wavelength	Width (Å)	Description	Camera
CLEAR	6200	5200	Clear aperture	WFC/HRC
F555W	5346	1193	Johnson V	WFC/HRC
F775W	7764	1528	SDSS i	WFC/HRC
F625W	6318	1442	SDSS r	WFC/HRC
F550M	5580	547	Narrow V	WFC/HRC
F850LP	9445	1229	SDSS z	WFC/HRC
POL0UV	2000–6000	-	0° UV polarizer	HRC[/WFC]
POL60UV	2000–6000	-	60° UV polarizer	HRC[/WFC]
POL120UV	2000–6000	-	120° UV polarizer	HRC[/WFC]
F892N	8917	154	Methane (2%)	HRC[/WFC]
F606W	5907	2342	Broad V	WFC/HRC
F502N	5022	57	[OIII] (1%)	WFC/HRC
G800L	5800–11,000	-	Grism (R~100)	WFC/HRC
F658N	6584	78	H $\alpha$ (1%)	WFC/HRC
F475W	4760	1458	SDSS g	WFC/HRC

Table 4.2: ACS WFC/HRC Filters in Filter Wheel #2

Filter Name	Central Wavelength	Width (Å)	Description	Camera
CLEAR	6000	5200	Clear aperture	WFC/HRC
F660N	6602	40	[NII] (1%)	WFC/HRC
F814W	8333	2511	Broad I	WFC/HRC
FR388N	3710–4050	2%	[OII] Ramp—middle segment	WFC/HRC
FR423N	4050–4420	2%	[OII] Ramp—inner segment	WFC
FR462N	4420–4820	2%	[OII] Ramp—outer segment	WFC
F435W	4297	1038	Johnson B	WFC/HRC
FR656N	6270–6850	2%	H $\alpha$ Ramp—middle segment	WFC/HRC
FR716N	6850–7470	2%	H $\alpha$ Ramp—inner segment	WFC
FR782N	7470–8160	2%	H $\alpha$ Ramp—outer segment	WFC
POL0V	4000–8000	-	0° Visible Polarizer	HRC[/WFC]

Filter Name	Central Wavelength	Width (Å)	Description	Camera
F330W	3354	588	HRC U	HRC
POL60V	4000–8000	-	60° Visible Polarizer	HRC[/WFC]
F250W	2696	549	Near-UV broadband	HRC
POL120V	4000–8000	-	120° Visible Polarizer	HRC[/WFC]
PR200L	2000–4000	-	NUV Prism (R~100 @ 200 nm)	HRC
F344N	3434	60	Ne V (2%)	HRC
F220W	2228	485	Near-UV broadband	HRC
FR914M	7570–10,710	9%	Broad Ramp—middle segment	WFC/HRC
FR853N	8160–8910	2%	IR Ramp—inner segment	WFC
FR931N	8910–9720	2%	IR Ramp—outer segment	WFC
FR459M	3810–5370	9%	Broad Ramp—middle segment	WFC/HRC
FR647M	5370–7570	9%	Broad Ramp—inner segment	WFC
FR1016N	9720–10,610	2%	IR Ramp—outer segment	WFC
FR505N	4820–5270	2%	[OIII] Ramp—middle segment	WFC/HRC
FR551N	5270–5750	2%	[OIII] Ramp—inner segment	WFC
FR601N	5750–6270	2%	[OIII] Ramp—outer segment	WFC

Table 4.3: ACS SBC Filter Complement

Filter Name	Description
F115LP	MgF <sub>2</sub> (1150 Å longpass)
F125LP	CaF <sub>2</sub> (1250 Å longpass)
F140LP	BaF <sub>2</sub> (1400 Å longpass)
F150LP	Crystal quartz (1500 Å longpass)
F165LP	Fused Silica (1650 Å longpass)
F122M	Ly- $\alpha$ ( $\lambda = 1200$ Å, $\Delta\lambda = 60$ Å)
PR110L	LiF Prism (R~100 @)
PR130L	CaF <sub>2</sub> Prism (R~100 @)

Figure 4.1: ACS Broad-band filters

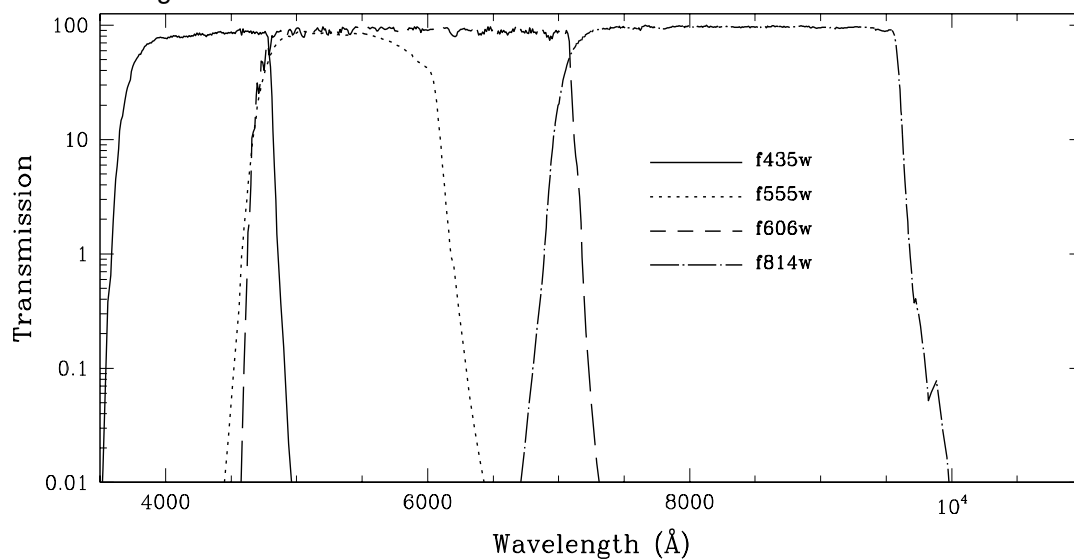


Figure 4.2: ACS SDSS filters

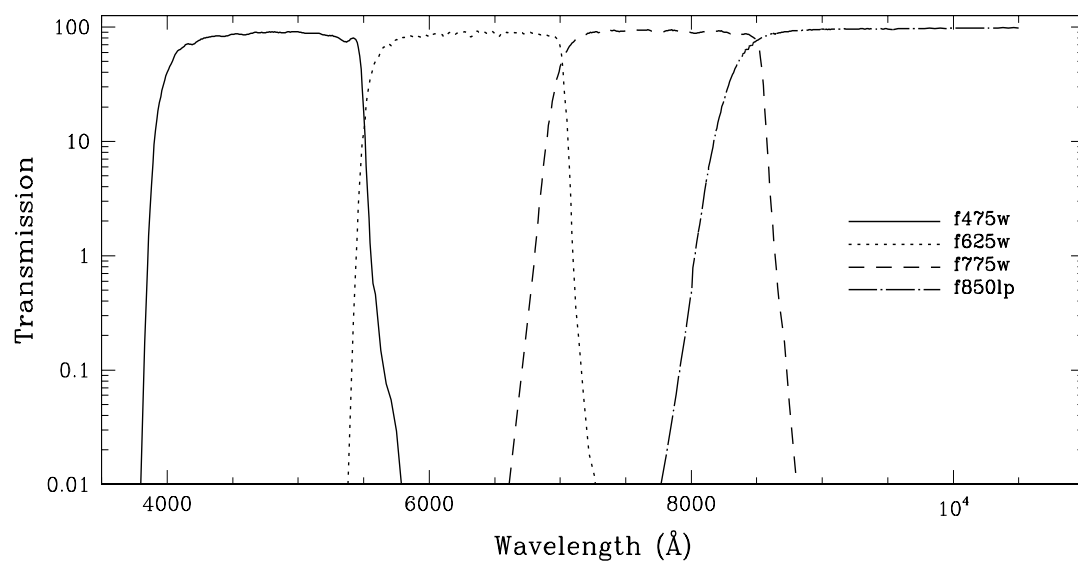


Figure 4.3: ACS UV and Medium-Band filters

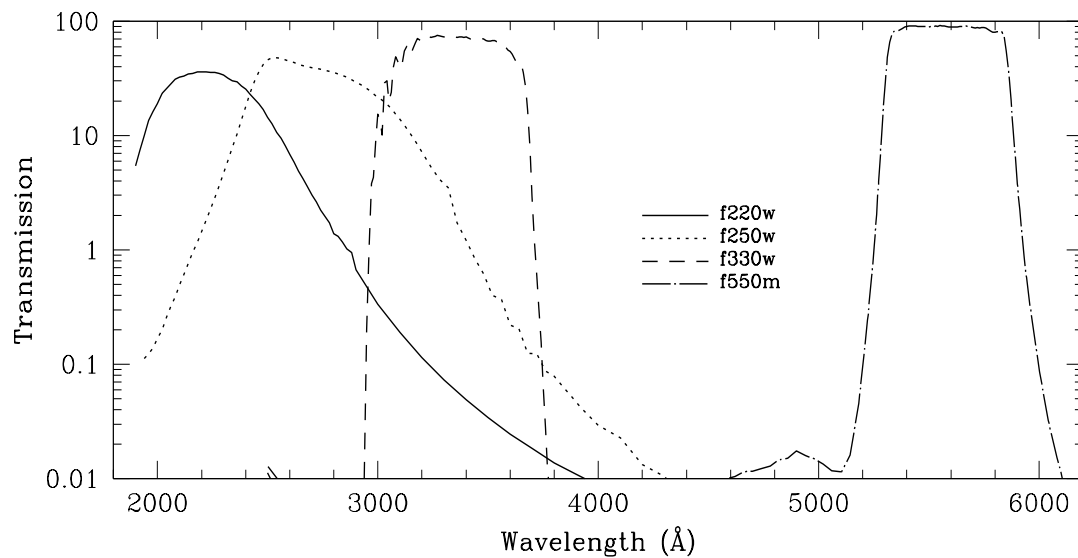


Figure 4.4: ACS Narrow-Band filters

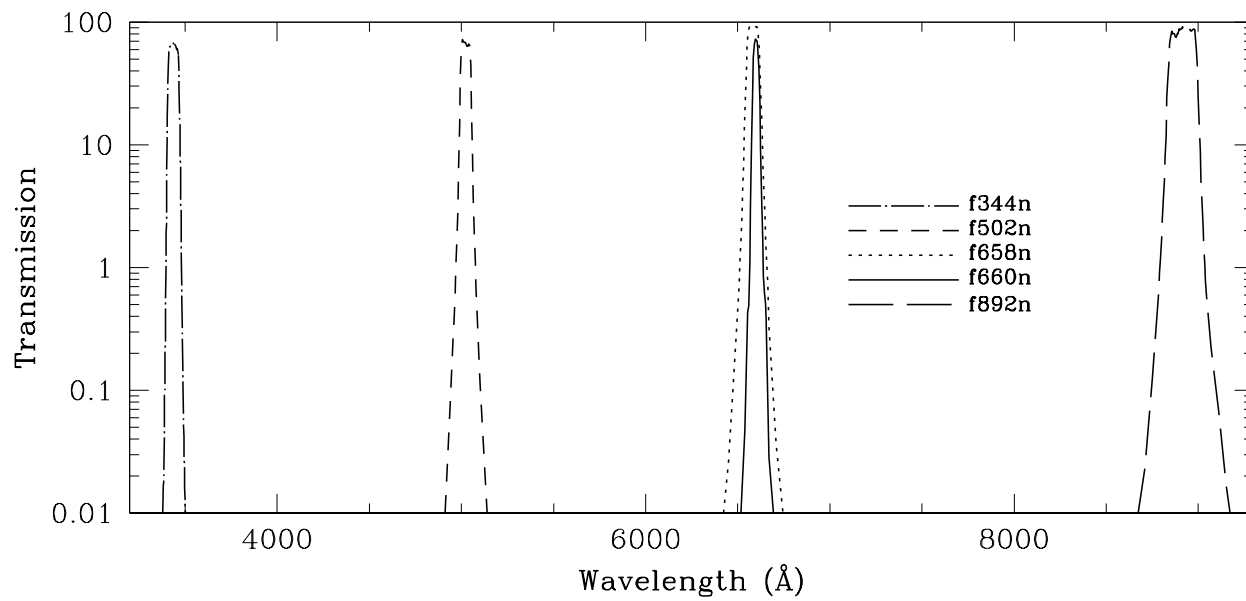
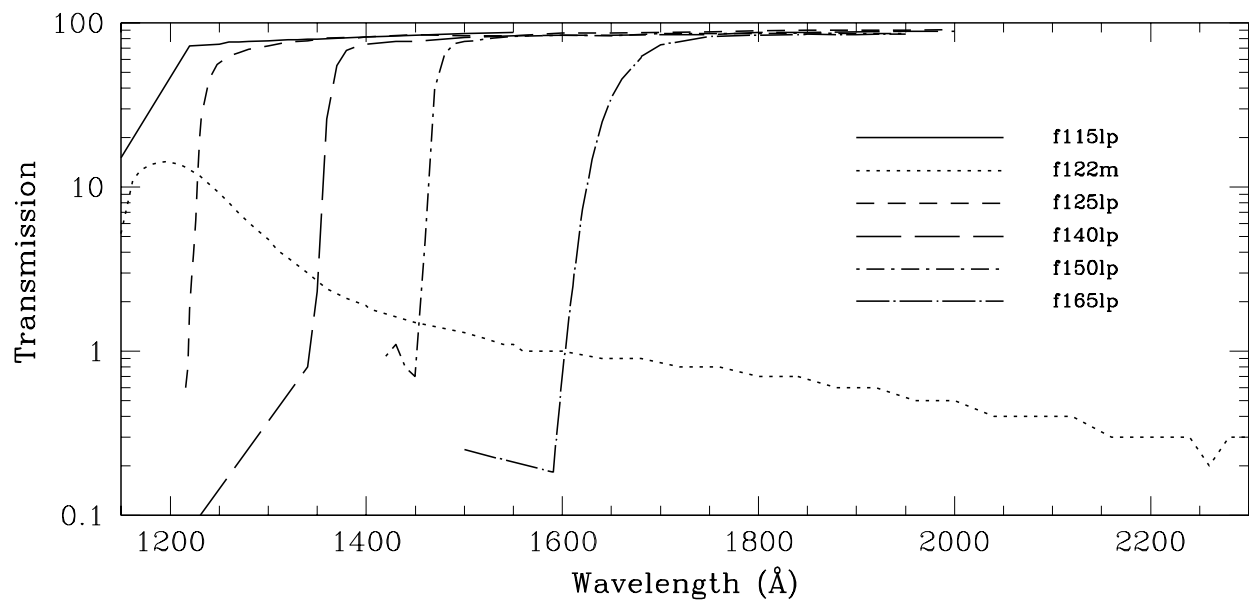


Figure 4.5: ACS SBC filters



## 4.2 Which instrument to use?

In this section, we compare briefly the performance of HST instruments with imaging and spectroscopic capability in the UV to near-IR spectral range. Important imaging parameters for all instruments are summarized in Table 4.4, followed by different sections where the ACS characteristics are compared to each other instrument.

Table 4.4: Characteristics of HST Imaging Instruments

Parameter	ACS		WFPC2	NICMOS	STIS	
<b>Wavelength range (Å)</b>	WFC HRC SBC	3700-11,000 2000-11,000 1150-1700	1150-11,000	8000-25,000	FUV-MAMA NUV-MAMA CCD	1150-1700 1700-3100 2000-11,000
<b>Detector(s)</b>	SITe CCDs, MAMA		Loral CCDs	HgCdTe	SITe CCD, MAMAs	
<b>Image format</b>	WFC HRC SBC	2×2048×4096 1024×1024 1024×1024	4×800×800	256×256 256×256 256×256	FUV-MAMA NUV-MAMA CCD	1024×1024 1024×1024 1024×1024
<b>FOV and pixel size</b>	WFC  HRC  SBC	202"×202" 0.05" /pix  29"×26" 0.027" /pix  35"×31" 0.032" /pix	150"×150" 0.1" /pixel  34"×34" 0.046" /pixel	11"×11" 0.043" /pixel  19"×19" at 0.075" /pixel  51"×51" at 0.2" /pixel	FUV-MAMA  NUV-MAMA  CCD	25"×25" 0.024" /pix  25"×25" 0.024" /pix  51"×51" 0.05" /pix
<b>Read noise</b>	WFC HRC SBC	5.0 e <sup>-</sup> 4.7 e <sup>-</sup> 0 e <sup>-</sup>	5.5 e <sup>-</sup> 7.5 e <sup>-</sup>	30 e <sup>-</sup>	FUV-MAMA NUV-MAMA CCD	0 e <sup>-</sup> 0 e <sup>-</sup> 5.4 e <sup>-</sup>
<b>Dark current</b>	WFC HRC SBC	0.002 e <sup>-</sup> /s/pix 0.0025 e <sup>-</sup> /s/pix 1.2×10 <sup>-5</sup> e <sup>-</sup> /s/pix	0.004 e <sup>-</sup> /s/pix	<0.1 e <sup>-</sup> /s/pix	CCD NUV FUV.	0.004 e <sup>-</sup> /s/pix 0.001 e <sup>-</sup> /s/pix 7×10 <sup>-6</sup> e <sup>-</sup> /s/pix
<b>Saturation</b>	WFC HRC	84,700 e <sup>-</sup> (gain 2) 155,000 e <sup>-</sup> (gain 4)	53,000 e <sup>-</sup> (gain 15)	200,000 e <sup>-</sup>	144,000 e <sup>-</sup> (gain 4)	

### 4.2.1 Comparison of ACS and WFPC-2

Advantages of each instrument may be summarized as follows:

ACS advantages are:

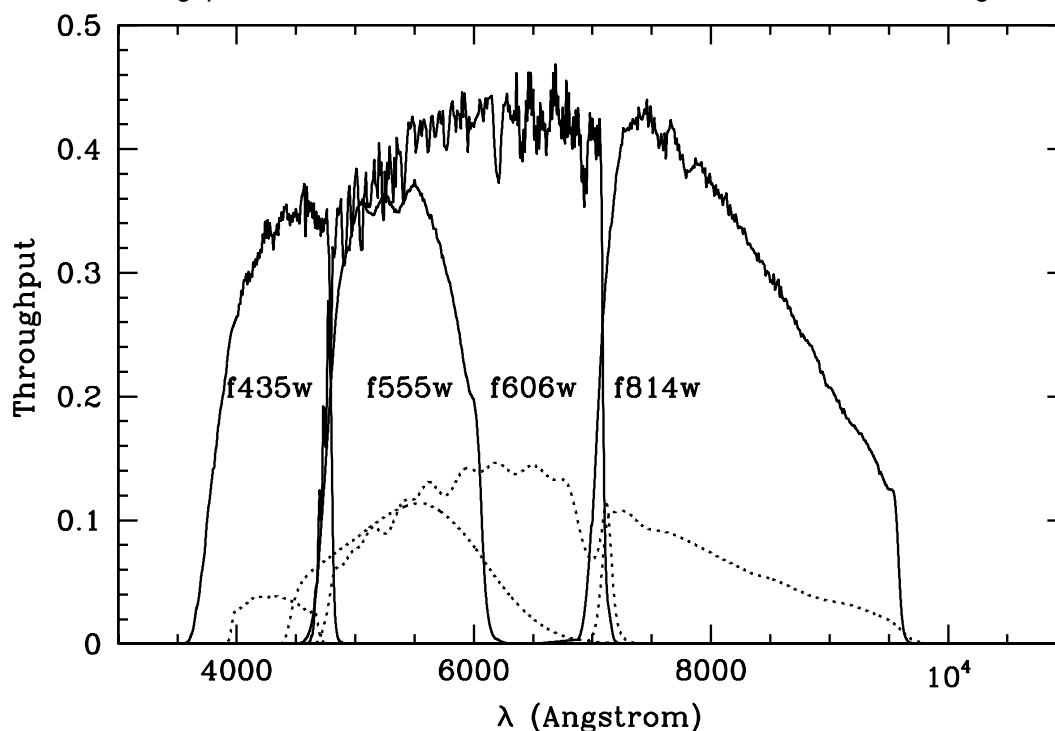
- Wider field of view, 202"×202" vs. 150"×150" or less.
- Higher throughput at wavelengths >3700 Å (see Figure 4.6).
- Better resolution: ACS offers 0.027" pixels vs. 0.046" on WFPC2 (PC).
- Better dynamic range: lower and well sampled read noise, longer sampled full well depth.
- Spectroscopic and coronagraphic observations are possible.
- ACS ramp filters have a higher throughput and FOV than those in WFPC2 (see Figures 4.6-4.9) and offer complete wavelength coverage from 3710Å to 10,710Å.
- Polarization observations on ACS can be made with 3 polarizer angles of 0°, 60°, 120° over the whole HRC FOV.
- For high contrast imaging, the WFPC2 PC has a higher scattered light floor than ACS HRC.
- ACS has uniform PSFs over the entire field-of-view.

WFPC2 advantages are:

- Some special filters are available that are not found in ACS. These are the narrow filters (F343N, F375N (OII), F390N, F437N, F469N, F487N, F588N, F631N, F673N, F953N). ACS can do narrow-band imaging with the ramp filters, with a smaller FOV and has higher throughput and lower read noise.
- Wide-field UV observations are possible with the following filters: F122M, F160BW, F170W, F185W, F218W, F255W, F300W, F336W.



Figure 4.6: Comparison between the system efficiency (or throughput) of ACS WFC and WFPC2 for the filters: Johnson B, Johnson V, Broad V and Broad I. The solid lines are for ACS and the dashed lines for WFPC2. ACS total system throughput is at least a factor of 3-4 better than WFPC2 at these wavelengths.



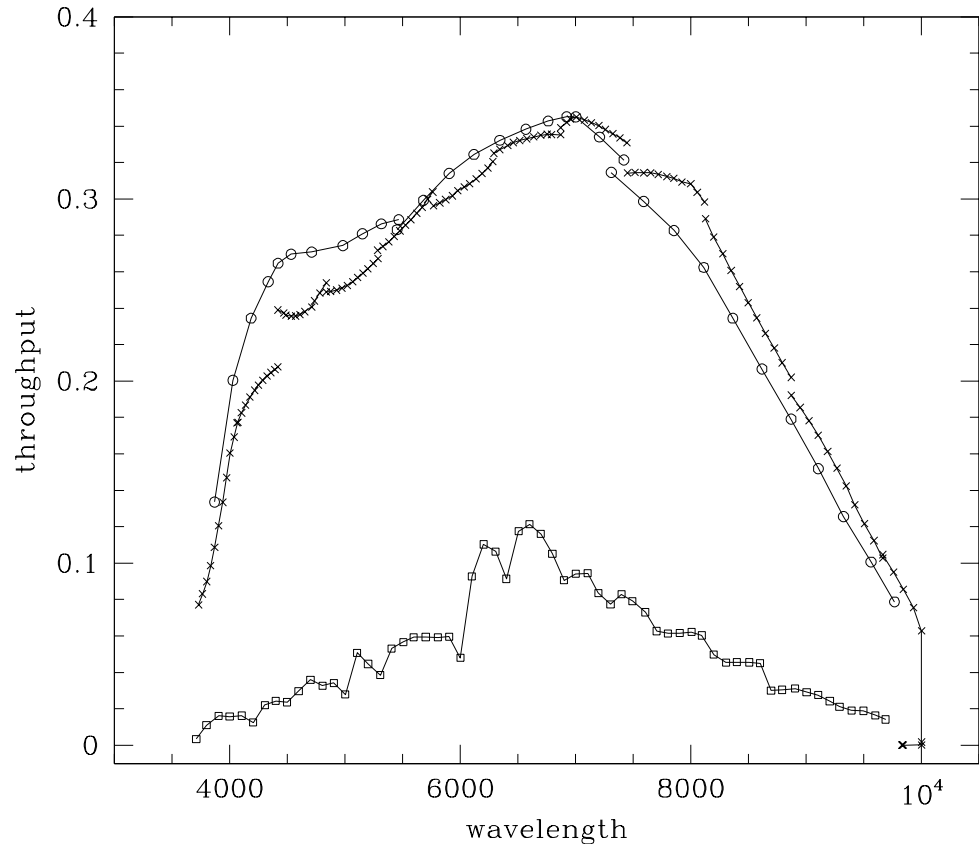
## 4.2.2 Comparison of ACS and NICMOS

ACS and NICMOS have a small overlap in imaging capability for filters at around  $9000\text{\AA}$ . At longer wavelengths NICMOS must be used; at shorter wavelengths either ACS, WFPC2 or STIS must be used. The following table compares the detective efficiency of ACS and NICMOS in the wavelength region where they both operate. Count rates for a  $V=20$  star of spectral class A1 are given for all filters at common wavelengths; the signal-to-noise (S/N) is also given for a 1 hour exposure of this same star.

Table 4.5: Near-IR capabilities of ACS compared to NICMOS

Instrument	Filter	Pivot Wavelength ( $\text{\AA}$ )	FWHM ( $\text{\AA}$ )	Count rate	S/N
ACS/WFC	F850LP	9103	1359	42.7	383
ACS/WFC	F892N	8915	175	4.3	117
NICMOS	F090M	9041	1318	17.1	69

Figure 4.7: Comparison between the ACS and WFPC2 ramp filters. The crosses and the open circles are for the ACS narrow and medium band ramps. The open squares are for the 4 WFPC2 ramps. For each of the ACS ramps the peak throughput that was calculated for eleven central wavelength values is plotted. For the WFPC2 ramps, the peak throughput calculated every 100Å within the field of view of any of the 4 chips and a 0° filter rotation angle (as mapped in Figs. 3.4 and 3.5 of the WFPC2 Instrument Handbook, version 3.0), is plotted.



### 4.2.3 Comparison of ACS and STIS

Both ACS and STIS are capable of imaging over the same wavelength range, between 1200Å and 11,000Å. At much longer wavelengths NICMOS must be used.

Advantages of each instrument may be summarized as follows:

ACS advantages are:

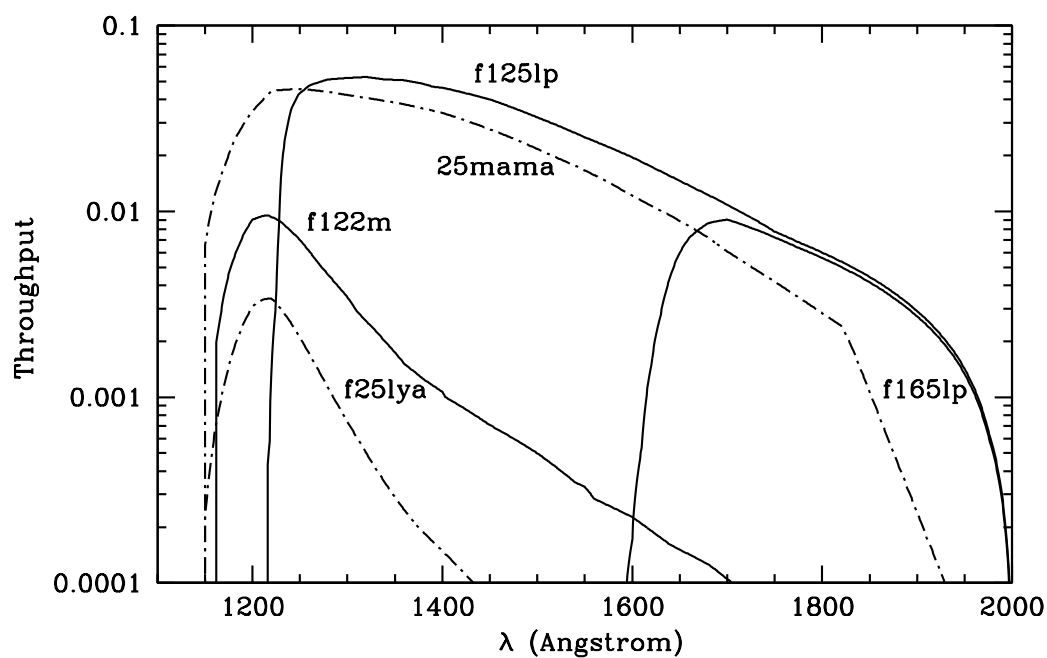
- Wider field-of-view at optical and near-infrared wavelengths, 202"×202" vs. 50"×50" or less.
- Greater selection of filters, including polarizers, are available.
- Higher sensitivity is possible.

STIS advantages are:

- MAMAs can be used in Time-Tag Mode.
- FUV-MAMA gives higher S/N than SBC due to the lower dark current.
- An OII filter centered at  $3727\text{\AA}$  is available that allows deep, high-resolution OII imaging.
- Narrow band filters at  $2800\text{\AA}$  and  $1900\text{\AA}$  allow imaging in MgII and CIII, respectively.
- Selectable aperture (slit) size for the MAMAs means that bright object concerns are lessened.

True to its name, ACS significantly enhances the imaging capabilities of HST. Due to the combination of sensitivity and field of view ACS has become the instrument of choice for UV/optical imaging on HST.

Figure 4.8: Comparison between the system efficiency of ACS SBC and STIS FUV-MAMA. For the ACS SBC the total system throughput for the f122m, f125lp and f165lp filters is plotted in the solid lines. For the STIS FUV-MAMA the system throughput for the Clear (25mama) and Lyman- $\alpha$  (f25lya) filters are given with the dashed line.



## 4.3 Caveats for ACS Imaging

There are a few characteristics of ACS that should be taken into account when imaging with ACS:

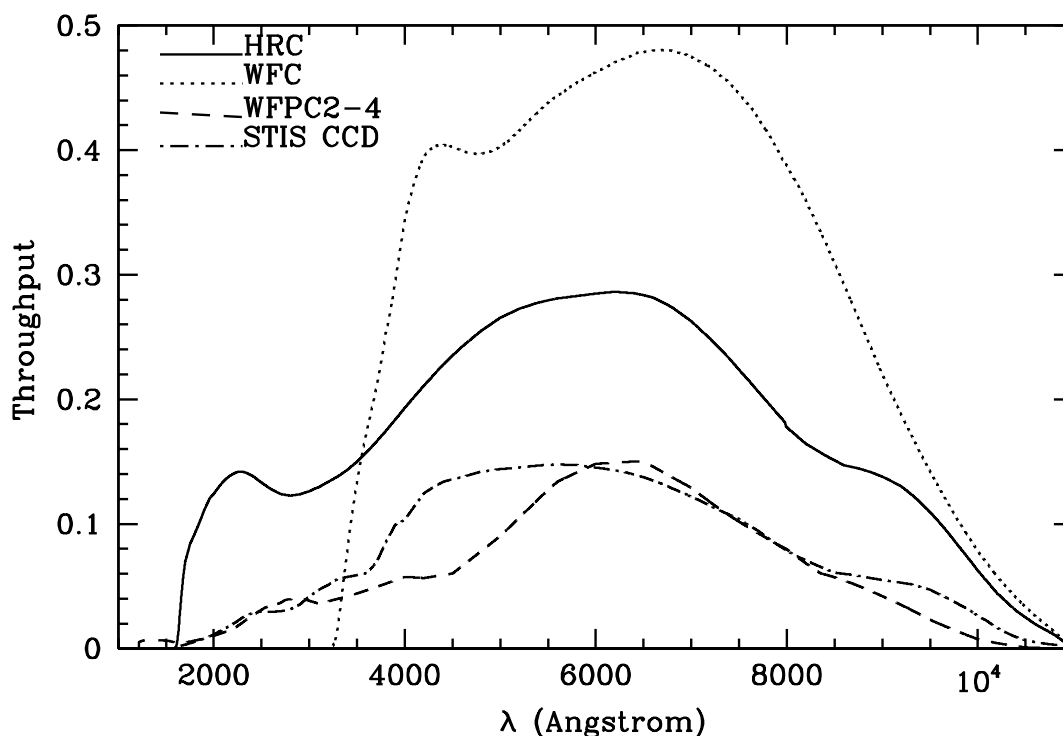
- The HRC and WFC filters are housed in two filter wheels shared by both cameras. As a consequence, when a filter is chosen for the primary camera the filter used in the parallel camera is not independently selectable (see Table 8.4).
- The ACS cameras are designed to be used with a single filter, and for this reason unfiltered imaging or imaging through two filters leads to significantly degraded imaging quality (particularly in the WFC) and is not normally used except for polarization observations, or bright target acquisitions with the HRC. The polarizer filters were designed with a zero optical thickness so that they can and should be used with another filter.
- The geometric distortion of the WFC is significant and causes the projected pixel area to vary by  $\pm 9\%$  over the field of view. This distortion affects both the photometric accuracy and the astrometric precision and must be accounted for when the required accuracy is better than 10%.
- The ratio of in-band vs. out-of-band transmission for the ACS CCD UV filters is similar to that of WFPC2, once the two detector QE curves are taken into account. This implies that for imaging in the UV of intrinsically red objects the effect of filter red-leaks needs to be calibrated.
- The cosmic ray fluxes for HRC and WFC are comparable, respectively, to those of the STIS CCD and WFPC2. As with these instruments typical imaging observations will need to be split or dithered for cosmic ray rejection.
- The default GAIN setting for WFC primary observations is `GAIN=1`. This allows for good sampling of the readout noise but it does not allow one to reach the full well counts of WFC. The readout noise for the WFC is still better than critically sampled at `GAIN=2`, which provides sampling of the full well depth as well (by contrast all WFPC2 results were obtained with a GAIN falling at least a factor of 3 short of critically sampling the readout noise). For HRC primary observations, the default gain is `GAIN=2`. For the HRC `GAIN=4` is needed to sample the detector full well depth, but this does result in modest undersampling of the readout noise. For HRC ACQ data, the default setting is `GAIN=4`. Users may select the GAIN they wish to use for their ACS observations by using the GAIN Optional Parameter in their Phase II proposal.

- At wavelengths longward of  $\sim 8000\text{\AA}$ , internal scattering in the HRC CCD produces an extended PSF halo. This should affect only a minority of observations since at these wavelengths the WFC camera should normally be preferred. The WFC CCDs include a front-side metallization that eliminates the large angle, long wavelength halo problem for  $7000 < \lambda < 10,000\text{\AA}$ .
- The ACS filter complement is not as rich as that in WFPC2. In particular, the Strömgren filter set and several narrow band filters available in WFPC2 (F375N, F390N, F437N, F469N, F487N, F588N, F631N, F656N, F673N, F953N) are not available on ACS. In general, these filters were not heavily used by the GO community. For most applications they can be replaced with the ACS medium and narrow ramps but it is conceivable that for some specialized applications the WFPC2 will still be preferred.

### 4.3.1 Throughputs and Limiting Magnitudes

In Figure 4.9 below, we show the throughput of the two unfiltered ACS CCD cameras: WFC and HRC. Superposed on this plot, we show the unfiltered WFPC2 (WF4) and the clear STIS throughputs. In Figure 4.8 the ACS SBC system throughput is compared to that of the STIS FUV-MAMA.

Figure 4.9: ACS CCD System Throughputs Versus those of STIS and WFPC2



### 4.3.2 Limiting Magnitudes

In Table 4.6, we give the V magnitude, in the Johnson-Cousins system, reached for an A0V star during a one-hour integration (**CR-SPLIT=2**) which produces a signal-to-noise ratio of 10 integrated over the number of pixels needed to encircle ~80% of the PSF flux. More precisely, for the WFC a boxsize of 5x5 pixels was used (encircling 84% of the PSF flux), for the HRC, a 9x9 pixel boxsize (81% of flux) and for the SBC, a 15x15 pixel boxsize (80% of the flux). The last column gives the limiting magnitude assuming an optimally weighted PSF fit. The observations are assumed to take place in **LOW-SKY** conditions for the Zodiacal light and **SHADOW** of the Earthshine. Note that the assumed sky backgrounds are therefore much better than average conditions; these are best case limits.

Table 4.6: ACS limiting V magnitudes for A stars

ACS Camera	Filter	Magnitude	
		Aperture	PSF Fit
WFC	F606W	27.83	28.32
WFC	F814W	26.99	27.50
HRC	F330W	24.52	25.45
HRC	F606W	27.29	28.05
SBC	F125LP	23.55	24.35

### 4.3.3 Signal-To-Noise Ratios

In Chapter 10, we present, for each imaging mode, plots of exposure time versus magnitude to achieve a desired signal-to-noise ratio. These plots, which are referenced in the individual imaging-mode sections below, are useful for getting an idea of the exposure time you need to accomplish your scientific objectives. More accurate estimates will require the use of the ACS Exposure Time Calculator.

### 4.3.4 Saturation

Both CCD and SBC imaging observations are subject to saturation at high total accumulated counts per pixel: the CCDs, due either to the depth of the full well or to the 16 bit data format, and the SBC, due to the 16-bit format of the buffer memory (see Section 7.2.1 and Section 7.4.1). In Chapter 10, saturation levels as functions of source magnitude and exposure time are presented in the S/N plots for each imaging mode.

## 4.4 Wide Field Optical CCD Imaging

The Wide Field Channel of ACS was designed primarily for high throughput observations in the visible. The use of protected silver mirror coatings, the small number of reflections and the use of a red sensitive CCD have provided the high throughput required for this camera at the expense of a 3700 Å blue cutoff. The WFC detectors are two butted 2k by 4k thinned, backside-illuminated, SITe CCDs with a red optimized coating and long- $\lambda$  halo fix. The plate scale is 0.050 arcsecond per pixel which provides a good compromise between adequately sampling the PSF and a wide field of view. The WFC PSF is critically sampled at 11,600 Å and undersampled by a factor 3 at the blue end of the WFC sensitivity range (3700 Å). For well-dithered observations we expect that it will be possible to achieve a final reconstructed FWHM of  $\sim 0.070$  arcsec, i.e., a diffraction limited PSF at  $\sim 8100$  Å and longward. See Section 8.2 for more discussion of how to use dithered observations to optimally sample the PSF.

The optical design of the camera introduces a two-component geometric distortion. The detectors themselves are at an angle with respect to the optical axis. This produces an 8% stretching of one pixel diagonal compared to the other. As a result WFC pixels project on the sky as rhombuses rather than squares. This effect is purely geometrical and easy to correct if necessary. The second component of geometric distortion is more complex. This distortion causes up to  $\pm 9\%$  variation in effective pixel area and needs to be taken into account when doing accurate photometry or astrometry as the effective area of the detector pixels varies nonlinearly with field position.

### 4.4.1 Filter Set

#### WFPC2 and Johnson-Cousins filters

All of the most commonly used WFPC2 filters are included in the ACS filter set. In addition to a medium and a broad V band filter (F550M and F606W), there is a complete Johnson-Cousins *BVI* set (F435W, F555W, F814W).

#### Sloan Digital Sky Survey filters

The Sloan Digital Sky Survey (SDSS) *griz* filter set (F475W, F625W, F775W, F850LP) are designed to provide high throughput for the wavelengths of interest and excellent rejection of out-of-band wavelengths. They were designed to provide wide, non-overlapping filter bands that cover the entire range of CCD sensitivity from the near UV to near-IR wavelengths.

### Narrow Band filters

The H $\alpha$  (F658N), [OIII] (F502N), and [NII] (F660N) narrow band filters are full-size, and can be used with both WFC and HRC.

### Ramp filters

ACS includes a complete set of ramp filters which provide full coverage of the WFC wavelength range at 2% and 9% bandwidth. Each ramp filter consists of 3 segments. The inner and outer filter segments can be used with the WFC only, while the central segments can be used by both WFC and HRC. Unlike the WFPC2 where the desired wavelength is achieved by offsetting the telescope, the wavelength of ACS ramps is selected by rotating the filter while the target is positioned in one of the pre-defined apertures. The monochromatic field of view of the ramp filters is approximately 40" by 80". Details of how to use the ramp filters are given in Section 8.5.2.

### Polarizer filters

The WFC/HRC filter wheels contain polarizers with pass directions spaced by 60°, optimized for both the UV (POL0UV, POL60UV and POL120UV) and the visible (POL0V, POL60V and POL120V). All the polarizer filters are sized for the HRC field of view, so will induce vignetting when used with the WFC, where the FOV will be about 72" by 72". More information on the use of the polarizers is given in Chapter 5.

### Grism and Prism

The CCD channels also have a grism (G800L) for use with both WFC and HRC from 5500Å to 11,000Å, and a prism (PR200L) for use with the HRC from 1600Å to 3500Å. Again, these are described more fully in Chapter 5.

## 4.4.2 Long wavelength halo fix

The PSF of the STIS CCD is characterized by a significant halo at long wavelengths which is due to photons crossing the CCD and being reflected back in random directions by the front side of the CCD. The problem becomes noticeable beyond 8000Å because only long wavelength photons can transverse the CCD without being absorbed. The so-called halo fix for the WFC consists of a metallization of the front side of the CCD which essentially reflects photons back to the original pixel. Based on initial inflight results we do not expect that the long wavelength halo will be a serious problem for WFC observations (now confirmed inflight).



## 4.5 High-Resolution Optical and UV Imaging

The High Resolution Channel of ACS is the prime ACS camera for near-UV imaging. HRC provides high throughput in the blue and a better sampling of the PSF than either the WFC or other CCD cameras on HST. The HRC pixel size critically samples the PSF at  $6300\text{\AA}$  and is undersampled by a factor 3.0 at the blue end of its sensitivity range ( $2000\text{\AA}$ ). In this capability, HRC functionally replaces the Faint Object Camera as the instrument able to critically sample the PSF in the V band. For this reason, although we expect that most of the usage of HRC will be for UV and blue imaging, HRC can also be convenient for imaging in the red when the PSF sampling is important. As an example, better PSF sampling is probably important for accurate stellar photometry in crowded fields and we expect that the photometric accuracy achievable by the HRC will be higher than that achievable with the WFC. Well-dithered observations with the HRC should lead to a reconstructed PSF FWHM of 0.03 arcsec, i.e. diffraction limited at  $\sim 4200\text{\AA}$  and longward. HRC also includes a coronagraph that will be discussed in Chapter 5. The HRC CCD presents a long wavelength halo problem similar to the STIS CCD since the front-side metallization correcting the halo problem for the WFC CCDs was implemented only after the HRC CCD had been procured. Given that most of the HRC imaging is likely to occur in the UV and in the blue we do not expect this to represent a significant problem for observers.

### 4.5.1 Filter set

The HRC-specific filters are mostly UV and blue. The set includes UV and visible polarizers (discussed in Chapter 5), a prism (PR200L, discussed in Chapter 5), three medium-broad UV filters (F330W, F250W, and F220W) and two narrow band filters (F344N and F892N). Use of the UV filters with the WFC is not supported because of the uncertainty of the WFC silver coating transmission below  $4000\text{\AA}$ .

All broad, medium and narrow band WFC filters can be used with the HRC whenever a better PSF sampling is required. In general, where their sensitivity overlaps the throughput of WFC is higher than that of HRC. Only some of the WFC ramp filters can be used with the HRC since only the middle ramp segment overlaps with the HRC FOV. In particular, HRC can use the FR459M and FR914M broad ramps, and the FR505N [OIII], FR388N [OII] and FR656N ( $H\alpha$ ) narrow ramps.

### 4.5.2 Multiple electron events

Like the STIS CCD but unlike WFPC2, the HRC CCD is directly sensitive to UV photons and for this reason is much more effective in detecting them. However, whenever a detector has non-negligible sensitivity over more than a factor two in wavelength, it becomes energetically possible for a UV photon to generate more than one electron, and so be counted more than once. This effect has indeed been seen in STIS and also during the ground testing of the HRC detector. The effect is only important shortward of 3200Å, and reaches a magnitude of approximately  $1.7e^-/\text{photon}$  at 2000Å. Multiple counting of photons has to be taken into account when estimating the detector QE and the noise level of a UV observation, since multiple photons cause a distortion in the Poisson distribution of electrons.

### 4.5.3 Red leaks

When designing a UV filter, a high suppression of off-band transmission, particularly in the red, has to be traded with overall in-band transmission. The very high blue quantum efficiency of the HRC compared to WFPC2 makes it possible to obtain an overall red leak suppression comparable to that of the WFPC2 while using much higher transmission filters. The ratio of in-band versus total flux is given in Table 4.7 for a few UV and blue HRC filters, where the cutoff point between in-band and out-of-band flux is defined as the filter's 1% transmission point. The same ratio is also listed for the equivalent filters in WFPC2. Clearly, red leaks are not a problem for F330W, F435W, and F475W. Red leaks are more important for F250W and F220W. In particular, accurate UV photometry of objects with the spectrum of an M star will require correction for the redleak in F250W and will be essentially impossible in F220W. For the latter filter a redleak correction will also be necessary for K and G types.

Table 4.7: In-band Flux as a Percentage of the Total Flux

	WFPC2 F218W	HRC F220W	WFPC2 F255W	HRC F250W	WFPC2 F300W	HRC F330W	WFPC2 F439W	HRC F435W	WFPC2 F450W	HRC F475W
O5V	99.8	99.8	99.6	99.7	99.9	99.9	99.9	99.9	99.9	99.9
B1V	99.7	99.7	99.6	99.7	99.9	99.9	99.9	99.9	99.9	99.9
A1V	99.4	99.1	99.2	99.3	99.2	99.9	99.9	99.9	99.9	99.9
F0V	98.5	97.8	98.8	99.0	98.8	99.9	99.9	99.9	99.9	99.9
G2V	92.5	90.2	97.4	98.4	97.4	99.9	99.9	99.9	99.8	99.9
K0V	71.7	69.6	95.0	97.3	95.0	99.9	99.9	99.9	99.8	99.9
M2V	0.03	2.5	45.5	71.9	45.4	99.9	99.9	99.9	99.6	99.9

## 4.6 Ultraviolet Imaging with the SBC

The Solar Blind Channel is the ACS camera optimized for far-UV imaging. The SBC uses the same optical train as the HRC and is comparable in performance to the FUV MAMA of STIS.

### 4.6.1 Filter Set

Like the STIS FUV MAMA, the SBC includes a Lyman  $\alpha$  narrow band filter (F122M), and a long pass quartz filter (F150LP). The STIS FUV clear and  $\text{SrF}_2$  filters are functionally replaced by the SBC  $\text{MgF}_2$  (F115LP) and  $\text{CaF}_2$  (F125LP) respectively. The SBC also includes two additional long pass filters not available in STIS (F140LP and F165LP) as well as prisms (discussed in Chapter 5).

### 4.6.2 Bright-Object Limits

The bright object limits are discussed in detail in Section 7.5.

### 4.6.3 Optical Performance

The optical performance of the SBC is comparable to that of the STIS FUV-MAMA. The use of the repeller wire increases the quantum efficiency of the detector by  $\sim 30\%$  or so, but adds a halo to the PSF.

### 4.6.4 Red-leaks

The visible light rejection of the SBC is excellent, but users should be aware that stars of solar type or later will have a significant fraction of the detected flux coming from outside the nominal wavelength range of the detector. Details are given below, in Table 4.8.

Table 4.8: Visible-Light Rejection of the SBC F115LP Imaging Mode

Stellar Type	Percentage of all Detected Photons which have $\lambda < 1800 \text{ \AA}$	Percentage of all Detected Photons which have $\lambda < 3000 \text{ \AA}$
O5	99.5	100
B1 V	99.4	100
A0 V	98.1	100
G0 V	72.7	99.8
K0 V	35.1	94.4

## 4.7 ACS Point Spread Functions

The ACS point spread function has been studied in ground test measurements, using models generated by the **TinyTIM** software of J. Krist and R. Hook and measured in on-orbit data. As with other HST instruments, the ACS point spread function is affected by both optical aberrations and geometric distortions. Also, point sources imaged with WFC and HRC experience blurring due to charge diffusion into adjacent pixels because of CCD subpixel variations, which reduces the limiting magnitudes that can be reached by WFC/HRC. The SBC PSF and the long-wavelength HRC PSF are additionally affected by a halo produced by the detectors themselves.

### 4.7.1 CCD pixel response function

The sharpness of the CCD PSF is somewhat degraded by photoelectron diffusion into adjacent pixels. The effect is usually described in terms of the pixel response function (PRF), which gives the distribution of flux from within the pixel into adjacent pixels. To quantify the PRF of the ACS CCDs, measurements have been made using a pinhole mask with a hole diameter of 2  $\mu\text{m}$ . The obtained PRF indicates that charge diffusion results in  $\sim 0.5$  mag loss in the WFC limiting magnitude at short wavelengths (the worst case). At longer wavelengths and at all wavelengths for the HRC the reduction in the limiting magnitude is  $\sim 0.2$  mag or less. At different wavelengths, the CCD pixel response functions can be represented by the following kernels:

$$K_{HRC} = \begin{bmatrix} 0.02 & 0.06 & 0.02 \\ 0.06 & 0.68 & 0.06 \\ 0.02 & 0.06 & 0.02 \end{bmatrix}, \quad K_{WFC} = \begin{bmatrix} 0.025 & 0.09 & 0.025 \\ 0.09 & 0.545 & 0.09 \\ 0.025 & 0.09 & 0.025 \end{bmatrix}$$

at  $\lambda = 4000\text{\AA}$ ,

$$K_{HRC} = \begin{bmatrix} 0.0175 & 0.05 & 0.0175 \\ 0.05 & 0.73 & 0.05 \\ 0.0175 & 0.06 & 0.0175 \end{bmatrix}, \quad K_{WFC} = \begin{bmatrix} 0.02 & 0.085 & 0.02 \\ 0.085 & 0.575 & 0.085 \\ 0.02 & 0.09 & 0.02 \end{bmatrix}$$

at  $\lambda = 5500\text{\AA}$ , and

$$K_{HRC} = \begin{bmatrix} 0.015 & 0.06 & 0.015 \\ 0.02 & 0.86 & 0.02 \\ 0.015 & 0.02 & 0.015 \end{bmatrix}, \quad K_{WFC} = \begin{bmatrix} 0.015 & 0.055 & 0.015 \\ 0.055 & 0.72 & 0.055 \\ 0.015 & 0.055 & 0.015 \end{bmatrix}$$

at  $\lambda = 8000\text{\AA}$ .

#### 4.7.2 Model PSFs

Table 4.9 gives the WFC/HRC model PSF in the central 5×5 pixel region in two wavelength bands (filters). Numbers listed are the fraction of the total energy received in each pixel. The models have been generated using **TinyTIM**, taking into account the HST optical aberrations and obscurations as well as the CCD pixel response function. Field dependent geometrical distortions are not included. The real PSF will also differ from the model because of the jitter in the HST pointing, HST focus variation (focus breathing), and other instrumental effects, some of which are briefly discussed below.

Table 4.9: Model ACS PSFs

WFC model PSF, filter F435W					WFC model PSF, filter F814W				
0.00	0.01	0.01	0.01	0.00	0.01	0.02	0.01	0.01	0.01
0.01	0.04	0.08	0.04	0.01	0.02	0.03	0.07	0.03	0.01
0.01	0.08	0.26	0.08	0.01	0.01	0.07	0.21	0.07	0.01
0.01	0.04	0.08	0.03	0.01	0.01	0.03	0.07	0.03	0.01
0.00	0.01	0.01	0.00	0.01	0.01	0.02	0.01	0.01	0.01
HRC model PSF, filter F435W					HRC model PSF, filter F814W				
0.01	0.01	0.01	0.01	0.01	0.00	0.01	0.02	0.01	0.00
0.02	0.03	0.06	0.03	0.01	0.01	0.04	0.05	0.04	0.01
0.01	0.06	0.16	0.06	0.01	0.02	0.05	0.08	0.05	0.02
0.01	0.03	0.07	0.03	0.01	0.01	0.04	0.05	0.04	0.01
0.01	0.02	0.01	0.01	0.01	0.00	0.01	0.02	0.01	0.00

As described in Section 4.4.2, long wavelength photons that are not readily absorbed in the thinned silicon CCD can be scattered by the glass material backing the CCD and detected as a broad halo surrounding a point source image. While a special reflective layer has been added to the WFC CCDs to ameliorate this effect, the HRC CCD was delivered before this anti-halation process was developed. Hence, at  $8000\text{\AA}$ , about 10% of the total flux detected from a point source in the HRC will be scattered from the image core into a broad halo roughly described by an exponential decay with  $1/e$  width of about 40 pixel. At 1 micron, where the silicon is more transparent, the fraction of light in the halo increases to about 30%; the effect is negligible below about  $7000\text{\AA}$ .

The SBC MAMA detector is also subject to a halation effect, due to the migration of photo-electrons created at the MicroChannel Plate surface from their creation site to neighboring microchannels. This effect, originally observed in STIS FUV-MAMA images, broadens the core and near wings of the PSF and also redistributes a small portion of the flux into a broad halo approximated by a gaussian with FWHM of  $\sim 20$  pixels. The peak flux for a point source centered on a pixel is reduced by 30% to 40%, depending on wavelength. The SBC PSF with the halation effect taken into account is shown in Table 4.10.

Table 4.10: Model ACS SBC PSFs

SBC PSF at 120 nm					SBC PSF at 160 nm				
<0.01	0.01	0.01	0.01	<0.01	<0.01	<0.01	<0.01	<0.01	<0.01
0.01	0.02	0.03	0.02	0.01	<0.01	0.02	0.04	0.02	<0.01
0.01	0.03	0.15	0.03	0.01	<0.01	0.04	0.20	0.04	<0.01
0.01	0.02	0.03	0.02	0.01	<0.01	0.02	0.04	0.02	<0.01
<0.01	0.01	0.01	0.01	<0.01	<0.01	<0.01	<0.01	<0.01	<0.01

### 4.7.3 Encircled Energy

The displayed encircled energy distribution within the channel's aperture (Figure 4.10) is from the PSF models generated by **TinyTIM**. The models take into account the CCD's pixel response function (for WFC and HRC) as well as optical aberrations produced by the HST optics. The model PSFs have been found to be quite consistent with the PSF measurements in ground tests. In general, the ACS channels encircled energy distribution has been found to be within the original instrument specifications. Figure 4.11 shows the encircled energy fraction for the SBC generated from data acquired during the servicing mission orbital verification.

Figure 4.10: Encircled energy for the CCD channels

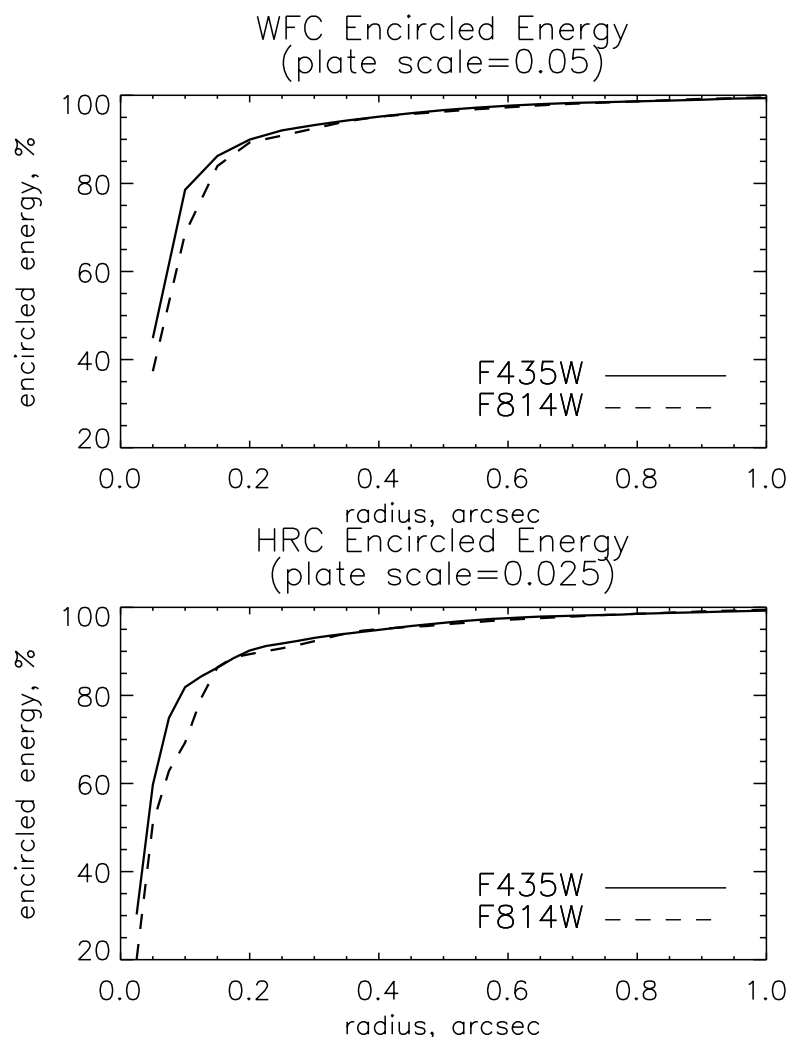
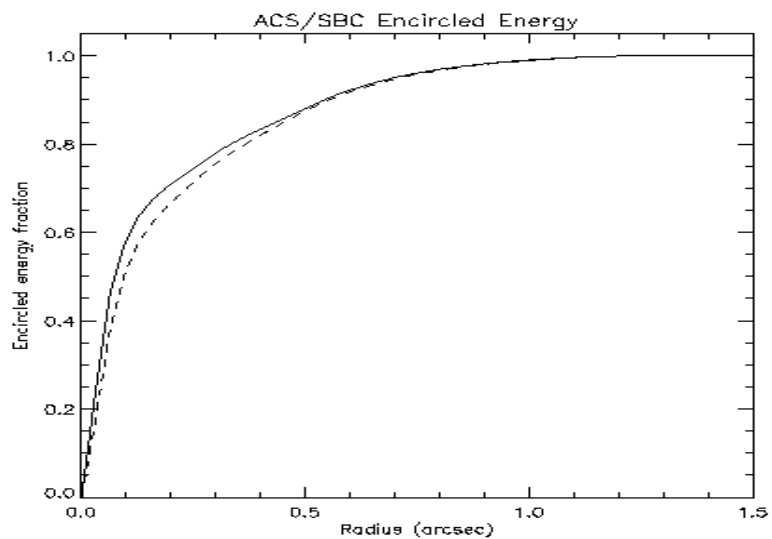


Figure 4.11: Encircled energy for the SBC



#### 4.7.4 Geometric Distortions

Geometric distortions will produce a significant impact on the shape of the PSF in all three of the ACS channels, as can readily be seen in Figure 4.12 and Figure 4.13, which display model WFC and HRC PSF images over  $\sim 3$  arcsec fields at  $8000 \text{ \AA}$ . The log stretch enhances the spider diffraction patterns, which the distortion renders non-perpendicular, and the outer Airy rings, which appear elliptical. The distortion owes primarily to the tilt of the focal surface to the chief ray at the large OTA field angles of the ACS apertures. The linear, field-independent, approximation for the WFC produces a difference in plate scale of about 8% between the two diagonals of the field and, in the HRC and SBC, about a 16.5% difference in scale between orthogonal directions rotated about 20 degrees from the aperture edges. Field-dependent distortions, measured as actual vs. predicted distances from field center, amount to about 2% peak in the WFC and about 1% in the HRC and SBC.

The distortions render the pixels, as projected on the sky, trapezoidal in shape and their area varies over the field by about 19% and 3.5% in the WFC and HRC/SBC, respectively. These variations have significant ramifications concerning appropriate techniques for flat-fielding and photometric calibration, especially when complicated by resampling in order to combine dithered image sets. A related issue is the manner in which the halation effects of the HRC and SBC detectors are removed and the treatment of spectra from the prisms and grism, which are not subject to the same distortion effects.

More details concerning geometric distortions in ACS can be found in “Distortion in the ACS” on page 234. A brief introduction to CALACS and **PyDrizzle** which apply corrections for geometric distortion are in Chapter 12.

#### 4.7.5 PSF at Extreme Red Wavelengths and the UV

The PSF in the far red with the WFC exhibits a characteristic shape in the far wings as shown in an F850LP image in Figure 4.13. In particular a linear feature may be seen along rows to the left of stellar sources, the field of view displayed in FIG is  $128 \times 128$  pixels, or 6.4 arcseconds. At 10 pixels to the left of stellar center the residual intensity is about 1% and at 20 pixels about 0.2%. These values are about a factor of 5 higher than intensities along diffraction spikes in the other directions. The effect is only noticeable for observations at wavelengths beyond  $9000 \text{ \AA}$ , e.g. the F814W filter is virtually free of this effect while it is seen in F850LP and ramp filter observations in the far red.

The HRC images above show that HRC exhibits a slight tail in the F220W image (left), which is not present in F435W image (center) and the F814W image (right). Only the near-UV images (F220W, F250W and F330W) exhibit this tail which is due to minor levels of a few low-order aberrations.



### 4.7.6 Residual Aberrations

The PSF quality has been optimized on-orbit to minimize the residual coma and defocus at the center of the WFC and HRC/SBC fields. The optical design introduces almost no other low-order aberrations at the field center, but at field positions away from the center of the WFC field there are small amounts of residual defocus, coma and astigmatism. Optical modelling predicts that the amplitude of these aberrations should amount to no more than a few hundredths of a wave at  $5000\text{\AA}$  and observations confirm that field dependencies of the PSF for the ACS cameras are low.

Figure 4.12: ACS WFC PSF - Model

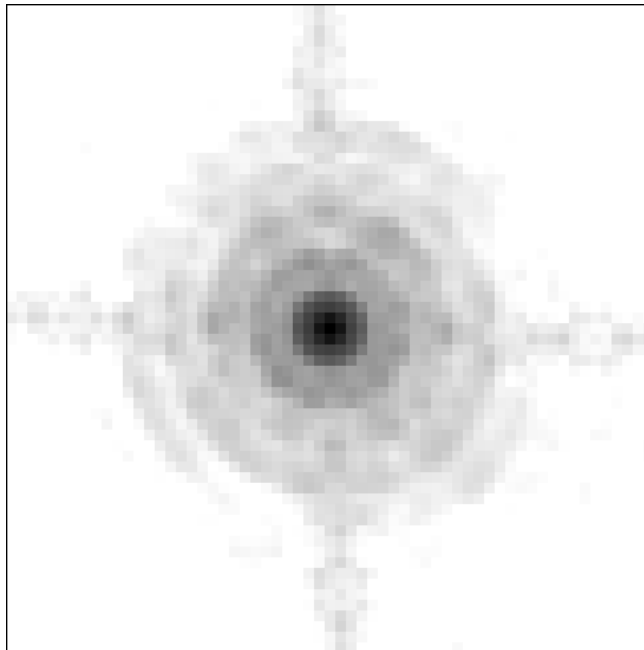


Figure 4.13: ACS HRC PSF - Model

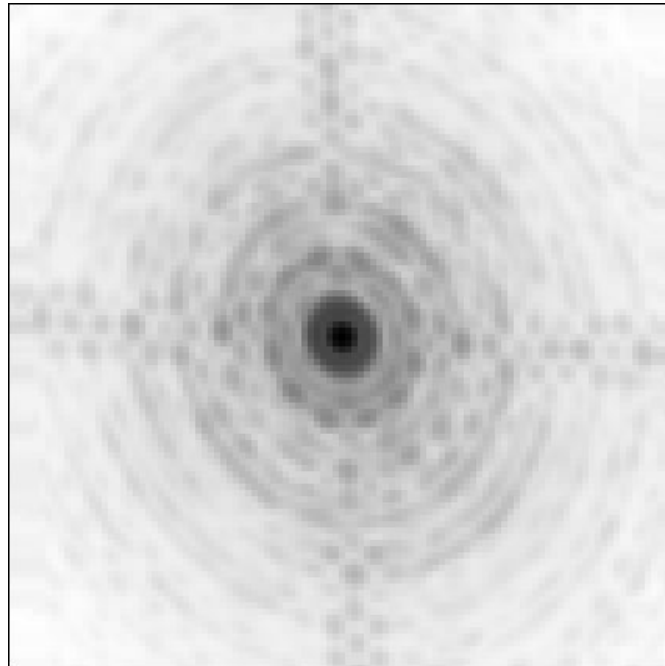


Figure 4.14: ACS WFC PSF in F850LP

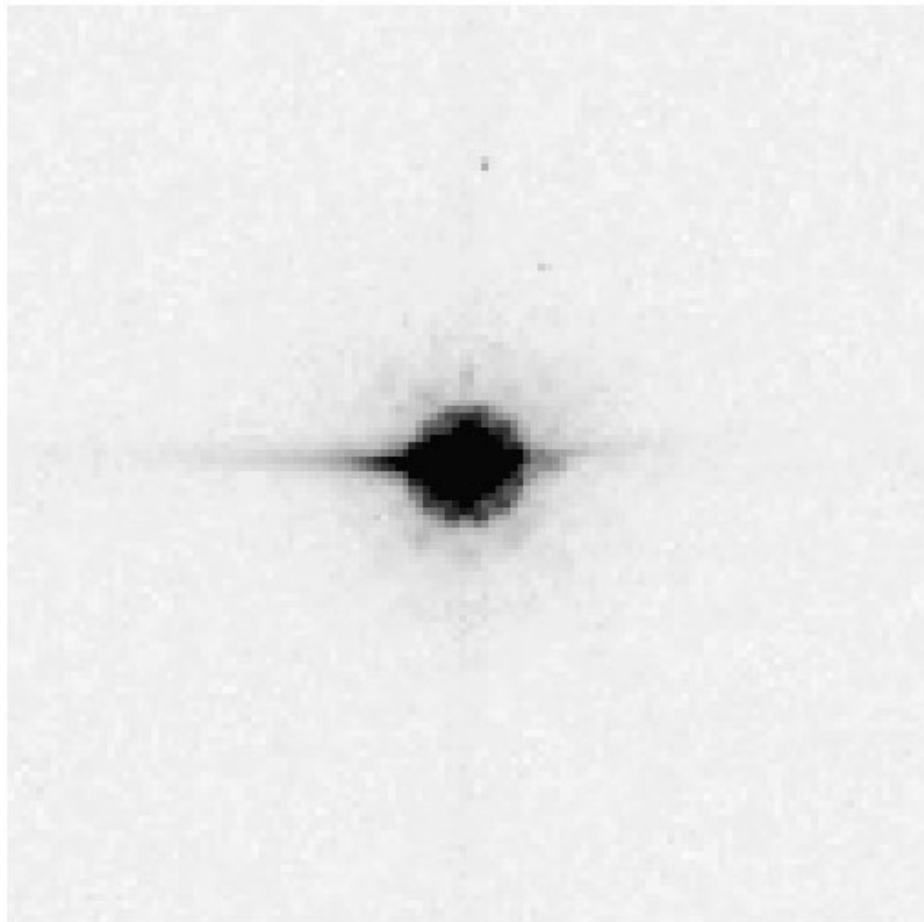
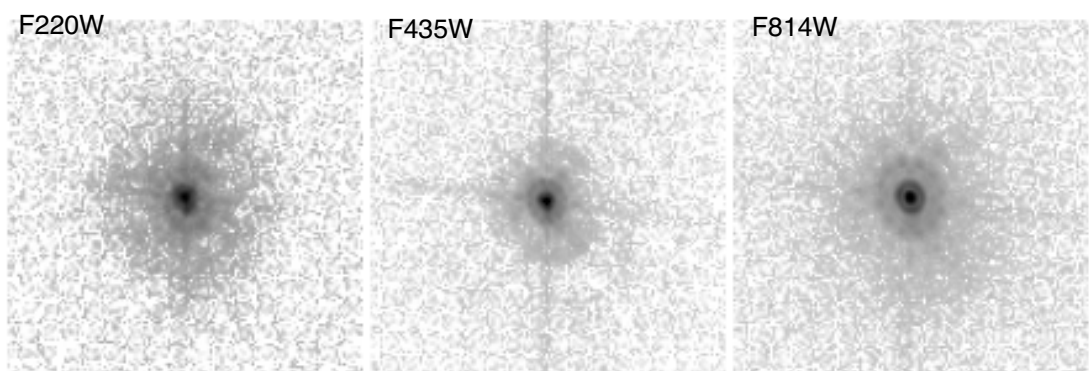


Figure 4.15: ACS HRC PSFs





CHAPTER 5:

# Polarimetry, Coronagraphy and Prism/Grism Spectroscopy

In this chapter. . .

5.1 Polarimetry / 63 5.2 Coronagraphy / 68 5.3 Grism/Prism Spectroscopy / 86
--

In this chapter we provide an overview of the special observing capabilities offered by ACS. These capabilities are optical and near-UV imaging polarimetry, coronagraphy with an aberrated beam coronagraph and low resolution ( $R \sim 100$ ) optical and near-UV spectroscopy.

---

## 5.1 Polarimetry

The Advanced Camera has a straightforward, robust imaging polarimetric capability. Polarization observations require a minimum of three images taken using polarizing optics with different polarization characteristics in order to solve for the source polarization unknowns (polarization degree, position angle and total intensity). To do this, ACS offers two sets of polarizers, one optimized for the blue (POLUV) and the

other for the red (POLVIS). These polarizers can be used in combination with most of the ACS filters (see Table 5.1) allowing polarization data to be obtained in both the continuum and in line emission; and to perform rudimentary spectropolarimetry by using the polarizers in conjunction with the dispersing elements. Due to the large number of possibilities in combination with ramp and dispersing elements, and heavy calibration overheads, observers wishing to use those modes should request additional calibration observations. For normal imaging polarization observations, the target remains essentially at rest on the detector with a suitable filter in beam, and an image is obtained with each of the appropriate polarizing elements in turn. The intensity changes between the resulting images provide the polarization information.

Each set of polarizers comprises three individual polarizing filters with relative position angles  $0^\circ$ ,  $60^\circ$  and  $120^\circ$ . The polarizers are designed as aplanatic optical elements and are coated with “Polacoat 105UV” for the blue optimized set and HN32 polaroid for the red set. The blue/near-UV optimized set is also effective all through the visible region, giving a useful operational range from approximately  $2000\text{\AA}$  to  $8500\text{\AA}$ . The second set is optimized for the visible region of the spectrum and is fully effective from  $4000\text{\AA}$  to about  $7500\text{\AA}$ .

The relative performance of the UV-optimized versus the visible optimized polarizers is shown in Figure 5.1. The visible polarizers clearly provide superior rejection for science in the  $4000\text{--}7500\text{\AA}$  bandpass, while the UV optimized coatings deliver lower overall rejection across a wider range into the near-UV,  $2000\text{--}7500\text{\AA}$ . While performance of the polarizers begins to degrade at wavelengths longer than about  $7500\text{\AA}$ , useful observations should still be achievable to approximately  $8500\text{\AA}$  in the red. In this case, allowance for imperfect rejection of orthogonally polarized light should be made at the analysis stage.

A further caveat is that imperfections in the flat fields of the POLVIS polarizer set have been found which may limit the optimal field of view somewhat. Potential users are encouraged to check the STScI ACS web site for the latest information.

In normal use across most of the wavelength range, the ACS polarizers should serve as three essentially perfect polarizers. The Stokes parameters (I, Q, U) in the most straightforward case of three images obtained with three perfect polarizers at  $60^\circ$  relative orientation, can be computed using simple arithmetic.

Using  $im1$ ,  $im2$ , and  $im3$  to represent the images taken through the polarizers POL0, POL60, and POL120 respectively, the Stokes parameters are as follows:

$$Q = \frac{2}{3}(2im1 - im2 - im3)$$

$$U = \frac{2}{\sqrt{3}}(im3 - im2)$$

$$I = \frac{2}{3}(im1 + im2 + im3)$$

These values can be converted to the degree of polarization  $P$  and the polarization angle  $\theta$ , measured counterclockwise from the  $x$  axis as follows:

$$P = \frac{\sqrt{Q^2 + U^2}}{I}$$

$$\theta = \frac{1}{2}\tan^{-1}(U/Q)$$

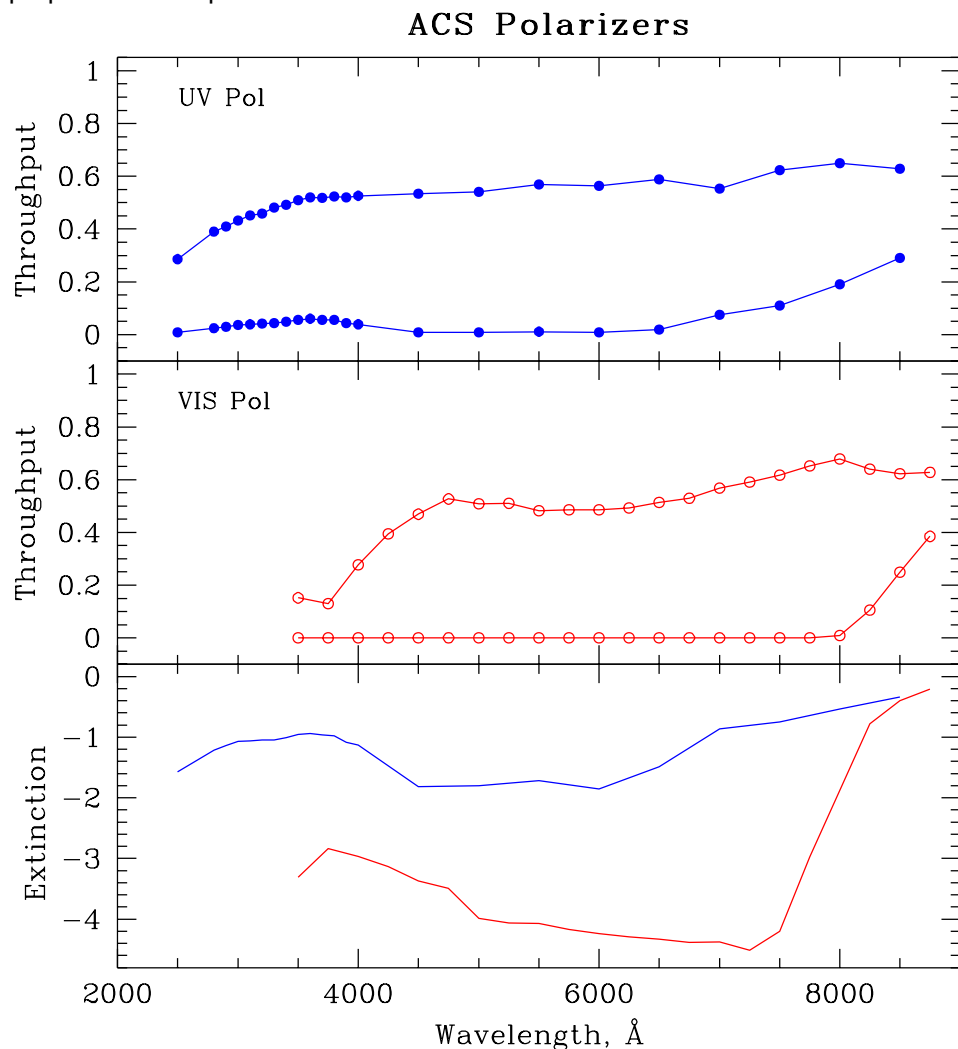
A more detailed analysis, including allowance for imperfections in the polarizers may be found in Sparks & Axon 1999 *PASP*, **111**, 1298. They find that the important parameter in experiment design is the product of expected polarization degree and signal-to-noise. A good approximation for the case of three perfect polarizers oriented at the optimal  $60^\circ$  relative position angles (as in ACS) is that the error on the polarization degree  $P$  (which lies in the range 0 for unpolarized to 1 for fully polarized) is just the inverse of the signal-to-noise per image. Specifically, they found

$$\log\left(\frac{\sigma_P}{P}\right) = -0.102 - 0.9898\log(P\langle S/N \rangle_i)$$

where  $\langle S/N \rangle_i$  is the signal to noise of the  $i$ th image; and

$$\log \sigma_\theta = 1.514 - 1.068\log(P\langle S/N \rangle_i)$$

Figure 5.1: Throughput and rejection of the ACS Polarizers. In the top two boxes, the upper curve is the parallel transmission, while the lower curve is the perpendicular transmission. The bottom panel shows the logarithm of the ratio of perpendicular to parallel transmission



The implementation of the ACS polarizers is designed for ease of use. Once a target has been acquired a polarimetric observation may be made by crossing each of the three polarimetric elements with the selected filter in turn. Polarizer specific apertures have been provided, so that the target remains at approximately the same location in the field of view for each of the three observations. The use of polarizer-specific apertures, which are selected automatically by the ground system, in addition to removing image shifts, allows selection of a clear location in the presence of flat-field irregularities.

Since the ACS near-UV and visible filter complement is split between two filter wheels, there are restrictions on which filters the polarizer sets can be combined with. The choices available were determined by the

relative performance of the polarizers and the near-UV limitations of the WFC resulting from the silver mirror coatings.

The near-UV optimized polarizers are mounted on Filter Wheel 1 and may be crossed with the near-UV filter complement, which are mounted on Filter Wheel 2. The visible optimized polarizers are mounted on Filter Wheel 2 and can be crossed with filters on Filter Wheel 1, namely the primary broadband filters, and discrete narrowband filters  $H\alpha$ , [OII] and their continuum filters. Due to the calibration overhead required, it is not planned to support the use of ramp filters with the UV polarizer set. GOs are, therefore, required to include calibration observations, if they plan to use the ramp filters with the UV polarizer set.

The polarizer sets are designed for use on the HRC where they offer a full unvignetted field of view,  $29\times 26$  arcsec with any of the allowable filter and coronagraph combinations including those ramps and spectroscopic elements that may also be used on the HRC (although see above re. additional calibrations). The same allowable combinations, either UV or visible optimized, may also be used on the WFC where an unvignetted field of view of diameter 70 arcsec is obtained. This does not fill the field of view of the WFC due to the small size of the polarizing filters. However it does offer an areal field approximately five times larger than that obtained on the HRC.

Table 5.1: Filters that can be used in conjunction with the ACS Polarizers

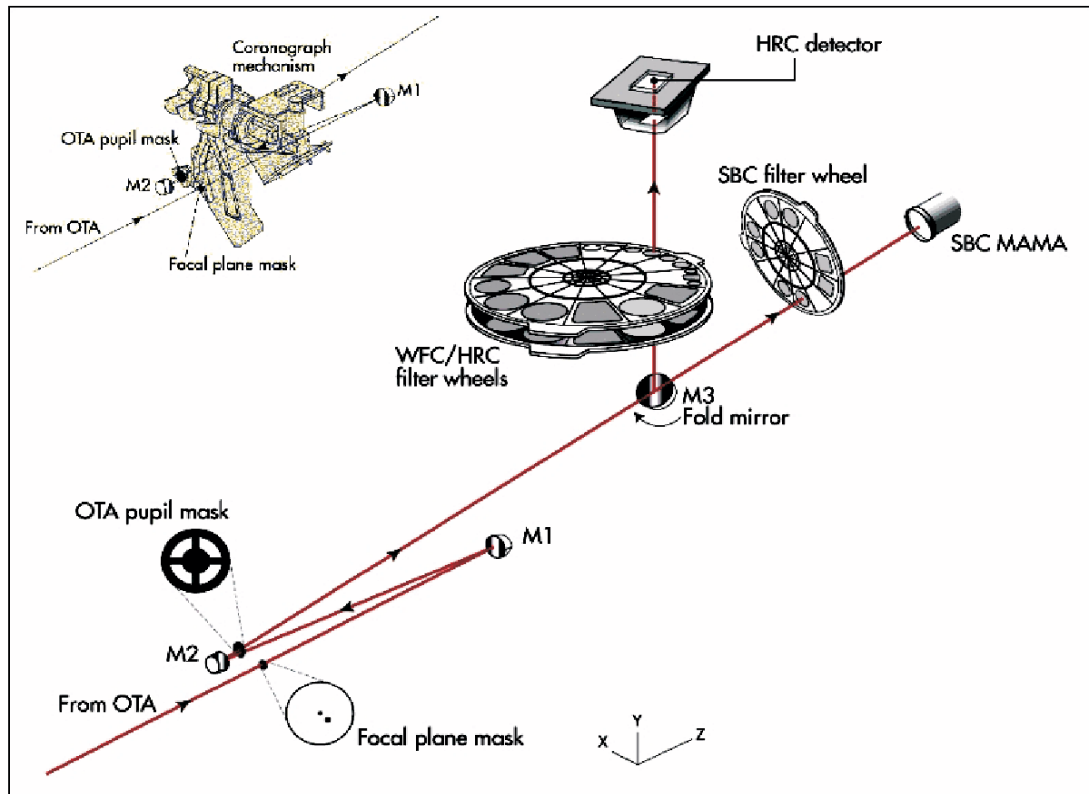
Polarizer set	Filters	Filter Comments
POL0UV	F220W	HRC NUV short
POL60UV	F250W	HRC NUV long
POL120UV	F330W	HRC U
	F435W	Johnson B
	F814W	broad I
POL0V	F475W	SDSS g
POL60V	F606W	Johnson V
POL120V	F625W	SDSS r
	F658N	$H\alpha$
	F775W	SDSS i

The filters specified in Table 5.1 are those that we expect users to choose for their polarization observations. We will calibrate the most popular of these filters. Filter combinations not on this list will most probably not be calibrated, so potential users who have a strong need for such a polarizer/filter combination should include any necessary calibrations themselves.

## 5.2 Coronagraphy

The ACS High Resolution Camera (HRC) has a user-selectable coronagraphic mode for the imaging of faint objects (circumstellar disks, substellar companions) near bright point sources (stars or luminous quasar nuclei). The coronagraph suppresses the diffracted light (diffraction spikes and rings) of the central source to below the level of the scattered light, most of which is caused by surface errors in the HST optics. The coronagraph was added after ACS construction began, at which point it was impossible to insert it into the aberration-corrected beam. Instead, the system is used in the aberrated beam, which is corrected after the coronagraph. While not as efficient as a corrected-beam coronagraph, especially for imaging close to the central source, it does provide a significant improvement to the high-contrast imaging capabilities of HST. Care must be taken, however, to design an observation plan that properly optimizes the coronagraph's capabilities and accounts for its limitations.

Figure 5.2: Schematic layout of the ACS HRC coronagraph. The upper left inset shows a schematic of the coronagraph mechanism that can be flipped in-and-out of the HRC optical path.



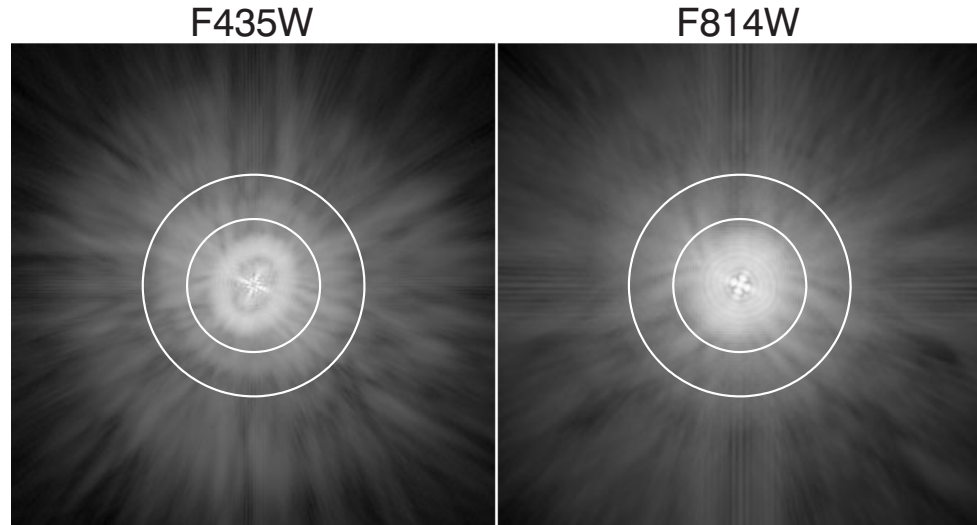


### 5.2.1 Coronagraph Design

A schematic layout of the ACS coronagraph is shown in Figure 5.2. The aberrated beam from the telescope first encounters one of two occulting spots. The beam continues to the M1 mirror, which forms an image of the HST entrance pupil on the M2 mirror, which corrects for the spherical aberration in the HST primary mirror. The coronagraph's Lyot stop is placed in front of M2. A fold mirror directs the beam onto the CCD detector. The field is 29" by 26" with a mean scale of 0.026"/pixel (geometric distortion results in effectively non-square pixels). The coronagraph can be used over the entire HRC wavelength range of  $\lambda=200\text{--}1000\text{ nm}$  using a variety of broad-to-narrowband filters.

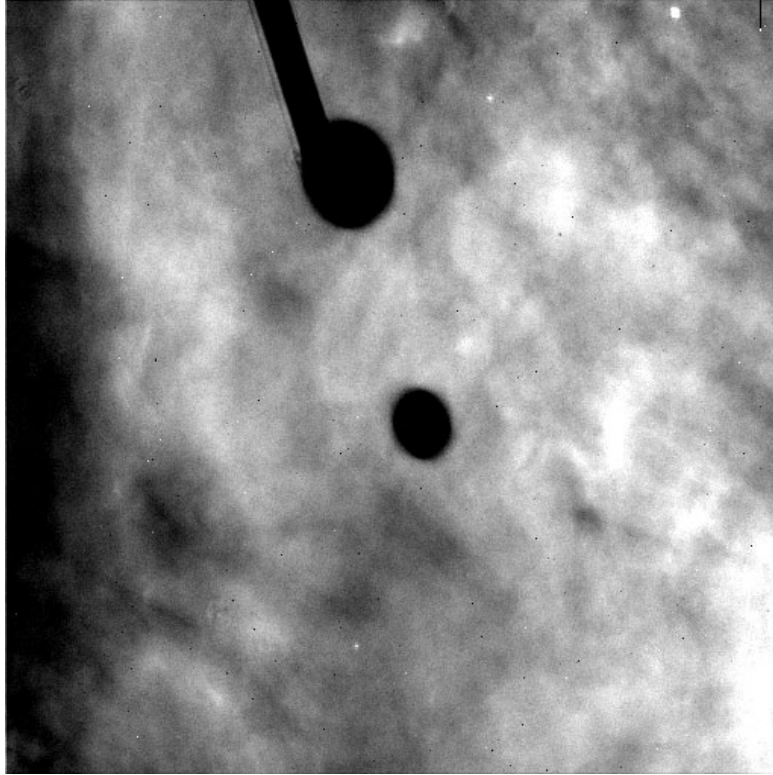
The occulting spots are placed in the plane of the circle of least confusion, near where the unaberrated HST focal plane would be. At this location the balance of defocus and spherical aberration provides a good compromise between maximal occulted flux and minimal spot radius. The angular extent of the PSF in this plane necessitates larger spots than would be used in an unaberrated system (Figure 5.3). The ACS spots are solid (unapodized) metallic coatings deposited on a glass substrate (which reduces throughput by 4.5%). The smaller spot is 1.8" in diameter and is at the center of the field. It is selected with the aperture CORON-1.8. A 3.0" diameter spot is near a corner (Figure 5.4) and is designated CORON-3.0. The smaller spot is used for the majority of the coronagraphic observations, as it allows imaging closer to the central source. The larger one may be used for very deep imaging of bright targets with less saturation around the spot edge than would occur with the smaller spot. Its position at the edge of the field also allows imaging of material out to 20" from the central source. The Lyot stop is located just in front of the M2 aberration correction mirror, where an image of the HST primary is formed. The stop is a thin metal mask that covers all of the diffracting edges in the HST system at the reimaged pupil (outer aperture, secondary mirror baffle, secondary mirror support vanes, and primary mirror support pads). The sizes of the stop and occulting spots were chosen to reduce the diffracted light below the level of the scattered light, which is unaltered by the coronagraph. The stop reduces the throughput by 48%, and it broadens the field PSF due to the smaller aperture and larger central obscuration relative to the beam diameter. The spots and Lyot stop are located on a panel attached to the ACS calibration door mechanism, which allows them to be flipped out of the beam when not in use. The inside surface of this door can be illuminated by a lamp to provide flat field calibration images for direct-mode imaging. However, the arrangement prevents the acquisition of internal flat fields in coronagraphic mode.

Figure 5.3: Computed point spread functions at the plane of the occulting spots through filters F435W and F814W. The elliptical, cross-shaped patterns in the cores are due to astigmatism at the off-axis location of the ACS aperture. It is corrected later by the ACS optics. The sizes of the two occulting spots ( $D=1.8''$  and  $3.0''$ ) are indicated. Logarithmic intensity scaled.



In addition to the combination of the occulting spots and Lyot stop that comprise the coronagraph, there is a  $0.8''$  wide,  $5''$  long occulting finger (OCCULT-0.8) permanently located at the window of the CCD dewar. It does not provide any suppression of diffracted light because it occurs after the Lyot stop. It was to be used to image closer to stars than is possible with the occulting spots while preventing saturation of the detector. However, because the finger is located some distance from the image plane, there is significant vignetting around its edges, reducing its effectiveness. Originally aligned to cover the central portion of the  $3.0''$  spot, shifting of the spots relative to the beam during launch now places the finger along that spot's edge. Because of vignetting and the sensitivity of the PSF wings to the centering of the star, unocculted, saturated observations of sources will likely be more effective than using the occulting finger.

Figure 5.4: Region of the Orion Nebula observed with the coronagraph in filter F606W. The silhouettes of the occulters can be seen superposed against the background nebulosity. The 1.8" spot is located at the center and the 3.0" spot towards the top. The finger is aligned along one edge of the larger spot. This image has not been geometrically corrected, so the spots appear elliptical.



### 5.2.2 Acquisition procedure and pointing accuracy

The central source must be placed precisely behind the occulting spot to ensure the proper suppression of the diffracted light. The absolute pointing accuracy of HST is about 1", too crude to ensure accurate positioning. An on-board acquisition procedure, borrowed from the STIS coronagraph, is used to provide better alignment. The observer must request an acquisition image immediately before using the coronagraph and must specify a combination of filter and exposure time that provides an unsaturated image of the source. An acquisition image is taken by specifying **HRC-ACQ** as the aperture and **ACQ** as the opmode in the RPS2 proposal file. A "campaign" acquisition mode will likely be made available for Cycle 12 (see Section 5.2).

During acquisition the unocculted star is imaged within a predefined 200 by 200 pixel subarray. To prevent saturation of the CCD, narrowband or crossed filters may be used for bright sources. Allowable filter combinations are F220W+F606W, F220W+F550M, and F220W+F502N, in order of decreasing throughput. Two exposures are taken and the

minimum value for each pixel is computed to avoid contamination by cosmic rays. The subarray is then boxcar-smoothed with a 3 by 3 pixel box (or 5 by 5 if crossed filters are used, which introduce a small amount of defocus). The maximum value is identified and the moment-of-mass centroid around that pixel is calculated. The telescope is then commanded by the ACS computer to slew the star to the location of the specified occulting spot. All of this happens on-board during an acquisition sequence without any additional intervention from the observer.

Initial results from multiple on-orbit observations indicate that the combined acquisition and slew errors are on the order of  $\pm 0.25$  pixels ( $\pm 6$  mas). While small, these shifts necessitate the use of subpixel registration techniques to subtract one coronagraphic PSF from another (Section 5.2.5). The position of the spots relative to the detector also varies by about  $\pm 0.25$  pixels every time the masks are inserted into the beam. This further alters the PSF, resulting in subtraction residuals. The “campaign” acquisition and observation sequence may reduce this problem (Section 5.2).

### 5.2.3 Vignetting and flat fields

The large angular extent of the aberrated PSF results in significant vignetting of objects at considerable distances around the occulters’ edges. One can visualize this as the convolution of the spots with the PSFs shown in Figure 5.3. The effects of vignetting can be seen directly in the images of the Orion Nebula (Figure 5.4). Vignetting is corrected by dividing out the flat field response of the system (Figure 5.5).

The normal HRC flat fields cannot be used to correct coronagraphic data. Besides the regions around the spots, there are large variations in the illumination pattern across the field due to the Lyot stop. Coronagraphic flats were taken during ground tests using an externally illuminated source and have been modified for application to on-orbit data (the spots shifted by about  $1''$  during launch). As of the time of writing, coronagraphic flats were being generated for the calibration pipeline. Contact STScI to find out the status of the flats in the pipeline.

Figure 5.5: (Left) Region of the Orion Nebula around the  $D=1.8''$  spot. The spot edge appears blurred due to vignetting. The image has not been geometrically corrected. (Right) The same region after the image has been corrected by dividing the flat field. The interior of the spot has been masked.

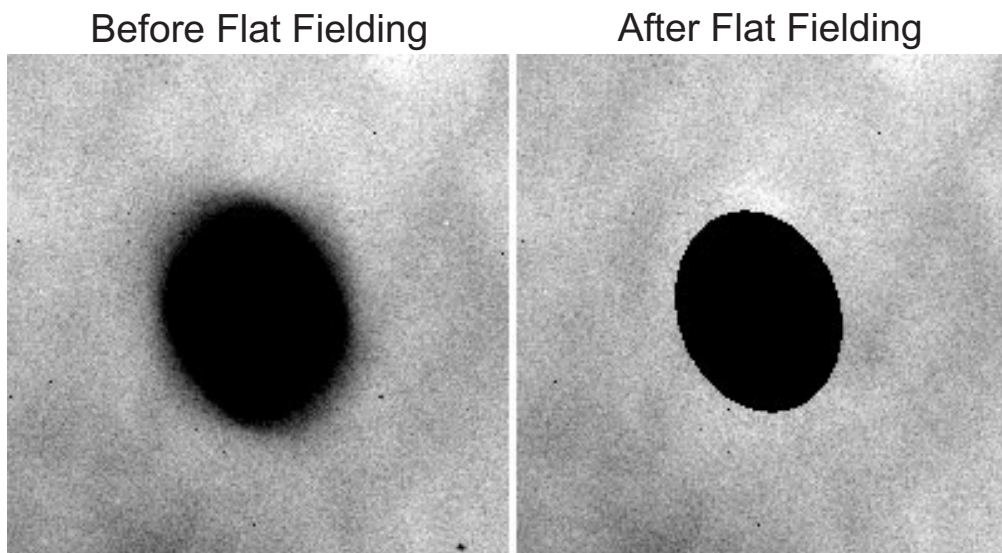
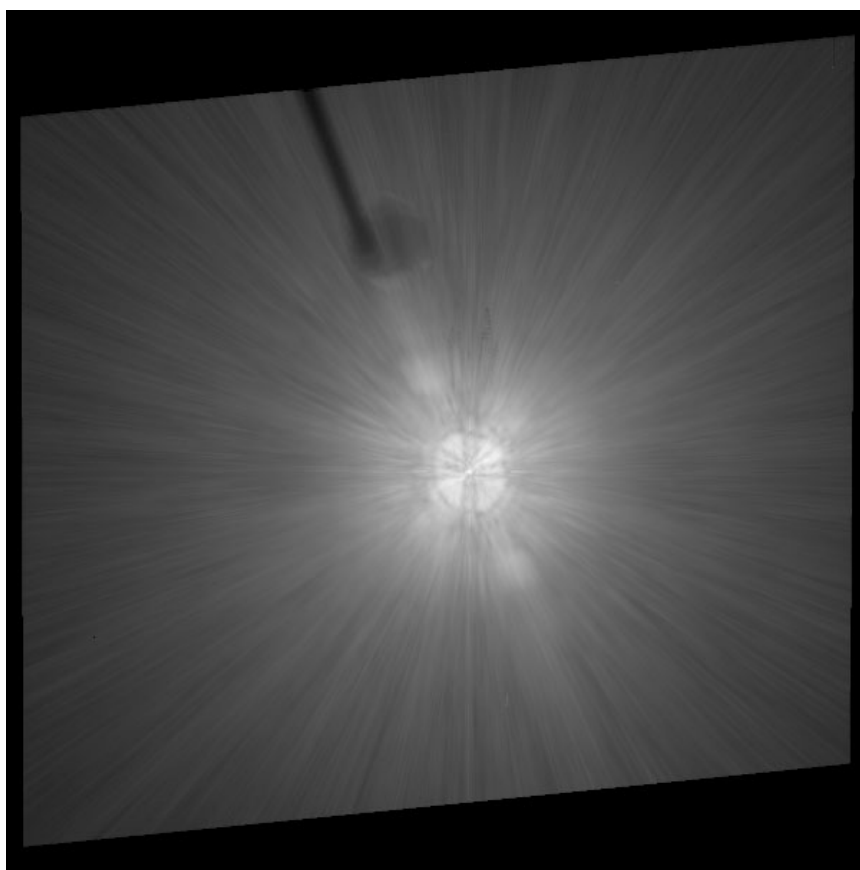


Figure 5.6: Geometrically corrected ( $29''$  across) image of Arcturus observed in F814W behind the  $1.8''$  spot. This is a composite of short, medium, and long (280s) exposures. The “bar” can be seen extending from the upper left to lower right. The shadows of the occulting finger and large spot can be seen against the scattered light background. Logarithmic intensity scale.



### 5.2.4 Coronagraphic Performance

Early in Cycle 11 coronagraphic performance verification images were taken of the  $V=0$  star Arcturus (Figures 5.6 & 5.7). This star has an angular diameter of 25 mas and is thus unresolved by the coronagraph. The coronagraphic image of a star is quite unusual. Rather than appearing as a dark hole surrounded by residual light, as would be the case in an aberration-free coronagraph, the interior of the spot is filled with a diminished and somewhat distorted image of the central source. This is due to correction by the M2 mirror of aberrated light from the star that is not blocked by the spot. The small spot is filled with light, while the large one is relatively dark. Broad, ring-like structures surround the spots, extending their apparent radii by about  $0.5''$ . These are due to diffraction in the wings of the aberrated PSF by the occulting spot itself. A consequence of these features is that stars may saturate the interior and edges of the spot within a short time. Within the small spot, the brightest pixels can become saturated in less than one second for a  $V=0.0$  star, while pixels at edge of the larger spot will saturate in about 14 seconds.

The measured radial surface brightness profiles (Figure 5.7) show that the coronagraph is well aligned and operating as expected. The light diffracted by the HST obscurations is suppressed below the level of the scattered light – there are no prominent diffraction spikes, rings, or ghosts beyond the immediate proximities of the spots. At longer wavelengths ( $\lambda > 600$  nm) the diffraction spikes appear about as bright as the residual scattered light (at longer wavelengths, the diffraction pattern is larger and therefore not as well suppressed by the coronagraph). The spikes are more prominent in images with the large spot than the small one. This can be explained by the fact that the Lyot stop is not located exactly in the pupil plane but is instead slightly ahead of it, so the beam can “walk” around the stop depending on the field angle of the object. Because the large spot is at the edge of the field, the beam is slightly shifted, allowing more diffracted light to pass around the mask edges.

The residual background is dominated by radial streaks that are caused primarily by scattering from zonal surface errors in the HST mirrors. This halo increases in brightness and decreases in size towards shorter wavelengths. One unexpected feature is a diagonal streak or “bar” seen in both direct and occulted star images. It is about 5x brighter than the mean azimuthal surface brightness in the coronagraphic images. This structure was not seen in the ground-test images and is likely due to scattering introduced by the HST optics. There appears to be a corresponding feature in STIS as well.

Figure 5.7: Regions around the occulting spots in different filters. The occulting finger can be seen in the 3" spot images. Logarithmic intensity scaled.

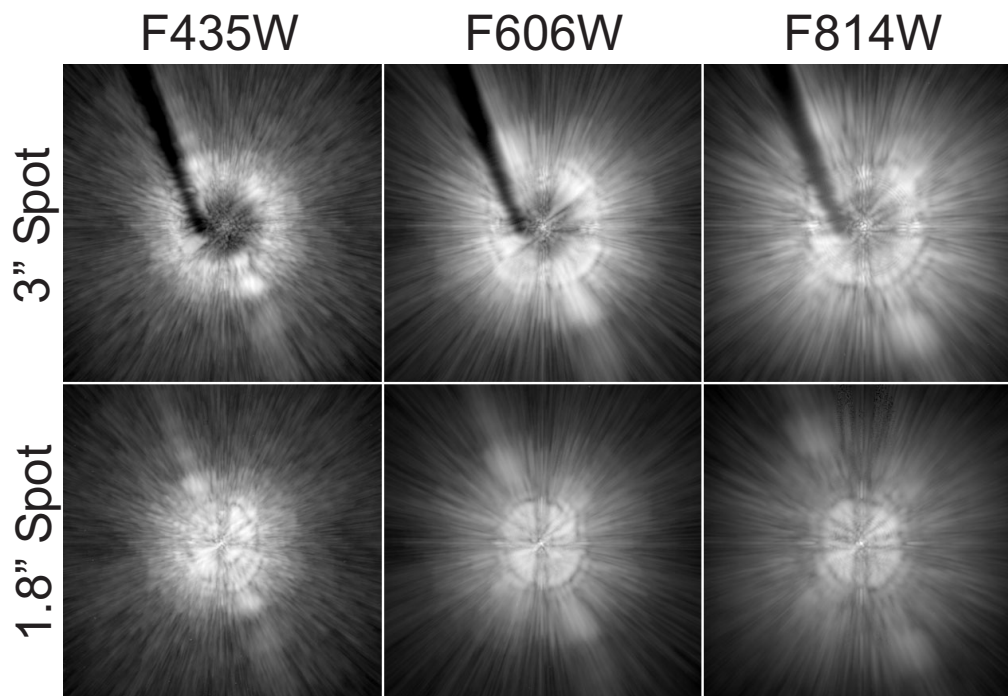
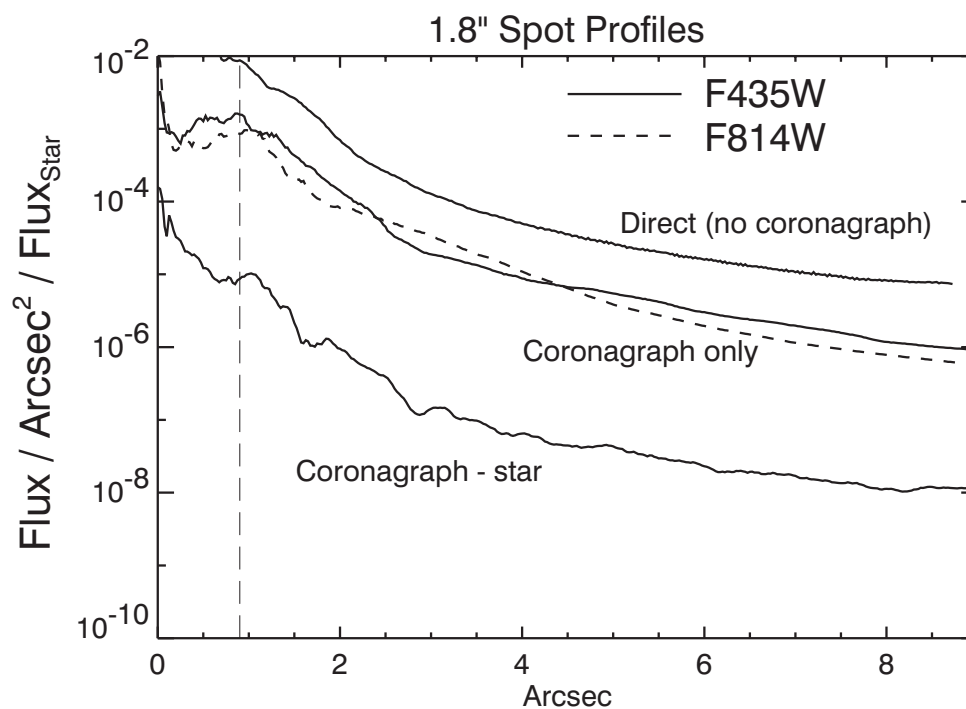
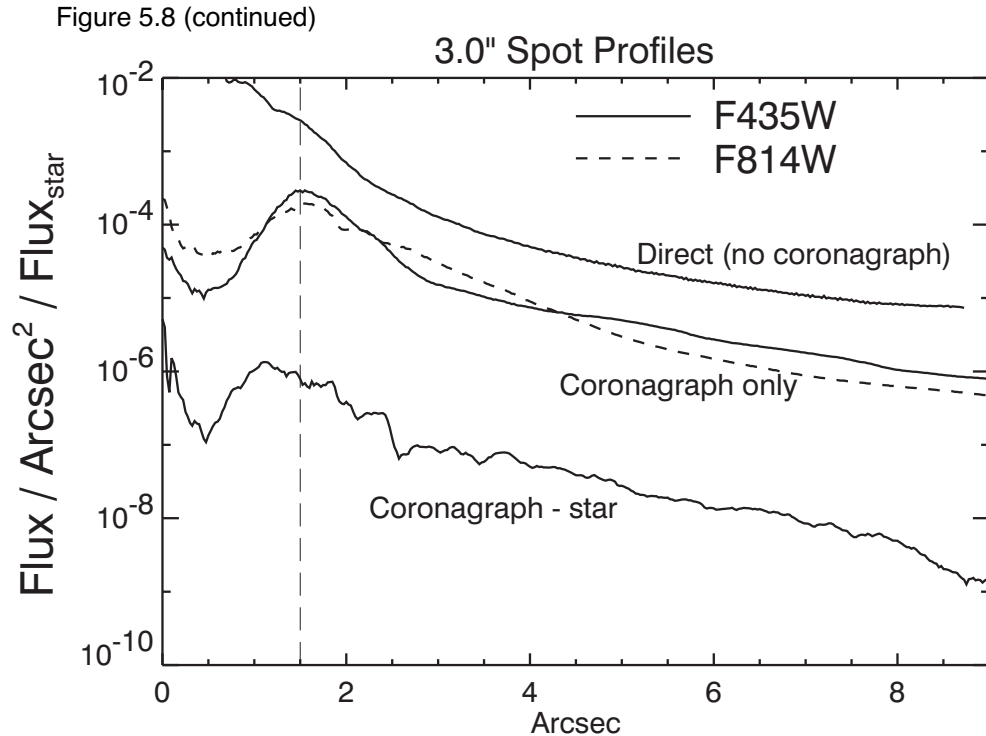


Figure 5.8: Surface brightness plots derived by computing the median value at each radius. The brightness units are relative to the total flux of the star. The direct profile is predicted; the coronagraphic profiles are measured from on-orbit images of Arcturus. "Coronagraph-star" shows the absolute median residual level from the subtraction of images of the same star observed in separate visits.





### 5.2.5 Residual light subtraction

While the coronagraph suppresses the diffracted light from the central star, the scattered light still overwhelms faint, nearby sources. It is possible to subtract most of the remaining halo using an image of another occulted star. PSF subtraction has been successfully used with images taken by other HST cameras, with and without a coronagraph. The quality of the subtraction depends critically on how well the target and reference PSFs match.

As mentioned above, for any pair of target and reference PSF observations there is likely to be a difference of 5-20 mas between the positions of the stars. Because the scattered light background is largely insensitive to small errors in star-to-spot alignment (it is produced before the coronagraph), most of it can be subtracted if the two stars are precisely registered and normalized. Due to the numerous sharp, thin streaks that form the scattered light background, subtraction quality is visually sensitive to registration errors as small as 0.03 pixels (0.75 mas). To achieve this level of accuracy, the reference PSF may be iteratively shifted and subtracted from the target until an offset is found where the streaks are minimized. This method relies on the judgment of the observer, as any circumstellar material could unexpectedly bias a registration optimization algorithm. A higher-order sampling method, such as cubic convolution interpolation, should be used to shift the reference PSF by subpixel



amounts; simpler schemes such as bilinear interpolation degrade the fine PSF structure too much to provide good subtractions.

Normalization errors as small as 1-4% between the target and reference stars may also create significant residuals. However, derivation of the normalization factors from direct photometry is often not possible. Bright, unocculted stars will be saturated in medium or broadband filters at the shortest exposure time (0.1 sec). An indirect method uses the ratio of saturated pixels in unocculted images (the accuracy will improve with greater numbers of saturated pixels). A last-ditch effort would rely on the judgment of the observer to iteratively subtract the PSFs while varying the normalization factor.

In addition to registration offsets, positional differences can alter the diffraction patterns near the spots' edges. The shape and intensity of these rings are very sensitive to the location of the star relative to the spot. They cannot be subtracted by simply adjusting the registration or normalization. These errors are especially frustrating because they increase the diameter of the central region where the data are unreliable. The only solution to this problem is to observe the target and reference PSF star in adjacent orbits without flipping the masks out of the beam between objects. See Section 5.2.8 for details on "campaign" mode observations.

Color differences between the target and reference PSF can be controlled by choosing an appropriate reference star. As wavelength increases, the speckles that make up the streaks in the halo move away from the center while their intensity decreases (Figure 5.7). The diffraction rings near the spots' edges will expand as well. These effects can be seen in images through wideband filters – a red star will appear to have a slightly larger PSF than a blue one. Thus, an M-type star should be subtracted using a similarly red star – an A-type would result in significant residuals. Even the small color difference between A0V and B8V stars, for example, may be enough to introduce bothersome errors (Figure 5.9).

A focus change can also alter the distribution of light in the PSF. The telescope focus changes over timescales of minutes to months. Within an orbit, the separation between the primary and secondary mirrors varies on average by 3  $\mu\text{m}$  (resulting in 1/28 wave RMS of defocus @  $\lambda=0.5 \mu\text{m}$ ) – an effect called *breathing*. This is caused by the occultation of the telescope's field of view by the warm Earth, which typically occurs during half of each 97-minute orbit. This heats HST's interior structure, which expands. After occultation the telescope gradually shrinks. Large changes in the pointing attitude relative to the Sun can also introduce 3-10  $\mu\text{m}$  of expansion, which decays back to normal over several orbits. The main result of these small focus changes is the redistribution of light in the wings (Figure 5.10).

Figure 5.9: Predicted absolute mean subtraction residual levels for cases where the target and reference stars have color mismatches. The brightness units are relative to the total flux of the target star.

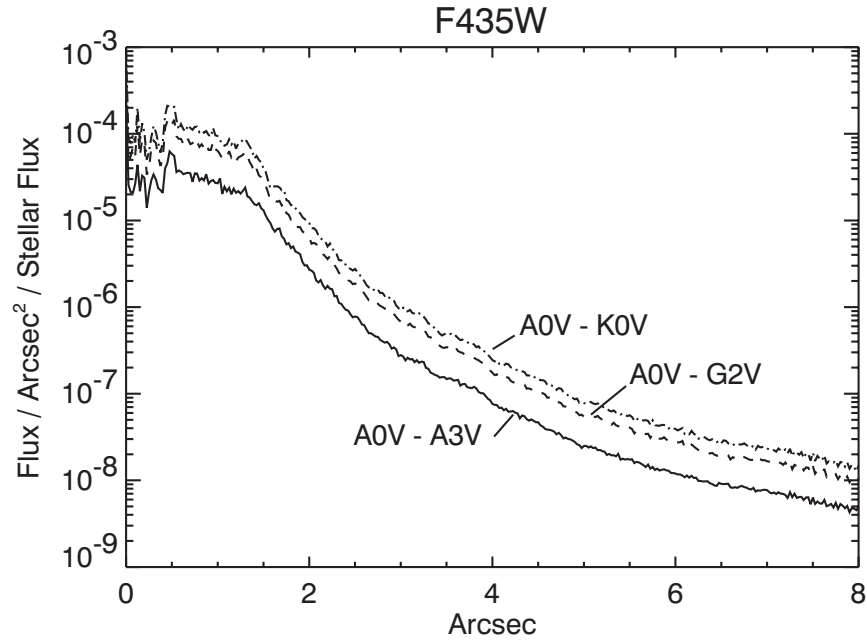
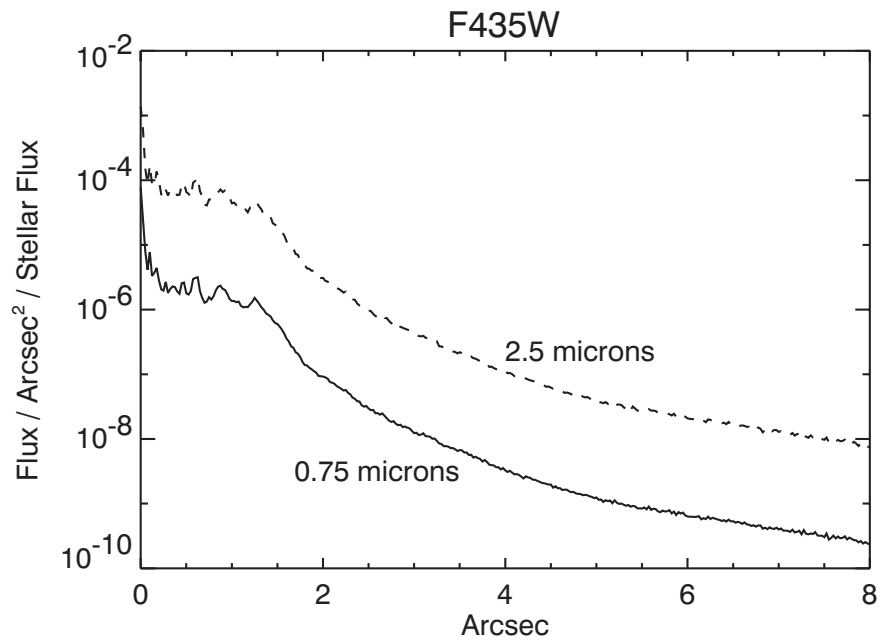


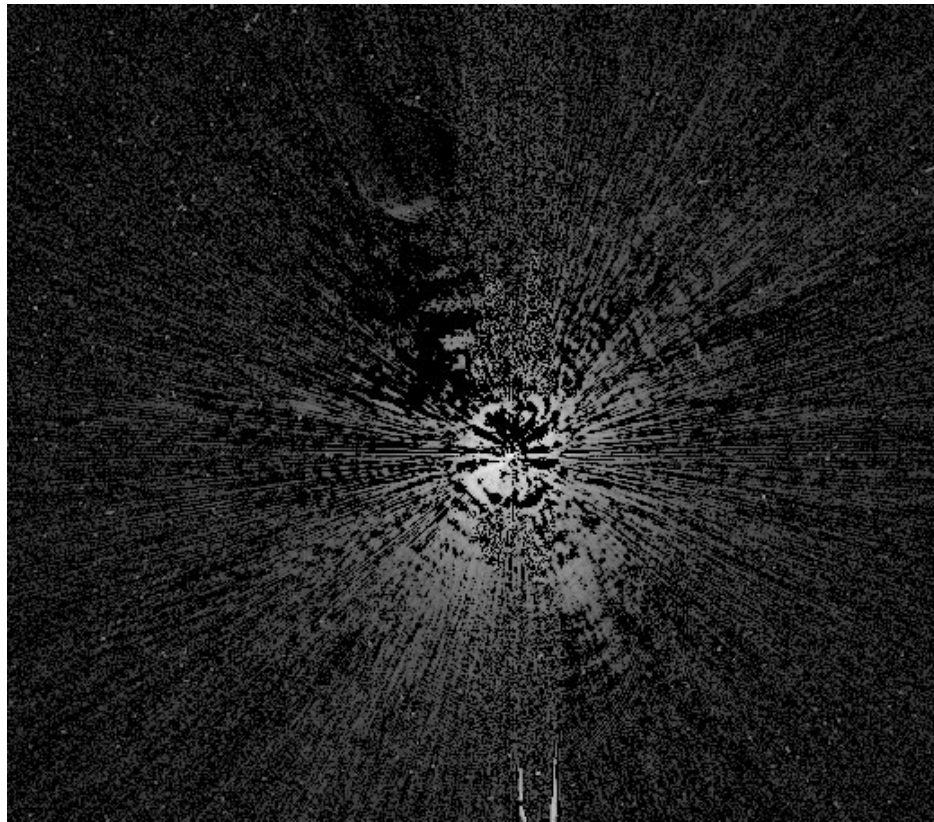
Figure 5.10: Predicted absolute mean subtraction residual levels for cases where the target and reference stars are imaged at different breathing-induced focus positions. The offset (0.75 or 2.5  $\mu\text{m}$ ) from perfect focus (0  $\mu\text{m}$ ) is indicated with respect to the change in the primary-secondary mirror separation (the typical breathing amplitude is 3-4  $\mu\text{m}$  within an orbit). The brightness units are relative to the total flux of the target star.



Plots of the azimuthal median radial profiles after PSF subtraction are shown in Figure 5.8. In these cases, images of Arcturus were subtracted from others of itself taken a day later. The images were registered as previously described. Combined with PSF subtraction, the coronagraph reduces the median background level by 250-2500x, depending on the radius and filter. An example of a PSF subtraction is shown in Figure 5.11. The mean of the residuals is not zero. Because of PSF mismatches, one image will typically be slightly brighter than the other over a portion of the field (such as shown in Figure 5.12). The pixel-to-pixel residuals can be more than 10x greater than the median level (Figure 5.13). Note that these profiles would be worse if there were color differences between the target and reference PSFs.

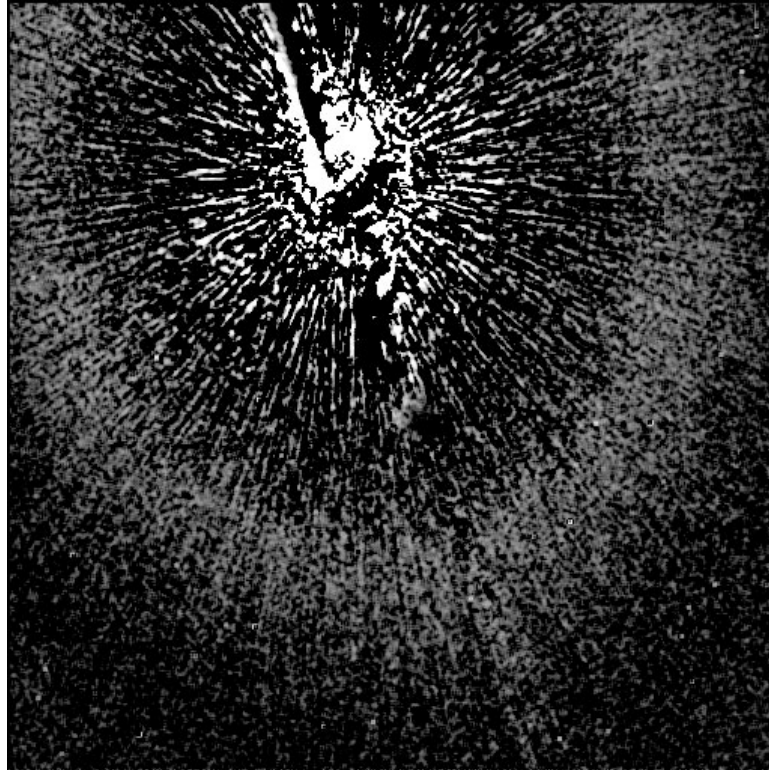
One way to get around both the color and normalization problems is to take images of the central source at different orientations and subtract one from the other (*roll subtraction*). This can be done by either requesting a roll of the telescope about the optical axis (up to 30° total) between orbits or by revisiting the object at a later date when the default orientation of the telescope is different. This technique only works when the nearby object of interest is not azimuthally extended. It is the best method for detecting point source companions or imaging strictly edge-on disks (e.g. Beta Pictoris). This method can also be used to reduce the pixel-to-pixel variations in the subtraction residuals by rotating and coadding the images taken at different orientations (this works for extended sources if another PSF star is used). Ideally, the subtraction errors will decrease as the square root of the number of orientations.

Figure 5.11: Residual errors from the subtraction of one image of Arcturus from another taken in a different visit (filter=F435W, D=1.8" spot). The image is 29" across and has not been geometrically corrected. Logarithmic intensity scaled.



The large sizes of the occulting spots severely limit how close to the central source one can image. It may be useful to combine coronagraphic imaging with direct observations of the target, allowing the central columns to saturate (additional observations at other rolls would help). PSF subtraction can then be used to remove the diffracted and scattered light.

Figure 5.12: Subtraction of Arcturus from another image of itself taken during another visit using the large ( $D=3.0''$ ) spot and F435W filter. The image has been rebinned, smoothed, and stretched to reveal very low level residuals. The broad ring at about  $13''$  from the star is a residual from some unknown source – perhaps it represents a zonal redistribution of light due to focus differences (breathing) between the two images. The surface brightness of this ring is  $20.5 \text{ mag arcsec}^{-2}$  fainter than the star. The diameter, brightness, and thickness of this ring may vary with breathing and filter. The image has not been geometrically corrected.



### 5.2.6 The Off-Spot PSF

Objects that are observed in the coronagraphic mode but that are not placed behind an occulting mask have a PSF that is defined by the Lyot stop. Because the stop effectively reduces the diameter of the telescope and introduces larger obscurations, this PSF is wider than normal, with more power in the wings and diffraction spikes (Figure 5.14). In addition, the stop and spot substrate reduce the throughput by 52.5%. In F814W, this PSF has a peak pixel containing 4.3% of the total (reduced) flux and a sharpness (including CCD charge diffusion effects) of 0.010 (compare these to 7.7% and 0.026, respectively, for the normal HRC PSF). In F435W the peak is 11% and the sharpness is 0.025 (compared to 17% and 0.051 for the normal F435W PSF). Observers need to take the reduced throughput and sharpness into account when determining detection limits for planned observations.

Figure 5.13: Plots of the azimuthal RMS subtraction residual levels at each radius for the large (3") spot. The flux units are counts per pixel relative to the total unocculted flux from the central source. These plots were derived from Arcturus-Arcturus subtractions represent the best results one is likely to achieve. The undistorted HRC scale assumed here is 25 mas/pixel.

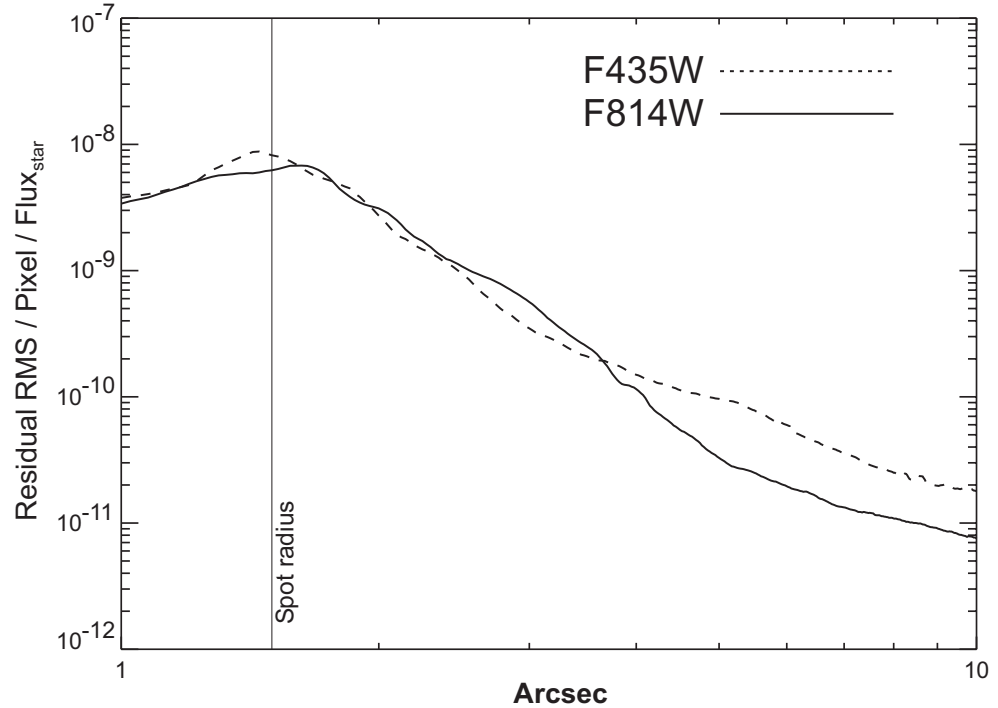
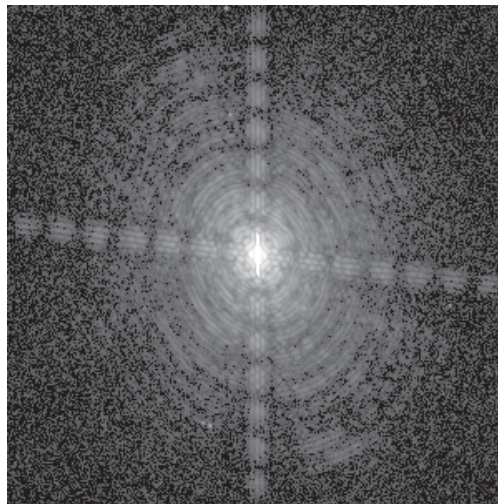


Figure 5.14: Image of Arcturus taken in coronagraphic mode with the star placed outside of the spot. The coronagraphic field PSF has more pronounced diffraction features (rings and spikes) than the normal HRC PSF due to the effectively larger obscurations introduced by the Lyot stop. The central portion of this image is saturated. It was taken through a narrowband filter (F660N) and is not geometrically corrected



## 5.2.7 Planning ACS Coronagraphic Observations

### Exposure Time Estimation

The estimation of exposure time for coronagraphic observations is similar to direct-mode time calculations, except that the additional background contribution from the central source's PSF has to be accounted for. Generally, most coronagraphic observations are limited by the central source's PSF wings. The APT Exposure Time calculator includes a coronagraphic mode for estimating exposure times. We will now demonstrate how exposure times for coronagraphic observations can be determined using the web-based version of the ACS Exposure Time Calculator. The following steps are required:

- Determine which occulting mask to use
- Calculate the count rate for the target
- Calculate the count rate for the central source
- Calculate the background contribution from the surface brightness of the central source's PSF wings at the location of the target.
- Verify that background+target does not saturate at this location in exposure time  $t_{\text{exp}}$  (or use exposure times of increasing length)
- Calculate the signal-to-noise ratio  $\Sigma$ , given by:

$$\Sigma = \frac{Ct}{\sqrt{Ct + N_{\text{pix}}(B_{\text{sky}} + B_{\text{det}} + B_{\text{PSF}})t + N_{\text{pix}}N_{\text{read}}R^2}}$$

Where:

- $C$  = the signal from the astronomical target in electrons  $\text{sec}^{-1}$  from the CCD.
- $N_{\text{pix}}$  = the total number of detector pixels integrated over to achieve  $C$ .
- $B_{\text{sky}}$  = the sky background in counts  $\text{sec}^{-1} \text{ pixel}^{-1}$ .
- $B_{\text{det}}$  = the detector dark current in counts  $\text{sec}^{-1} \text{ pixel}^{-1}$ .
- $B_{\text{PSF}}$  = the background in counts  $\text{sec}^{-1} \text{ pixel}^{-1}$  from the wings of the central source's PSF at the same distance from the central source as the target.
- $N_{\text{read}}$  = the number of CCD readouts.
- $t$  = the integration time in seconds.
- $R$  is the readout noise of the HRC CCD =  $4.7e^-$ .

In order to illustrate a calculation we shall consider the case where we are trying to determine the S/N achieved in detecting a M6V star with a V magnitude of 20.5 at a distance of 4.25 arcsec from a F0V star with a V

magnitude of 6, for an exposure time of 1000 seconds with an F435W filter. Using the ACS Exposure Time Calculator and considering the case for the 3.0" occulting mask:

- Target count rate =  $5.9 \text{ e}^-/\text{sec}$  for a  $5 \times 5$  aperture (including 47.5% throughput of coronagraph)  
Sky count rate =  $0.003 \text{ e}^-/\text{sec/pixel}$   
Detector dark rate =  $0.003 \text{ e}^-/\text{sec/pixel}$
- Central star count rate =  $3.3 \times 10^7 \text{ e}^-/\text{sec}$  for a  $101 \times 101$  aperture ( $101 \times 101$  aperture used to estimate total integrated flux)
- At a distance 4.25 arcsec from the central star, from Figure 5.8, the fraction of flux per  $0.026'' \times 0.026''$  pixel in the PSF wings is  $5 \times 10^{-9}$ .  
 $B_{\text{PSF}} = 3.3 \times 10^{-9} * 5 \times 10^7 = 0.165 \text{ e}^-/\text{sec/pixel}$
- Using the equation above we find the signal to noise for a 1000 sec exposure is 57. Note that a M6V star with a V magnitude of 20.5 observed with the HRC in isolation would yield a S/N of 129.

### Observing sequence for point source companions

The best way to detect faint stellar or substellar companions is to use roll subtraction to avoid color differences between the target and reference PSFs. This also provides duplicate observations that make it easier to verify true companions from noise. It is best to roll the telescope between visits and repeat the image sequence in a new orbit. This way, you can better match the breathing cycle of the telescope than if you rolled the telescope in the middle of an orbital visibility window. You can force this to happen by selecting both orientation and time-sequencing constraints in the visit special requirements. Remember that the coronagraphic field PSF is somewhat broader than the normal HRC PSF, which may influence your assumed signal-to-noise ratio. Off-spot PSF models can be generated with the Tiny Tim PSF software. You can estimate the residual background noise level using Figure 5.13.

Suggested point-source companion observing sequence:

1. Obtain an acquisition image
2. Execute image sequence.
3. Request telescope roll offset (use **ORIENT  $\theta_1$  TO  $\theta_2$  FROM  $n$**  special requirement in visit).
4. Obtain another acquisition.
5. Repeat image sequence.
6. Repeat 3-5 as necessary.



### **Observing sequence for extended sources (e.g. circumstellar disks and AGN host galaxies)**

When imaging extended objects, the remaining scattered light must be subtracted using a reference star image, which should match the color of your target as closely as possible. It helps the reference PSF is bright enough to provide higher signal-to-noise ratios in the wings than the target source, to reduce the impact of noise in the subtracted images. If possible, select a reference star that is nearby ( $<20^\circ$ ) and request that it be observed immediately before or after the target source. This reduces the chance that there will be large focus differences between the two visits. In order to better discriminate between subtraction artifacts and real structure, it may also help to obtain images of the target at two or more orientations of the telescope (there is no need to get reference PSF images at different rolls). You can estimate the residual background noise level using Figure 5.13.

Suggested extended source observing sequence:

1. Obtain direct images of the science target in each filter to derive normalization factors
2. Obtain an acquisition image of the science target.
3. Take image sequence of science target.
4. Request a new telescope orientation.
5. Repeat steps 2-3.
6. In a new visit, point at the reference star.
7. Obtain direct images of the reference star in each filter to derive normalization factors
8. Obtain an acquisition image of reference star.
9. Take image sequence of reference star.

Because the occulting spots are large, you may wish to image closer to the source using additional direct observations without the coronagraph. Multiple roll angles are necessary in this case because portions of the inner region will be affected by saturated columns and diffraction spikes. Direct observations of the reference star will be required as well to subtract both the diffracted and scattered light. Color and focus mismatches between the target and reference PSFs will be even more important in the direct imaging mode than with the coronagraph because the diffracted light is not suppressed. However, there are no mismatches caused by star-spot alignment to worry about.

### **5.2.8 “Campaign” Mode**

The occulting spots vary slightly in position every time the coronagraph is enabled, so it would be advantageous to observe a series of targets without moving the calibration door mechanism on which the masks are

mounted. By default, acquisition images are first taken without the coronagraph and then the masks are inserted. So every time the target changes or another acquisition is requested after rolling the telescope, the masks are taken out, an acquisition image is taken, and the masks inserted again.

A new observing sequence *may* be available for Cycle 12 called “coronagraphic campaign mode” in which multiple targets are observed in adjacent orbits without flipping the masks in-and-out of the beam. At the beginning of the sequence, the masks are inserted. Every acquisition will then occur with the masks inserted and the target located outside of the occulting spot. The exact procedure for defining campaign mode observations has not yet been finalized (check the ACS web site or contact the Institute to obtain the current procedures). Most likely it will require specifying an aperture for acquisitions that is different from HRC-ACQ and forcing observations to occur in back-to-back orbits with time constraints in the visit special requirements section of the Phase II proposal. If both direct and coronagraphic images are being taken, then separate visits should be used outside of campaign mode for the direct observations.

---

## 5.3 Grism/Prism Spectroscopy

The ACS filter wheels include four dispersing elements for low resolution slitless spectrometry over the field of view of the three ACS channels. One grism (G800L) provides low resolution spectra over the 5500-11000Å range for both the WFC and HRC; a prism (PR200L) in the HRC covers the range 1600 to beyond 3900Å; in the SBC a LiF prism covers the wavelength range 1150 to ~1800Å (PR110L) and a CaF2 prism is useful over the 1250 to ~1800Å range (PR130L). Table 5.2 summarizes the essential features of the four ACS dispersers in the five available modes. The grism provides first order spectra with dispersion almost linear with wavelength but have second order overlap beyond about 10000Å; the prisms however have non-linear dispersion with maximum resolution at shorter wavelengths but much lower resolution at longer wavelengths. The two-pixel resolution is listed for each grism or prism at a selected wavelength in Table 5.2. The pixel scale for the prisms is given at the selected wavelength. The tilt of the spectra to the detector X axis (close to the spacecraft V2 axis) is also listed.

Table 5.2: Optical Parameters of ACS Dispersers

Disperser	Channel	Wavelength range (Å)	Resolution	Å/pixel	Tilt <sup>1</sup> (deg)
G800L	WFC	1st order: 5500-11000	100@8000Å	39.7 <sup>2</sup>	-2
G800L	WFC	2nd order: 5000-9500	200@8000Å	20.7 <sup>2</sup>	-2
G800L	HRC	1st order: 5500-11000	140@8000Å	24.4	-39
G800L	HRC	2nd order: 5500-9500	280@8000Å	12.0	-39
PR200L	HRC	1600-3900	59@2500Å	21.3	-1
PR110L	SBC	1150-1800	79@1500Å	9.5	0
PR130L	SBC	1250-1800	96@1500Å	7.8	0

1. Tilt with respect to the positive X-axis of the data frame.

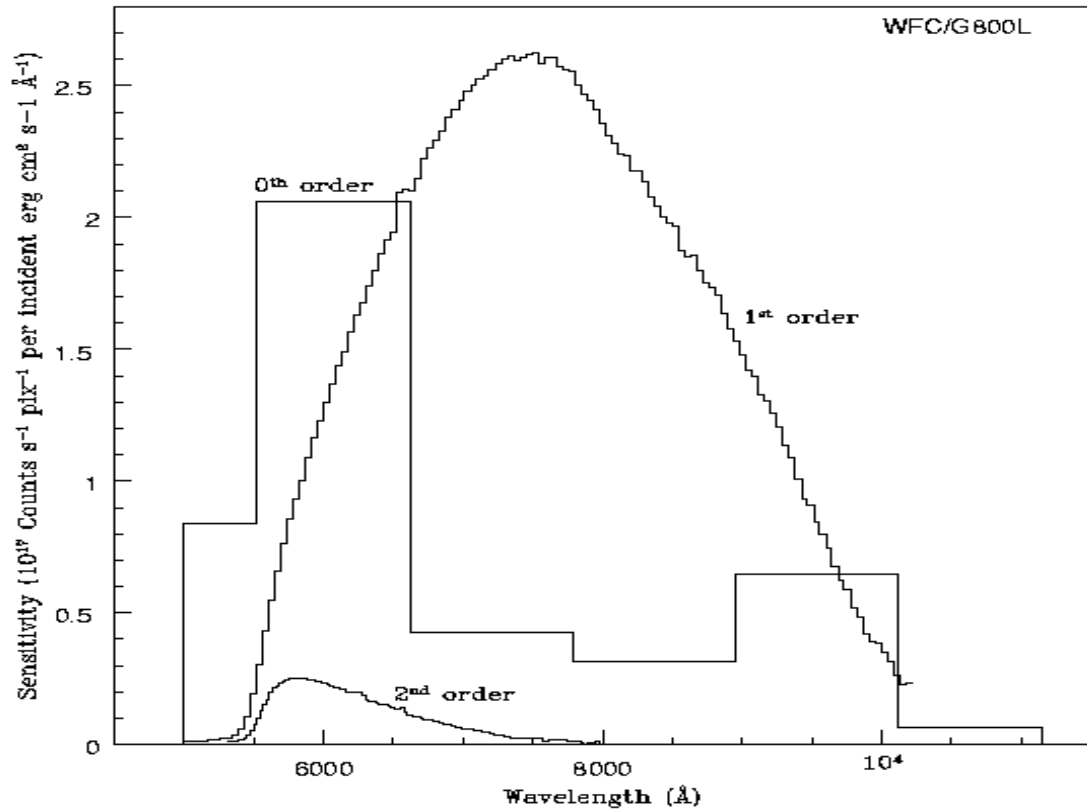
2. The dispersion varies over the field by +/- 12%; the tabulated value refers to the field center.

### 5.3.1 WFC G800L

The G800L grism and the WFC provide two-pixel resolution from 69 (at 5500Å) to 138 (at 11000Å) for first order spectra over the whole accessible field of 202x202". Table 5.2 lists the linear dispersion, but a second order dispersion solution provides a better fit. Figure 5.15 shows the wavelength extent and sensitivity for the zeroth, first, and second order spectra when used with the WFC; Figure 5.16 shows the same plot in pixel extent. The 0 position refers to the position of the direct image and the pixel size is 0.05". Note that there is contamination of the 1st order spectrum above 10000Å by the second power. The total power in the zeroth order is 2.5% of that in the first order, so locating the zeroth order may not be an effective method of measuring the wavelengths of weak spectra. The default method will be to obtain a matched direct image-grism pair. There is also sensitivity of about a percent of first order in the third and fourth orders and about half a percent in the negative orders. The full extent the spectrum of a bright source (orders -2, -1, 0, 1, 2 and 3) covers is 1200 pix (60"). Figure 5.17 shows the full spectrum extent for a 60s exposure of the white dwarf GD153 (V=13.35) with the individual orders indicated. When observing bright objects, the signal in fainter orders may be mistaken for separate spectra of faint sources and in crowded fields many orders from different

objects can overlap. The wavelength solution is field dependent on account of the tilt of the grism to the optical axis and the linear dispersion varies by  $\pm 12\%$  from center to corner. This field dependence has been calibrated to allow wavelength determination to better than 0.5 pixels over the whole field.

Figure 5.15: Sensitivity versus wavelength for WFC G800L

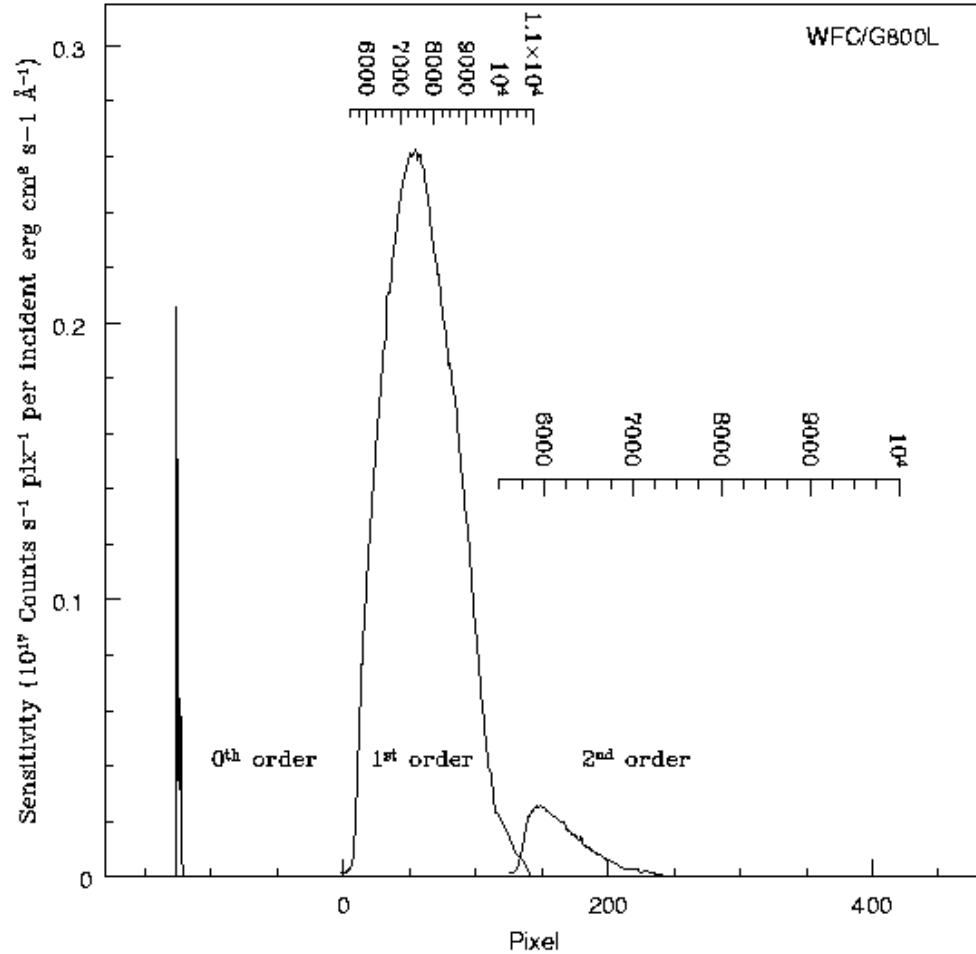


### 5.3.2 HRC G800L

When used with the HRC, the G800L grism provides higher spatial resolution ( $0.028''$ ) pixels than the WFC and also higher spectral resolution. However, the spectra are tilted at  $-39$  degrees to the detector X axis. Figure 5.18 shows the wavelength extent and sensitivity in the zero, first and second orders, with the pixel extent shown in Figure 5.19. Figure 5.20 shows the observed spectrum of the standard star GD153. Again there is contamination of the first order spectrum by the second order beyond  $9500 \text{ Å}$ . The total extent of the spectrum (orders -1 and +2) in Figure 5.20 covers about 70% of the 1024 detector pixels, and a much greater number of spectra will be formed by objects situated outside the HRC direct image, or will have their spectra truncated by the chip edges, than for the WFC.

The variation of the grism dispersion over the HRC field is about  $\pm 4\%$  from center to corner and has been calibrated.

Figure 5.16: Sensitivity versus pixel position for WFC G800L



### 5.3.3 HRC PR200L

The maximum pixel resolution of the prism is  $5.3\text{\AA}$  at  $1800\text{\AA}$ . At  $3500\text{\AA}$ , the dispersion drops to  $91\text{\AA}/\text{pix}$  and is  $515$  at  $5000\text{\AA}$ . The result is a bunching up of the spectrum to long wavelengths with about 8 pixels spanning  $1500\text{\AA}$ . For bright objects, this effect can lead to blooming of the HRC CCD from filled wells; the overfilled pixels bleed in the detector Y direction, and would thus affect other spectra. Figure 5.21 shows the sensitivity versus wavelength for PR200L and the wavelength extent of the pixels is indicated. The variation of the dispersion across the detector for PR200L amounts to about  $\pm 3\%$ . The angle of the prism causes a large deviation between the position of the direct object and the region of the dispersed spectrum. The pixel numbers on Figure 5.21 indicate the size of the offset from the direct image. On account of the size of this offset, special apertures have been defined in the observation scheduling system

so that the spectrum of the target centered on the direct image occurs near the center of the field in the prism image.

Figure 5.17: Full Dispersed Spectrum for White Dwarf GD153 with WFC/G800L

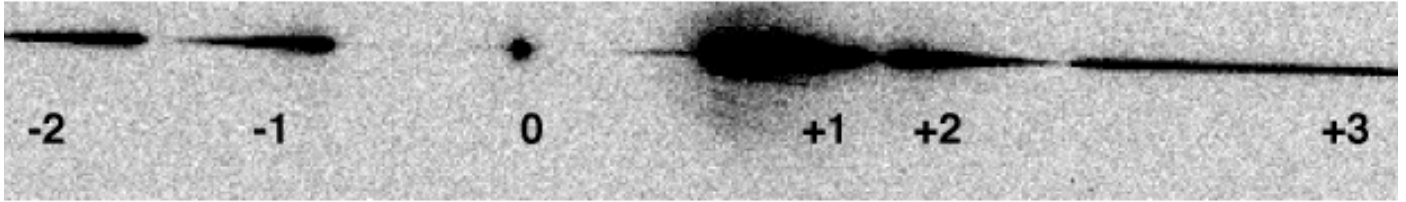
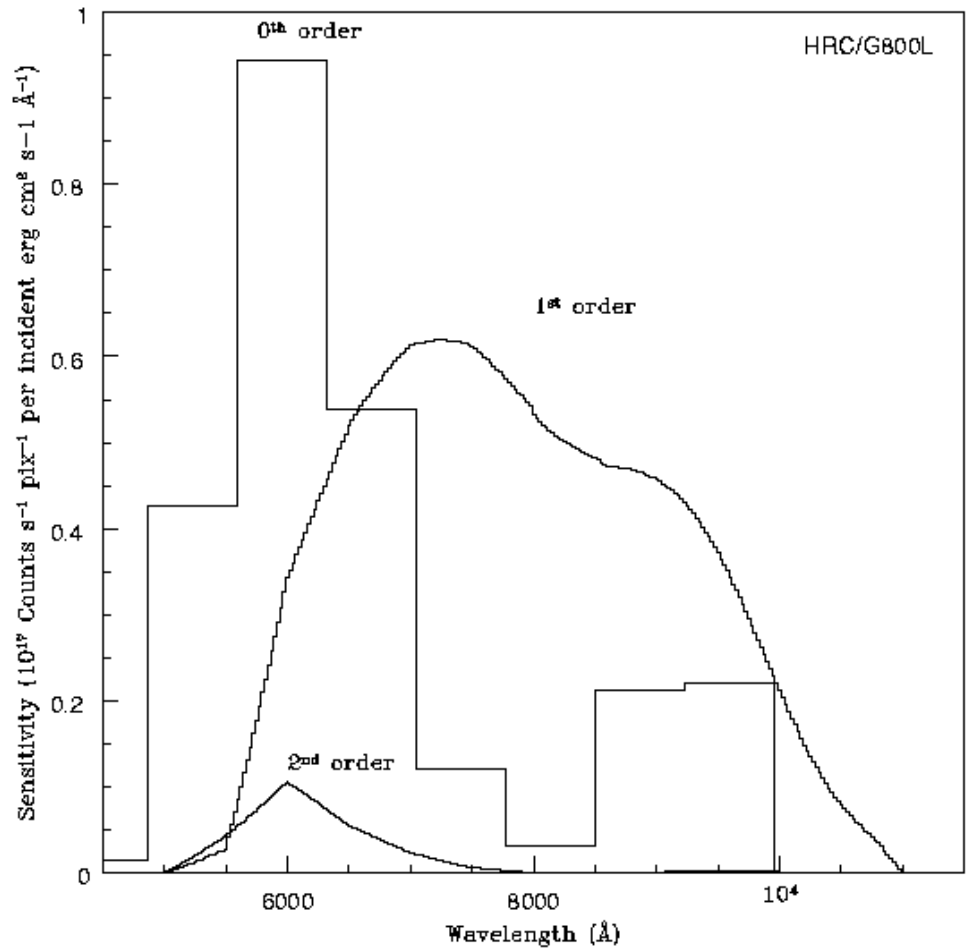


Figure 5.18: Sensitivity versus wavelength for HRC G800L



### 5.3.4 SBC PR110L

The PR110L prism is sensitive to below 1200Å and includes the geo-coronal Lyman-alpha line, so it is subject to high background. The dispersion at Lyman-alpha is 2.6Å per pixel. Figure 5.22 shows the sensitivity with wavelength and the wavelength width of the pixels. The

long wavelength cut-off of the CsI MAMA detector at  $\sim 1800\text{\AA}$  occurs before the long wavelength build-up of flux; the dispersion at  $1800\text{\AA}$  is  $21.6\text{\AA}/\text{pixel}$ . However the detected counts at the long wavelength edge must be within the MAMA Bright Object Protection Limits; these limits must include the contribution of the geo-coronal Lyman-alpha flux per SBC pixel. The numbers in Figure 5.22 show the offset of the spectrum from the direct image.

### 5.3.5 SBC PR130L

The short wavelength cut-off of the PR130L prism at  $1250\text{\AA}$  excludes the geocoronal Lyman-alpha line, making it the disperser of choice for faint object detection in the  $1250\text{--}1800\text{\AA}$  window. The dispersion varies from  $1.65\text{\AA}$  at  $1250\text{\AA}$  to  $20.2\text{\AA}$  at  $1800\text{\AA}$ . Figure 5.23 shows the sensitivity versus wavelength and the pixel widths in angstroms. Bright Object Protection considerations similar to the case of PR110L also apply to the use of this prism, except that the background count rate is lower.

Figure 5.19: Sensitivity versus pixel position for HRC G800L

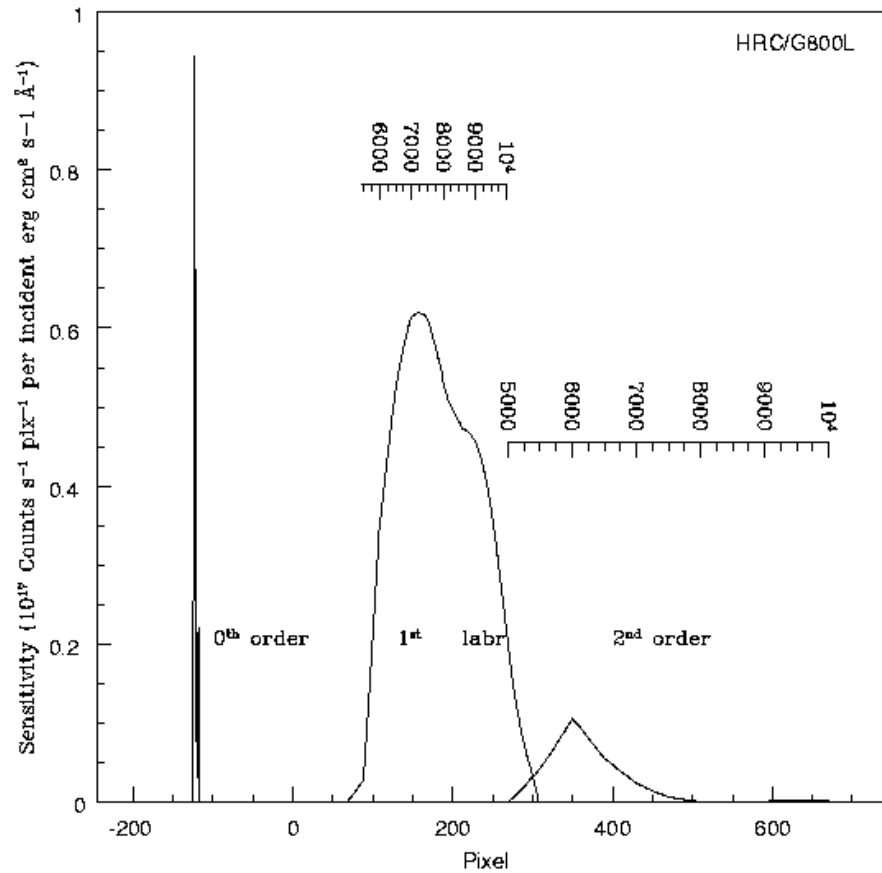
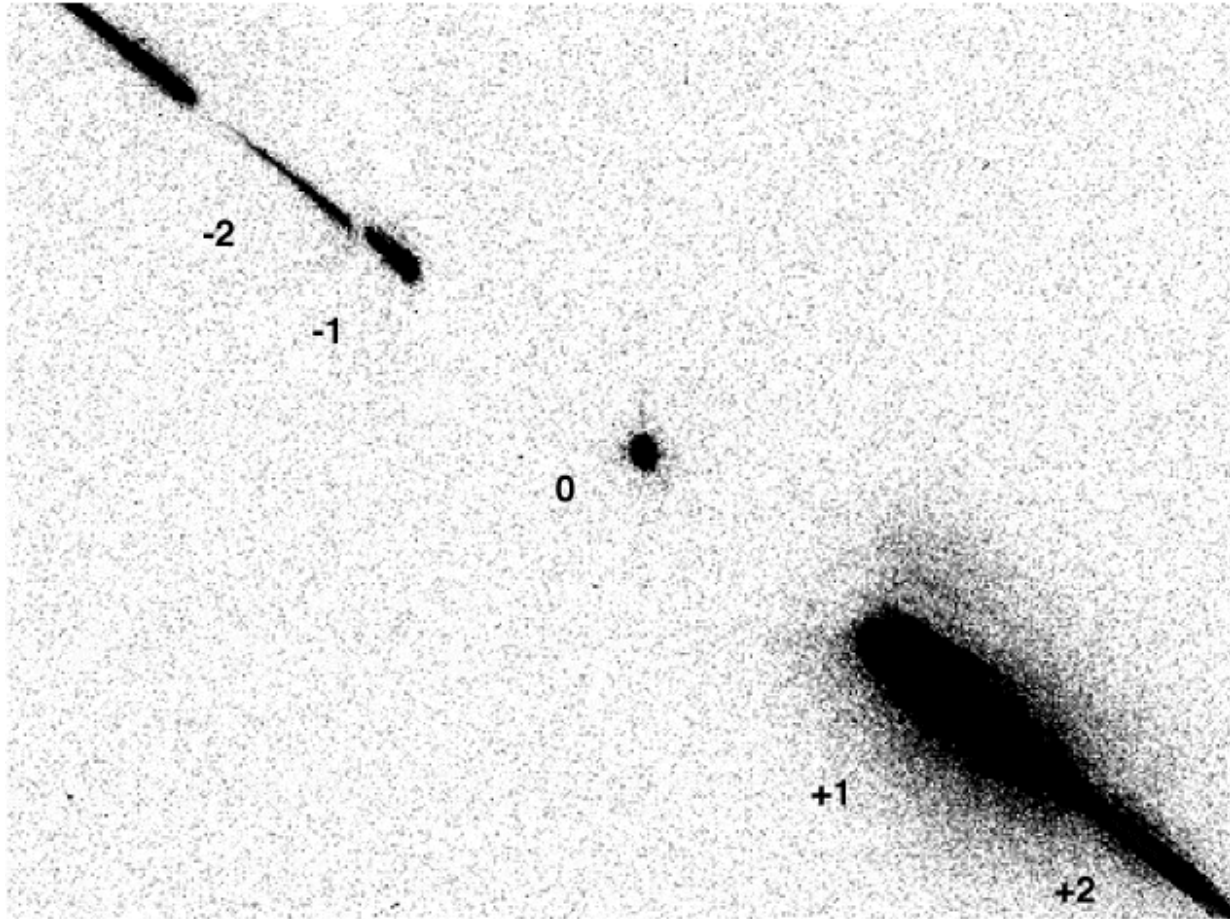


Figure 5.20: Full Dispersed Spectrum of White Dwarf GD153 with HRC/G800L



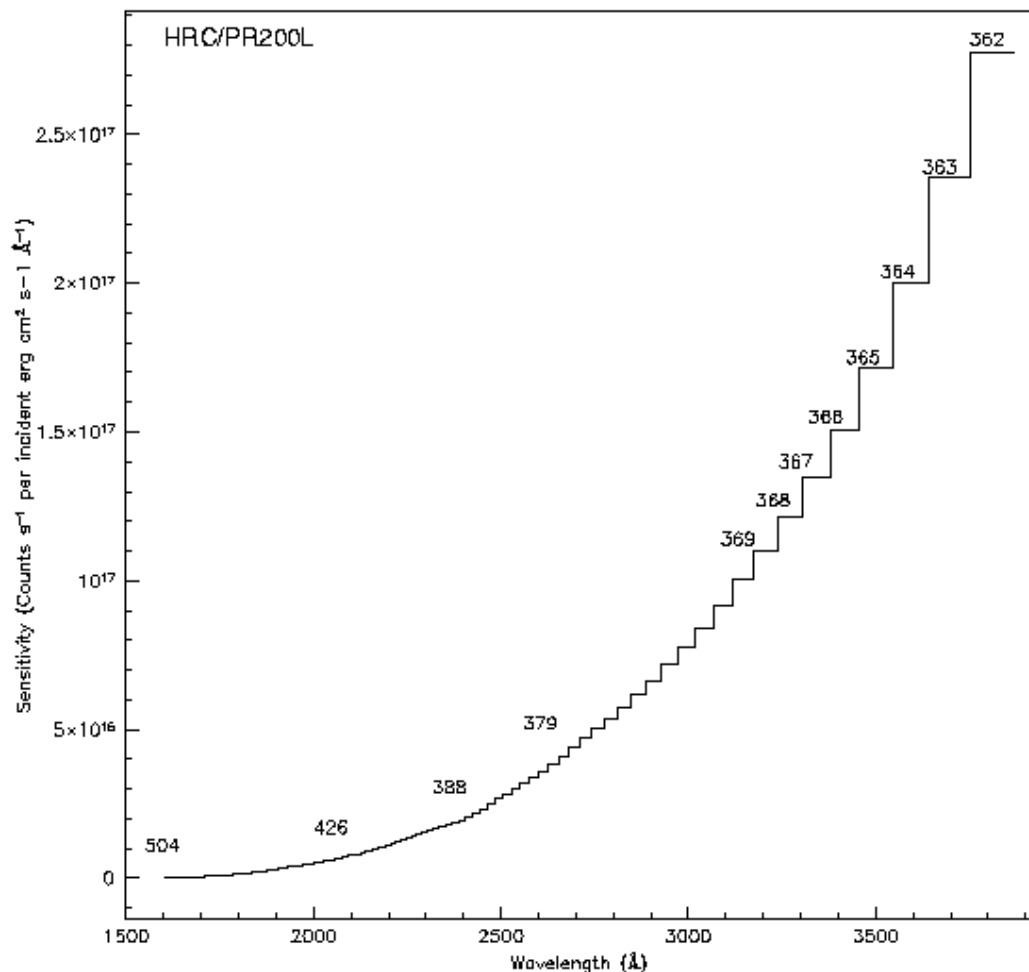
### 5.3.6 Observation Strategy

The default observing mode for all ACS WFC grism and HRC grism and prism modes will be to obtain a direct image of the field followed by a dispersed grism/prism image. This combination will then allow the wavelength calibration of the individual target spectra by reference to the corresponding target on the direct image. The direct image will be added by default to the dispersed image by the scheduling system (AUTOIMAGE=YES). For the WFC and HRC G800L spectra an F606W exposure will be employed; for the HRC PR200L prism an F330W image will be applied. The companion direct image can be switched off by AUTOIMAGE=NO, allowing, for example, a separate direct image in a different filter to be specified if desired. For the SBC, the default mode will be to obtain spectra without an accompanying direct image on account of the need for Bright Object Protection (BOP). The user can separately specify a direct image to accompany the prism image, which should be



scheduled immediately before or after the prism image in the same orbit. The direct image must also of course pass the BOP check.

Figure 5.21: Sensitivity versus wavelength for HRC/PR200L, numbers in figure show offset in pixels from direct image.



All exposures with the SBC prisms must fall within the Bright Object Protection limits. In the case of spectra, the most important determination is that the flux at the longest wavelength must not exceed 50 counts/s/pix. Table 5.3 lists for the PR110L and PR130L prisms, the observed magnitudes of stars of various spectral types whose spectra are expected to just exceed this BOP limit.

Table 5.3: BOP limits for SBC Prism spectra

Spectral Type	PR110L	PR130L
O5V	15.8	15.6
A1V	11.0	10.9
G2V	2.9	2.9

Figure 5.22: Sensitivity versus wavelength for SBC PR110L, numbers in figure show offset from direct image.

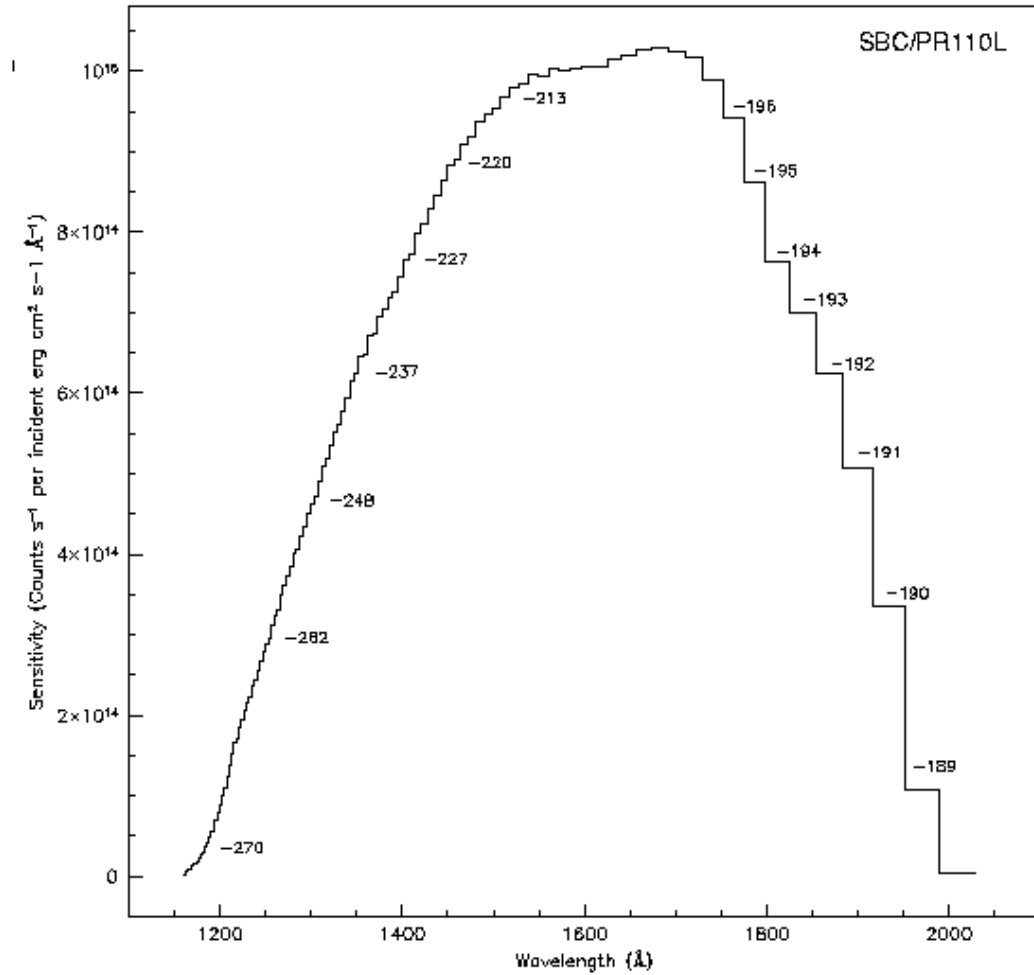


Table 5.4 lists the V detection limits for the ACS grism/prism modes for various spectral types without reddening. An exposure time of 1 hour was assumed with LOW Zodiacal background and a signal-to-noise of 5 per resolution element. For the WFC and HRC exposures, a CR-SPLIT of two was used and GAIN=1.

Table 5.4: V detection limits for the ACS Grism/Prism modes

Mode	V limit for a given spectral type		
	O5V	A1V	K4V
WFC/G800L	23.8	24.1	25.1
HRC/G800L	23.0	23.3	24.3
HRC/PR200L	25.9	23.6	19.3
SBC/PR110L	23.8	19.6	1.9
SBC/PR130L	24.6	20.4	2.6

Figure 5.15 through Figure 5.23 can be used to compute the detected count rate in the various orders of the gratings and prisms given the flux of the source spectra. Chapter 6 provides details of the calculations. Depending on the wavelength region, the background must also be taken into account in computing the signal-to-noise ratio. The background at each pixel consists of the sum of all the dispersed light in all the orders from the background source. For complex fields, the background consists of the dispersed spectrum of the unresolved sources; for crowded fields, overlap in the spectral direction and confusion in the direction perpendicular to the dispersion may limit the utility of the spectra.

The ACS Exposure Time Calculator supports all the available spectroscopic modes of the ACS and is available for more extensive calculations at [http://stdas.stsci.edu/ETC/ACS/acs\\_spec\\_etc.html](http://stdas.stsci.edu/ETC/ACS/acs_spec_etc.html). The current version employs the on-orbit determinations of the dispersion solution and sensitivity determination where available.

For more detailed simulations of ACS spectra, an image-spectral simulator, called **SLIM**, is available. This tool allows synthetic target fields to be constructed and dispersed images from spectrum templates to be formed. **SLIM** can simulate spectra for all the ACS spectral modes. The simulator runs under Python and an executable version is available at: <http://www.stecf.org/software/SLIM/SLIM10/index.html>. Version 1.0 uses a Gaussian PSF but this has been found to be an adequate representation to the **Tiny Tim** model of the ACS PSF. A detailed description of the tool and examples of its use are given by Pirzkal et al. (2001), available at <http://www.stsci.edu/hst/acs/documents/isrs/isr0103.pdf>.

### 5.3.7 Extraction and Calibration of Spectra

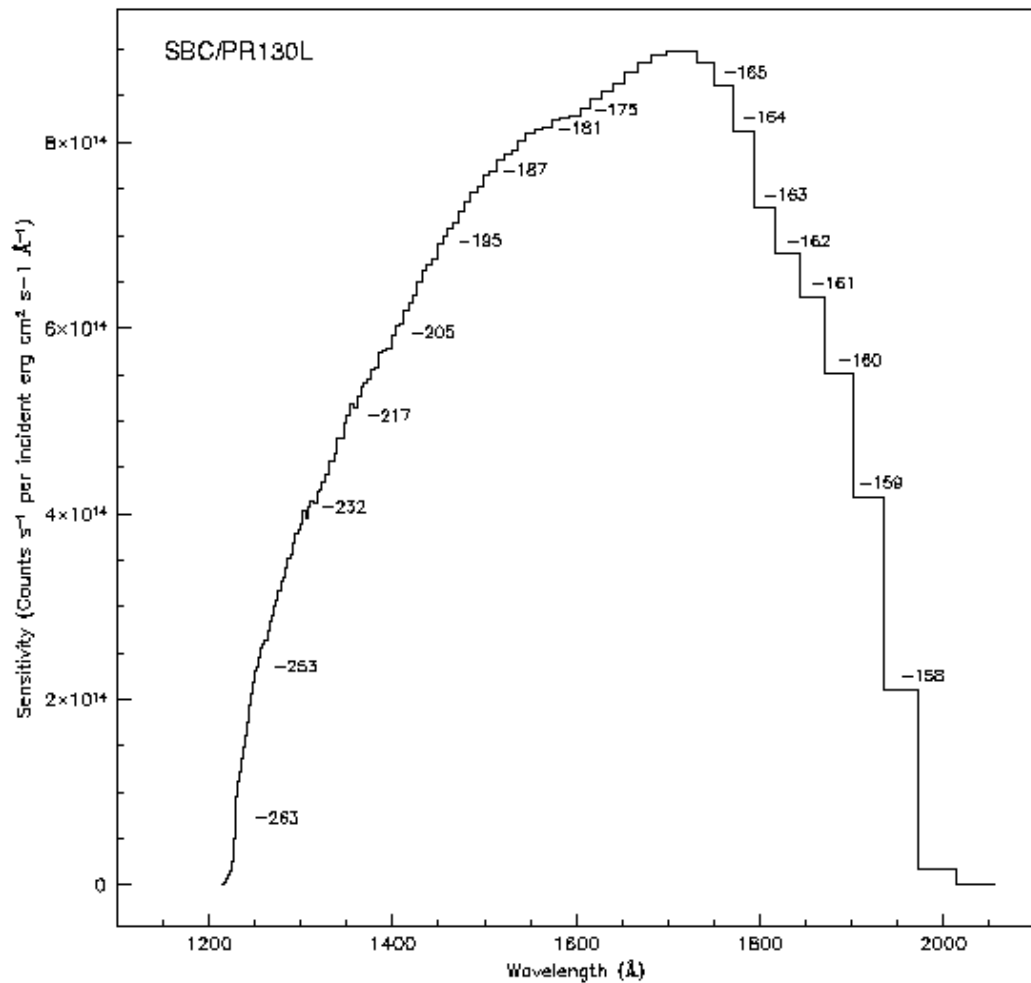
Since there is no slit in the ACS, the Point Spread Function of the target modulates the spectral resolution. In the case of extended sources it is the extension of the target in the direction of dispersion which sets the achievable resolution. Simulations show that for elliptical sources, the spectral resolution depends on the orientation of the long axis of the target to the dispersion direction and is described in more detail in Pasquali et al. (2001) <http://www.stsci.edu/hst/acs/documents/isrs>. The dispersion of the gratings and prisms is well characterized, but for the wavelength zero point it is important to know the position of the target in the direct image. For the gratings, the zeroth order will generally be too weak to reliably set the wavelength zero point. Given the typical spacecraft jitter, wavelength zero points to  $\pm 0.2$  pixels should be routinely achievable using the direct image taken just before or after the slitless spectrum image.

The wavelength extent of each pixel for the WFC and HRC G800L modes in the red is small enough that fringing modulates the spectra. Ground tests show that for the HRC, the peak-to-peak fringe amplitude is about 30% at 9500 Å, similar to STIS. For the WFC, the fringing

peak-to-peak amplitude is 25%. Modelling of the resultant fringing of the CCD structure by an optical model allows the fringe amplitude per pixel to be reduced below 4% peak-to-peak. In addition for a point source<sup>3</sup>, the fringe amplitude measured in the spectrum will be reduced on account of the finite extent of the PSF in the dispersion direction. For a point source, the fringe amplitude will be reduced on account of the finite extent of the PSF in the dispersion direction. Ground-based narrow-band fringe flats will be applied to reduce the effect of the fringing on extracted spectra to below ~5%.

An extraction software package, **aXe**, is available to extract, wavelength calibrate, flat field and flux calibrate ACS grism and prism spectra. Full details can be found at: <http://www.stecf.org/software/aXe/> The package is also available in STSDAS.

Figure 5.23: Sensitivity versus wavelength for SBC/PR130L



# Exposure-Time Calculations

In this chapter. . .

6.1 Overview / 97
6.2 Determining Count Rates from Sensitivities / 98
6.3 Computing Exposure Times / 104
6.4 Detector and Sky Backgrounds / 105
6.5 Extinction Correction / 111
6.6 Exposure-Time Examples / 112
6.7 Tabular Sky Backgrounds / 116

---

## 6.1 Overview

In this chapter, we explain how to use sensitivities and throughputs to determine the expected count rate from your source and how to calculate exposure times to achieve a given signal-to-noise ratio for your ACS observations taking various background contributions into account. At the end of this chapter in “Exposure-Time Examples”, you will find examples to guide you through specific cases.

### 6.1.1 The ACS Exposure Time Calculator

The ACS Exposure-Time Calculator (ETC) is available to help with proposal preparation via the ACS web page. This ETC calculates count rates for given source and background parameters, and signal-to-noise ratios for a given exposure time, or count rates and exposure time for a given signal-to-noise ratio for imaging and for spectroscopic observations. A calibrated spectrogram of your source can be provided directly to the Exposure-Time Calculator. The ETC also determines peak per-pixel count

rates and total count rates to aid in feasibility assessment. Warnings appear if the source exceeds the local or global brightness limits for SBC observations (see Section 7.5). The ETC has online help for its execution and interpretation of results. Alternatively, users can use **synphot** to calculate count rates and the wavelength distribution of detected counts.

## 6.2 Determining Count Rates from Sensitivities

In this Chapter, specific formulae appropriate for imaging and spectroscopic modes are provided to calculate the expected count rates and the signal-to-noise ratio from the flux distribution of a source. The formulae are given in terms of sensitivities, but we also provide transformation equations between the throughput ( $QT$ ) and sensitivity ( $S$ ) for imaging and spectroscopic modes.

Throughputs are presented in graphical form as a function of wavelength for the prisms and for the imaging modes in Chapter 10. Given your source characteristics and the sensitivity of the ACS configuration, calculating the expected count rate over a given number of pixels is straightforward, since the ACS PSF is well characterized. The additional required information is the encircled energy fraction ( $\epsilon_f$ ) in the peak pixel, the plate scale, and the dispersions of the prisms. This information is summarized in Tables 6.1 to 6.3.

Table 6.1: Useful Quantities for the ACS WFC

Filter	Pivot $\lambda$ (Å)	$\int Q_\lambda T_\lambda d\lambda/\lambda$	AB mag zero point	$\int S_\lambda d\lambda$	encircled energy	Flux in central pixel	Background sky rate
<b>F435W</b>	4311.8	0.0735	25.66	$3.14 \times 10^{18}$	0.82	0.24	0.0284
<b>F475W</b>	4747.6	0.1042	26.04	$5.41 \times 10^{18}$	0.83	0.22	0.0609
<b>F502N</b>	5022.4	0.0032	22.27	$1.88 \times 10^{17}$	0.83	0.22	0.0020
<b>F550M</b>	5582.2	0.0378	24.94	$2.71 \times 10^{18}$	0.83	0.22	0.0280
<b>F555W</b>	5363.7	0.0776	25.72	$5.13 \times 10^{18}$	0.83	0.22	0.0545
<b>F606W</b>	5915.4	0.1592	26.50	$1.29 \times 10^{19}$	0.84	0.20	0.1358
<b>F625W</b>	6305.3	0.0916	25.90	$8.33 \times 10^{18}$	0.84	0.20	0.0825
<b>F658N</b>	6584.0	0.0050	22.75	$5.03 \times 10^{17}$	0.82	0.20	0.0045
<b>F660N</b>	6599.5	0.0019	21.68	$1.88 \times 10^{17}$	0.82	0.20	0.0017
<b>F775W</b>	7697.3	0.0735	25.66	$1.00 \times 10^{19}$	0.80	0.17	0.0780
<b>F814W</b>	8064.6	0.0951	25.94	$1.42 \times 10^{19}$	0.80	0.17	0.1044
<b>F850LP</b>	9103.3	0.0372	24.92	$7.04 \times 10^{18}$	0.76	0.15	0.0415
<b>F892N</b>	8914.9	0.0036	22.38	$6.54 \times 10^{17}$	0.76	0.15	0.0039
<b>G800L</b>	7558.3	0.1439	26.39	$1.89 \times 10^{19}$	0.80	0.17	0.1526
<b>CLEAR</b>	6280.8	0.3855	----	$3.51 \times 10^{19}$	----	----	0.3580

Table 6.2: Useful Quantities for the ACS HRC

Filter	Pivot $\lambda$ (Å)	$\int Q_{\lambda} T_{\lambda} d\lambda/\lambda$	AB mag zero point	$\int S_{\lambda} d\lambda$	encircled energy	Flux in central pixel	Background sky rate
<b>F220W</b>	2256.7	0.0107	23.57	$1.25 \times 10^{17}$	0.74	0.16	0.0001
<b>F250W</b>	2714.2	0.0126	23.75	$2.15 \times 10^{17}$	0.80	0.16	0.0003
<b>F330W</b>	3361.7	0.0170	24.07	$4.41 \times 10^{17}$	0.80	0.16	0.0006
<b>F344N</b>	3432.9	0.0017	21.56	$4.57 \times 10^{16}$	0.80	0.16	0.0001
<b>F435W</b>	4310.3	0.0435	25.09	$1.85 \times 10^{18}$	0.82	0.14	0.0043
<b>F475W</b>	4774.9	0.0640	25.51	$3.34 \times 10^{18}$	0.83	0.12	0.0120
<b>F502N</b>	5021.1	0.0021	21.82	$1.24 \times 10^{17}$	0.83	0.12	0.0003
<b>F550M</b>	5580.0	0.0241	24.45	$1.72 \times 10^{18}$	0.83	0.12	0.0048
<b>F555W</b>	5357.5	0.0500	25.24	$3.29 \times 10^{18}$	0.83	0.12	0.0099
<b>F606W</b>	5882.3	0.0986	25.98	$7.87 \times 10^{18}$	0.84	0.10	0.0238
<b>F625W</b>	6289.7	0.0547	25.34	$4.98 \times 10^{18}$	0.84	0.10	0.0148
<b>F658N</b>	6581.9	0.0030	22.17	$2.95 \times 10^{17}$	0.84	0.10	0.0008
<b>F660N</b>	6581.4	0.0011	21.11	$1.10 \times 10^{17}$	0.84	0.10	0.0003
<b>F775W</b>	7674.0	0.0361	24.89	$4.90 \times 10^{18}$	0.72	0.07	0.0111
<b>F814W</b>	8121.0	0.0500	25.24	$7.52 \times 10^{18}$	0.72	0.07	0.0161
<b>F850LP</b>	9207.7	0.0232	24.41	$4.52 \times 10^{18}$	0.61	0.05	0.0075
<b>F892N</b>	8913.7	0.0021	21.82	$3.91 \times 10^{17}$	0.61	0.05	0.0007
<b>G800L</b>	7586.3	0.0805	25.76	$1.07 \times 10^{19}$	0.72	0.07	0.0250
<b>PR200L</b>	5639.9	0.2741	27.09	$2.00 \times 10^{19}$	0.80	0.16	0.0624
<b>CLEAR</b>	5449.3	0.3207	----	$2.18 \times 10^{19}$	----	-----	0.0683

Table 6.3: Useful Quantities for the ACS SBC

Filter	Pivot $\lambda$ (Å)	$\int Q_{\lambda} T_{\lambda} d\lambda/\lambda$	AB mag zero point	$\int S_{\lambda} d\lambda$	encircled energy	Flux in central pixel	Background sky rate
<b>F115LP</b>	1406.1	0.0148	23.92	$6.71 \times 10^{16}$	0.80	0.18	0.0238
<b>F122M</b>	1273.7	0.0009	20.95	$3.56 \times 10^{15}$	0.80	0.16	0.0042
<b>F125LP</b>	1437.5	0.0122	23.71	$5.81 \times 10^{16}$	0.81	0.19	0.0027
<b>F140LP</b>	1527.0	0.0069	23.09	$3.68 \times 10^{16}$	0.80	0.18	0.0000
<b>F150LP</b>	1610.7	0.0038	22.45	$2.27 \times 10^{16}$	0.81	0.19	0.0000
<b>F165LP</b>	1757.9	0.0010	21.02	$7.30 \times 10^{15}$	0.83	0.22	0.0000
<b>PR110L</b>	1429.4	0.0120	23.69	$5.62 \times 10^{16}$	0.81	0.19	0.0129
<b>PR130L</b>	1438.8	0.0119	23.68	$5.65 \times 10^{16}$	0.81	0.19	0.0027

In each Table, the following quantities are listed:

- The pivot wavelength, a source-independent measure of the characteristic wavelength of the bandpass, defined such that it is the same if the input spectrum is in units of  $f\lambda$  or  $f\nu$ :

$$\lambda_p = \sqrt{\frac{\int Q(\lambda) T(\lambda) d\lambda}{\int Q(\lambda) T(\lambda) ((d\lambda)/\lambda)}}$$

- The integral  $\int Q_\lambda T_\lambda d\lambda/\lambda$ , used to determine the count rate when given the astronomical magnitude of the source.
- The ABmag zero point, defined as the AB magnitude of a source with a constant  $F_\nu$  source that gives 1 count/sec with the specified configuration
- The sensitivity integral, defined as the count rate that would be observed from a constant  $F_\lambda$  source with flux  $1 \text{ erg cm}^{-2} \text{ s}^{-1} \text{ \AA}^{-1}$ .
- The encircled energy, defined as the fraction of PSF flux enclosed in the default photometry aperture (5×5 pixels for the WFC, 9×9 pixels for the HRC, and 15×15 pixels for the SBC)
- The fraction of PSF flux in the central pixel, useful for determining the peak count rate to check for overflow or bright object protection possibilities
- The sky background count rate, which is the count rate that would be measured with average zodiacal background, and average earthshine. It does not include the contribution from the detectors, tabulated separately in Table 6.4.

Here, we describe how to determine two quantities:

1. The counts  $\text{sec}^{-1}$  ( $C$ ) from your source over some selected area of  $N_{\text{pix}}$  pixels, where a signal of an electron on a CCD is equivalent to one count.
2. The peak counts  $\text{sec}^{-1} \text{ pixel}^{-1}$  ( $P_{\text{cr}}$ ) from your source, which is useful for avoiding saturated CCD exposures and for assuring that SBC observations do not exceed the bright-object limits.

We consider the cases of point sources and diffuse sources separately in each of the imaging and spectroscopy sections following.



## 6.2.1 Imaging

### Point Source

For a point source, the count rate,  $C$ , can be expressed as the integral over the bandpass of the filter:

$$C = A \int F_{\lambda} \frac{\lambda}{hc} Q_{\lambda} T_{\lambda} \epsilon_f d\lambda = \int F_{\lambda} S_{\lambda} \epsilon_f d\lambda$$

Where:

- $A$  is the area of the unobstructed 2.4 meter telescope (i.e., 45,239 cm<sup>2</sup>)
- $F_{\lambda}$  is the flux from the astronomical source in erg sec<sup>-1</sup>cm<sup>-2</sup>Å<sup>-1</sup>
- $h$  is Planck's constant
- $c$  is the speed of light
- The factor  $\lambda/hc$  converts ergs to photons.
- $Q_{\lambda}T_{\lambda}$  is the system fractional throughput, i.e. the probability of detecting a count per incident photon, including losses due to obstructions of the full 2.4 m OTA aperture. It is specified this way to separate out the instrument sensitivity  $Q_{\lambda}$  and the filter transmission  $T_{\lambda}$ .
- $\epsilon_f$  = the fraction of the point source energy encircled within  $N_{pix}$  pixels.
- $S_{\lambda}$  is the total imaging point source sensitivity with units of counts sec<sup>-1</sup> Å<sup>-1</sup> per incident erg sec<sup>-1</sup>cm<sup>-2</sup>Å<sup>-1</sup>.

The peak counts sec<sup>-1</sup> pixel<sup>-1</sup> from the point source, is given by:

$$C_{peak} = \int F_{\lambda} S_{\lambda} \epsilon_f(1) d\lambda$$

Where:

- $F_{\lambda}$ , and  $S_{\lambda}$  are as above.
- $\epsilon_f(1)$  is the fraction of energy encircled within the peak pixel.

Again, the integral is over the bandpass.

If the flux from your source can be approximated by a flat continuum ( $F_{\lambda}$  = constant) and  $\epsilon_f$  is roughly constant over the bandpass, then:

$$C = F_{\lambda} \epsilon_f \int S_{\lambda} d\lambda$$

We can now define an equivalent bandpass of the filter ( $B_{\lambda}$ ) such that:

$$\int S_{\lambda} d\lambda = S_{peak} B_{\lambda}$$

Where:

- $S_{peak}$  is the peak sensitivity.
- $B_\lambda$  is the effective bandpass of the filter.

The count rate from the source can now be written as:

$$C = F_\lambda \epsilon_f S_{peak} B_\lambda$$

In Tables 6.1–6.3, we give the value of  $\int S_\lambda d\lambda$  for each of the filters. Alternatively, we can write the equation in terms of V magnitudes:

$$C = 2.5 \times 10^{11} \epsilon_f \left( \int QT d\lambda / \lambda \right) \times 10^{-0.4(V + AB_v)}$$

where V is the visual magnitude of the source, the quantity under the integral sign is the mean sensitivity of the detector+filter combination and is tabulated in Tables 6.1–6.3, and  $AB_v$  is the filter-dependent correction for the deviation of the source spectrum from a constant  $F_v$  spectrum. This latter quantity is tabulated for several different astronomical spectra in Tables 10.1 to 10.3 in Chapter 10.

### Diffuse Source

For a diffuse source, the count rate,  $C$ , per pixel, due to the astronomical source can be expressed as:

$$C = \int I_\lambda S_\lambda m_x m_y d\lambda$$

Where:

- $I_\lambda$  = the surface brightness of the astronomical source, in  $\text{erg sec}^{-1} \text{cm}^{-2} \text{\AA}^{-1} \text{arcsec}^{-2}$ .
- $S_\lambda$  as above.
- $m_x$  and  $m_y$  are the plate scales along orthogonal axes.

### Emission Line Source

For a source where the flux is dominated by a single emission line, the count rate can be calculated from the equation

$$C = 2.23 \times 10^{12} \cdot (QT)_\lambda \cdot F(\lambda) \cdot \lambda$$

where  $C$  is the observed count rate in counts/sec,  $(QT)$  is the system throughput at the wavelength of the emission line,  $F(\lambda)$  is the emission line flux in units of  $\text{erg cm}^{-2} \text{s}^{-1}$ , and  $\lambda$  is the wavelength of the emission line in Angstroms.  $(QT)_\lambda$  can be determined by inspection of the plots in Chapter 10. See Section 6.6.4 for an example of emission-line imaging using ACS.

## 6.2.2 Spectroscopy

### Point Source

For a point source spectrum with a **continuum flux distribution**, the count rate,  $C$ , is per pixel in the dispersion direction and is integrated over a fixed extraction height  $N_{spix}$  in the spatial direction perpendicular to the dispersion:

$$C = F_{\lambda} S'_{\lambda} \epsilon'_{N_{spix}} = F_{\lambda} A \frac{\lambda}{hc} T_{\lambda} \epsilon'_{N_{spix}} d$$

Where:

- $S'_{\lambda}$  is the total point source sensitivity in units of counts  $\text{sec}^{-1}$  per incident  $\text{erg sec}^{-1} \text{cm}^{-2} \text{\AA}^{-1}$ ; and  $S_{\lambda} = S'_{\lambda} \cdot d$
- $d$  is the dispersion in  $\text{\AA}/\text{pix}$ .
- $\epsilon'_{N_{spix}}$  is the fraction of the point source energy within  $N_{spix}$  in the spatial direction.
- the other quantities are defined above.

For an **unresolved emission line** at  $\lambda = L$  with a flux of  $F_L$  in  $\text{erg sec}^{-1} \text{cm}^{-2}$  the total counts recorded over the  $N_{spix}$  extraction height is:

$$C = F_{\lambda} S'_{\lambda} / d$$

These counts will be distributed over pixels in the wavelength direction according to the instrumental line spread function.

In contrast to the case of imaging, sensitivity  $S_{\lambda}$ , the spectroscopic point source sensitivity calibration ( $S_{\lambda} \times \epsilon_{N_{spix}}$ ) for a default extraction height of  $N_{spix}$  is measured directly from observations of stellar flux standards after insertion of ACS into HST. Therefore, the accuracy in laboratory determinations of  $T_{\lambda}$  for the ACS prisms and grisms is NOT crucial to the final accuracy of their sensitivity calibrations.

The peak counts  $\text{sec}^{-1} \text{pixel}^{-1}$  from the point source, is given by:

$$P_{cr} = \epsilon'_f(1) F_{\lambda} S'_{\lambda}$$

Where:

- $\epsilon'_f(1)$  is the fraction of energy contained within the peak pixel.
- the other quantities are as above.

## 6.3 Computing Exposure Times

To derive the exposure time to achieve a given signal-to-noise ratio, or to derive the signal-to-noise ratio in a given exposure time, there are four principal ingredients:

- Expected counts  $C$  from your source over some area.
- The area (in pixels) over which those counts are received ( $N_{pix}$ ).
- Sky background ( $B_{sky}$ ) in counts  $\text{pixel}^{-1} \text{sec}^{-1}$ .
- The detector background, or dark, ( $B_{det}$ ) in counts  $\text{sec}^{-1} \text{pixel}^{-1}$  and the read noise ( $R$ ) in counts of the CCD.
- Section 6.4 provides the information for determining the sky-plus-detector background.

### 6.3.1 Calculating Exposure Times for a Given Signal-to-Noise

The signal-to-noise ratio,  $\Sigma$  is given by:

$$\Sigma = \frac{Ct}{\sqrt{Ct + N_{pix}(B_{sky} + B_{det})t + N_{pix}N_{read}R^2}}$$

Where:

- $C$  = the signal from the astronomical source in counts  $\text{sec}^{-1}$ , or electrons  $\text{sec}^{-1}$  from the CCD. The actual output signal from a CCD is  $C/G$  where  $G$  is the gain. You must remember to multiply by  $G$  to compute photon events in the raw CCD images.
- $G$  = the gain is always 1 for the SBC and  $\sim 1, 2, 4$  or  $8$  for the CCDs, depending on **GAIN**.
- $N_{pix}$  = the total number of detector pixels integrated over to achieve  $C$ .
- $B_{sky}$  = the sky background in counts  $\text{sec}^{-1} \text{pixel}^{-1}$ .
- $B_{det}$  = the detector dark current in counts  $\text{sec}^{-1} \text{pixel}^{-1}$ .
- $R$  = the read noise in electrons; = 0 for SBC observations, 5.0 and 4.7 for WFC and HRC respectively
- $N_{read}$  = the number of CCD readouts.
- $t$  = the integration time in seconds.

This equation assumes the optimistic (and often realistic) condition that the background zero point level under the object is sufficiently well known (and subtracted) to not significantly contribute; in crowded fields this may not be true.

Observers using the CCD normally take sufficiently long integrations that the CCD read noise is not important. This condition is met when:

$$Ct + N_{pix}(B_{sky} + B_{det})t > 2N_{pix}N_{read}R^2$$

For the CCD in the regime where read noise is not important and for all SBC observations, the integration time to reach a signal-to-noise ratio  $\Sigma$ , is given by:

$$t = \frac{\Sigma^2 [C + N_{pix}(B_{sky} + B_{det})]}{C^2}$$

If your source count rate is much brighter than the sky plus detector backgrounds, then this expression reduces further to:

$$t = \frac{\Sigma^2}{C}$$

i.e. the usual result for Poisson statistics of  $\Sigma = \sqrt{totalcounts}$ .

More generally, the required integration time to reach a signal to noise ratio  $\Sigma$  is given by:

$$t = \frac{\Sigma^2 [C + N_{pix}(B_{sky} + B_{det})] + \sqrt{\Sigma^4 [C + N_{pix}(B_{sky} + B_{det})]^2 + 4\Sigma^2 C^2 [N_{pix}N_{read}R^2]}}{2C^2}$$

---

## 6.4 Detector and Sky Backgrounds

When calculating expected signal-to-noise ratios or exposure times, the background from the sky and the background from the detector must be taken into account.

### 6.4.1 Detector Backgrounds

Table 6.4 shows the read-noise and dark-current characteristics of the detectors. See Table 7.3 for further details including variations by amplifier and GAIN for the CCDs.

Table 6.4: Detector Backgrounds

	WFC	HRC	SBC
Read noise (electrons pix <sup>-1</sup> )	~5	~4.7	0
Dark current (electrons sec <sup>-1</sup> pix <sup>-1</sup> )	2.2×10 <sup>-3</sup>	2.5×10 <sup>-3</sup>	1.2×10 <sup>-5</sup>

### 6.4.2 Sky Background

The sources of sky background which will affect ACS observations include:

- Earth shine (ES).
- Zodiacal light (ZL).
- Geocoronal emission (GC).

The background in counts sec<sup>-1</sup> pixel<sup>-1</sup> for **imaging observations** can be computed as:

$$B_{sky} = \int I_{\lambda} S_{\lambda} m_x m_y d\lambda$$

Where:

- $I_{\lambda}$  is the surface brightness of the sky background, in erg sec<sup>-1</sup> cm<sup>-2</sup> Å<sup>-1</sup> arcsec<sup>-2</sup>.
- $S_{\lambda}$  is the point source sensitivity for the imaging mode.
- $m_x$  and  $m_y$  are the plate scales along orthogonal axes.

The image of the sky through a disperser is not uniform, since some wavelengths fall off the detector for regions of sky near the edge of the field of view (FOV). Since the ACS grism spectra are of order 200 pixels long, the regions of lower sky will be strips at the long and short wavelength edges of the FOV. The maximum width of the strips from where the signal starts to decline to the edge, where the signal is down by roughly 2X, is about half the total length of a spectrum of a point source, i.e. roughly 100 pixels in the case of a sky background with a **continuum** of wavelengths. In the case of the HRC, the sky for the dispersed mode will not have the low background strips, since the FOV is not masked to the detector size. These small strips of lower sky background in the SBC and the WFC are ignored in the following formulae. Furthermore in the SBC and the WFC, since the spectra do not lie along the direction of the anamorphic distortion,

the plate scales of  $m_x$  and  $m_y$  above must be replaced by the plate scales  $m_s$  and  $m_\lambda$  in the orthogonal spatial and dispersion directions, respectively. Interior to the strips, a point on the detector sees a region of sky over the full wavelength coverage of the disperser. Thus, for **spectroscopic observations**:

$$B_{sky}^\lambda = \int I_\lambda S'_\lambda m_s m_\lambda d\lambda$$

For a **monochromatic** sky emission line at  $\lambda = L$  like Lyman- $\alpha$ , which will dominate the background through the LiF prism:

$$B_{sky}^\lambda = I_L S'_\lambda m_s m_\lambda / d$$

where

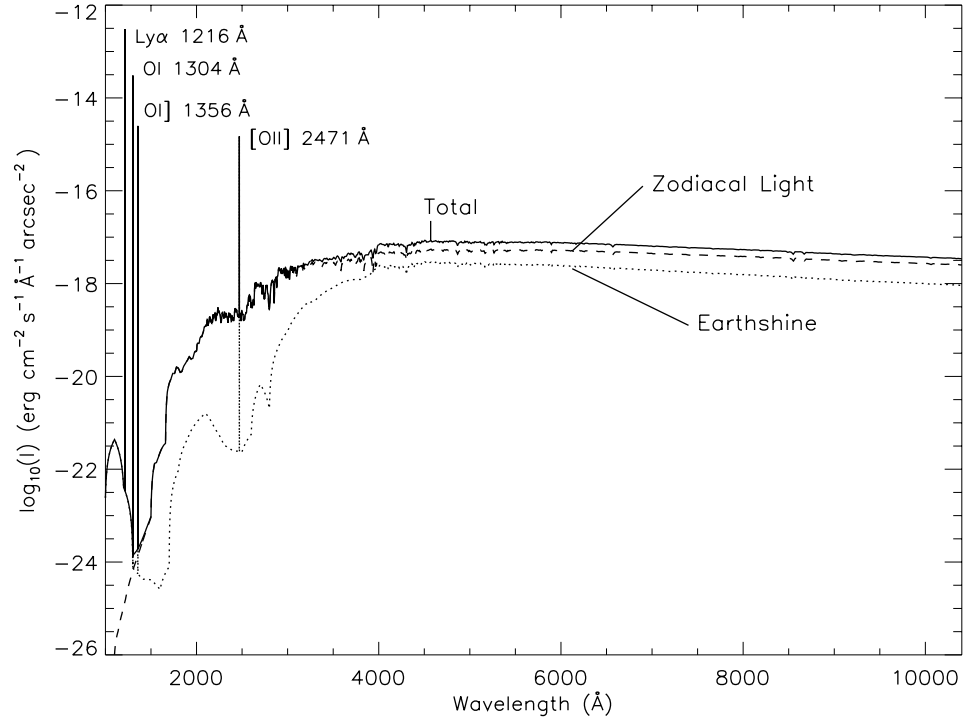
- $I_L$  is the monochromatic intensity of a line at wavelength  $L$  in  $\text{erg sec}^{-1} \text{cm}^{-2} \text{arcsec}^{-2}$ .

The total sky background is:

$$B_{sky} = B_{sky}^\lambda + B_{sky}^L$$

Figure 6.1 and Table 6.7 show high sky background intensity as a function of wavelength, identifying the separate components which contribute to the background. The “shadow” and “average” values of the Earthshine contribution in the ACS Exposure Time Calculator correspond, respectively, to 0 and 50% of the “high” values in Figure 6.1 and Table 6.7. For the zodiacal sky background, the values in Table 6.7 correspond to the typical value of  $m_V = 22.7$  from Table 6.5, while the “low” and “high” zodiacal light is scaled to  $m_V = 23.3$  and 22.1, respectively.

Figure 6.1: High Sky Background Intensity as a Function of Wavelength. The zodiacal contribution (ZL) is at ecliptic latitude and longitude of 30,180 degrees, and corresponds to  $m_v = 22.7$  per square arcsec. The Earthshine (ES) is for a target which is 24 degrees from the limb of the sunlit Earth. Use Figure 6.2 to estimate background contributions at other angles. The daytime geo-coronal line intensities are in  $\text{erg cm}^{-2} \text{s}^{-1} \text{arcsec}^{-2}$  (see Table 6.6).



### Background Variations and LOW-SKY

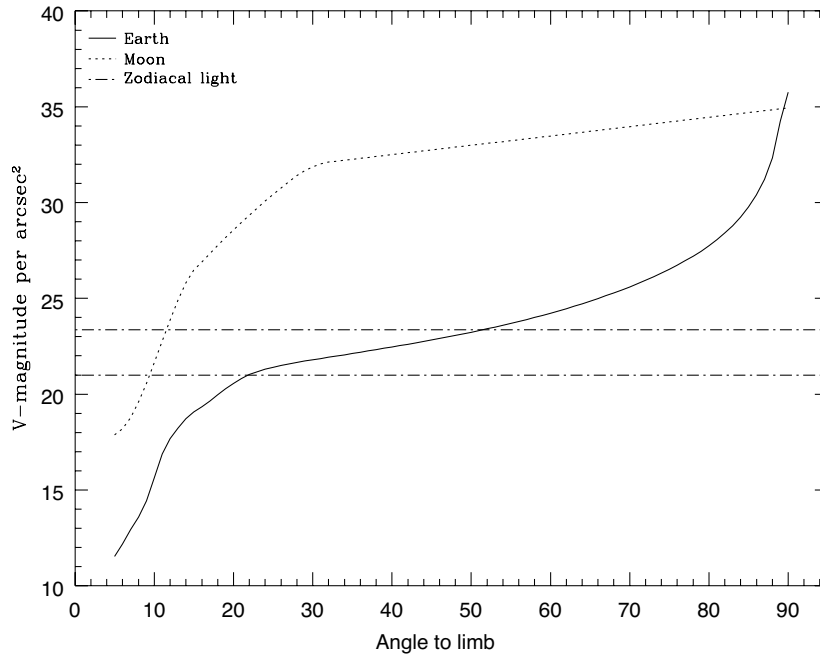
In the ultraviolet, the background contains bright airglow lines, which vary from day to night and as a function of HST orbital position. The airglow lines may be the dominant sky contributions in the UV both for imaging-mode and spectroscopic observations. Away from the airglow lines, at wavelengths shortward of  $\sim 3000 \text{ Å}$ , the background is dominated by zodiacal light, where the small area of sky that corresponds to a pixel of the high resolution HST instrumentation usually produces a signal that is much lower than the intrinsic detector background. The contribution of zodiacal light does not vary dramatically with time and varies by only a factor of about three throughout most of the sky. Table 6.5 gives the variation of the zodiacal background as a function of ecliptic latitude and longitude. For a target near ecliptic coordinates of (50,0) or (-50,0), the zodiacal light is relatively bright at  $m_v=20.9$ , i.e. about 9 times the faintest values of  $m_v=23.3$ . Deep imaging applications must carefully consider expected sky values!

On the other hand, Earthshine varies strongly depending on the angle between the target and the bright Earth limb. The variation of the Earthshine as a function of limb angle from the sunlit Earth is shown in Figure 6.2. The Figure also shows the contribution of the moon, which is



typically much smaller than the zodiacal contribution, for which the upper and lower limits are shown. For reference, the limb angle is approximately  $24^\circ$  when the HST is aligned toward its orbit pole (i.e., the center of the CVZ). The Earthshine contribution shown in Figure 6.1 and Table 6.7 corresponds to this position.

Figure 6.2: Background Contributions in V Magnitude per arcsec<sup>2</sup> due to the zodiacal light, Moon, and the Sunlit Earth as a Function of Angle Between the Target and the Limb of the Earth or Moon. The two zodiacal light lines show the extremes of possible values.



For observations taken longward of  $3500 \text{ \AA}$ , the Earthshine dominates the background at small ( $<22^\circ$ ) limb angles. In fact, the background increases exponentially for limb angles  $<22^\circ$ . The background near the bright limb can also vary by a factor of  $\sim 2$  on timescales as short as two minutes, which suggests that the background from Earthshine also depends upon the reflectivity of the terrain over which HST passes during the course of an exposure. Details of the sky background as it affects ACS, as well as STIS, are discussed by Shaw et al. (STIS ISR 98-21).

Table 6.5: Approximate Zodiacal Sky Background at V as a Function of ecliptic latitude and ecliptic longitude (in V magnitudes per square arcsec)

Ecliptic Longitude (deg)	Ecliptic Latitude (deg)			
	0	30	60	90
180	22.1	22.7	23.2	23.3
145	22.4	22.9	23.3	23.3
110	22.3	22.9	23.3	23.3
50	20.9	22.2	22.9	23.3

Observations of the faintest objects may need the special requirement **LOW-SKY** in the Phase II observing program. **LOW-SKY** observations are scheduled during the part of the year when the zodiacal background light is no more than 30% greater than the minimum possible zodiacal light for the given sky position. **LOW-SKY** in the Phase II scheduling also invokes the restriction that exposures will be taken only at angles greater than 40 degrees from the bright Earth limb to minimize Earthshine and the UV airglow lines. The **LOW-SKY** special requirement limits the times at which targets within 60 degrees of the ecliptic plane will schedule, and limits visibility to about 48 minutes per orbit.

The ETC provides the user with the flexibility to separately adjust both the zodiacal (low, average, high) and Earthshine (shadow, average, high) sky background components in order to determine if planning for use of **LOW-SKY** is advisable for a given program. However, the absolute sky levels that can be specified in the ETC may not be achievable for a given target; e.g., as shown in Table 6.5 the zodiacal background minimum for an ecliptic target is  $m_v = 22.4$  which is still brighter than both the low and average options with the ETC. By contrast, a target near the ecliptic pole would always have a zodiacal=low background in the ETC. The user is cautioned to carefully consider sky levels as the backgrounds obtained in HST observations can cover significant ranges.

### Geocoronal Emission and Shadow

Background due to geocoronal emission originates mainly from hydrogen and oxygen atoms in the exosphere of the Earth. The emission is concentrated in the four lines listed in Table 6.6. The brightest line is Lyman- $\alpha$  at 1216Å. The strength of the Lyman- $\alpha$  line varies between about 2 and 30 kilo-Rayleighs (i.e., between  $6.1 \times 10^{-14}$  and  $9.2 \times 10^{-13}$  erg  $\text{sec}^{-1} \text{cm}^{-2} \text{arcsec}^{-2}$  where 1 Rayleigh =  $10^6$  photons  $\text{sec}^{-1} \text{cm}^{-2}$  per  $4\pi$  steradian) depending on the position of HST with respect to the day-night terminator and the position of the target relative to the Earth limb. The next strongest line is the OI line at 1302 Å, which rarely exceeds 10% of Lyman- $\alpha$ . The typical strength of the OI 1302 Å line is about 2

kilo-Rayleighs (which corresponds to about  $5.7 \times 10^{-14} \text{ erg sec}^{-1} \text{ cm}^{-2} \text{ sec}^{-1} \text{ arcsec}^{-2}$ ) on the daylight side and about 150 times fainter on the night side of the HST orbit. OI 1356 Å and OI 2470 Å lines may appear in observations on the daylight side of the orbit, but these lines are at least 3 times weaker than the OI 1302 Å line. The width of the lines also vary with temperature, the line widths given in Table 6.6 are representative values assuming a temperature of 2000 K.

Except for the brightest objects (e.g. planets), a filter or prism mode which does not transmit at Lyman- $\alpha$  should be employed. To minimize geocoronal emission the special requirement SHADOW can be requested. Exposures using this special requirement are limited to roughly 25 minutes per orbit, exclusive of the guide-star acquisition (or reacquisition) and can be scheduled only during a small percentage of the year. SHADOW reduces the contribution from the geocoronal emission lines by roughly a factor of ten while the continuum Earthshine is set to zero. SHADOW requirements must be included in your Phase I proposal (see the Call for Proposals).

Table 6.6: Geocoronal emission lines

Wavelength (Å)	ID	Line Width (Å)	Intensity			
			Day		Night	
			kilo- Rayleighs	$\text{erg s}^{-1} \text{ cm}^{-2} \text{ arcsec}^{-2}$	kilo- Rayleighs	$\text{erg s}^{-1} \text{ cm}^{-2} \text{ arcsec}^{-2}$
1216	Ly- $\alpha$	0.04	~20	$6.1 \times 10^{-13}$	2	$6.1 \times 10^{-14}$
1302	OI	0.013	~2	$5.7 \times 10^{-14}$	0.013	$3.8 \times 10^{-16}$
1356	OI	0.013	~0.2	$\sim 5 \times 10^{-15}$	~0.001	$\sim 3 \times 10^{-17}$
2470	OI	0.023	< 0.2	$< 3 \times 10^{-15}$	< 0.001	$< 1.5 \times 10^{-17}$

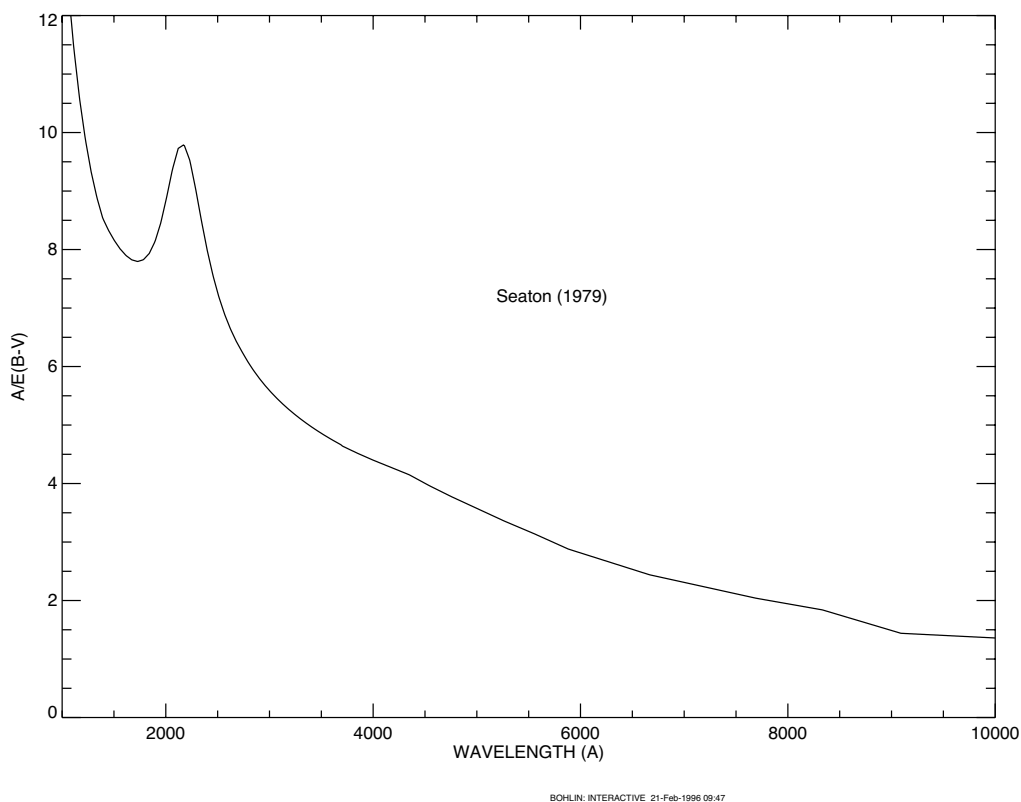
## 6.5 Extinction Correction

Extinction can dramatically reduce the counts expected from your source, particularly in the ultraviolet. Figure 6.3 shows the average  $A_v / E(B - V)$  values for our galaxy, taken from (Seaton, *MNRAS*, **187**, 73P, 1979). Large variations about the average are observed (Witt, Bohlin, Stecher, *ApJ*, **279**, 698, 1984).

Extinction curves have a strong metallicity dependence, particularly in the UV wavelengths. Sample extinction curves can be seen in Koornneef and Code, *ApJ*, **247**, 860 1981 (LMC); Bouchet et al., *A&A*, **149**, 330 1985 (SMC); and Calzetti, Kinney and Storchi-Bergmann, *ApJ*, **429**, 582, 1994, and references therein. At lower metallicities, the 2200Å bump which is so

prominent in the galactic extinction curve disappears; and  $A_V / E(B - V)$  may increase monotonically at UV wavelengths.

Figure 6.3: Extinction versus Wavelength



## 6.6 Exposure-Time Examples

In the following you will find a set of examples for the three different channels and for different types of sources. The examples were chosen in order to present typical objects for the three channels and also to present interesting cases as they may arise with the use of ACS.

### 6.6.1 Example 1: WFC imaging a faint point source

What is the exposure time needed to obtain a signal to noise of 10 for a point source of spectral type F5V, normalized to  $V=26.5$ , when using the WFC, F555W filter? Assume a GAIN of 1 and a photometry box size of 11x11 pixels, and average sky values.

The ACS Exposure Time Calculator (ETC) gives a total exposure time of 6124s to obtain this S/N in a single exposure. Since such an exposure would be riddled with cosmic rays and essentially useless, it is necessary to

specify how many exposures to split the observation into. ACS WFC observations generally should be split if the exposure time is larger than about 5 minutes, but for multi-orbit observations, splitting into 2 exposures per orbit is generally sufficient.

For a typical object visibility of 53 minutes, after applying the requisite overheads, there is time for two 1200s exposures per orbit. The required exposure time can thus be reached in 5 exposures, but re-running the ETC using `CR-SPLIT=5` raises the required exposure time to 7052s (because of the extra noise introduced by the four extra readouts). To achieve the required exposure time would require `CR-SPLIT=6`, or three orbits.

Using the pencil and paper method, Table 6.1 gives the integral  $QTd\lambda/\lambda$  as 0.0776, and the  $AB_v$  correction term can be retrieved from Table 10.1 as 0.043. According to Figure 4.10, a circular aperture of radius 0.3 arcsec (which has an area of 116 pixels, close to the 121 pixel box specified) encloses about 90% of the light from a star. The count rate is then  $2.5 \times 10^{11} * 0.0776 * 0.9 * 10^{-0.4(26.5+0.043)} = 0.421$  counts/sec, which agrees with the ETC-returned value of 0.422. The exposure time can then be found by using the equation

$$t = \frac{\Sigma^2 [C + N_{pix}(B_{sky} + B_{det})]}{C^2}$$

to give  $t=5835s$ , which is close to the ETC-derived value of 6124s. We have inserted the background rate from Table 6.1 ( $B_{sky}=0.055$ ) and Table 6.4 ( $B_{det}=0.002$ ) and assumed that the noise on the background is much greater than the readout noise.

Note that this can be greatly shortened by specifying a smaller analysis box (for example, 5x5) and using `LOW-SKY`. Dropping the aperture size to 5x5 at average sky which still encloses 83% of the light requires 1830s. Including both the smaller 5x5 box and `LOW-SKY` (Zodiacal=LOW, Earthshine=AVERAGE) using the ETC gives the required exposure time as only 1608s (using `CR-SPLIT=1`), or 1806s with `CR-SPLIT=2`. The `LOW-SKY` visibility per orbit is 47 minutes, which allows a total on-target exposure time of 2000s in one orbit with `CR-SPLIT=2`.

Note also that the count rate from WFPC2 would be 0.167 electrons/sec, a factor of 2.2 lower.

### 6.6.2 Example 2: SBC Objective prism spectrum of a UV spectrophotometric standard star

What is the peak count rate using the PR110L prism in the SBC for the HST standard star HS2027+0651 ( $V=16.9$ ) that was used for the STIS prism calibration (this spectrum is not in the ETC list, therefore we quote below the flux which could be found by dearchiving the STIS spectrum)?

The sensitivity peaks in the 1500-1600Å region. To find the count rate at 1537Å, inspection of Figure 5.22 gives the sensitivity of  $9.6 \times 10^{14}$  counts/sec per  $\text{erg}/\text{cm}^2/\text{s}/\text{Å}$ . Multiplying by the stellar flux of  $5.8 \times 10^{-14}$  gives 55.7 counts/sec, summed in the cross dispersion direction. For the fraction of light in the central pixel  $\epsilon=0.31$ , the brightest pixel at 1500Å is 17.3 counts/sec/pixel, well below the bright object limit.

The SBC has no readout noise, and the dark current rate is negligible, while the main sky contribution for PR110L is from Lyman- $\alpha$ . For daytime Ly- $\alpha$  intensity of  $20\text{kR}=6.1 \times 10^{-13} \text{ erg cm}^{-2} \text{ s}^{-1} \text{ arcsec}^{-2}$ ,  $S'=1.7 \times 10^{14}$  and  $d$ , the dispersion in Å/pixel, is 2.58. Therefore, the background count rate is  $6.1 \times 10^{-13} * 1.7 \times 10^{14} * 0.032^2 / 2.58 = 0.041$  counts/sec/pixel. This value varies somewhat over the field, as the plate scale varies from the nominal 0.032 arcsec/pixel. For faint source spectroscopy, it is better to use PR130L, which is on a  $\text{CaF}_2$  substrate to block Ly- $\alpha$ .

### 6.6.3 Example 3: WFC VIS Polarimetry of the jet of M87

What signal to noise ratio is reached in three one orbit exposures (~2400s each) for M87, when using the WFC, F555W for one orbit each in the three VIS polarizers? Gain is 2, box size is 5x5 pixels, CR-SPLIT=2 and average sky.

If the M87 jet region has  $\mu_V=17$  mag/square arcsec, using the ETC with a flat continuum spectral distribution and an exposure time of 2400s (CR-SPLIT=2), gives  $S/N=128$  for an observation with each VIS polarizer filter (which is an average of the polarizer at the 3 available position angles  $0^\circ$ ,  $60^\circ$  and  $120^\circ$ ). If the polarization  $P$  is 20%, then  $P*S/N = 25.6$ , so using

$$\log\left(\frac{\sigma_P}{P}\right) = -0.102 - 0.9898 \log(P \langle S/N \rangle_i)$$

from Chapter 5,  $\sigma_P/P = 0.032$ , or  $\sigma_P=0.016$ , which is the error on the fractional polarization. The error on the position angle should be  $1.0^\circ$  using the formula, again from Chapter 5, of

$$\log \sigma_\theta = 1.514 - 1.068 \log(P \langle S/N \rangle_i)$$

### 6.6.4 Example 4: SBC imaging of Jupiter's aurora at Lyman-alpha

What signal to noise ratio is reached in a one orbit exposure (2000s) observing Jupiter's aurora in Ly- $\alpha$  using the SBC and F122M filter?

The equation from the Section , “Emission Line Source,” on page 102 can be used to calculate the expected count rate. The aurora is variable, up to ~100kR. The value of (QT) for the SBC+F122M filter at 1216Å is 0.009, from inspection of Figure 10.106 on page 224. For a surface brightness of 40kR =  $1.22 \times 10^{-12}$  erg cm<sup>-2</sup> s<sup>-1</sup> arcsec<sup>-2</sup> (See “Geocoronal Emission and Shadow” on page 110. for conversion), the total counts per pixel are approximately  $2.23 \times 10^{12} \times 0.009 \times 1.22 \times 10^{-12} \times 1216 \times (0.032)^2 \times 2000 = 61.0$  counts. The background contributions are the detector dark of  $1.2 \times 10^{-5}$  counts/pixel/sec (which can be ignored in this case) and a sky background which is dominated by geocoronal Lyman- $\alpha$ . During the daytime, the geocoronal background is 20kR, or 30.5 counts, while at night the background drops to one tenth of this, or 3.05 counts.

Finally, we calculate the signal to noise ratio  $\Sigma$  for a 2x2 pixel resolution element: in the daytime,  $\Sigma = 61.0 \cdot 4 / \sqrt{(61.0 + 30.5) \cdot 4} = 12.7$ , while at night,  $\Sigma = 61.0 \cdot 4 / \sqrt{(61.0 + 3.05) \cdot 4} = 15.2$

### 6.6.5 Example 5: Coronagraphic imaging of the Beta-Pictoris disk

In the final example we shall consider the case where we are trying to determine the S/N achieved on the Beta Pictoris disk, assuming a disk surface brightness of R magnitude of 16 arcsec<sup>-2</sup> at a distance of 6 arcsec from the central star with a V magnitude of 3.9, for an exposure time of 1000 seconds with an F435W filter. Assume that the star and disk have an A5V-type spectrum. Using the ACS Exposure Time Calculator and considering the case for the 3.0" occulting mask:

- Disk count rate = 26.6 e<sup>-</sup>/sec for a 5x5 aperture (including 47.5% throughput of coronagraph) Sky count rate = 0.003 e<sup>-</sup>/sec/pixel, Detector dark rate = 0.0025 e<sup>-</sup>/sec/pixel
- In 1000s, this gives 26,600 e<sup>-</sup>/5x5 aperture in the disk region.
- Central star count rate =  $2.7 \times 10^8$  e<sup>-</sup>/sec for a 101x101 aperture (101x101 aperture used to estimate total integrated flux)
- At a distance 6 arcsec from the central star, the fraction of flux per square arcsec in the PSF wings is  $3.0 \times 10^{-6}$ .  
 $B_{\text{PSF}} = 2.7 \times 10^{11} \times 3.0 \times 10^{-6} = 8.1 \times 10^5$  e<sup>-</sup> per square arcsec. Over 25 pixels  $\times 0.025^2 \times 5^2 = 12600$ .
- The S/N in a 5x5 box is then  $26000 / \sqrt{26,600 + 12,600} = 134$ .

## 6.7 Tabular Sky Backgrounds

We provide a table of the *high* sky background numbers as plotted in Figure 6.1. See the text and the caption in Figure 6.1 for more details. These high sky values are defined as the earthshine at  $24^\circ$  from the limb and the high zodiacal light of  $m_V = 22.7$ .

Table 6.7: High Sky Backgrounds

Wavelength	Earthshine	Zodiacal Light	Total Background
$\text{\AA}$	$\text{erg sec}^{-1} \text{cm}^{-2} \text{\AA}^{-1} \text{arcsec}^{-2}$	$\text{erg sec}^{-1} \text{cm}^{-2} \text{\AA}^{-1} \text{arcsec}^{-2}$	$\text{erg sec}^{-1} \text{cm}^{-2} \text{\AA}^{-1} \text{arcsec}^{-2}$
1000.	1.32E-22	2.56E-28	1.32E-22
1100.	3.38E-22	1.37E-26	3.38E-22
1200.	8.25E-23	1.27E-25	8.26E-23
1400.	4.65E-25	2.68E-24	3.14E-24
1500.	3.97E-25	4.60E-23	4.64E-23
1600.	3.42E-25	3.32E-22	2.33E-22
1700.	1.24E-23	6.49E-21	6.50E-21
1800.	1.26E-22	1.35E-20	1.37E-20
1900.	4.69E-22	2.13E-20	2.18E-20
2000.	1.02E-21	4.22E-20	4.32E-20
2100.	1.42E-21	1.21E-19	1.22E-19
2200.	8.02E-22	2.00E-19	2.01E-19
2300.	3.73E-22	1.97E-19	1.97E-19
2400.	2.59E-22	2.14E-19	2.14E-19
2500.	2.80E-22	2.05E-19	2.06E-19
2600.	1.29E-21	4.73E-19	4.75E-19
2700.	5.42E-21	8.26E-19	8.31E-19
2800.	7.72E-21	7.48E-19	7.56E-19
2900.	4.43E-20	1.52E-18	1.56E-18
3000.	1.01E-19	1.72E-18	1.56E-18
3100.	2.12E-19	1.92E-18	2.14E-18
3200.	3.50E-19	2.24E-18	2.59E-18
3400.	6.39E-19	2.65E-18	3.28E-18



Table 6.7: High Sky Backgrounds (Continued)

Wavelength	Earthshine	Zodiacal Light	Total Background
$\text{\AA}$	$\text{erg sec}^{-1} \text{cm}^{-2}$ $\text{\AA}^{-1} \text{arcsec}^{-2}$	$\text{erg sec}^{-1} \text{cm}^{-2}$ $\text{\AA}^{-1} \text{arcsec}^{-2}$	$\text{erg sec}^{-1} \text{cm}^{-2}$ $\text{\AA}^{-1} \text{arcsec}^{-2}$
3500.	2.28E-19	1.92E-18	2.14E-18
3600.	1.05E-18	2.53E-18	3.50E-18
3700.	1.20E-18	3.03E-18	4.23E-18
3800.	1.26E-18	2.87E-18	4.13E-18
3900.	1.59E-18	2.83E-18	4.42E-18
4000.	2.33E-18	4.22E-18	6.55E-18
4250.	2.31E-18	4.42E-18	6.73E-18
4500.	2.70E-18	5.16E-18	7.86E-18
4750.	2.75E-18	5.23E-18	7.98E-18
5000.	2.65E-18	5.10E-18	7.75E-18
5250.	2.56E-18	5.02E-18	7.58E-18
5500.	2.55E-18	5.16E-18	7.71E-18
5750.	2.53E-18	5.25E-18	7.78E-18
6000.	2.43E-18	5.14E-18	7.57E-18
6250	2.31E-18	5.00E-18	7.31E-17
6500.	2.18E-18	4.80E-18	6.98E-18
6750.	2.08E-18	4.69E-18	6.77E-18
7000.	1.94E-18	4.48E-18	6.42E-18
7250.	1.83E-18	4.30E-18	6.13E-18
7500.	1.74E-18	4.13E-18	5.87E-18
7750.	1.64E-18	3.97E-18	5.62E-18
8000.	1.56E-18	3.83E-18	5.39E-18
8250.	1.48E-18	3.68E-18	5.15E-18
8500.	1.38E-18	3.47E-18	4.84E-18
8750.	1.30E-18	3.31E-18	4.61E-18



# Feasibility and Detector Performance

In this chapter. ..

7.1 The CCDs / 119
7.2 CCD Operations and Limitations / 126
7.3 The SBC MAMA / 131
7.4 SBC Operations and Limitations / 134
7.5 SBC Bright-Object Limits / 138

ACS employs two fundamentally different types of detectors: CCDs for use from the near UV to the near IR, and a Multi-Anode Microchannel Array detector, known as a MAMA, for use in the ultraviolet. The CCD and the MAMA detectors are used in different ways and impose their own unique limitations on the feasibility of observations performed with them. In this chapter we present the properties of the ACS detectors, describe how to use them to optimize scientific programs, and list the steps you should take to ensure the feasibility of your observations.

---

## 7.1 The CCDs

### 7.1.1 Detector Properties

#### WFC Properties

The WFC/CCD consists of two 2048×4096 charge-coupled devices that are sensitive from the near UV to the near IR. They are thinned,

backside-illuminated devices manufactured by Scientific Imaging Technologies (SITE). They are butted together along their long dimension to create an effective  $4096 \times 4096$  array with a gap corresponding to approximately 50 pixels between the chips.

As with STIS, the CCD camera design incorporates a warm dewar window, designed to prevent buildup of contaminants on the window, which were found to cause a loss of UV throughput for the WFPC2 CCDs. A summary of the ACS/CCDs' performance is given in Table 7.1. The performance values on read noise and dark current are those valid as of August 2002.

Table 7.1: ACS CCD Detector Performance Characteristics

Characteristic	WFC Performance	HRC Performance
Architecture	Thinned, backside illuminated anti-reflection coated multi-phase pinned	Thinned, backside illuminated anti-reflection coated multi-phase pinned
Wavelength range	3700–11000 Å	2000–11000 Å
Pixel format	2 butted 2048×4096	1024×1024
Field of view	202×202 arcsec	29×26 arcsec
Pixel size	15×15 μm	21×21 μm
Pixel plate scale	0.05 arcsec	0.027 arcsec
Quantum efficiency	~77% @ 4000 Å ~83% @ 6000 Å ~67% @ 8000 Å	~33% @ 2500 Å 69% @ 6000 Å ~53% @ 8000 Å
Dark count	~0.002 e <sup>-</sup> sec <sup>-1</sup> pix <sup>-1</sup>	0.0025 e <sup>-</sup> sec <sup>-1</sup> pix <sup>-1</sup>
Read noise	~5 e <sup>-</sup> rms	~4.7 e <sup>-</sup> rms
Full well	~ 84700 e <sup>-</sup>	~155000 e <sup>-</sup>
Gain (max. 65, 535 DN)	1, 2, 4 and 8 e <sup>-</sup> /dn	1, 2, 4 and 8 e <sup>-</sup> /dn

### HRC

The HRC CCD is a flight-spare STIS 1024×1024 CCD also manufactured by SITE. They are also thinned, backside-illuminated devices, but are coated using a process developed by SITE to provide good quantum efficiency in the near-ultraviolet. The performance characteristics and specifications are given in Table 7.1

## 7.1.2 CCD Spectral Response

### WFC

The spectral response of the unfiltered WFC CCD is shown in Figure 4.9. This figure illustrates the excellent quantum efficiency in the visible and near infrared part of the spectrum, along with the violet cutoff imposed by the silver coatings on the optical elements.

### HRC

The HRC spectral response is also shown in Figure 4.9. As well as excellent quantum efficiency in the visible and near-infrared part of the spectrum, the sensitivity in the near ultraviolet is improved over that of the STIS CCD by means of the coating.

## 7.1.3 Quantum Efficiency Hysteresis

Based on current data, the ACS CCDs do not suffer from Quantum Efficiency Hysteresis (QEH)—that is, the CCD responds in the same way to light levels over its whole dynamic range, irrespective of the previous illumination level.

## 7.1.4 CCD Long-Wavelength Fringing

Like most CCDs, the ACS CCDs exhibit fringing in the red, longward of  $\sim 7500 \text{ \AA}$ . The amplitude of the fringes is a strong function of wavelength and spectral resolution. At the time of writing we do not have good figures for the amplitude of the fringing, so it is difficult to assess the impact of fringing on astronomical observations.

The fringe pattern can be corrected by rectification with an appropriate flat field. The fringe pattern is a convolution of the contours of constant distance between the front and back surfaces of the CCD and the wavelength of the light on a particular part of the CCD. The fringe pattern has been shown to be very stable in similar devices, as long as the wavelength of light on a particular part of the CCD stays constant. In practice, this means that the fringe pattern is dependent on the spectrum of the light incident on the detector, with the sensitivity to the source spectrum a function of the bandwidth of the filter.

## 7.1.5 Optical Performance

Testing of the WFC and HRC optics and detectors, following fine alignment activities on-orbit, has shown that the optical quality objectives of the cameras are met. The encircled energy requirements for the ACS

channels are given in Table 7.2 The column labelled “measured” gives the value obtained from observations made in SMOV.

Table 7.2: Encircled energy requirements for the ACS channels

Channel	Encircled Energy		Measured
	Center of Field	Edge of Field	
WFC at 632.8nm in 0.25 arcsec diameter	> 75 percent Goal: > 80 percent	> 75 percent Goal: > 80 percent	80.0% center 79.4% edge
HRC at 632.8nm in 0.25 arcsec diameter	> 75 percent Goal: > 80 percent	> 75 percent Goal: > 80 percent	81.8% center 81.6% edge
SBC at 121.6nm in 0.10 arcsec diameter	> 30 percent Goal: > 30 percent	> 30 percent Goal: > 30 percent	28% center

## 7.1.6 Readout Format

### WFC

Each CCD chip is read out as a  $4144 \times 2068$  array, including physical and virtual overscans. This is made up of 24 columns of physical overscan, 4096 columns of pixel data and then 24 further columns of physical overscan. Each column consists of 2048 rows of pixel data followed by 20 rows of virtual overscan. The orientation of the chip is such that for the grism spectra, the dispersed images have wavelength increasing from left to right in the positive x-direction.

### HRC

The HRC chip is read out as a  $1062 \times 1044$  array, including physical and virtual overscans. There are 19 columns of physical overscan, followed by 1024 columns of pixel data and then 19 more columns of physical overscan. Each column consists of 1024 rows of pixel data followed by 20 rows of virtual overscan. As with WFC, the orientation of the chip was chosen so that grism images have wavelength increasing from left to right.

## 7.1.7 Analog-To-Digital Conversion

Electrons which accumulate in the CCD wells are read out and converted to data numbers (DN) by the analog-to-digital converter (ADC). The ADC output is a 16-bit number, producing a maximum of 65,535 DN in one pixel.

The CCDs are capable of operating at gains of 1, 2, 4 or 8  $e^-/\text{DN}$ . In principle, use of a lower gain value can increase the dynamic range of faint source observations by reducing the quantization noise; however, in practice this improvement is not significant. Table 7.3 shows the actual gain

levels and readout noise in electrons for the 4 WFC amps and the default C amp used for the HRC.

Table 7.3: CCD Gain and Readout Noise

Chip	Amp	Gain=1		Gain=2		Gain=4	
		Gain	Noise	Gain	Noise	Gain	Noise
WFC1	A	1.000	4.99	2.018	5.28	---	---
WFC1	B	0.972	4.89	1.960	5.12	---	---
WFC2	C	1.011	5.16	2.044	5.42	---	---
WFC2	D	1.018	4.82	2.010	5.15	---	---
HRC	C	1.185	4.55	2.216	4.71	4.289	5.94

For the WFC, gain factors of 1 and 2 are fully supported, and so are gain values of 2 and 4 for the HRC. The remaining two gain factors for each camera are available but unsupported, i.e. users of the latter modes must plan their own calibration. It is worth noticing that, for the WFC, the readout noise associated with GAIN=2 is on average only 0.28 e<sup>-</sup> higher per amplifier than that of GAIN=1. The noise increase brought about by the use of GAIN=2 is equivalent to that produced by adding a mere 1.7 e<sup>-</sup> of noise in quadrature to the noise of the GAIN=1 configuration: when the number of detected photons is larger than 3, the Poisson noise alone on the combination of source and sky would exceed this level. Thus, in terms of readout noise, the advantage of using GAIN=1 is minimal, whereas by adopting the higher gain value one would extend by 0.32 magnitude the ability of doing accurate photometry before saturation, would increase the number of bright unsaturated sources to provide cross-image registration and, for point sources, could perform photometry several magnitudes beyond saturation in some cases.

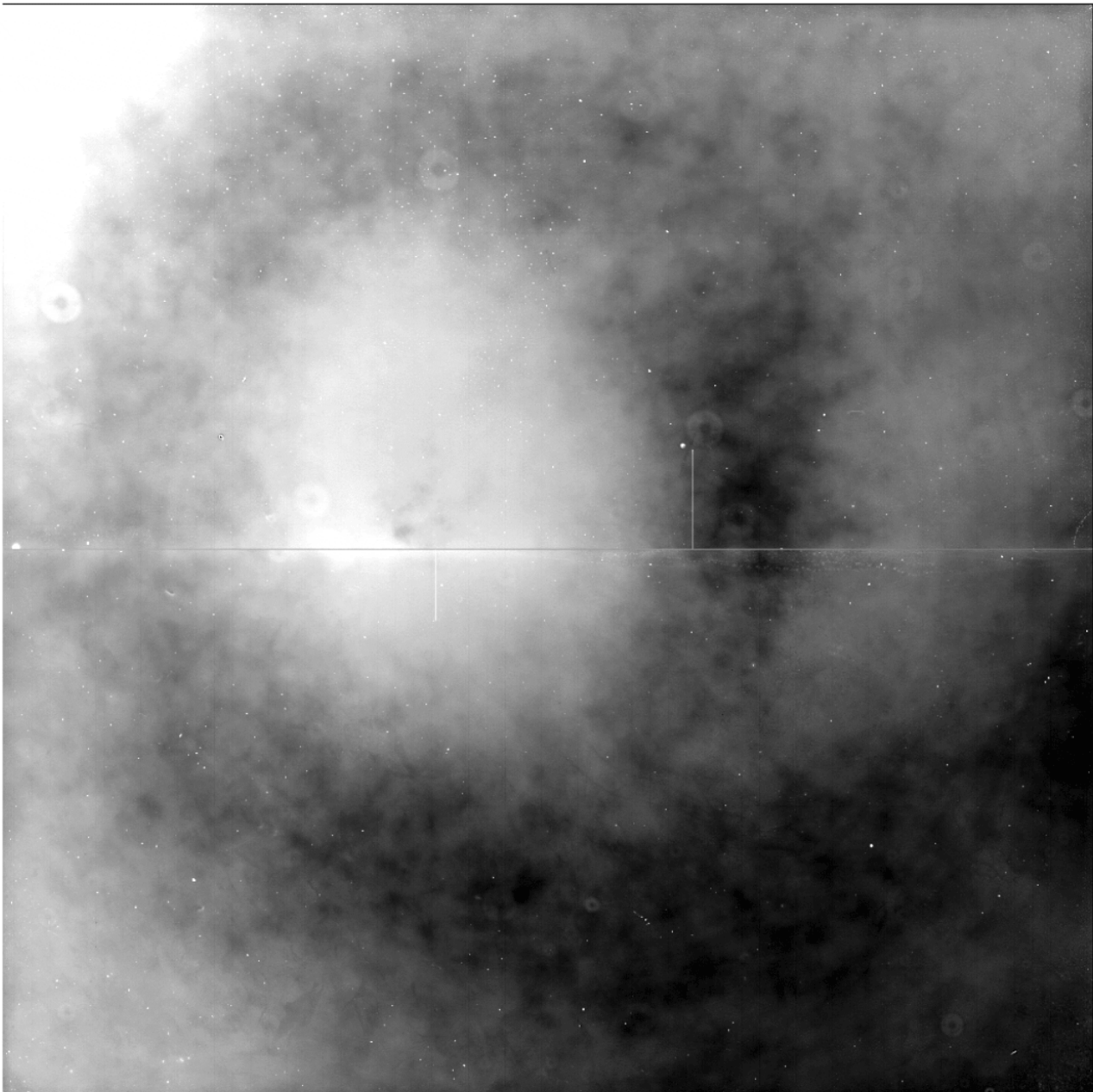
## 7.1.8 Flat Fields

### WFC

The flat fields for WFC now combine information from two sources. Ground-based flat fields using a stimulus to simulate the illumination expected on-orbit were obtained at high S/N for all filters. In-flight observations of a rich stellar field (see ISR 2002-008, J. Mack et al.) with large-scale, repeated dithers have been used to refine the low-frequency domain of the flat fields in order to obtain the proper corner-to-corner

gradients. Following these 10-18% corrections, the resulting flat field has  $S/N \sim 300$  for pixel-to-pixel variations and supports photometry to  $< \sim 1\%$  over the full field of view. Figure 7.1 shows the WFC1 and WFC2 flats for the F555W filter; **note that on the sky a gap of 50 pixels exists between the top and bottom halves that is not shown here.** For further discussion of flat field features including impacts of dust motes, see a number of existing ISRs.

Figure 7.1: WFC Flat Field

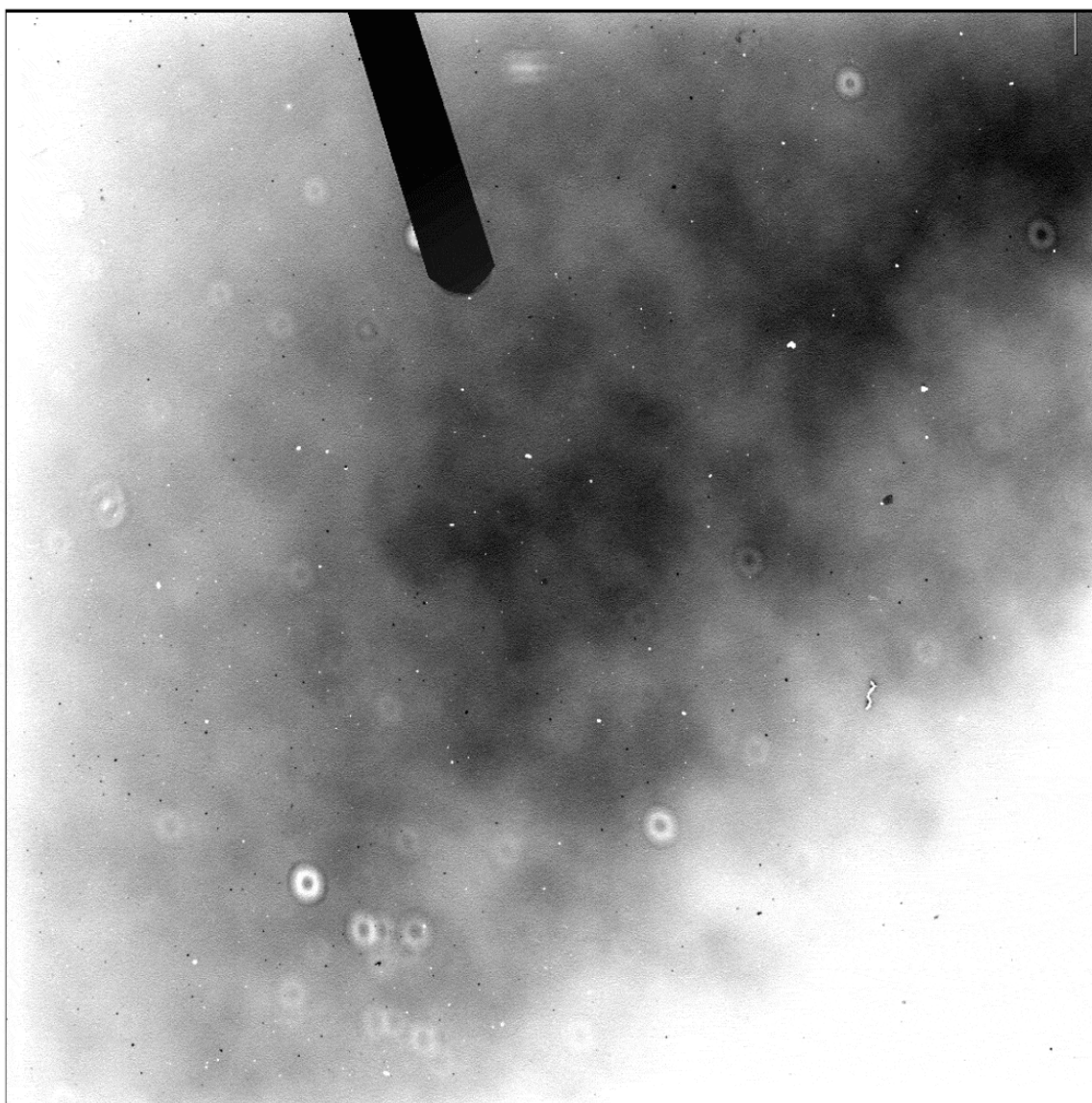




## HRC

The flat fields for HRC now combine information from two sources. Ground-based flat fields using a stimulus to simulate the illumination expected on-orbit were obtained at high S/N for all filters. In-flight observations of a rich stellar field with large scale, repeated dithers have been used to refine the low-frequency domain of the flat fields, in order to obtain the proper corner-to-corner gradients. Following these 5-10% corrections, the resulting flat field has  $S/N \sim 300$  for pixel-to-pixel variations and supports photometry to  $< \sim 1\%$  over the full field of view. Figure 7.2 shows the HRC flat for the F555W filter. For further discussion of flat field features including impacts of dust motes, see a number of existing ISRs.

Figure 7.2: HRC Flat Field



## 7.2 CCD Operations and Limitations

### 7.2.1 CCD Saturation: the CCD Full Well

The full well capacity for the ACS CCDs is given in Table 7.1 as 84,700  $e^-$  for the WFC and 155,000  $e^-$  for the HRC. This is somewhat dependent on the position on the chip. If the CCD is over-exposed, blooming will occur. This happens when a pixel becomes full, so excess charge flows into the next pixels along the column. However, extreme overexposure is not believed to cause any long-term damage to the CCDs, so there are no bright object limits for the ACS CCDs. When using  $GAIN = 2$  on the WFC and  $GAIN = 4$  on the HRC, it has been shown that the detector response remains linear to well under 1% up to the point when the central pixel reaches the full well depth. On-orbit tests have demonstrated that when using aperture photometry and summing over the pixels bled into, linearity to  $\leq 1\%$  holds even for cases in which the central pixel has received up to 10 times the full well depth.

### 7.2.2 CCD Shutter Effects

The ACS camera includes a very high-speed shutter, so that even the shortest exposures are not significantly affected by the finite traversal time of the shutter blades. Calibration of shutter shading corrections will be supplied if they are found to be necessary.

### 7.2.3 Cosmic Rays

Initial studies have been made of the characteristics of cosmic ray impacts on the two ACS imaging cameras, HRC and WFC. The fraction of pixels affected by cosmic rays varies from 1.5% to 3% during a 1000 second exposure for both cameras, similar to what was seen on WFPC2 and STIS. This number provides the basis for assessing the risk that the target(s) in any set of exposures will be compromised. The affected fraction is the same for the WFC and HRC despite their factor of two difference in pixel areas because the census of affected pixels is dominated by charge diffusion, not direct impacts. Observers seeking rare or serendipitous objects as well as transients may require that every single WFC pixel in at least one exposure among a set of exposures is free from cosmic ray impacts. For the CR fractions of 1.5% to 3% in 1000 sec, a single  $\sim 2400$  sec orbit must be broken into 4 exposures (4 CR splits of 500 to 600 sec each) to reduce the number of uncleanable pixels to 1 or less. (It is also

recommended that users dither these exposures to remove hot pixels as well.)

The flux deposited on the CCD from an individual cosmic ray does not depend on the energy of the cosmic ray but rather the length it travels in the silicon substrate. The electron deposition due to individual cosmic rays has a well defined cut-off with negligible events of less than 500 electrons and a median of  $\sim 1000$  electrons (see Figure 7.3 and Figure 7.4).

Figure 7.3: Electron deposition by cosmic rays on WFC.

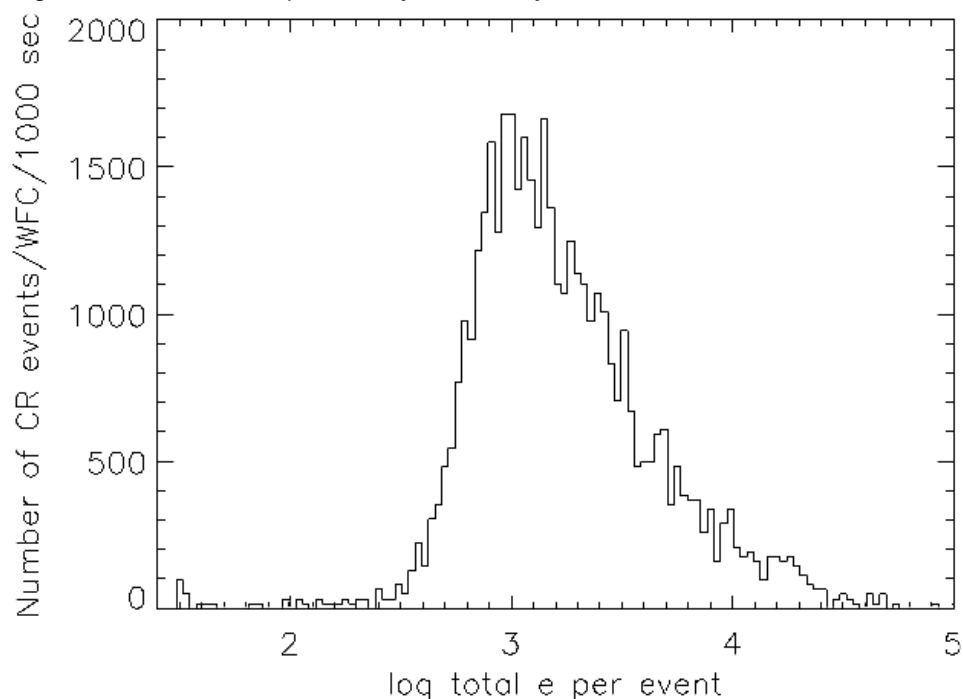
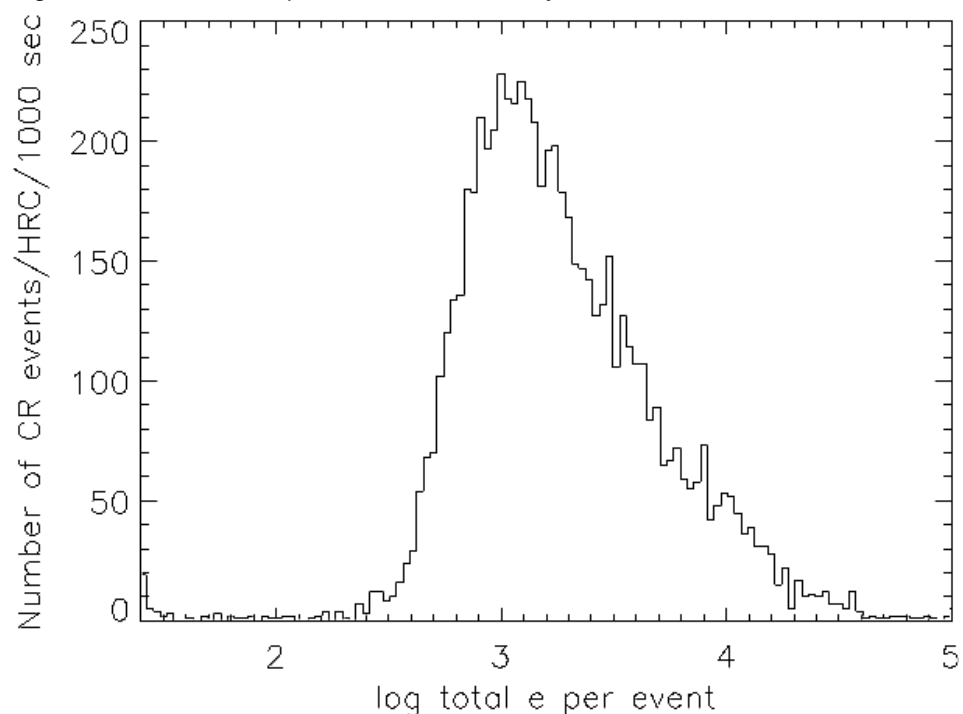


Figure 7.4: Electron deposition of Cosmic Rays on HRC.



The distribution of the number of pixels affected by a single cosmic ray is strongly peaked at 4 to 5 pixels. Although a few events are seen which encompass only one pixel, examination of these events indicate that at least some and maybe all of these sources are actually transient hot pixels or unstable pixels which can appear hot in one exposure (with no charge diffusion) and normal in the next. Such pixels are very rare but do exist. There is a long tail in the direction towards increasing numbers of attached pixels.

Distributions of sizes and anisotropies can be useful for distinguishing cosmic rays from astrophysical sources in a single image. The size distribution for both chips peaks near 0.4 pixels as a standard deviation (or 0.9 pixels as a FWHM). This is much narrower than for a PSF and is thus a useful discriminant between unresolved sources and cosmic rays.

### 7.2.4 Hot Pixels

We have made an initial study of the dark current and the "hot" pixels on the ACS CCDs. These pixels appear similar to those seen on previous CCDs flown on HST and are likely caused by radiation damage.

The dark current distribution is well described by a Gaussian with a center at  $0.0022 \text{ e}^-/\text{sec}$  and rms of  $0.0029 \text{ e}^-/\text{sec}$  for the WFC and  $0.0025 \text{ e}^-/\text{sec}$  and rms of  $0.0015 \text{ e}^-/\text{sec}$  for the HRC. As expected from experience with earlier HST cameras, very significant tails in these distributions are seen from much "warmer" or "hotter" pixels. We have chosen a conservative limit of twice that, or  $0.04 \text{ e}^-/\text{sec}$  for WFC and  $0.08 \text{ e}^-/\text{sec}$  for HRC as a threshold above which we consider a pixel to be "hot" and not part of the normal distribution of pixel dark current. Figure 7.5 and Figure 7.6 show the daily growth of these hot pixels. For WFC we find a growth rate of approximately 1200 new hot pixels per day with dark current greater than  $0.04 \text{ e}^-/\text{sec}$ . For HRC the number of new hot pixels per day above the threshold is approximately 90. Because the distribution of dark current in hot pixels is strongly peaked near the threshold, the specific number of such pixels is necessarily a strong function of the chosen threshold.

Figure 7.5: Hot Pixel Trends for WFC.

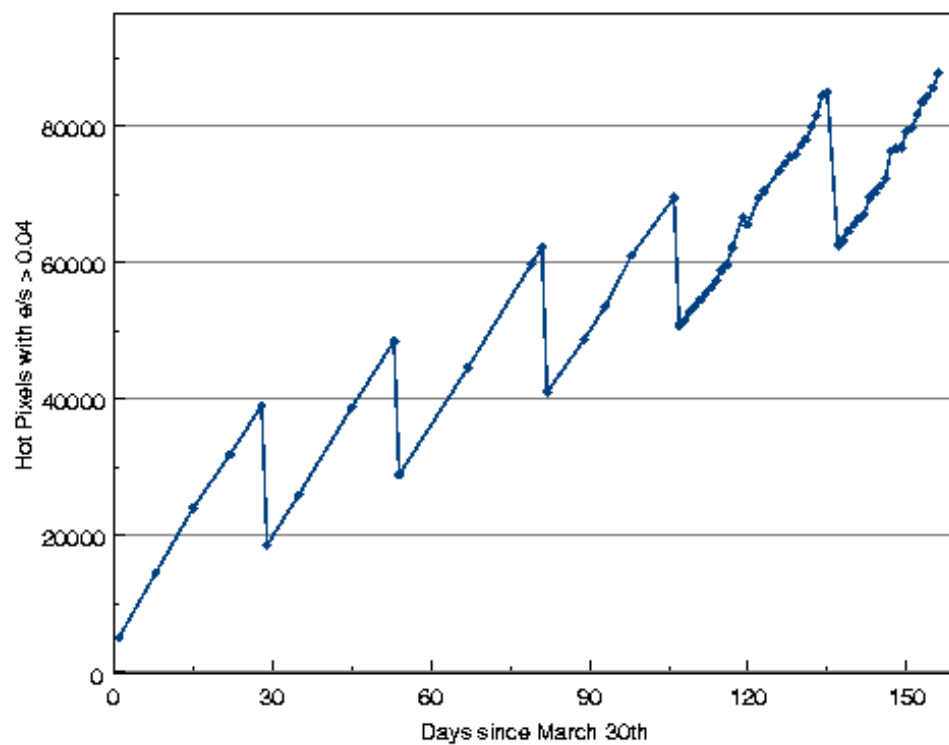
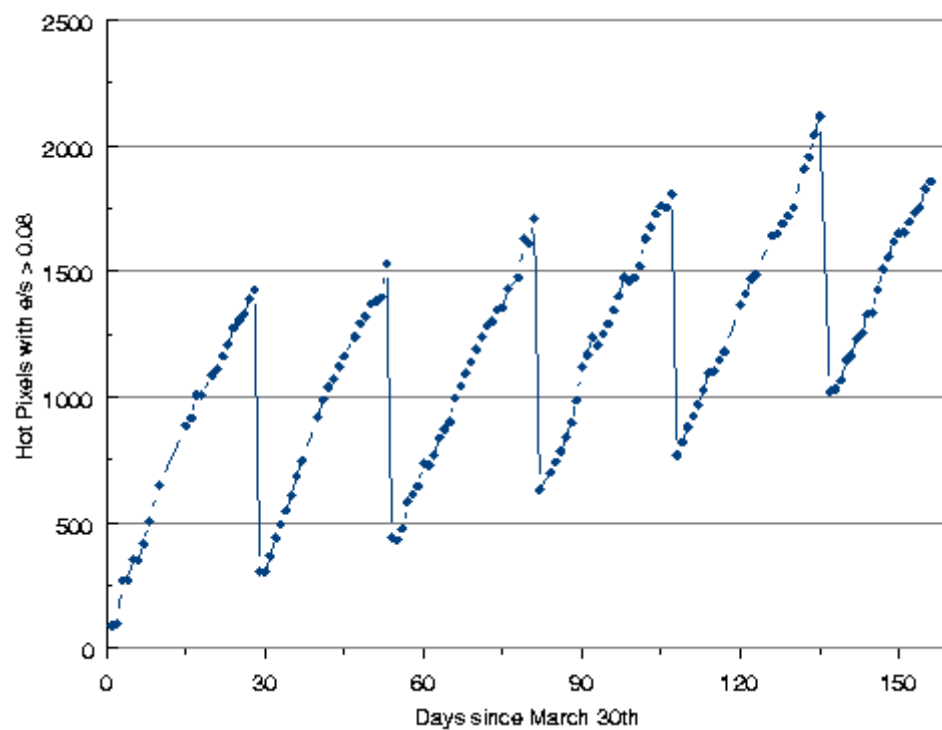


Figure 7.6: Hot Pixel Trends for HRC.



The first two anneals for HRC healed 80% of new hot pixels, similar to what is seen with WFPC2 and STIS. The first two anneals on WFC healed only 45%-50% of hot pixels.

Subtraction of a superdark frame from a science image can remove the dark current from hot pixels just as it does for normal pixels. However, hot pixels are often orders of magnitude noisier than normal pixels, which in many cases limits their ability to provide useful measurements of flux. In rare cases (but not without precedents), hot pixels can spontaneously "heal", a circumstance which could create false positive detections in some science programs.

### 7.2.5 Charge Transfer Efficiency

Charge Transfer Efficiency (CTE) is a measure of how effective the CCD is at moving charge from one pixel location to the next when reading out the chip. A perfect CCD would be able to transfer 100% of the charge as the charge is shunted across the chip and out through the serial register. In practice, small traps in the silicon lattice are able to compromise this process by holding on to electrons, releasing them at a significantly later time (seconds rather than microseconds). For large charge packets (several thousands of electrons), losing a few electrons along the way is not a serious problem, but for smaller ( $\sim 100$  electrons or less) signals, it can have a substantial effect.

CTE is typically measured as a pixel transfer efficiency, and would be 1 for a perfect CCD. The CTE numbers for the ACS CCDs at the time of writing are given in Table 7.4. While the numbers look impressive, remember that reading out the WFC CCD requires 2048 parallel and 2048 serial transfers, so that almost 2% of the charge from a pixel in the corner opposite the readout amplifier is lost.

Table 7.4: Charge Transfer Efficiency measurements for the ACS CCDs

Chip	Parallel	Serial
WFC1	0.999995	0.999999
WFC2	0.999995	0.999999
HRC	0.999983	0.999994

Also, the CTE numbers are significantly different for images where the pixels have a low intensity compared to those where the intensity is high.

Both the WFPC2 and STIS CCDs have been found to suffer from a significant degradation in CTE since their installation in 1993 and 1997, respectively. More details can be found in the latest versions of the *WFPC2 Instrument Handbook* and the *STIS Instrument Handbook*. While we do not know exactly how the ACS CCDs will fare on orbit, we can expect that

their CTE degradation will mirror that experienced by WFPC2 and STIS. Measurements made only 2-3 months after installation have not shown any indication of degradation; further monitoring will provide very sensitive results. The results we can expect for ACS are that the parallel CTE falls by  $10^{-4}$  per year for faint sources (50-150 electrons) on a low background ( $3e^-/\text{pixel}$ ). Brighter targets, or targets on a higher background, will suffer less CTE degradation. As an example, for STIS it was found that the CTE degradation for a background of  $5e^-/\text{pixel}$  is less than half of that for a background of  $3e^-/\text{pixel}$ . The growth rate of the serial CTE is lower by an order of magnitude.

For a star in the middle of one of the WFC CCD chips, 1024 parallel transfers are required. At the end of 1 year, when the projected parallel CTE is 0.9999, this means that  $1 - (0.9999)^{1024}$ , or 10%, of the flux will be lost. For a faint star near the WFC reference point, 1824 parallel transfers are required, so the resulting loss will be 17%. These numbers will rise to 19% and 30% respectively after 2 years, and 27% and 43% after 3 years.

For this reason, a post-flash capability has been included in the ACS. This can add a relatively low amount of charge to the general background and hence mitigate the effect of CTE degradation. However, the addition of this charge will of course elevate the background contribution to the noise.

For most broad-band, deep imaging programs using the WFC, the sky background will be high enough to make CTE effects small for at least the first few years of operation.

## 7.2.6 UV Light and the HRC CCD

In the optical, each photon generates a single electron. However, in the near UV, shortward of  $\sim 3200 \text{ \AA}$  there is a finite probability of creating more than one electron per UV photon (see Christensen, O., *J. App. Phys.* **47**, 689, 1976). This effect is accounted for in developing sensitivities. The interested reader may wish to see Chapter 6 of the *STIS Instrument Handbook* for details on Signal-to-Noise treatment.

---

## 7.3 The SBC MAMA

### 7.3.1 MAMA Properties

The ACS MAMA detector is the STIS flight spare STF7 and provides coverage from 1150 to  $1700 \text{ \AA}$ . The MAMA detector is a photon-counting device which processes events serially. The ACS MAMA only operates in the accumulate (ACCUM) mode in which a time-integrated image is produced. Unlike the STIS MAMAs, the ACS does not offer the

high-resolution ( $2048 \times 2048$ ) mode nor the time-tagged data acquisition. The primary benefits afforded by the STIS and ACS MAMAs, in comparison with previous HST UV spectroscopic detectors such as those of the GHRS and FOS, are high spatial resolution, two-dimensional imaging over a relatively large field of view, and low background for point sources.

Figure 7.7: Design of the SBC MAMA

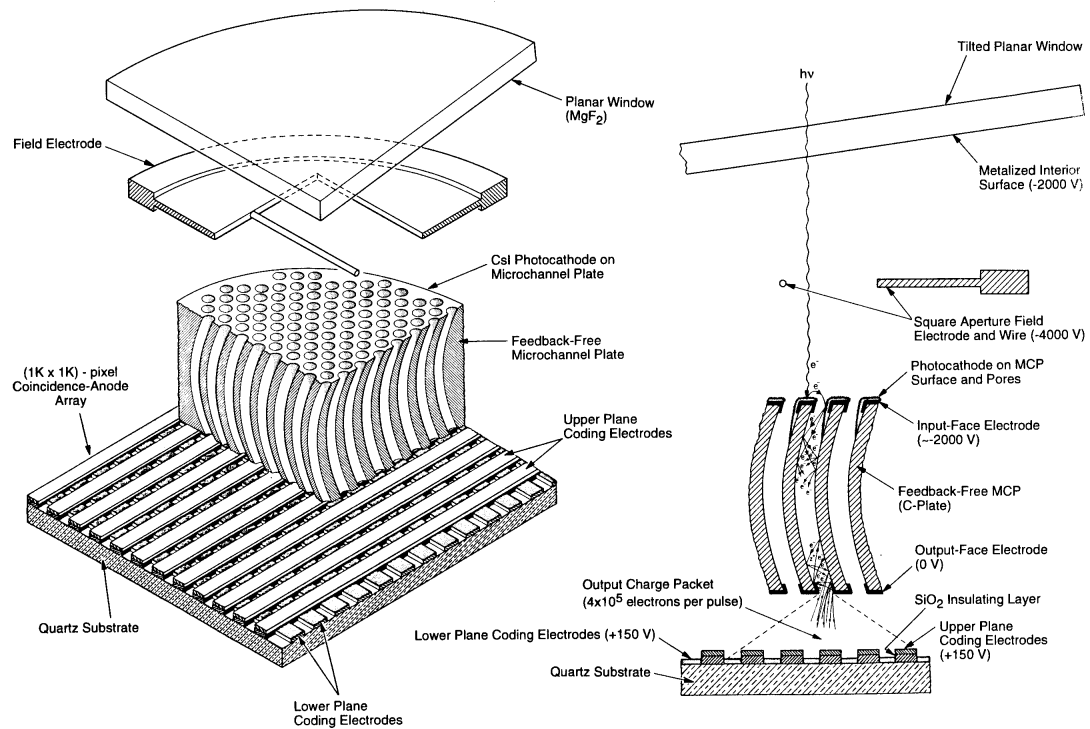


Figure 7.7 illustrates the design of the MAMA which has an opaque CsI photocathode deposited directly on the face of the curved microchannel plate (MCP). Target photons strike the photocathode, liberating single photoelectrons which pass into the microchannel plate (MCP). There they are multiplied to a pulse of  $\sim 4 \times 10^5$  electrons. The pulse is recorded by an anode array behind the photocathode and detected by the MAMA electronics which process it, rejecting false pulses and determining the origin of the photon event on the detector.

The field electrode, or *repeller wire*, repels electrons emitted away from the microchannel plate back into the channels. This provides an increase in quantum efficiency of the detector at the price of an increase in the detector PSF halo. The repeller wire voltage is always on for SBC observations.



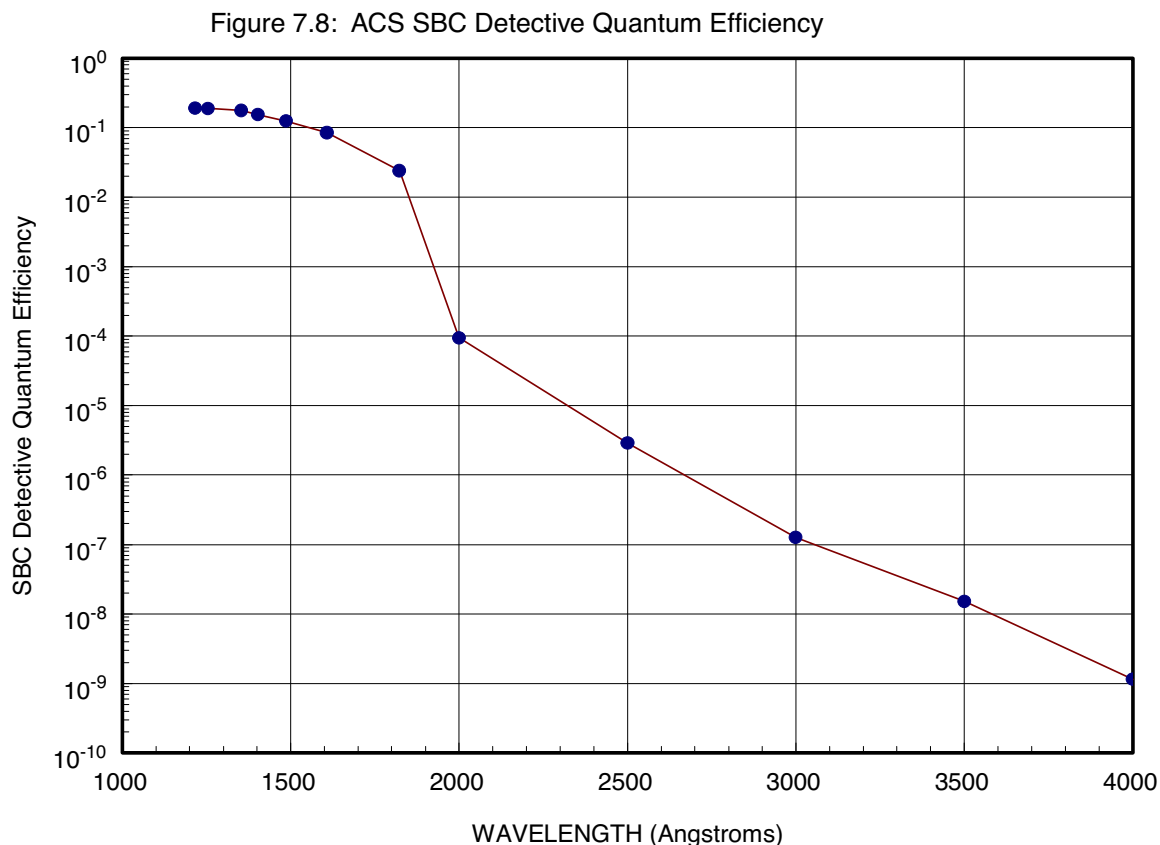
Table 7.5: SBC Detector Performance Characteristics

Characteristic	SBC MAMA Performance
Photocathode	CsI
Wavelength range	1150–1700 Å
Pixel format	1024×1024
Pixel size	25×25 μm
Plate scale	0.034×0.030 arcseconds/pixel
Field of view	34.6 x 30.8 arcseconds
Quantum efficiency	19.2% @ 1216 Å
Dark count	$1.2 \times 10^{-5}$ counts sec <sup>-1</sup> pix <sup>-1</sup>
Global count-rate linearity limit <sup>1</sup>	360,000 counts sec <sup>-1</sup>
Local count-rate linearity limit	~350 counts sec <sup>-1</sup> pix <sup>-1</sup>
Visible light DQE	$< 1.2 \times 10^{-9}$ above 400 nm

1. Rate at which counting shows 10% deviation from linearity. These count rates are well above the bright-object screening limits.

### 7.3.2 SBC Spectral Response

The spectral response of the unfiltered SBC is illustrated in Figure 7.8. The peak photocathode response occurs at Lyman- $\alpha$ . Its spectral response is defined by the cutoff of the MgF<sub>2</sub> window at 1150 Å at short wavelengths, and by the relatively steep decline of the CsI photocathode at long wavelengths. Out-of-band QE at longer wavelengths (>4000 Å) is  $< 10^{-8}$  yielding excellent solar-blind performance.



### 7.3.3 Optical Performance

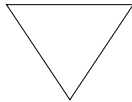
The SBC exhibits low-level extended wings in the detector point-spread function (PSF). Sample MAMA detector PSF profiles are shown in Figure 7.9.

## 7.4 SBC Operations and Limitations

### 7.4.1 MAMA Overflowing the 16 Bit Buffer

The MAMA is a photon-counting detector: as each photon is recorded, it is placed into buffer memory. The buffer memory stores values as 16-bit integers; hence the maximum number it can accommodate is 65,535 counts per pixel in a given ACCUM mode observation. When accumulated counts per pixel exceed this number, the values will wrap. As an example, if you are counting at 25 counts  $\text{sec}^{-1}$  pixel $^{-1}$ , you will reach the MAMA “accumulation” limit in ~44 minutes.

One can keep accumulated counts per pixel below this value by breaking individual exposures into multiple identical exposures, each of which is short enough that fewer than 65,536 counts are accumulated per pixel. There is no read noise for MAMA observations, so no penalty is paid in lost signal-to-noise ratio when exposures are split. There is only a small overhead for each MAMA exposure (see Section 9.2).

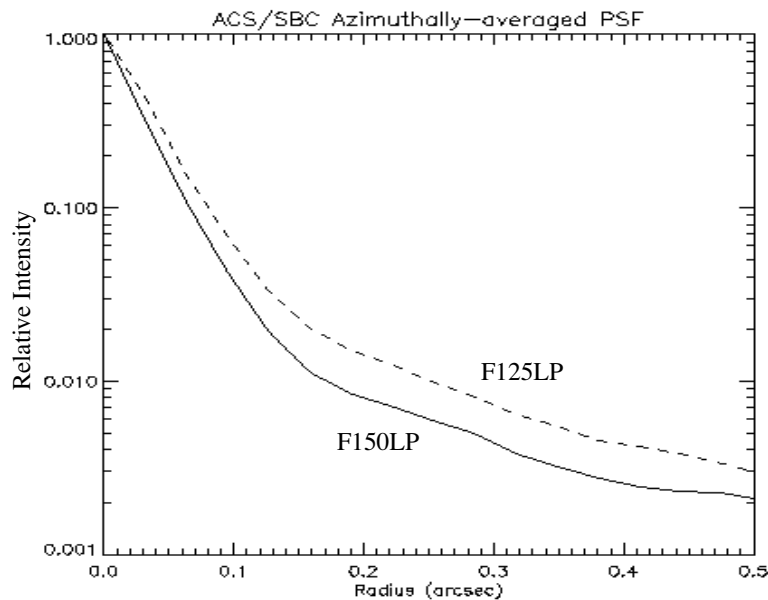



---

***Keep the accumulated counts per pixel below 65,536, by breaking single exposures into multiple exposures, as needed.***

---

Figure 7.9: MAMA Point Spread Function



### 7.4.2 MAMA Darks

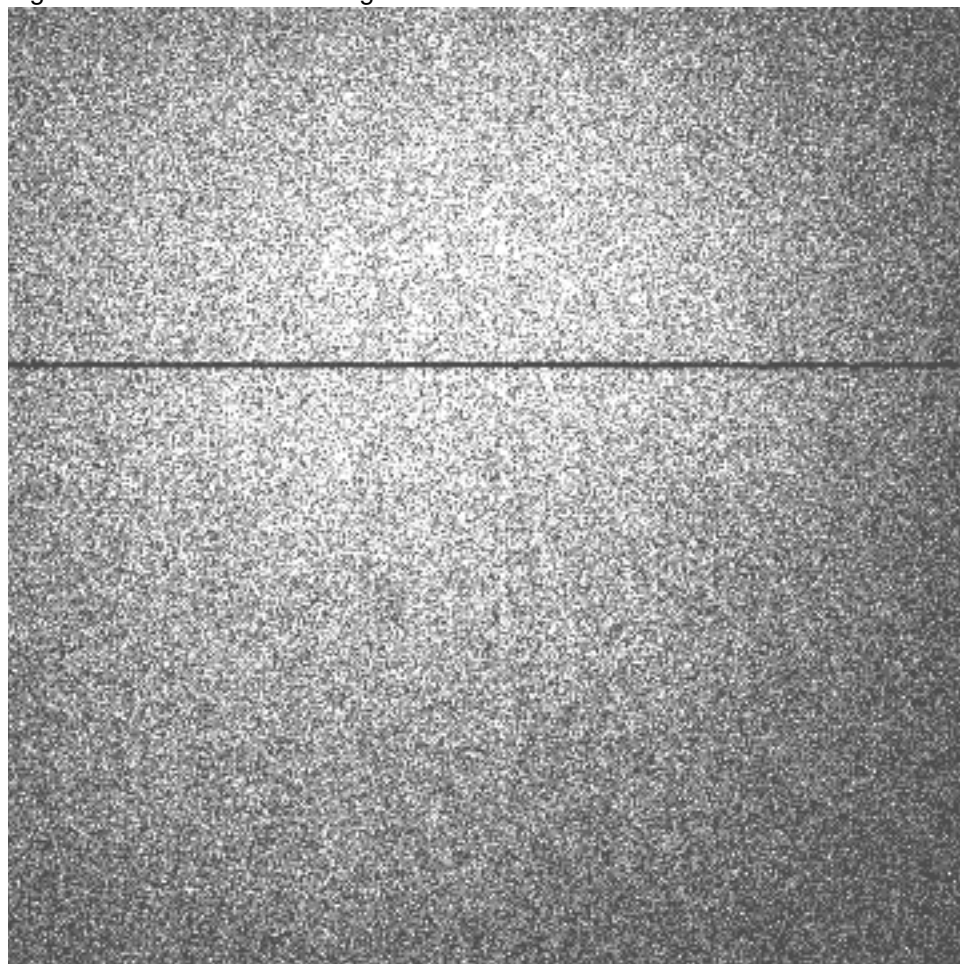
MAMA detectors have intrinsically low dark currents. Ground test measurements of the ACS MAMA showed count rates in the range of  $10^{-5}$  to  $10^{-4}$  counts per pixel per second as the temperature varied from 28 to 35 degrees. The count rate increased by about 30% for one degree increase in temperature. In-flight measurements, taken weekly throughout June and July, show count rates between  $8 \times 10^{-6}$  and  $10^{-5}$ . These measurements were taken as soon as the MAMA was turned on and were therefore at the lower end of the temperature range. A 10 hour observation in SMOV, long enough for nominal temperatures to be reached yield a dark current of

$1.2 \times 10^{-5}$  counts per second. However, uncertainty remains in values to be expected in normal operations.

The ACS MAMA has a broken anode which disables the seven rows 599 to 605. There are three dark spots, smaller than 50 microns at positions (334,977), (578,964) and (960,851) and two bright spots at (55,281) and (645,102) with rates which fluctuate but are always less than 3 counts per second.

An example of the dark current variation across the detector can be seen in Figure 7.10 below.

Figure 7.10: MAMA Dark Image



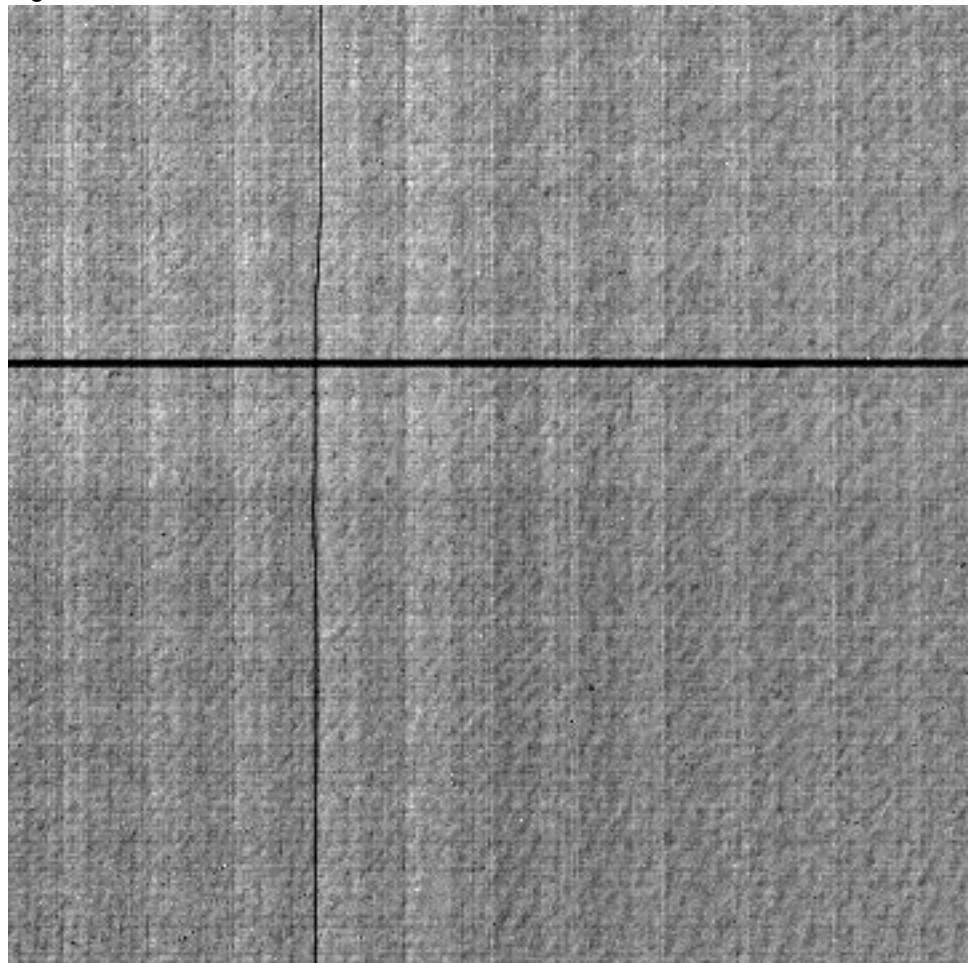
### 7.4.3 SBC Signal-to-Noise Ratio Limitations

MAMA detectors are capable of delivering signal-to-noise ratios on the order of 100:1 per resolution element ( $2 \times 2$  pixels) or even higher. Tests in orbit have demonstrated that such high S/N is possible with STIS (Kaiser et al., *PASP*, **110**, 978; Gilliland, STIS ISR 98-16.)

For targets observed at a fixed position on the detector, the signal-to-noise ratio is limited by systematic uncertainties in the small-scale spatial and spectral response of the detector. The MAMA flats show a fixed pattern that is a combination of several effects including beating between the MCP array and the anode pixel array, variations in the charge-cloud structure at the anode, and low-level capacitive cross-coupling between the fine anode elements. Intrinsic pixel-to-pixel variations are 6% but are stable to <1%.

#### 7.4.4 SBC Flatfield

Figure 7.11: Mama Flat Field



The flat field image illustrates several features. The low frequency response is extremely uniform except a change of response can be seen in the four image quadrants. The rows 601 to 605, disabled due to the broken anode, are clearly displayed as is the shadow of the repeller wire running vertically near column 640. A regular fixed “tartan” pattern is visible showing the effect of the discrete anodes.

### 7.4.5 SBC Nonlinearity

#### Global

The MAMA detector begins to experience nonlinearity (photon impact rate not equal to photon count rate) at global (across the entire detector) count rates of 200,000 counts  $\text{sec}^{-1}$ . The nonlinearity reaches 10% at 360,000 counts  $\text{sec}^{-1}$  and can be corrected for in post-observation data processing at the price of a loss of photometric reliability. Additionally, the MAMA detector plus processing software are not able to count reliably at rates exceeding 285,000 count  $\text{sec}^{-1}$ . For this reason and to protect the detectors, observations beyond this rate are not allowed (see Section 7.5).

#### Local

The MAMA detector remains linear to better than 1% up to  $\sim 22$  counts  $\text{sec}^{-1} \text{ pixel}^{-1}$ . At higher rates, they experience local (at a given pixel) nonlinearity. The nonlinearity effect is image dependent—that is, the nonlinearity observed at a given pixel depends on the photon rate affecting neighboring pixels. This property makes it impossible to correct reliably for the local nonlinearity in post-observation data processing. In addition, MAMA detectors are subject to damage at high local count rates (see the discussion of MAMA bright-object limits below).

---

## 7.5 SBC Bright-Object Limits

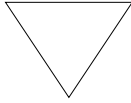
STScI has responsibility to ensure that the MAMA detectors are not damaged through over-illumination. Consequently, we have developed procedures and rules to protect the MAMA. We ask all potential users to share in this responsibility by reading and taking note of the information in this section and designing observing programs which operate in the safe regime for these detectors.

### 7.5.1 Overview

The SBC detector is subject to catastrophic damage at high global and local count rates and cannot be used to observe sources which exceed the defined safety limits. The potential detector damage mechanisms include over-extraction of charge from the microchannel plates causing permanent reduction of response, and ion feedback from the microchannel plates causing damage to the photocathode and release of gas which can overpressure the tube.

To safeguard the detector, checks of the global (over the whole detector) and local (per pixel) illumination rates are automatically performed in flight for all SBC exposures. The *global illumination rate* is monitored

continuously; if the global rate approaches the level where the detector can be damaged, the high voltage on the detector is automatically turned off. This event can result in the loss of all observations scheduled to be taken with that detector for the remainder of the calendar ( $\sim 1$  week). The *peak local illumination rate* is measured over the SBC field at the start of each new exposure. If the local rate approaches the damage level, the SBC filter wheel will be used to block the light, since there is no "shutter". Also, all subsequent SBC exposures (in the obset) will be lost until a new filter is requested.




---

*Sources that would over-illuminate the SBC detector cannot be observed. It is the responsibility of the observer to avoid specifying observations that exceed the limits described below.*

---

### 7.5.2 Observational Limits

To ensure the safety of the SBC detector and the robustness of the observing timeline, we have established observational limits on the incident count rates. Observations which exceed the allowed limits will not be scheduled. The allowed limits are given in Table 7.6, which includes separate limits for nonvariable and irregularly-variable sources. The global limits for irregular variable sources are a factor 2.5 more conservative than for sources with predictable fluxes. Predictable variables are treated as nonvariable for this purpose. Examples of sources whose variability is predictable are Cepheids or eclipsing binaries. Irregularly variable sources are, for instance, cataclysmic variables or AGN.

Table 7.6: Absolute SBC Count-Rate Limits for Nonvariable and Variable Objects

Target	Limit Type	Mode	Screening Limit
Nonvariable	Global	All modes	200,000 counts sec <sup>-1</sup>
Nonvariable	Local	Imaging	50 counts sec <sup>-1</sup> pix <sup>-1</sup>
Irregularly Variable <sup>1</sup>	Global	All modes	80,000 counts sec <sup>-1</sup>
Irregularly Variable	Local	Imaging	50 counts sec <sup>-1</sup> pix <sup>-1</sup>

1. Applies to the phase when the target is brightest.

Table 7.7: Limiting V-band Magnitudes for SBC observations in various filters

Spectral type	$\log T_{\text{eff}}$	f122m	f115lp	f125lp	f140lp	f150lp	f165lp	pr110l	pr130l
O5V	4.648	17.5	20.7	20.6	20.0	19.5	18.0	16.6	16.4
B1V	4.405	16.6	19.9	19.8	19.2	18.6	17.3	15.8	15.6
B3V	4.271	15.7	19.1	19.0	18.5	18.0	16.6	15.1	14.9
B5V	4.188	15.0	18.5	18.4	18.0	17.4	16.1	14.5	14.3
B8V	4.077	13.6	17.4	17.4	17.0	16.5	15.2	13.6	13.4
A1V	3.965	11.0	15.4	15.4	15.3	15.1	14.0	12.0	11.9
A3V	3.940	9.5	14.3	14.3	14.3	14.2	13.5	11.6	11.5
A5V	3.914	8.6	13.6	13.6	13.6	13.6	13.2	11.1	11.0
F0V	3.857	7.1	12.3	12.3	12.4	12.4	12.1	10.4	10.3
F2V	3.838	6.4	11.6	11.6	11.6	11.6	11.4	9.7	9.6
F5V	3.809	4.7	10.1	10.1	10.1	10.1	9.9	8.0	8.0
F8V	3.792	3.6	9.0	9.0	9.0	9.0	8.8	6.8	6.8
G2V	3.768	2.6	7.3	7.3	7.3	7.3	7.1	5.2	5.1
G5V	3.760	2.6	6.7	6.7	6.7	6.7	6.5	4.7	4.6
G8V	3.746	2.6	6.6	6.6	6.2	5.9	5.1	3.5	3.8
K0V	3.720	---	6.6	6.6	6.2	5.9	5.1	3.5	3.8
Double <sup>1</sup>	---	15.8	19.0	18.9	18.3	17.8	16.3	15.9	15.7
AG Peg <sup>2</sup>	---	14.4	17.5	17.4	16.9	16.5	14.8	15.7	15.6

1. System made of a main sequence late-type star with an O5V star contributing 20% to the total light in the V band. In the UV, the O5 component dominates and sets the same limiting magnitude for types A-M. A one magnitude safety factor has been added, as for the O5V case.

2. Star with a flux distribution like AG Peg.

### 7.5.3 How Do You Determine if You Violate a Bright Object Limit?

As a first step, you can check your source V magnitude and peak flux against the bright-object screening magnitudes in Table 7.7 for your chosen observing configuration. In many cases, your source properties will be much fainter than these limits, and you need not worry further.

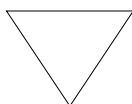
However, if you are near these limits (within 1 magnitude or a factor of 2.5 of the flux limits), then you need to carefully consider whether your source will be observable in that configuration. Remember the limits in these tables assume zero extinction. Thus you will want to correct the



limits appropriately for your source's reddening and the aperture throughput.

You can use the information presented in Section 6.2 to calculate your peak and global count rates. Perhaps better, you can use the ACS Exposure-Time Calculator to calculate the expected count rate from your source. It has available to it a host of template stellar spectrograms. If you have a spectrum of your source (e.g., from IUE, FOS, or GHRS) you can also input it directly to the calculator. The calculator will evaluate the global and per pixel count rates and will warn you if your exposure exceeds the absolute bright-object limits. We recommend you use the ACS exposure time calculator if you are in *any doubt* that your exposure may exceed the bright-object MAMA limits.

#### 7.5.4 Policy and Observers' Responsibility in Phase I and Phase II




---

*It is the observers' responsibility to ensure that their observations do not exceed the bright-object count limits stated in Table 7.6.*

---

It is your responsibility to ensure that you have checked your planned observations against the brightness limits prior to proposing for Phase I. If your proposal is accepted and we, or you, subsequently determine (in Phase II), that your source violates the absolute limits, then you will either have to change the target, if allowed, or lose the granted observing time. We encourage you to include a justification in your Phase I proposal if your target is within 1 magnitude of the bright-object limits for your observing configuration. For SBC target-of-opportunity proposals, please provide in your Phase I proposal an explanation of how you will ensure your target can be safely observed.

STScI will screen all ACS observations that use the MAMA detector to ensure that they do not exceed the bright-object limits. In Phase II, you will be required to provide sufficient information to allow screening to be performed.

Here we describe the required information you must provide.

##### **Prism Spectroscopy**

To allow screening of your target in Phase II for spectroscopic MAMA observations you must provide the following for your target (i.e., for all sources which will illuminate the detector during your observations):

- V magnitude.

- Expected source flux at observing wavelength.
- Spectral type (one of the types in the screening tables).
- E(B-V).
- B-V color.

If you wish to observe a target which comes within one magnitude (or a factor of 2.5 in flux) of the limits in the spectroscopic bright-object screening table (Table 7.7) for your configuration, after correction for reddening, but which you believe will not exceed the absolute limits in Table 7.7 and so should be observable, you must provide auxiliary information to justify your request. Specifically:

- You must provide an existing UV spectrum (e.g., obtained with IUE, FOS, GHRS or STIS) of the star which proves that neither the global nor the local absolute limits will be exceeded.
- If you do not have such data, then you must obtain them, by taking a “pre-exposure” in a MAMA-safe configuration (e.g., using the STIS FUV-MAMA with a ND filter in place) before we will schedule your observations. *Be sure to include the time (1 orbit in a separate visit) for such an observation in your Phase I Orbit Time Request, as needed.*

### Imaging

The SBC imaging bright-object screening magnitudes are very stringent, ranging from  $V = 15$  to  $V = 20.5$  for the different imaging apertures, and apply to all sources imaged onto the MAMA detector (i.e., not just the intended target of interest). Table 7.7 can be used to determine if the target of interest is above the bright-object limit. Starting in Cycle 8, STScI has been using the second-generation Guide-Star Catalog (GSC II) to perform imaging screening for objects in the field of view other than the target itself. The GSC II contains measurements from photometrically calibrated photographic plates with color information for magnitudes down to at least  $V = 22$  mag. This information will be used to support bright-object checking for fixed and for moving targets (major planets). STScI will make a best effort to perform the imaging screening using GSC II. However, observers should be prepared for the possibility that under exceptional circumstances GSC II may be insufficient. For instance, fields close to the Galactic plane may be too crowded to obtain reliable photometry. If for any reason the screening cannot be done with GSC II, the observer is responsible for providing the required photometry. In the case of moving targets, STScI will identify “safe” fields, and the observations will be scheduled accordingly. Observers will be updated on the status of their observations by their Contact Scientists. We anticipate that bright-object considerations will not have a significant effect on the scheduling of such observations.

### Policy on Observations Which Fail Because they Exceed Bright-Object Limits

If your source passes screening, but causes the automatic flight checking to shutter your exposures or shut down the detector voltage causing the loss of your observing time, *then that lost time will not be returned to you*; it is the observer's responsibility to ensure that observations do not exceed the bright-object limits.

#### 7.5.5 What To Do If Your Source is Too Bright for Your Chosen Configuration?

If your source is too bright, there may be no way of performing the observation with the SBC. The SBC has no neutral-density filters and only low resolution prism dispersing modes. The options open to you if your source count rate is too high in a given configuration include:

- Change configurations totally to observe a different portion of the spectrum of your target (e.g., switching to the CCD).
- Attempt to locate an equivalent but less bright target.
- Consider using the STIS MAMA which has neutral-density filters and a selection of slit widths and higher dispersion modes.

#### 7.5.6 Bright-Object Protection for Solar System Observations

Observations of planets with ACS require particularly careful planning due to the very stringent overlight limits of the SBC. In principle Table 7.6 and Table 7.7 can be used to determine if a particular observation of a solar-system target exceeds the safety limit. In practice the simplest and most straightforward method of checking the bright object limits for a particular observation is to use the ACS Exposure-Time Calculator. With a user-supplied input spectrum, or assumptions about the spectral energy distribution of the target, the ETC will determine whether a specified observation violates any bright object limits.

Generally speaking, for small ( $< \sim 0.5$ – $1$  arcsec) solar-system objects the local count rate limit is the more restrictive constraint, while for large objects ( $> \sim 1$ – $2$  arcsec) the global limit is much more restrictive.

As a first approximation, small solar system targets can be regarded as point sources with a solar (G2V) spectrum, and if the V magnitude is known, Figure 7.6 and Table 7.7 can be used to estimate whether an observation with a particular ACS prism or filter is near the bright-object limits. V magnitudes for the most common solar-system targets (all planets and satellites, and the principal minor planets) can be found in the

*Astronomical Almanac*. This approximation should provide a conservative estimate, particularly for the local limit, because it is equivalent to assuming that all the flux from the target falls on a single pixel, which is an overestimate, and because the albedos of solar-system objects in the UV are almost always significantly less than their values in the visible part of the spectrum (meaning that the flux of the object will be less than that of the assumed solar spectrum at UV wavelengths where the bright-object limits apply). A very conservative estimate of the global count rate can be obtained by estimating the peak (local) count rate assuming all the flux falls on one pixel, and then multiplying by the number of pixels subtended by the target. If these simple estimates produce numbers near the bright-object limits, more sophisticated estimates may be required to provide assurance that the object is not too bright to observe in a particular configuration.

For large solar-system targets, checking of the bright-object limits is most conveniently done by converting the integrated V magnitude ( $V_0$ , which can be found in the *Astronomical Almanac*) to V magnitude/arcsec<sup>2</sup> as follows:

$$V/(\text{arcsec}^2) = V_0 - 2.5 \log(1/\text{area})$$

where *area* is the area of the target in arcsec<sup>2</sup>. This  $V / \text{arcsec}^2$  and the diameter of the target in arcsec can then be input into the ETC (choose the Kurucz model G2 V spectrum for the spectral energy distribution) to test whether the bright-object limits can be satisfied.

# Observing Techniques

**In this chapter . . .**

8.1 Operating Modes / 145
8.2 Patterns and Dithering / 149
8.3 A Road Map for Optimizing Observations / 152
8.4 CCD Gain Selection / 155
8.5 ACS Apertures / 156
8.6 Fixing Orientation on the Sky / 163
8.7 Parallel Observations / 166

In this Chapter we describe how to carry out observations with the ACS. We include a description of the operating modes, some suggestions on how to split exposures for cosmic ray rejection and a description of the use of subarrays and dithering patterns.

---

## 8.1 Operating Modes

ACS supports two types of operating modes:

- ACCUM for each of the cameras. This is the standard data taking mode and it is the one most generally used by observers.
- ACQ (acquisition). This is the mode used to acquire a target for coronagraphic observations. ACQ is only available on the HRC.

### 8.1.1 WFC ACCUM Mode

In this mode the WFC CCD accumulates signal during the exposure in response to photons. The charge is read out at the end of the exposure and translated by the A-to-D converter into a 16 bit data number (DN, ranging from 0 to 65,535). The number of electrons per DN can be specified by the user as the GAIN value. The full well of the WFC CCD is about 85,000 electrons and consequently all GAIN values larger than 1 will allow the observer to count up to the full well capacity. For GAIN=1 only 75% of full well capacity is reached when the DN value saturates at 65,535. The read-out noise of the WFC CCD is about 5 electrons rms and thus it is critically sampled even at GAIN=2. WFC can make use of an user-transparent, lossless, on-board compression algorithm, the benefits of which will be discussed in the context of parallel observations. The algorithm is more effective with higher GAIN values, i.e. when the noise is undersampled.

A total of six apertures are accessible to WFC users. WFC1-FIX and WFC2-FIX select the geometric centers of the two WFC camera chips. WFC, WFC1 and WFC2 are approximately located near the field of view center and the centers of chips 1 and 2, respectively. Their location has been chosen to be free of detector blemishes and hot pixels and they are to be preferred for typical observations. The WFCENTER corresponds to the geometric center of the combined WFC field and will be useful for facilitating mosaics and obtaining observations at multiple orientations. See Section 8.5 for more details about ACS apertures. Usually each CCD is read from two amplifiers to minimize Charge Transfer Efficiency (CTE) problems and minimize read-out time. As a result the two 2k by 2k portions in a single chip may have slightly different read-out noise. The WFC chips have both physical and virtual overscan which can be used to estimate the bias level and the read-out noise on each single image.

The ACS internal buffer can only store a single full frame WFC image. When this image is compressed, and depending on the compression factor, the buffer can store a number of additional HRC and SBC images. As a consequence of the implementation of the compression strategy, under no circumstance can more than one full frame WFC image be stored in the buffer. Note also that the adopted policy is not to compress primary WFC observations. The present flight software does not allow reading an ACS frame directly into the HST on-board recorder. Images have to be first stored in the internal buffer. When more than one WFC image is obtained during an orbit a buffer dump must occur during the visibility period so as to create space in the buffer for a new WFC image. If each exposure is longer than approximately 338 seconds, buffer dumps can occur during the integration of the following image with no impact on observing efficiency. Conversely, short, full frame, integrations with the WFC during the same orbit will cause buffer dumps to be interleaved with observations and will

negatively affect the observing efficiency. See Chapter 9, *Overheads and Orbit-Time Determination*, for more details about ACS overheads.

### WFC CCD Subarrays

It is possible to read-out only a portion of a detector thus obtaining a subarray which has a smaller size than the full frame. Subarrays are mostly useful to reduce the data volume, to store more frames in the internal buffer (thus avoiding the efficiency loss due to buffer dumps), or to read only the relevant portion of the detector when imaging with ramp filters or with HRC filters (which produce a vignetted field of view on WFC). WFC subarrays have some limitations:

1. they can be specified only on a single WFC chip
2. they only have physical but no virtual overscan
3. they cannot include the CCD edge (i.e. the maximum subarray size is 4140 by 2046) and
4. they are read through a single amplifier. A consequence of the latter limitation is that subarrays may be more affected by CTE problems than standard images.

Subarrays appropriate to the use of HRC filters, and the ramp filters are supplied, as well as a small selection of square apertures (512, 1024, and 2048 pixels on a side with physical overscan added) placed at the B Amp corner of WFC1 and D Amp corner of WFC2. In addition on an available-but-unsupported basis subarrays of nearly arbitrary size and location can be specified; users requesting such would need to obtain special bias calibrations as desired.

### Ramp Filters

Unlike WFPC2, ACS ramp filter observations at different wavelengths are obtained at the same location on the CCD, thus simplifying data processing in, e.g., continuum subtraction of emission line data. To select the desired wavelength, the ramp filter is rotated to move the appropriate part of the filter over the specified pointing. Observations with different ramp filters do not generally occur at the same pointing. The precise location where a given observation will be performed can be found from Table 8.1 where for each ramp filter we list the fiducial pointing for the inner IRAMP, middle MRAMP, and outer ORAMP filter segment. The inner segment corresponds to the WFC1 chip, while the outer to the WFC2 chip. The middle segment can be used with either of the WFC chips but is used by default with WFC1. For any ramp filter observation three ramp filters will end up in the FOV even though the target is properly positioned only for the requested one. Table 4.1 and Table 4.2 can be used to determine the remaining two ramp filters which can be of interest for serendipitous observations.

### 8.1.2 HRC ACCUM Mode

In this mode the HRC CCD accumulates signal during the exposure in response to photons. The charge is read out at the end of the exposure and translated by the A-to-D converter into a 16 bit data number (DN, ranging from 0 to 65,535). The number of electrons per DN can be specified by the user as the **GAIN** value. The full well of the HRC CCD is about 155,000 electrons. As a consequence, in order not to overflow the 16-bit pixel word size, one needs to use **GAIN=4**. In many applications **GAIN=2** is adequate since it still allows critical sampling of the read-out noise of HRC (about 4.7 electrons rms) and for this reason it has been chosen as the default **GAIN** ratio. For typical HRC observations the observer should specify the HRC aperture which is approximately located at the center of the field of view in a location free of detector blemishes and hot pixels. The **HRC-FIX** aperture is located at the geometric center of the field-of-view. Additional apertures are used for coronagraphic observations - see Table 8.3 for more details of HRC apertures.

Up to 16 HRC images can be stored in the ACS buffer. Alternatively, HRC images can share the buffer with some SBC images and/or a single compressed WFC image. The number of HRC images will depend in the latter case on the WFC compression factor.

#### HRC CCD Subarrays

Similarly to the WFC, a subarray is obtained when only a portion of the detector is read-out and transmitted to the ground. Generally the smaller size of the HRC CCD reduces the usefulness of subarrays. However, subarrays are used during on-board coronagraphic target acquisition which is similar to the STIS target acquisition and cannot be changed. A square subarray of 512x512 pixels in the C Amp readout corner, and a 512 pixel square aperture centered on the 1.8" coronagraphic spot are available. In addition, on an available-but-unsupported basis nearly arbitrary sizes and locations for subarrays can be specified. When coupling use of subarrays with **PATTERNS** or **POS TARGS** the issue arises of whether to keep the subarray fixed in pixel space or have it track and stay centered on the target. With **PATTERNS** the subarray stays fixed in pixel space, using (Phase II terminology) **POS TARGS** the observer can decide which mode to adopt.

### 8.1.3 SBC ACCUM Mode

The SBC **ACCUM** mode accumulates photons into a 1024 by 1024 array, 16 bits per pixel. At the end of the exposure the data are sent to the onboard recorder via the internal ACS memory buffer. The high-res mode used in the STIS MAMAs is not available for the SBC. Note that **ACCUM** is the only mode available for SBC observations since the Time Tag mode of STIS is also not available on ACS. The minimum SBC exposure time is 0.1 seconds and the maximum 1.0 hours. The minimum time between SBC



exposures is 40 seconds. Note that the SBC, like the STIS MAMAs, has no read-out noise. As a consequence there is no scientific driver for longer exposure times apart from the small overhead between successive images, described in Section 9.2.

Up to 17 SBC images can be stored in the internal buffer. SBC images can also share the buffer with HRC images and/or a single, compressed WFC image.

#### 8.1.4 HRC ACQ Mode

The HRC target acquisition mode is used to place a target under the occulting finger or the coronagraphic mask. Observations through two (non-polarizer) filters are allowed in ACQ images to cut down the flux to acceptable levels for very bright targets. Due to the optical design of HRC the simultaneous use of two filters leads to a degraded imaging quality which is however still acceptable for a successful target acquisition. The ACS IDT has identified a number of filter combinations that effectively act as neutral density filters and allow the observer to acquire a very bright target that would otherwise saturate the CCD. These filter pairs are F220W+F606W, F220W+F550M and F220W+F502N in order of decreasing transmission. A more complete description of the Target Acquisition procedure is given in Section 5.2.2.

---

## 8.2 Patterns and Dithering

A number of different patterns are available for ACS to support dithered observations, i.e., observations where the pointing is shifted between frames. The size of the offsets can be very different depending on the purpose of offsetting the pointing between exposures; in particular it is useful to distinguish between *mosaicing* and *dithering*. Mosaicing is done with the aim of increasing the area coverage of a particular set of exposures. Dithering is done for a variety of goals, namely

- better removal of detector blemishes
- straightforward removal of hot pixels
- improving the PSF sampling
- improving the photometric accuracy by averaging over flat fielding errors
- obtaining a contiguous field of view for the WFC.

Patterns have been defined to allow ACS users to easily carry out both mosaicing and dithering. Using patterns allows exposures to be

automatically associated in **CALACS** pipeline processing. Pattern exposures that can be associated are restricted to those exposures obtained within a single visit and those patterns where the cumulative offset is under the  $\sim 100$  arcsec guide star limitation. For the latter, these patterns include dither patterns for all three cameras, HRC and SBC mosaic patterns and the 2-point ACS-WFC-MOSAIC-LINE pattern. All patterns designed with POS TARGs will not be associated. These are described in detail in ACS ISR 01-07.

The plate scale for the WFC varies by about  $\pm 5\%$ , and so a one pixel dither near the center will be 0.95 or 1.05 pixels near the corners. For this reason, the patterns designed purely for dithering should be kept as compact as possible. Large displacements will have varying sub-pixel properties across the image.

In addition to the plate scale variation associated with the significant ACS geometric distortion, there can also be a temporal variation of overall plate scale. Some CR-SPLIT images taken during SMOV testing, in which the two components were separated by the scheduling system across orbital occultations (about one hour gap), showed registration differences of about 0.5 pixels corner-to-corner. Thus for programs that wish to combine multiple images to create oversampled images at the resolution ACS is capable of providing, the user may need to allow for the general problem of combining distorted, misregistered images. A variety of tools are being made available within STSDAS and **pyraf** to assist with these tasks including PyDrizzle.

### 8.2.1 How to obtain dithered data

Whenever possible observers should make use of the pre-defined mosaic and dither patterns. For WFC exposures requiring a contiguous field of view, offsets by 2.5 arcsec or more are required to cover the interchip gap. The STSDAS **dither** package is the recommended software package for processing dithered observations. It includes tools for rejecting CR affected pixels from data sets with a single image at each pointing so that CR-SPLITting observations at each pointing is not necessary. New software is also being developed in **pyraf** to enhance and simplify the functionality of the STSDAS **dither** package. The program PyDrizzle provides an easy-to-use interface to Drizzle for ACS and other HST instruments. The following are suggestions on the optimal number of exposures for a dithered data set:

- a minimum of 3 images are required to cover the WFC interchip gap (so that in the interchip region, the data allow for cosmic ray rejection)
- at least 2 images are always required for CR rejection. If dithering is performed it is not necessary to do a CR-SPLIT as well.

- for exposures filling one orbit the recommended minimum number of images for a good CR rejection is 3 for small dithers not bridging the gap and 4 for dithers bridging the gap.
- programs attempting to improve the PSF sampling should always use at least 4 exposures, more would be better.

Given the relatively low read-out noise and the high throughput of the WFC, broad-band optical images longer than about 1000 seconds will be background limited.

## 8.2.2 Supported Patterns

As for the other instruments, a suite of carefully designed ACS dither and mosaic "convenience patterns" is available for Phase II proposers. These patterns accomplish the familiar goals of removing detector features (including the WFC interchip gap), and providing sub-pixel PSF sampling (optimized for the number of dither points). Both **Line** and **Box** patterns are available for each detector, with designation **DITHER** or **MOSAIC** depending on the intended purpose of the pattern. Default parameters are available for these convenience patterns, although observers may override these and specify their own patterns if desired. Detailed description of the use of these patterns and syntax to employ in developing a Phase II proposal may be found in the Phase II Proposal Instructions, and in the ACS Instrument Science Report "ACS Dither and Mosaic Pointing Patterns" 2001-07.

## 8.2.3 How to combine dithered observations

The nonlinear geometric distortion makes simple shift-and-add schemes inadequate for the proper combination of ACS dithered exposures since, e.g., a shift by an integer number of pixels in the chip center will not in general be integer at the edge. In the case of WFC the effect can be very significant since a shift by 50 pixels, as required to bridge the interchip gap, will be different by 2.5 pixels at the edge of the CCD so that stars in different exposures will not be aligned across the FOV by applying a simple shift to the images.

The STSDAS **dither/PyDrizzle** package allows the user to combine images taken at different offsets including also a correction for geometric distortion. Experience with the WFPC2, STIS and NICMOS shows that well dithered observations can be combined with the **drizzle** task included in the **dither** package even in the presence of imperfect offsets and rotation between the images. For undersampled data the reconstructed PSF will have a FWHM approaching the pixel size of the original observations. Final reconstructed PSFs with a FWHM of 1.35 of the initial pixel size

have been obtained for intensively observed WFPC2 fields and similar limits are anticipated for ACS. Usually, the final PSF obtained by reconstructing CCD observations remains larger than the theoretical limit because CCDs have a non negligible pixel-transfer function, i.e., electrons can diffuse to neighboring pixels as is the case for both WFPC2 and ACS. As described in Section 8.2.1, enhancements to this software approach have been provided and development work is ongoing.

### 8.2.4 How to determine the offsets

Within a single visit the commanded relative positions and the positions that are actually achieved are in very good agreement, often to better than  $0''.01$ . Thus within one visit the commanded offsets are usually a very good starting point for image combination. On occasion the guide star acquisition leads to a false lock. In this case, the commanded position can be incorrect even by  $0''.5$  or more. The jitter files allow the observer to track such false locks since they also contain information on the rms of the pointing, on the guide star separation and on the guide star separation rms. During false locks one or more of these indicators are normally anomalous. Across different visits the mismatch between commanded and achieved offsets can instead be significant. In these cases the offsets derived from the jitter files are better than the commanded ones, although they are only good to about  $0''.02$  rms. For accurate combination of images the recommended strategy is then that of deriving the offsets from cross-correlation of the images themselves, or by using matched object catalogues derived from the images. The **dither** package includes software to carry out such cross-correlations.

---

## 8.3 A Road Map for Optimizing Observations

Dithering and CR-SPLITting more than the minimum recommended values tends to yield higher quality images with fewer residual detector defects, hot pixels or CR signatures in the final combined image. Unfortunately, splitting a given exposure time into several exposures reduces its signal-to-noise when the image is read-out noise limited. WFC images taken through the broad band filters and longer than about 500 seconds are background limited, while shorter exposures and narrow band images are read-out noise limited for all practical exposure times. Thus, the optimal number of CR-splits and dithering positions is a result of a trade-off between completeness of the CR-rejection, final image quality, and optimal S/N. A schematic flow chart of this trade-off is given in Figure 8.1. The main steps in this, possibly iterative, process are the following:

1. determine the exposure time required to achieve the desired S/N
2. determine the maximum number of acceptable residual CR in the final combined image. This number depends critically on the scientific objective since for e.g. a survey of distant galaxies or a globular cluster color magnitude diagram a few residual CR will not compromise the scientific output of the observations. In contrast, in, e.g., a search for an optical counterpart of some radio or gamma ray selected object even one residual CR would not be acceptable over the region of interest. In this latter case, since we expect about 5 percent (range of ~4-7%) of the pixels to be affected by CR hits during a one orbit exposure on the WFC, the requirement that no pixel in the final image is affected by CR hits would force one to use at least 4 CR-SPLITS. For an experiment in which the number of allowed false alarms is zero, e.g. a search for cosmological supernovae, observers may wish to consider using a number of CR-SPLITS at least twice the number required to formally avoid coincidences. Note also that given the large number of pixels in the WFC even a few thousand residual CR hits would correspond to only a small fraction of the total number of pixels. In general, the number of pixels affected by coincident CR hits for a given total exposure time and number of CR-SPLITS  $N$  will be:

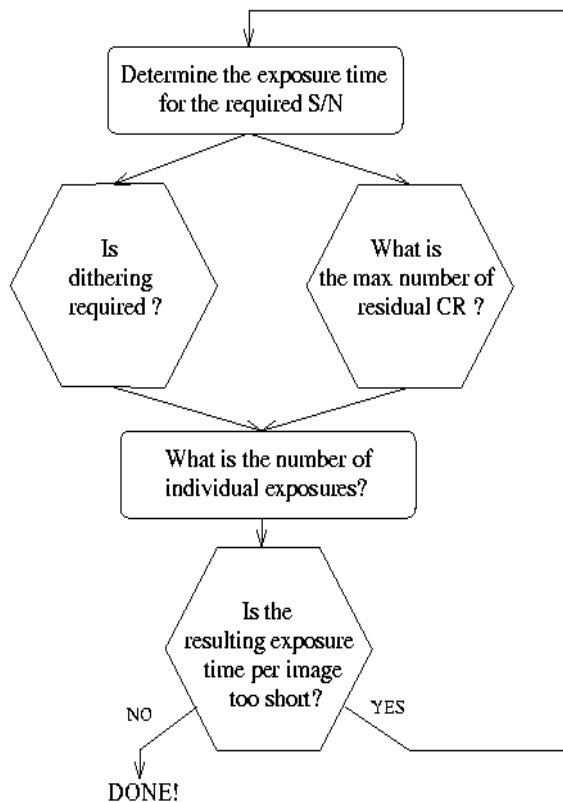
$$\left(0.05 \times \frac{ExposureTime}{2400s \times N}\right)^N \times 4096^2$$

3. determine whether dithering is required. CR-SPLITS of course have no effect on hot pixels which form due to CCD radiation damage and which persist for ~weeks. If such features would critically effect the science, then dithering is required to remove them. For some imaging programs the spatial resolution provided by the WFC and the presence of some detector defects and hot pixels in the final image are acceptable. For such observations dithering would not be required and one would simply split the exposure time for CR hit correction. For observations where several orbits worth of data are obtained with each filter the best strategy is to observe using a sub-pixel dither pattern *without* obtaining multiple images at each position. Since each CR hit will now influence more than one output pixel the requirement on the number of separate exposures is more stringent than in the simple CR-SPLIT case, but when 10 or more images (and a fast CPU with a lot of memory) are available one will obtain both a high image quality and a negligible number of residual CR hits. If the total exposure with each filter is short, one will have to compromise between S/N and image quality. In general, dithering with sub-pixel steps increases the number of individual exposures required to eliminate CR hits. Given that the geometric distortion of WFC makes any dithering step non-integer somewhere in the field of view (unless the

dither steps are very small,  $<5$  pixels), the size of the high image quality field of view also comes into play. If the high quality area is small, one may make do with integer pixel dithers. In this case a few CR-SPLITS may be obtained at each dithering position and the combined images may then be combined together using **drizzle**. On the edges of the field the CR-rejection quality will be lower than in the field center. A minimum number of 4 images for a two position dither and 8 for a four position dither is required.

4. once the required number of individual exposures has been established on the basis of CR rejection and dithering requirements, the observer will need to verify whether the resulting read-out noise affects the achieved S/N.

Figure 8.1: Schematic flow-chart of the CR-split vs. dithering vs. S/N trade-off.



## 8.4 CCD Gain Selection

As quantified in Table 7.3 both the WFC and HRC CCDs have selectable gain values near 1, 2, 4, and 8 electrons per digital number. Various factors should influence the gain selected in Phase II for your science program: level of support and calibrations provided, influence of associated readout noise on data quality, dynamic range on the bright end, and for the WFC in limited applications data compressibility.

### 8.4.1 WFC Gain

GAINS 1 and 2 are fully supported for the WFC, since GAIN = 1 provides the smallest readout noise, while GAIN = 2 (or above) is needed to sample the available full well depth. It is the goal to provide equal calibration support for data taken in these two supported gains, although more calibration data will be taken in the default GAIN = 1 setting. Calibration support will not be provided for the "available-but-unsupported" GAIN = 4 and 8 settings; users proposing their use should provide special justification and discussion of calibrations to be used.

While the readout noise is lower at GAIN = 1, the advantage over GAIN = 2 ( $< 0.3$  e- extra rms) is modest. GAIN = 2 has the offsetting advantage of fully sampling the full well depth of nearly 85,000 e- thus providing a  $> 0.3$  magnitude dynamic range extension before saturation is reached. The latter could be advantageous even for programs in which the prime targets are very faint, if serendipitous objects in the field of view can be used to support image-to-image registration solutions as needed for optimal dithered image combinations. Furthermore, to first order charge is conserved even beyond filling the full well depth, for point sources at GAIN = 2 it is possible to obtain valid aperture photometry several magnitudes beyond saturation by summing over all pixels bled into. Both GAINS 1 and 2 provide better than critical sampling of the readout noise supporting robust background sky-level determination even at low values.

The large pixel count for WFC can create data rate problems if images are acquired as quickly as possible for multiple orbits. The available-but-unsupported mode COMPRESSION is more effective when the noise is undersampled which could result in special circumstances for which the GAIN values of 4 or 8 are preferred.

### 8.4.2 HRC Gain

GAINS 2 and 4 are fully supported for the HRC, and analogous to the supported WFC values provide a low readout noise case and a GAIN that provides sampling of the physical full well depth.

GAIN = 4 on the HRC, which is needed if high dynamic range on the bright end is desired does not provide critical sampling of the readout noise. Not only is the readout noise penalty in going from GAIN = 2 to 4 non-trivial, background estimation will be less robust without critical noise sampling. As with WFC, when the full well depth is sampled with GAIN = 4 the detector response remains accurately linear up to and even well beyond saturation. Compression is not an issue for the small HRC images, therefore rationales for use of the unsupported GAIN = 8 are not anticipated. GAIN = 1 is available-but-unsupported, but the very modest improvement of readout noise in comparison to GAIN = 2 ( $< 0.2$  e- higher rms) seems unlikely to present compelling need for its use.

---

## 8.5 ACS Apertures

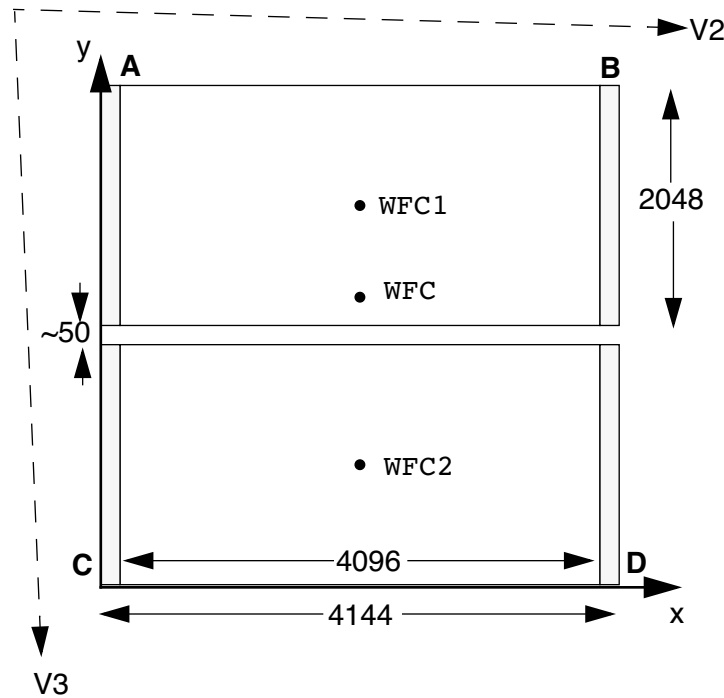
As discussed in Section 3.2, the ACS consists of three cameras: the WFC, the HRC and the SBC. The WFC is constructed of two CCDs each nominally 2048 by 4096 pixels, with their long sides adjacent to form a roughly square array, 4096 pixels on a side. The HRC CCD and the SBC MAMA detectors are each 1024 pixels square.

### 8.5.1 WFC Apertures

The active image area of each WFC detector is 4096 by 2048. The mean scale is 0.04945 arcsec/pixel and the combined detectors cover an approximately square area of 202 arcseconds on a side. In establishing reference pixel positions we have to consider the overscanned pixel areas which extend 24 pixels beyond the edges in the long direction. So each CCD must be regarded as a 4144 by 2048 pixel area. The gap between the two CCDs is equivalent to about 50 pixels. In Table 8.2 the letters A, B, C and D show the corner locations of the four readout amps.



Figure 8.2: WFC Aperture Definitions



We define apertures named WFC1 and WFC2 which represent the two CCDs, with their reference points initially at the geometric center of each chip, at pixel positions (2072,1024). The science images delivered will be 4144 by 2048 pixels (including physical overscans) and the reference position will be at (2072,1024) within the image. If we find that these positions are on undesirable parts of the chips due to some blemish, we will define new reference positions nearby. However, we keep two other apertures named WFC1-FIX and WFC2-FIX at the original locations. For extended sources, choosing new positions may not be of any advantage and it may be more effective to use these fixed positions.

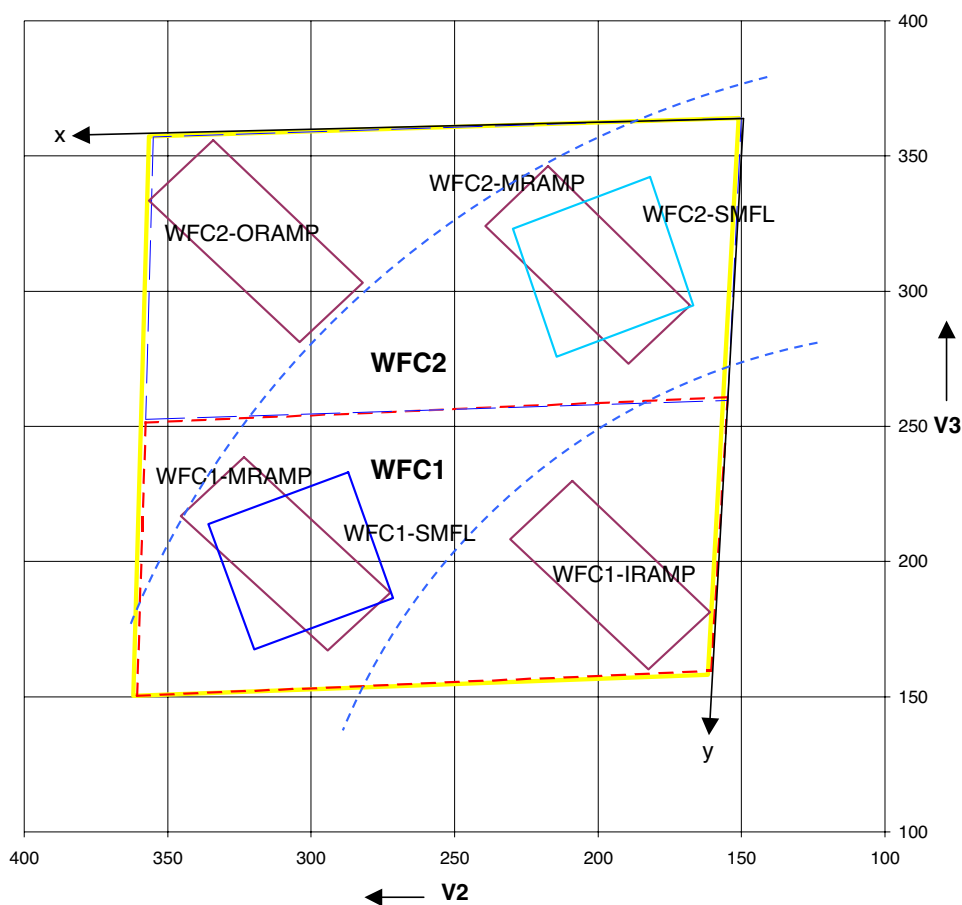
The aperture WFC encompasses both detectors and has its reference point near the overall center but about 10 arcsec away from the interchip gap. This has been chosen to be position (2072,200) on the WFC1 CCD. Again, this is the initial selection for the aperture named WFC which might be shifted later, but the reference point for WFC-FIX will remain at this value. Selection of WFC1, WFC2 or WFC only changes the pixel where the target will be positioned. In all three cases data is normally delivered in a file containing two imsets, one for each detector. See Section 11.1 for details of the ACS data format. Reading out a subarray, which consists of part of only one of the chips, is done only if requested.

WFCCENTER is similar to WFC, but is placed at the precise geometric center of the combined WFC full field. Selection of WFCCENTER can be of use in obtaining observations with maximum overlap at unique orientations and for mosaics.

### 8.5.2 Ramp filter apertures

There are 3 ramp filters which can be rotated across the WFC field of view as indicated in Figure 8.3. The IRAMP filter can only be placed on WFC1 in a location which will define the aperture WFC1-IRAMP and the ORAMP only on WFC2 creating the aperture WFC2-ORAMP. The MRAMP filter can lie on WFC1 or WFC2 with corresponding apertures WFC1-MRAMP and WFC2-MRAMP. The approximate aperture locations are indicated in Figure 8.3, while actual data obtained during ground calibrations are overlaid on an image of a ramp filter in Figure 8.4. Operationally, a fixed reference point will be defined for each detector and filter combination and the ramp filter will be rotated to place a required wavelength at the reference position.

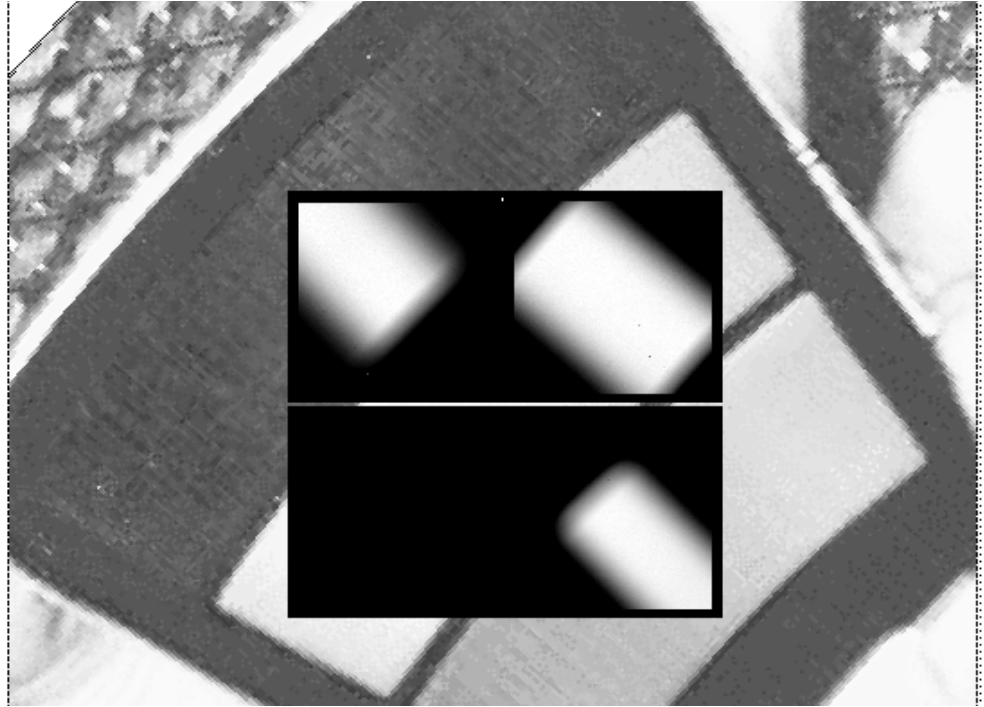
Figure 8.3: Schematic WFC apertures and Ramp Filters



The reference positions for all defined apertures are given in Table 8.1 in pixels and in the telescope V2,V3 reference frame, where values are measured in arcseconds. The values given here are based on in-flight calibration results. The x and y axis angles are measured in degrees from the V3 axis towards the V2 axis. This is in the same sense as measuring

from North to East on the sky. The "extent" of the ramp filter apertures given in Table 8.1 are the FWHM of the monochromatic patches (visible in Figure 8.4) measured from a small sample of ground calibration data.

Figure 8.4: Monochromatic patches in ground calibration data showing actual aperture sizes through ramp filters (superimposed on photo of ramp filters).



### 8.5.3 The Small Filter Apertures

When a filter designed for the HRC is used on the WFC, it only covers a small area on either WFC1 or WFC2. The projected filter position may be placed on either chip by selection of the filter wheel setting. Figure 8.3 shows how the filter projection may be placed so as to avoid the borders of the chips. Apertures `WFC1_SMFL` and `WFC2_SMFL` will be defined and automatically assigned when a WFC observation is proposed using an HRC filter. Reference positions at or near the center of these apertures will be defined so that a target may be placed in the region covered by the chosen filter.

The axis angles given in Table 8.1 do not refer to the edges of the apertures as drawn, but rather to the orientation of the x and y axes at the WFC reference pixel. These angles vary slightly with position due to geometric distortion.

For the ramp and small filter apertures, the default will be to read out a subarray. The subarray will be a rectangular area with sides parallel to the

detector edges which encompasses the indicated filtered areas. Optionally the whole chip may be read.

Table 8.1: WFC Aperture Parameters

Aperture Name active area	Extent (arcsec)	Reference pixel	Reference V2,V3 (arcsec)	x-axis angle	y-axis angle
				(degrees from V3 through V2)	
WFC 4096 × 4096	202 × 202	(2072,200) <i>on WFC1</i>	(258,239)	92.0	177.5
WFC-FIX 4096 × 4096	202 × 202	(2072, 200)	(258,239)	92.0	177.5
WFCENTER 4096 × 4096	202 × 202	(2115, 2029)	(259,252)	92.0	177.4
WFC1 4096 × 2048	202 × 102	(2072, 1024)	(260,198)	92.3	177.3
WFC1-FIX 4096 × 2048	202 × 102	(2072, 1024)	(260,198)	92.3	177.3
WFC2 4096 × 2048	202 × 102	(2072, 1024)	(255,302)	91.4	177.7
WFC2-FIX 4096 × 2048	202 × 102	(2072, 1024)	(255,302)	91.4	177.7
WFC1-IRAMP 600 × 1500	45 × 85	(1048,1024)	(200,200)	92.7	176.9
WFC1-MRAMP 600 × 1500	65 × 100	(3096,1024)	(310,196)	92.0	177.8
WFC2-MRAMP 600 × 150	65 × 100	(1048,1024)	(205,303)	91.7	177.4
WFC2-ORAMP 600 × 1500	60 × 85	(3096,1024)	(306,301)	91.2	178.0
WFC1-SMFL 1024 × 1024	72 × 72	(3096,1024)	(310,196)	92.0	177.8
WFC2-SMFL 1024 × 1024	72 × 72	(1048,1024)	(205,303)	91.7	177.4

### 8.5.4 Polarizer Apertures

Apertures have been provided for use with the polarizer sets similar to the SMFL apertures. They will attempt to eliminate image shifts that are introduced by small filter-to-polarizer planar mis-alignments. In addition, such apertures can be used to select a clear region of the field of view, free of defects. These apertures are selected automatically when a polarizing spectral element is used, and a single WFC chip quadrant readout is obtained.

### 8.5.5 HRC Apertures

The HRC has an area of 1062 by 1024 including 19 physical overscan pixels at each end in the x direction. The active area is 1024 by 1024 pixels. The mean scales along the x and y directions are 0.028 and 0.025 arcseconds/pixel, thus providing a field of view of about 29 by 26 arcseconds in extent. The anisotropy and variation of scales is discussed in a later section of this handbook. The reference point for the aperture labelled **HRC-FIX**, and initially for HRC, is at the geometric center, (531,512). As with the WFC apertures, there may be reason to move the HRC reference point later.

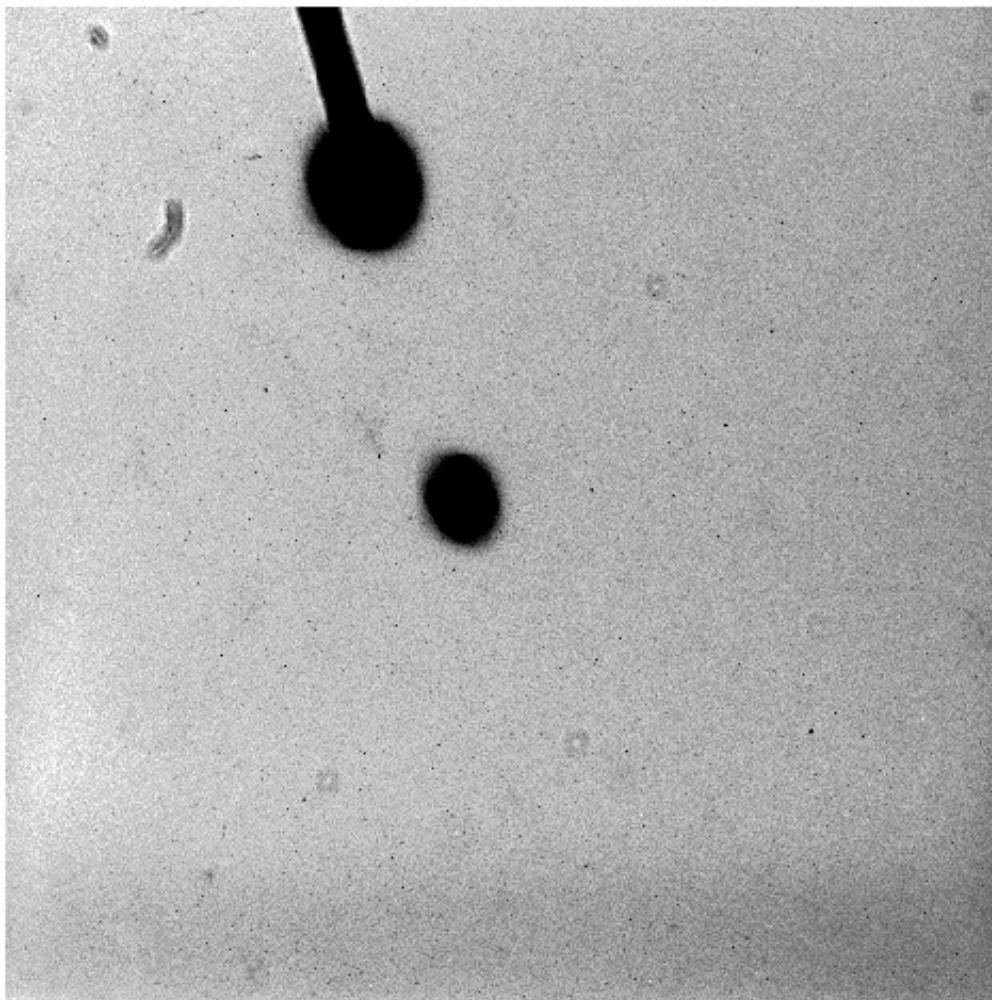
The HRC is equipped with two coronagraphic spots, nominally 1.8 and 3.0 arcseconds in diameter and a coronagraphic finger, 0.8 arcseconds in width. Apertures **HRC-CORON1.8**, **HRC-CORON3.0** and **HRC-OCCULT0.8** are defined to correspond to these features. In addition we define a target acquisition aperture, **HRC-ACQ** designed for acquiring targets which are subsequently automatically placed behind a coronagraphic spot or the occultation finger. **HRC-ACQ** is currently coincident with the **HRC-CORON1.8**, with the idea that the target can be acquired in this position and the coronagraphic stop subsequently moved into the beam. To use the other features will require a target offset, which is added automatically by the scheduling system when needed. A modification to this procedure is in work to enable target acquisition of the coronagraphic mechanism already in place.

### 8.5.6 SBC Apertures

The SBC aperture is 1024 pixel square. There are no overscan pixels to consider. The x and y scales are 0.034 and 0.030 arcseconds/pixel leading to a coverage on the sky of 35 by 31 arcseconds. The reference point will initially be at (512,512). As with the CCDs we will maintain an **SBC-FIX** aperture which will always have this same position even if SBC has to be altered. MAMA detectors slowly lose efficiency with exposure and we might shift the SBC reference point if the initial position shows a measurable degree of this effect.

The (512,512) reference point falls at the same position in (V2,V3) as the HRC, namely (207, 471) and the x and y axis angles are -83.9 and 0.4 degrees.

Figure 8.5: HRC Coronagraphic finger and spots



The HRC aperture parameters are summarized in the following table.

Table 8.2: HRC Aperture Parameters

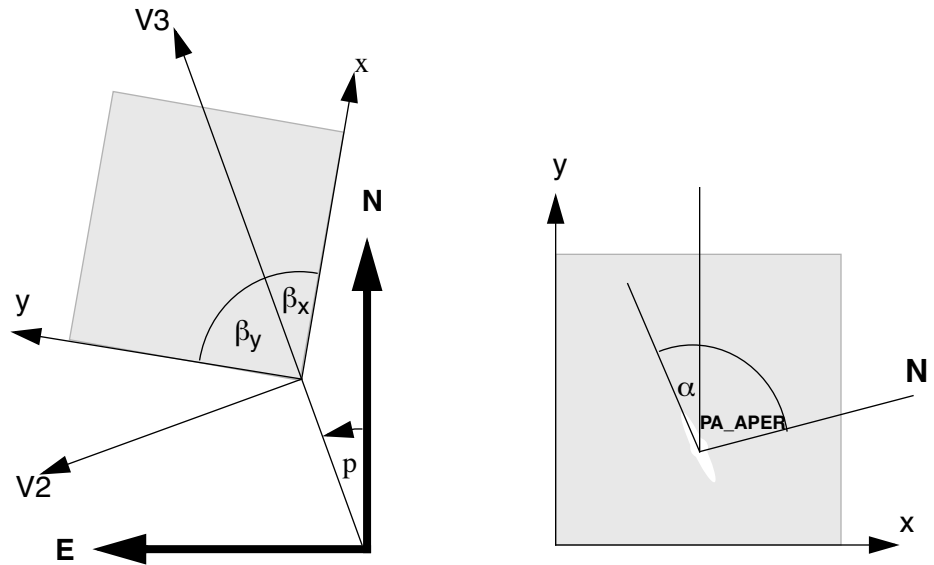
Aperture Name active area	Extent (arcsec)	Reference pixel	Reference V2,V3 (arcsec)	x-axis angle	y-axis angle
HRC 1024 × 1024	29 × 26	(531, 512)	(207,471)	-83.9	0.4
HRC-FIX 1024 × 1024	29 × 26	(531, 512)	(207,471)	-83.9	0.4
HRC-CORON1.8	-	(570,469)	(206,470)	-83.9	0.3
HRC-CORON3.0	-	(472,795)	(209,478)	-84.0	0.4
HRC-OCCULT0.8	-	(443,791)	(210,478)	-84.0	0.4
HRC-ACQ	-	(577,461)	(206,470)	-83.9	0.3

## 8.6 Fixing Orientation on the Sky

Determining the orientation of an image requires knowledge of the telescope roll and the angle of the aperture relative to the telescope's coordinate frame. Additionally a target may need to be specially oriented on a detector, particularly when spectroscopy is to be performed.

All HST aperture positions and orientations are defined within a right angled coordinate system labelled V1,V2,V3, in which V1 is nominally along the telescope roll axis. Apertures are therefore in the V2,V3 plane. A V3 position angle  $p$ , is defined as the angle of the projection of the V3 axis on the sky, measured from North towards East measured at the aperture. This is almost identical to the telescope roll angle. (There is a small difference between roll angles measured at the V1 axis and those measured at the aperture. This can amount to several tenths of a degree depending on the target declination.) When the position angle is zero, V3 points North and V2 points East. In the V2V3 coordinate system, aperture orientations are defined by  $\beta_x$  and  $\beta_y$ , the angles their x and y axes make with the V3 axis measured in an anti-clockwise direction. (The value of  $\beta_x$  as illustrated would be considered negative.) Hence, the angles these axes make with North are found by adding the axis angles to the position angle.

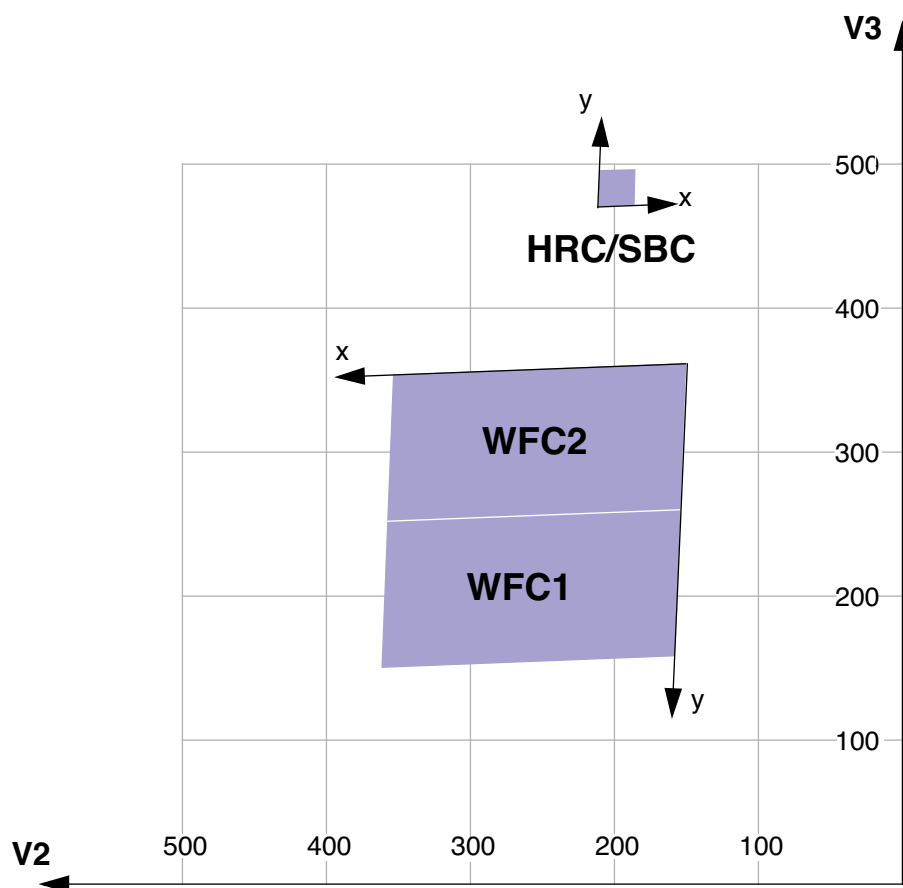
Figure 8.6: Aperture and image feature orientation



The science image header supplies the value of ORIENTAT, the angle the detector y axis makes with North and is equal to  $p + \beta_y$ . Another angle

keyword supplied is `PA_APER` which is the angle the aperture y axis makes with North. Both angles are defined at the aperture so using them does not involve the displacement difference. Normally the aperture and detector y axes are parallel and so `PA_APER = ORIENTAT`. Several STIS slit apertures were not aligned parallel to the detector axes and so this distinction was meaningful, but ACS has no slit apertures so this difference will probably not arise. In any case, it is always correct to use `PA_APER`. Beyond establishing the direction of the aperture axes, it will often be required to know the orientation of a feature, such as the plane of a galaxy, within an image. Conversely, we need to know what direction within an image corresponds to North. To this end we define a feature angle  $\alpha$  within the aperture as measured on the science image, anti-clockwise from the y-axis so that it is in the same sense as the previously defined angles. For an orthogonal set of aperture axes the direction of this feature would be `PA_APER +  $\alpha$`  and the image direction of North would be the value of  $\alpha$  which makes this angle zero, namely `-PA_APER`, still measured in an anti-clockwise direction from the y axis.

Figure 8.7: ACS apertures





The x and y axes projected on the sky are not necessarily orthogonal. For all instruments prior to the ACS the departure from orthogonality has been negligible, but for the ACS the angle between the axes is about 85 degrees. Figure 8.7 realistically represents the alignment of the ACS apertures and shows that the apertures are not square. The x and y axes indicated are those that will be used for the science images. The V2, V3 coordinates can be calculated from the x, y coordinates according to

$$V2 = V2_0 + s_x \sin \beta_x x + s_y \sin \beta_y y$$

$$V3 = V3_0 + s_x \cos \beta_x x + s_y \cos \beta_y y$$

where  $s_x$  and  $s_y$  are scales in arcsec per pixel along the image x and y axes.  $V2_0$  and  $V3_0$  are the coordinates of the aperture origin, but they do not enter into the angle calculations, Figure 8.7 shows that a rotation from x to y is in the opposite sense to a rotation from V2 to V3. This will be the arrangement for ACS apertures. This is significant in defining the sense of the rotation angles. For a direction specified by displacements  $\Delta x$  and  $\Delta y$  in the image, the angle  $\alpha$  is  $\arctan(-\Delta x/\Delta y)$ .

Because of the oblique coordinates, the angle  $\alpha_s$  on the sky will not be equal to  $\alpha$ . To calculate the sky angle, it is convenient to define another set of orthogonal axes  $x_s, y_s$ , similar to the V2V3 but rotated so that  $y_s$  lies along y, and  $x_s$  is approximately in the x direction. Let  $\omega = \beta_y - \beta_x$  be the angle between the projected detector axes and for simplicity let their origins be coincident. Then the transformation is

$$x_s = s_x \sin \omega x$$

$$y_s = s_x \cos \omega x + s_y y$$

By comparing differentials and defining  $\alpha_s$  as  $\arctan(-\Delta x_s/\Delta y_s)$  we find

$$\tan \alpha_s = \frac{s_x \sin \omega \sin \alpha}{s_y \cos \alpha - s_x \cos \omega \sin \alpha}$$

The equation as written will place the angle in the proper quadrant if the ATAN2 Fortran function or the IDL ATAN function is used. To get the true angle East of North, for a feature seen at angle  $\alpha$  in the image, calculate  $\alpha_s$  and add to PA\_APER.

The inverse relation is

$$\tan \alpha = \frac{s_y \sin \alpha_s}{s_x \sin(\alpha_s + \omega)}$$

To find the value of  $\alpha$  corresponding to North we need the value of  $\alpha_s$  such that  $\text{PA\_APER} + \alpha_s = 0$ . So substitute  $-\text{PA\_APER}$  for  $\alpha_s$  in the equation to get the angle  $\alpha$  in the image which corresponds to North. The values of the scales and axis angles for all instruments are maintained on an Observatory Science Group web page:

<http://www.stsci.edu/instruments/observatory/>

For the ACS apertures, the values in Table 8.3 have been derived from results of operating the ACS in the Refractive Aberrated Simulator. These should not be considered as true calibrations but they indicate some aperture features, such as the non-orthogonality of the aperture axes and the x and y scale differences for HRC and SBC.

Table 8.3: Plate scales and axis angles for the 3 ACS channels

	$s_x$	$s_y$	$\beta_x$	$\beta_y$	$\beta_y - \beta_x$
	arcsec/pixel		degrees		
WFC	.0494	.0494	92.2	177.8	85.5
HRC	.0284	.0248	-84.1	0.1	84.6
SBC	.0338	.0301	-85.0	-0.6	84.6

A particular orientation is specified in an HST Phase II proposal using yet another coordinate system: U2,U3. These axes are opposite to V2 and V3, so, for example,  $U3 = -V3$ . The angle ORIENT, used in a Phase II proposal to specify a particular spacecraft orientation, is the position angle of U3 measured from North towards East. The direction of the V3 axis with respect to North is  $PA\_APER - \beta_y$  and so

$$ORIENT = PA\_APER - \beta_y \pm 180^\circ.$$

The IRAF task **rotate** in the package **images.geom** takes an image and rotates it counter-clockwise by a specified angle. To orient an image so that its y axis becomes North, the angle to specify is  $PA\_APER$ . The x axis will then point approximately 5 degrees North of East.

## 8.7 Parallel Observations

### 8.7.1 Parallel Observing

Parallel observing allows HST to operate several instruments simultaneously, in addition to the instrument that executes the primary observations. While the primary instrument observes a fixed target at user-specified coordinates, the parallel observes at coordinates 5 to 10 arcminutes away, depending on the instrument and spacecraft orientation. The HST field of view following SM3B (Figure 3.3 on page 30) shows the general locations of the instrument apertures adjacent to one another on the sky. Accurate relative positions for all instruments can be found on STScI's Observatory web page under "Pointing"<sup>1</sup>. The recommended method of

1. Pointing page: <http://www.stsci.edu/instruments/observatory/taps.html>

determining the field of view for any instrument is the Visual Target Tuner (VTT). A Digital Sky Survey (or user supplied) image of the primary target area is displayed with an HST field of view overlay. Any desired coordinate and ORIENT combination for the primary target will then display the possible pointings of any instrument operated in parallel. If the primary will execute at a known (absolute) orient, the VTT will display the exact field of view for any instrument executed in parallel. If the primary will execute at a random (nominal) orient or range of orient values, the VTT allows the HST field of view to be rotated interactively about the primary pointing. The VTT can be an invaluable resource for parallel observing programs, especially those designed for or restricted to specific pointings for the parallel FOV.

Certain operating limits are in place to restrict use of configurations, modes, parameters, elements and requirements allowed for each instrument while used in parallel. Details on these limits are documented in the Cycle 12 Call For Proposals, Section 4.2: “Parallel Observations”. General information on ACS specific parallel operations are documented in the following sections for each of the three types of ACS parallel observing; coordinated, auto and pure.

### **ACS Coordinated Parallels**

Coordinated parallel observations are specified in the same Phase II observing program as the primary observations via the <parallel-exp-list> PAR WITH <primary-exp-list> Special Requirement. A single ACS channel may be used for a coordinated parallel observation, with, and only with, another instrument. (Unlike NICMOS, the PAR WITH requirement cannot be used to operate any of the ACS channels simultaneously.) ACS exposures may not be used in both the <primary-exp-list> and the <parallel-exp-list> of a PAR WITH special requirement. All ACS exposures in the <parallel-exp-list> must use the same configuration. In order to operate ACS channels simultaneously, the use of ACS auto-parallels are described in the following section. The filter choice for auto-parallels is restricted and thus implemented as auto-parallels instead of coordinated parallels.

In order to protect the ACS SBC detector from inadvertent over illumination, the ACS/SBC configuration may be used as a coordinated parallel only if an exact spacecraft orientation (ORIENTation) is specified, the coordinates of the parallel field are determined and the parallel target or field passes the same bright-object screening applied to SBC primary observations. The Visual Target Tuner will greatly assist in writing this type of ACS parallel program.

Currently ACS and WFPC2 cannot be used together in a coordinated parallel program when the ACS auto-parallel capability is enabled. This restriction is made to prevent potential conflicts between ACS buffer dumps and WFPC2 readouts. This may be corrected in future cycles. ACS and WFPC2 may be used together if one is part of a pure parallel program,

or if the ACS auto-parallel capability is disabled via optional parameter `PAREXP=NONE`.

### ACS Auto-Parallels

The ACS auto-parallel capability is intended to increase the scientific return of the instrument by adding exposures with the parallel detector while interfering as little as possible with the observer's primary program. When either the WFC or HRC is the primary channel, and the exposure in that channel meets the requirements stated below, an auto-parallel observation will be automatically scheduled in the other channel during Phase II processing. Parallel detector exposures will be added automatically for the longest possible exposure time that does not interfere with the primary program. In order for an auto-parallel to be scheduled, the primary observation must meet the specifications that depend primarily on the exposure time and the filter selection of the primary exposure.

The user has three control options: This is done by selecting the `PAREXP` optional parameter. A user may either choose to explicitly add the auto-parallels by choosing `PAREXP=MULTIPLE`; choose to have no auto-parallels added by selecting `PAREXP=NONE`; or leave the special requirement set to the default, `DEF`. When `DEF` is selected, auto-parallels will be added according to the same primary exposure requirements as those for the `MULTIPLE` option. When `MULTIPLE` is selected an auto-parallel will be added for each `CR-SPLIT` part of the primary exposure (see Figure 8.8). There is a simple algorithm that the Phase II software follows in order to determine if an auto-parallel is feasible:

1. The primary exposure must be for an external target, in `ACCUM` mode and either in the WFC or HRC channel. It is not possible to observe simultaneously with the HRC and SBC, since they share the same optical train up to the flip mirror, and simultaneous operation of the WFC and SBC is not supported.
2. The primary exposure must be taken with a filter from the list of primary/auto-parallel filter combinations (Table 8.4). HRC and WFC share the same filter wheels, so the filter selection for the primary camera predetermines which filter will be used for the simultaneous observation in the other channel, it cannot be independently selected. (The HRC primary/WFC parallel filter combination will not always be the inverse of the WFC primary/HRC parallel combination, because the WFC & HRC optical paths are not diametrically opposite each other in the filter wheel).
3. The primary exposure time must be greater than the minimum exposure time, defined in Table 8.5. These values are calculated such that all of the commanding associated with the auto-parallel is scheduled during the exposure time of the primary `CR-SPLIT` portion.

4. The primary exposure is not allowed to have any EXPAND, MIN DUR, MAX DUR or RT ANALYSIS special requirements.

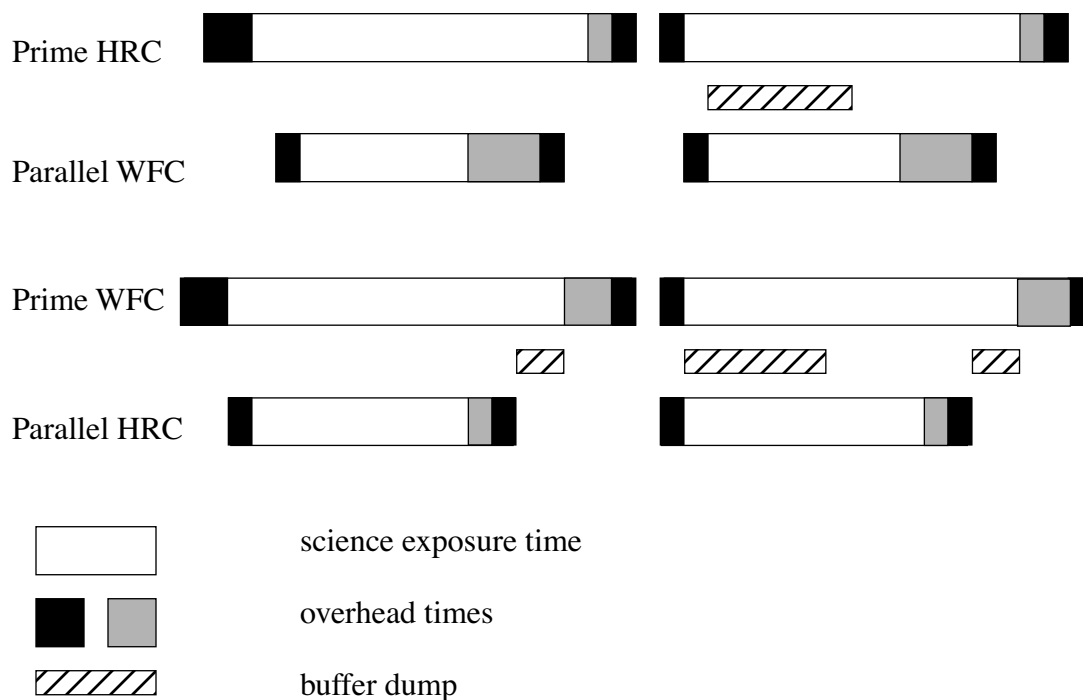
Table 8.4: Filter combinations for auto-parallels in the two cases of (i) HRC camera prime and (ii) WFC camera prime. Note that since the WFC and HRC apertures are not opposite each other on the filter wheels, filter pairs in columns 1 and 2 do not map to columns 3 and 4.

HRC Primary	WFC Auto-parallel	WFC Primary	HRC Auto-parallel
F892N	F775W	F475W	F850LP
F606W	F625W	F658N	F550M
F502N	F550M	G800L	F625W
G800L	F850LP	F502N	F775W
F555W	F606W	F606W	F555W
F775W	F502N	F850LP	G800L
F625W	G800L	F550M	F502N
F550M	F658N	F625W	F606W
F850LP	F475W	F775W	F892N
F330W	F660N	F660N	F330W
F250W	F814W	F814W	F250W
F220W	F435W	F435W	F220W

Table 8.5: Minimum primary exposure time (sec) to attach an auto-parallel for CR-SPLIT=n (if CR-SPLIT=NO then n=1, if CR-SPLIT not specified n=2)

primary exposure type	multiple auto-parallel scenario ( $n \geq 1$ )
HRC	$n \times 495$
WFC compressed	$n \times 406$
WFC uncompressed	$n \times 465$

Figure 8.8: Scheduling of Auto-parallels

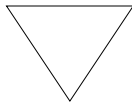


When the primary exposure meets these requirements an auto-parallel will be attached to each CR-SPLIT portion of the primary and the pair will be scheduled in an orbit. When the pair is too long to fit in the current orbit it will drop to the next orbit leaving unused time at the end of the first orbit. This prevents any primary/auto- parallel exposure pair from running into the occultation period.

There are a few things to remember to get the most out of your auto-parallels:

- In order to avoid the addition of serial buffer dumps in the primary program, group short HRC exposures and long WFC exposures separately. It takes approximately 338 seconds to dump a WFC image from the buffer. When WFC image is the parallel camera, this buffer dump can occur during the following exposure if its exposure time is greater than ~338 seconds, otherwise a serial buffer dump must be added. This can be avoided by scheduling long WFC full-frame exposures together.
- PATTERNS should not be affected, TRANS will look at each pointing in the offset pattern separately and evaluate whether auto-parallels can be attached based on the exposure time and CR-SPLIT value at that pointing.

- auto-parallels will not be assigned when the number of exposure iterations specified for the primary exposure is greater than one. It is assumed that the observer will use exposure iterations to obtain coarse time resolution. These exposures will in most cases be too short for auto-parallel observations.
- WFC auto-parallels will be readout with one 2048×2048 CCD quadrant compressed. In some cases there may be partial data loss from the compression.




---

*This data loss will be considered routine and it will be the policy of STScI not to repeat observations scheduled as auto-parallels which exhibit partial data loss due to the data compression.*

---

### **ACS Pure Parallels**

In ACS pure parallel observations, an observation is taken with ACS on an essentially random area of the sky while another instrument is making prime observations. The WFC will be a prominent instrument in pure parallel observing due to its sensitivity and field of view. The HRC is also available for pure parallel observing, however no SBC pure parallels will be allowed due to bright object concerns.

Unlike the previous two types of parallel programs, pure parallels contain only parallel visits. Use of the GO/PAR proposal category will make any visit in the program a pure parallel.

The Parallel Working Group met at STScI in February 2000 and made several ACS-specific recommendations. There is a non-proprietary default ACS parallel program using the SDSS g, r, i and z filters. Details on this program and policies relating to it can be found on the ACS web page.

Pure parallel observations are executed at every possible opportunity, although there are many constraints which can render pure parallels unschedulable in any given orbit. Pure parallels will always be given lower priority than primaries and are thus scheduled only on a non-interference basis.

### **ACS Auto-Parallels with ACS Coordinated and ACS Pure Parallels**

ACS auto-parallels can be added to ACS pure and ACS coordinated parallels by default if scheduling constraints allow. However auto-parallels cannot be added to log sheet lines that make use of EXPAND or MAX DUR special requirements. Therefore ACS pure parallels can either be crafted to expose for the maximum duration allowed in each individual orbit by using EXPAND/MAX DUR or have auto-parallels added, but not both.





# Overheads and Orbit-Time Determination

In this chapter . . .

9.1 Overview / 173
9.2 ACS Exposure Overheads / 174
9.3 Orbit Use Determination Examples / 177

This Chapter describes the overheads associated with ACS observations and it gives examples showing how to determine the number of orbits that your program will require.

---

## 9.1 Overview

After you establish the set of scientific exposures and any additional target-acquisition or calibration exposures that you require for your program, you are ready to determine the total number of orbits to request. Generally, this is a straightforward exercise involving compilation of the overheads on the individual exposures, packing the exposure plus overhead time into individual orbits, and tallying up the results to determine your total orbit request. In some cases, it may be an iterative process as you refine your exposure requests to more fully exploit the orbits.

The Phase I Call for Proposals includes proposal instructions that provide information on the Observatory policies and practices with respect

to orbit-time requests and on the orbit-determination advice. Below, we provide a summary of the ACS-specific overheads and give several examples that illustrate how to calculate your orbit requirements for Phase I Proposals.

---

## 9.2 ACS Exposure Overheads

The overheads on exposures are summarized in Table 9.1 and Table 9.2. All numbers given are approximate; they do not differentiate in detail the overheads for different ACS modes and configurations. These overhead times are to be used (in conjunction with the actual exposure times and the Phase I Proposal Instructions) to estimate the total number of orbits for your proposal. After your HST proposal is accepted, you will be asked to submit a Phase II proposal to support scheduling of your approved observations. At that time you will be presented with actual, up-to-date overheads by the scheduling software. *Allowing sufficient time for overhead in your Phase I proposal is important; additional time to cover unplanned overhead will not be granted later.*

The following list presents important points for each type of overhead:

- **Generic (Observatory Level) Overheads:**
  - The first time you acquire an object you must include the overhead for the guide-star acquisition (6.1 min).
  - In subsequent contiguous orbits you must include the overhead for the guide-star reacquisition (5.7 min); if you are observing in the Continuous Viewing Zone (see the Phase I Proposal Instructions), no guide-star *reacquisitions* are required.
  - Time needs to be allowed for each deliberate movement of the telescope; e.g., if you are performing a target-acquisition exposure on a nearby star and then offsetting to your target, or if you are taking a series of exposures in which you move the target on the detector, you must allow time for the moves (20 sec to 60 sec depending on the size of the slew, see Table 9.1 and Table 9.2).
- **Onboard Target-Acquisition Overheads:**
  - On-board target acquisitions in general only need to be done to place the target under one of the coronagraphic spots.
  - An on-board target-acquisition needs to be done only once in a series of contiguous orbits (i.e., once per visit).
  - The drift rate induced by the Observatory is less than 10 milli-arc-sec per hour. Thermal drifts internal to ACS are less still.
- **Scientific Exposures:**

- The overhead times are dominated by the time to move the filter wheel, the readout time (CCD), and any serial buffer dump that is necessary. Again, we stress that in Phase II the overheads will frequently be less, but it is important to plan Phase I using the conservative overheads given in Table 9.2 to ensure you will have adequate time for your scientific goals.
- *Spectroscopy:*
  - Each CCD spectroscopic observation is preceded by an imaging exposure used for calibration, with the exposure time 3 and 6 min. for grism and prism observations, respectively. SBC prism exposures are not preceded by an automatic calibration exposure. Technically this is an individual single exposure requiring all regular science exposure overheads. For the observer it represents, however, an additional overhead to include in the observation time budget, so we have included it in the table of instrument overhead times for science exposures.

Table 9.1: Science Exposure Overheads: General

Action	Overhead
<i>Generic (Observatory Level)</i>	
Guide-star acquisition	Initial acquisition overhead = 6.1 min Reacquisitions on subsequent orbits = 5.7 min per orbit
Spacecraft moves	For offsets less than 1.5 arcmin and more than 10 arcsec = 1 min. For offsets between 10 arcsec and 1 arcsec = 0.5 min For offsets less than 1 arcsec in size = 20 sec

Table 9.2: ACS Science Exposure Overhead Times (minutes).

Exposure Type	WFC	HRC	SBC
<i>Mode: Accum</i>			
Single exposure or the first exposure in a series of identical exposures	4.0	2.5	1.7
Subsequent identical exposures in series (within an orbit)	2.5	1.0	0.7
Additional overhead for each serial buffer dump (added when WFC exposures are less than 338 sec long, excluding last exposure in an orbit)	5.8	0.0	0.0
Predefined imaging exposure for prism spectroscopy	N/A	8.5	N/A
Predefined imaging exposure for grism spectroscopy	7	5.5	N/A
<i>Mode: Acq</i>			
For the specified acquisition exposure time, <i>tacq</i> , the total acquisition time is:	N/A	$3.5 + (2 \times tacq)$	N/A
<i>Additional Overheads</i>			
Additional overhead if switching over from HRC to SBC within an orbit		17.0	
Additional overhead if switching over from SBC to HRC within an orbit		14.0	

Note that identical exposures are generated automatically if the observer specifies the proposal optional parameters **CR-SPLIT** (for  $n > 1$ ) or **PATTERN** or if **Number\_of\_Iterations**  $> 1$  (if not specified, **CR-SPLIT** defaults to  $n=2$ ). In general, identical exposures are defined here as exposures at the same target and with the same detector and the same filter(s). **PATTERNS** also involve slews and therefore slew overheads

For **ACQ** mode, the overhead includes double the specified exposure time. The reason is that it is necessary to have two acquisition images, hence two exposures, in order to eliminate possible image defects which can interfere with target acquisition. The flight software ensures that two images are taken, the user does not need to specify them in the proposal.

The overhead time for serial buffer dumps arises in certain cases from the overheads associated with the on-board data management and switching over the cameras. The on-board buffer memory can hold no more than one WFC image. The next WFC image can be placed into the buffer only after the buffer dumps the previous image, which takes 338 sec. If the next exposure time is longer than 338 sec, the buffer dump will occur during that exposure, and no overhead is imposed. However, if the next exposure time is shorter than 338 sec, then the dump must occur between

the two exposures. Sequences of many short HRC or SBC exposures can also lead to serial dumps when the buffer becomes full. In this case the buffer dump time becomes an overhead to be included into the orbit time budget. This overhead can severely constrain the number of short exposures one can squeeze into an orbit. Subarrays can be used to lower the data volume for some applications.

A serious penalty is imposed for toggling between SBC and HRC within an orbit. The time to switch over from SBC to HRC is 480 sec. The opposite switch takes 650 sec, and in both cases there is an additional overhead of 6 min. associated with buffer dump. This consumes a significant portion of available orbital time. Thus, whenever possible, one should plan to use HRC and SBC in different orbits.

---

## 9.3 Orbit Use Determination Examples

The easiest way to learn to compute total orbit time requests is to work through a few examples. Below we provide five different examples:

- Example 1 is a simple WFC image in one filter.
- Example 2 is a set of short WFC exposures that may require large overheads associated with buffer dumps.
- Example 3 is a one-orbit coronagraphic observation in two filters.
- Example 4 is a two-orbit observation using dithering.
- Example 5 is a one orbit WFC grism spectroscopic observation.

These examples represent fairly typical uses of ACS.

### 9.3.1 Sample Orbit Calculation 1:

Consider a target to be imaged with WFC in a given filter in one orbit. Using the Exposure Time Calculator (ETC), we find that we need 2400 sec of exposure time to reach the desired level of signal-to-noise ratio. Given that the observation must be split into a series of two exposures by CR-SPLIT (CR-SPLIT=2), we map the overheads and the science exposure times onto the orbit as follows:

Table 9.3: Orbit Calculation for Example

Action	Time (min.)	Explanation
<i>Orbit 1</i>		
Initial guide-star acquisition	6.1	Needed at start of observation of a new target
WFC overhead for the first exposure	4.0	Includes filter change, camera set-up, and readout
First science exposure	20.0	
WFC overhead for the subsequent science exposure in the series	2.5	Includes readout
The next science exposure in the series	20.0	
Total time for science exposures	40.0	
Total used time in the orbit	52.6	

Thus, the two WFC exposures totaling 2400 sec make full use of the typically available time in one orbit. The exposure times can be adjusted if the actual target visibility time differs from the derived total used time.

### 9.3.2 Sample Orbit Calculation 2

This example illustrates the impact of short WFC exposures on the useful time in the orbit. We have one orbit to observe a target with WFC in two filters, so the observation consists of two series, each with two identical CR-SPLIT exposures. The ETC has shown that at the minimally accepted signal-to-noise ratio the exposure time must be 540 sec for each of the filters, so each of the CR-SPLITS must be at least 270 sec long. For the target declination, we find that the visibility time is 55 min. The time budget for the orbit is then as follows:

Table 9.4: Orbit Calculation for Example 2

Action	Time (min.)	Explanation
<i>Orbit 1</i>		
Initial guide-star acquisition	6.1	Needed at start of observation of a new target
WFC overhead for the first exposures in two series	$2 \times 4 = 8$	Includes filter change, camera set-up, and readout
WFC overhead for subsequent exposures in each of the two series	$2 \times 2.5 = 5$	Includes readout
Additional overhead for all but the last exposures in the orbit	$5.8 \times 3 \approx 17$	Needed to dump the buffer because the next exposure is too short (shorter than 338 sec) to accommodate the dump time.
Science exposures	$4 \times 4.5 = 18$	
Total time for science exposures	18	
Total used time in the orbit	54	

Comparing with the previous example, we see that although with the adopted minimum exposure times we can squeeze the observation into one orbit, the efficiency of the orbit use is very low because of the large overheads associated with buffer dumps. However, if we increase each of the four exposure times so that they are larger than 338 sec, we avoid these additional overheads. This would free ~17 min. of the orbit time for science, which allows us to almost double the science exposure time (35 min. instead of 18 min.) and thus significantly improve signal-to-noise.

### 9.3.3 Sample Orbit Calculation 3:

This example demonstrates orbit calculation for a coronagraphic observation. We want to obtain coronagraphic images of a star in two filters, F250W and F606W. The ETC has shown that the exposure times adequate for our scientific goals are 5 min. in F606W and 30 min. in F250W. From the orbit visibility table (see the *Call for Proposals* and Phase I Proposal Instructions) we find that at the target declination of 15 degrees the target visibility time is 52 min. With CR-SPLIT=2, we thus have to accommodate in that period 35 min. of four science exposures grouped in two series. The orbit calculation goes like this:

Table 9.5: Orbit Calculation for Example 3

Action	Time (min.)	Explanation
<i>Orbit 1</i>		
Initial guide-star acquisition	6.1	Needed at start of observation of a new target
Target acquisition	$3.5 + (2 \times 0.1) = 3.7$	Point-source acquisition on target
HRC overhead for the first exposures in the series	$2 \times 2.5 = 5$	Includes filter change, camera set-up, and readout
HRC overhead for the subsequent exposures in the series	$2 \times 1 = 2$	Includes readout
Science exposures in F606W	$2 \times 2.5 = 5$	
Science exposures in F250W	$2 \times 15 = 30$	
Total time for science exposures	40	
Total used time in the orbit	~52	

The derived total used time in the orbit shows that our target can indeed be imaged in the selected filters in one orbit. Since there remains 3 min. of unused time, we can adjust our exposure times to make full use of the available time.

### 9.3.4 Sample Orbit Calculation 4:

This example illustrates orbit calculation for a WFC observation with the ACS box pattern, which implements imaging at four offset pointings. The goal of the observation is to obtain a dithered image of a field in such a way that would allow us to bridge the 50-pixel interchip gap between the WFC CCDs in the combined image. Given the WFC plate scale of 0.05 arcsec/pix, this requires that the offsets in the dithering pattern are larger than 2.5 arcsec. Each offset will then take 0.5 min. to move the spacecraft from one pointing in the pattern to another. We have determined that the exposure time necessary to reach the desired signal-to-noise ratio is 80 min. The visibility time at our target declination is 58 min. In this observation we do not want to rely on cosmic ray removal provided by the dithering data reduction package, and set `CR-SPLIT=2` to be able to remove cosmic rays from the four individual images separately. As a result, the orbit calculation will involve a series of 8 exposures (two exposures at each of the four pointings in the dithering pattern) split across two orbits:

Table 9.6: Orbit Calculation for Example 4

Action	Time (min.)	Explanation
<i>Orbit 1</i>		
Initial guide-star acquisition	6.1	Needed at start of observation of a new target
WFC overhead for the first exposures in the series	4	Includes filter change, camera set-up, and readout
WFC overhead for the subsequent 3 exposures in the series	$3 \times 2.5 = 7.5$	Includes readout
Spacecraft slew	0.5	To offset from the first to the second pointing
Four science exposures	$4 \times 10 = 40$	Exposures at the first two pointings in the dither pattern
Total time for science exposures	40	
Total used time in the orbit	58.1	
<i>Orbit 2</i>		
Guide-star re-acquisition	5.7	Needed at start of a new orbit to observe the same target
WFC overhead for the remaining exposures in the series	$4 \times 2.5 = 10$	Includes readout
Spacecraft slews	$2 \times 0.5 = 1$	To offset to the third and fourth pointings
Four science exposures	$4 \times 10 = 40$	Exposures at the second two pointings in the dither pattern
Total time for science exposures	40	
Total used time in the orbit	58.7	



The total used time in the second orbit comes out a little bit larger than the visibility time. However, given the conservative nature of the adopted overhead times as well as a bit of flexibility in the adopted signal-to-noise ratio, the difference is not significant. It is to be remembered that the purpose of the above exercises is to estimate how many orbits to request for our science program rather than to exactly design the observation.

### 9.3.5 Sample Orbit Calculation 5:

This example illustrates orbit calculation for a simple 30 min. WFC grism spectroscopic observation broken down by CR-SPLIT=2 into a series of two exposures.

Table 9.7: Orbit Calculation for Example 5

Action	Time (min.)	Explanation
<i>Orbit 1</i>		
Initial guide-star acquisition	6.1	Needed at start of observation of a new target
Predefined imaging exposure for grism spectroscopy	10	Needed to co-locate the targets and their spectra in the FOV
WFC overhead for the first science exposure in the series	4.0	Includes filter change, camera set-up, and readout
WFC overhead for the subsequent science exposure in the series	2.5	Includes readout
Two science exposures	$2 \times 15.0 = 30$	
Total science exposure time	30.0	
Total used time in the orbit	52.6	

Unlike similar imaging exposures, here we have to take into account an additional imaging exposure before the sequence of spectroscopic exposures, which takes 10 min. off the available orbit time.





PART III:

# Supporting Material

---

The chapters in this Part present more detailed material in support of the User's Guide. Included is the imaging reference material.



## CHAPTER 10:

# Imaging Reference Material

### In this chapter . . .

10.1 Introduction / 186	HRC/F550M / 210
10.2 Using the Information in this Chapter / 186	HRC/F555W / 211
WFC/F435W / 189	HRC/F606W / 212
WFC/F475W / 190	HRC/F625W / 213
WFC/F502N / 191	HRC/F658N / 214
WFC/F550M / 192	HRC/F660N / 215
WFC/F555W / 193	HRC/F775W / 216
WFC/F606W / 194	HRC/F814W / 217
WFC/F625W / 195	HRC/F850LP / 218
WFC/F658N / 196	HRC/F892N / 219
WFC/F660N / 197	HRC/G800L / 220
WFC/F775W / 198	HRC/PR200L / 221
WFC/F814W / 199	HRC/CLEAR / 222
WFC/F850LP / 200	SBC/F115LP / 223
WFC/G800L / 201	SBC/F122M / 224
WFC/CLEAR / 202	SBC/F125LP / 225
HRC/F220W / 203	SBC/F140LP / 226
HRC/F250W / 204	SBC/F150LP / 227
HRC/F330W / 205	SBC/F165LP / 228
HRC/F344N / 206	SBC/PR110L / 229
HRC/F435W / 207	SBC/PR130L / 230
HRC/F475W / 208	10.3 Distortion in the ACS / 234
HRC/F502N / 209	

In this Chapter, we provide imaging reference material, in support of the information presented in Chapter 6.

---

## 10.1 Introduction

This chapter provides reference material to help you select your filter and detector configuration and determine your observing plan (e.g., total required exposure time, and number of exposures). This chapter is, for the most part, organized by *filter* and *detector*. For each imaging mode the following are provided:

- Plots of integrated system throughput as a function of wavelength.
- Plots of the time needed to achieve a desired signal-to-noise ratio vs. magnitude for all filters for a point source and a one arcsec<sup>2</sup> extended source.

---

## 10.2 Using the Information in this Chapter

### 10.2.1 Sensitivity Units and Conversions

This chapter contains plots of throughputs for each imaging mode. “Determining Count Rates from Sensitivities” on page 98 explains how to use these throughputs to calculate expected count rates from your source.

The first figure for each imaging mode gives the integrated system throughput. This is the combination of the efficiencies of the detector and of the optical elements in the light path. The throughputs in this handbook are based in part on ground test data. Although, at the time of writing the overall detector efficiency curve and most filter throughputs have been adjusted based on in-flight data. The throughput is defined as the number of detected counts per second per cm<sup>2</sup> of telescope area relative to the incident flux in photons per cm<sup>2</sup> per second. For the CCD “counts” is the number of electrons detected. For the MAMA, “counts” is the number of valid events processed by the detector electronics after passing through the various pulse-shape and anti-coincidence filters. In both cases the detected counts obey Poisson statistics. The throughput includes all obscuration effects in the optical train (e.g., due to the HST secondary). Comparisons of the throughput between ACS and the other instruments can be found in “Which instrument to use?” on page 43.

To recalculate the throughput with the most recent CCD QE tables in synphot, you can create total-system-throughput tables (instrument plus OTA) using the synphot calcband task. Calcband takes any valid obsmode command string as input and produces an STSDAS table with two columns of data called "wavelength" and "throughput" as its output. For example, to evaluate the throughput for the F475W filter and the WFC detector, chip 1,

you would use the command **calcband acs,wfc1,f475w sdssg\_thpt**. The resulting throughput table is stored in **sdssg\_thpt**.

### 10.2.2 Signal-To-Noise

For each imaging mode, plots are provided to estimate the signal-to-noise (S/N) for a representative source. The first figure shows S/N for point sources (**GAIN=1**). The second figure shows S/N for uniform extended sources of area 1 arcsec<sup>2</sup>.

The different line styles in the S/N figures delineate regions where different sources of noise dominate. A particular source of noise (readnoise for example) is presumed to dominate if it contributes more than half the total noise in the observations.

The point- and extended-source S/N figures are shown for average and low sky levels. An aperture size of 5x5 pixels has been used for the WFC, 9x9 pixels for HRC and 15x15 pixels for the SBC S/N evaluation. For the CCD the read noise has been computed assuming a number of readouts  $N_{\text{READ}} = \text{integer}(t / 1000 \text{ s})$ , where  $t$  is the exposure time, with a minimum  $N_{\text{READ}}=2$ . That is, each exposure has a minimum **CR-SPLIT=2**. Different line styles in the figures are used to indicate which source of noise dominates.

To the left of the vertical line in the SBC S/N plots, the count rate from the source exceeds the 150 counts sec<sup>-1</sup> pix<sup>-1</sup> local count rate limit. This is computed from the model PSF, which gives 14 to 22% of the flux in the central pixel.

In situations requiring more detailed calculations (non-stellar spectra, extended sources, other sky background levels, unknown target V magnitude, etc.), the ACS Exposure-Time Calculator, located at the ACS web page, should be used.

Follow these steps to use the signal-to-noise plots:

1. Determine the AB magnitude of your source at the wavelength of interest. There are several ways to do this.
  - Examine Table 10.1, 10.2 or 10.3 and find  $AB_V$  for the desired spectral type and filter. Sum the V magnitude of the target and  $AB_V$  derived from the table.
  - Alternatively, compute  $ABMAG (=V+AB_V)$  from the source flux, using the relation  $ABMAG = -2.5 \log f_V - 48.60$ , or  $ABMAG = -2.5 \log f_\lambda - 5 \log \lambda - 2.406$ .
2. Find the appropriate plot for the filter in question, and locate  $V+AB_V$  on the horizontal axis. Then read off the signal-to-noise ratio for the desired exposure time, or vice-versa.

The “x” characters at the top of each plot indicate the onset of saturation, in the case of the CCD. The “x” shows where the total number of counts exceeds the 16-bit buffer size of 65,535.

Note that the plots show the S/N as a function of source magnitude for exposure times as short as 0.1s, although the minimum exposure time for the WFC CCD channel is 0.5s.

### 10.2.3 Point Spread Functions

All information about the PSF are based on the modeled encircled energy data presented in “ACS Point Spread Functions” on page 56.



## WFC/F435W

### Description

Johnson B filter.

Figure 10.1: Integrated System Throughput for WFC/F435W

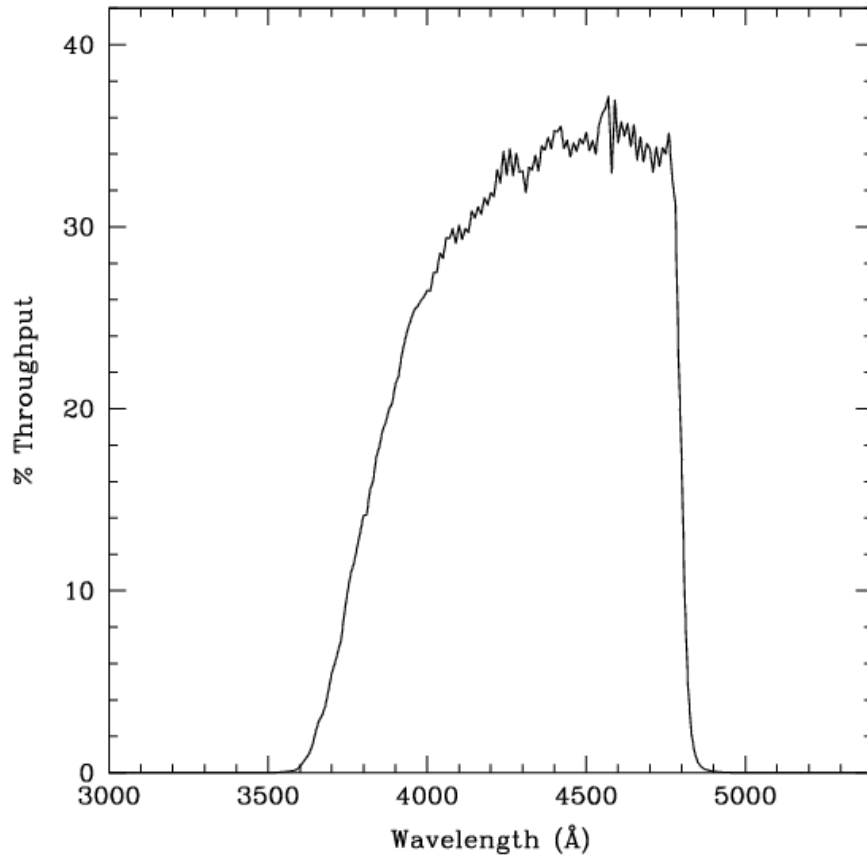


Figure 10.2: Point Source S/N vs.  $V+AB_v$  for the WFC/F435W filter. Top curves are for low sky; bottom curves are for average sky.

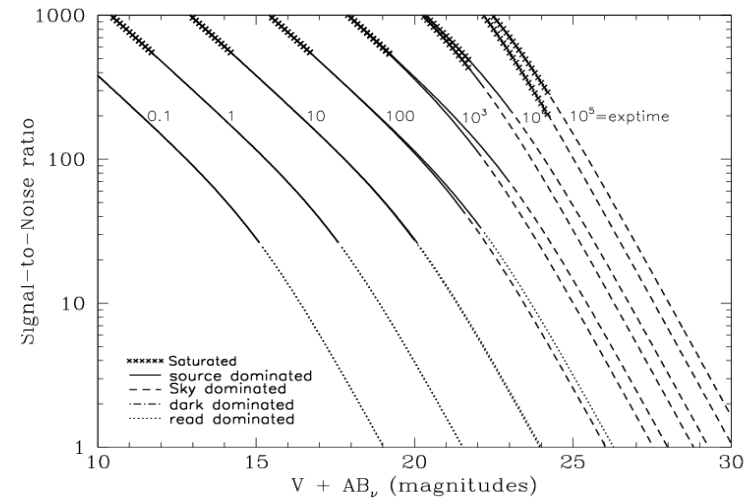
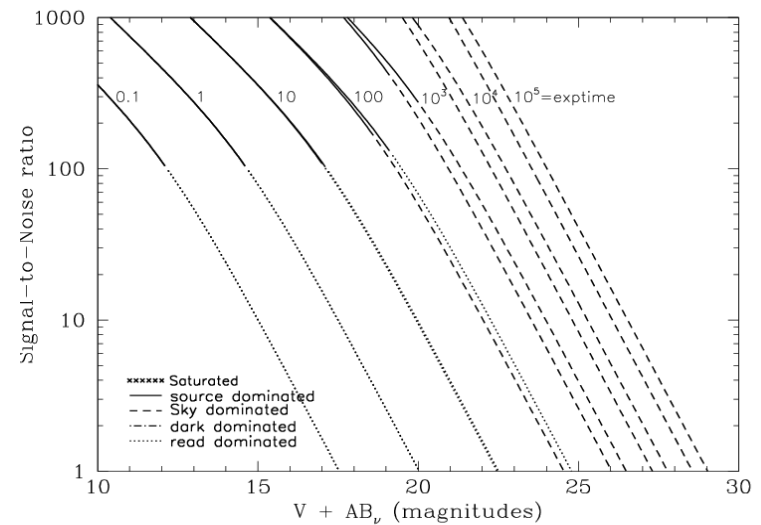


Figure 10.3: Extended Source S/N vs.  $V+AB_v$  for the WFC/F435W filter. Top curves are for low sky and bottom curves are for average sky for a 1 arcsec<sup>2</sup> area.



## WFC/F475W

### Description

Sloan Digital Sky Survey g filter.

Figure 10.4: Integrated System Throughput for WFC/F475W

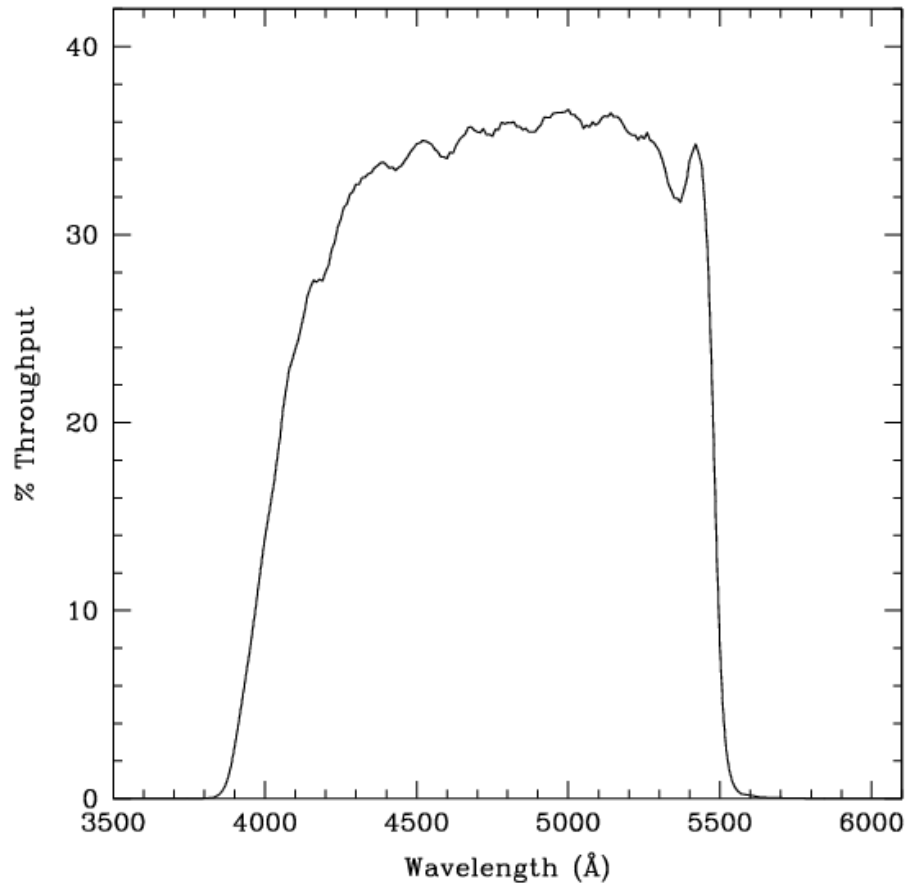


Figure 10.5: Point Source S/N vs.  $V+AB_v$  for the WFC/F475W filter. Top curves are for low sky; bottom curves are for average sky.

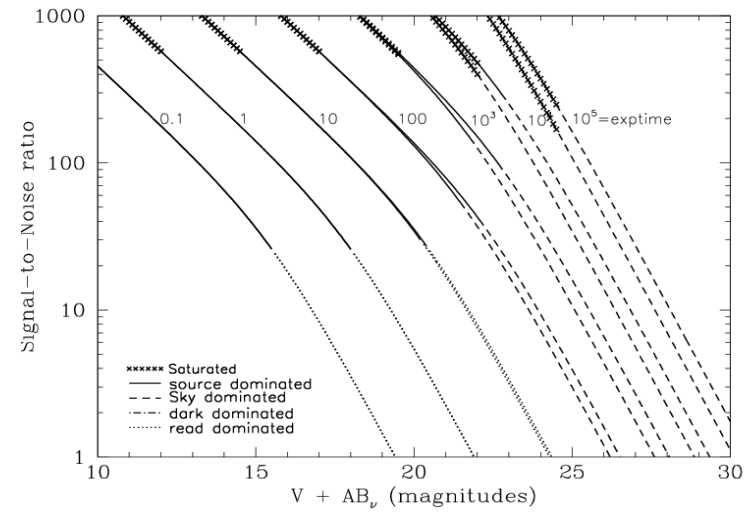
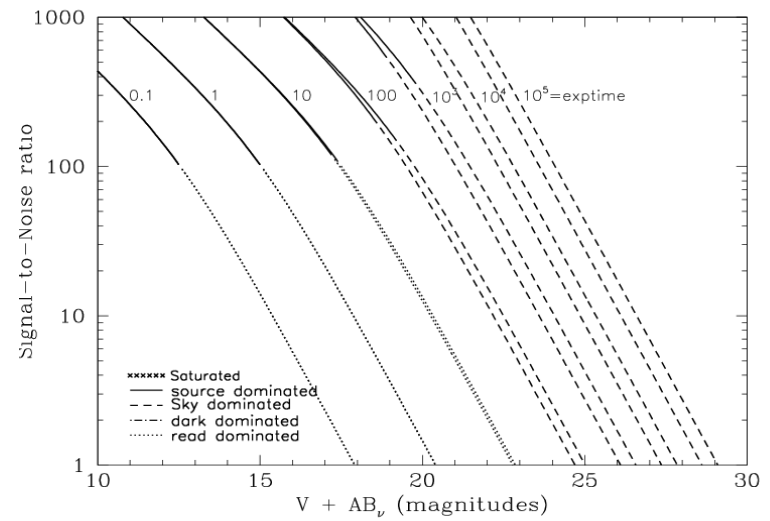


Figure 10.6: Extended Source S/N vs.  $V+AB_v$  for the WFC/F475W filter. Top curves are for low sky and bottom curves are for average sky for a 1 arcsec<sup>2</sup> area.



## WFC/F502N

### Description

OIII filter.

Figure 10.7: Integrated System Throughput for WFC/F502N

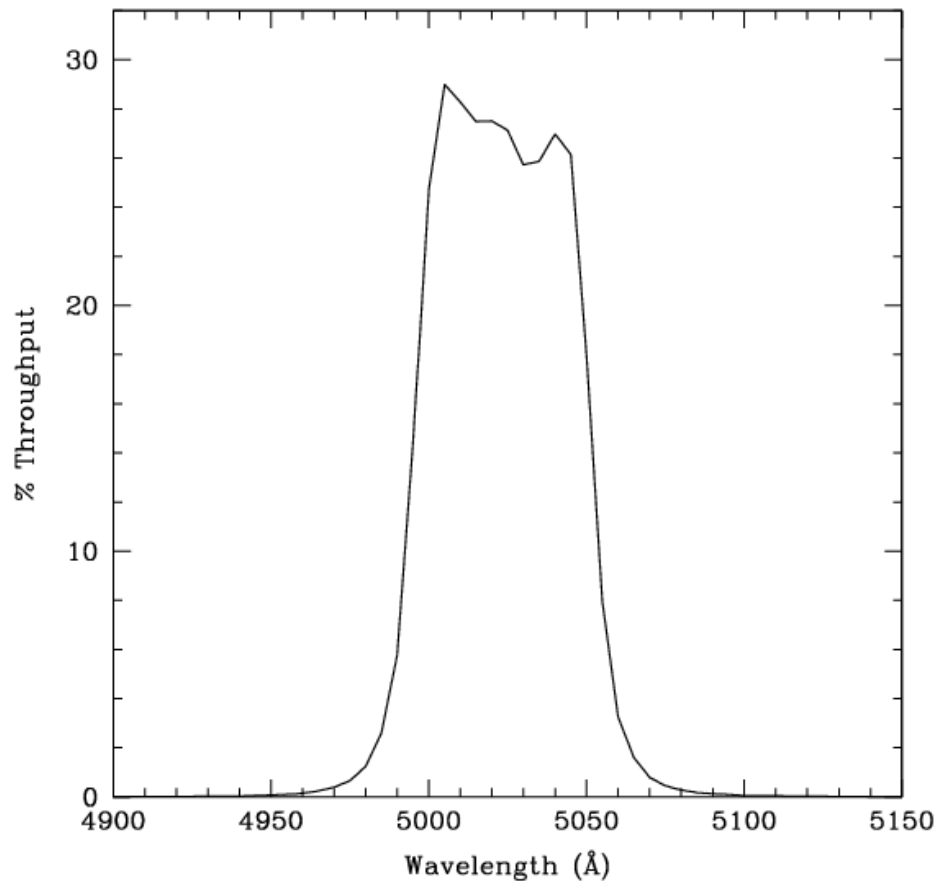


Figure 10.8: Point Source S/N vs.  $V+AB_v$  for the WFC/F502N filter. Top curves are for low sky; bottom curves are for average sky.

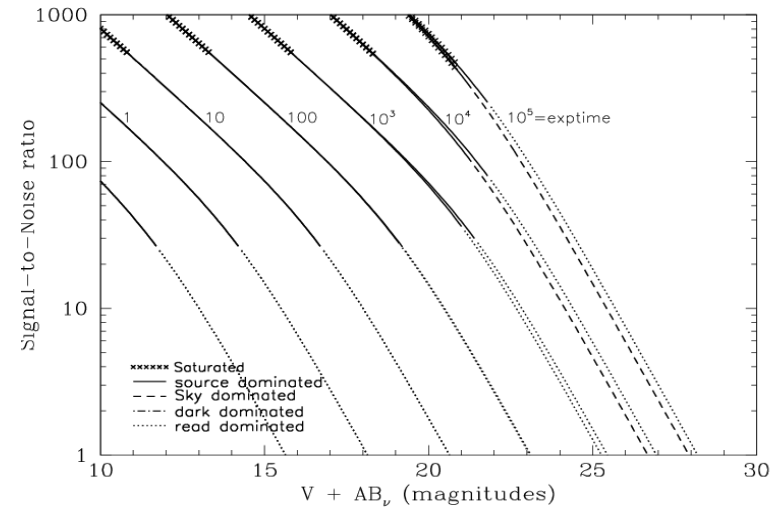
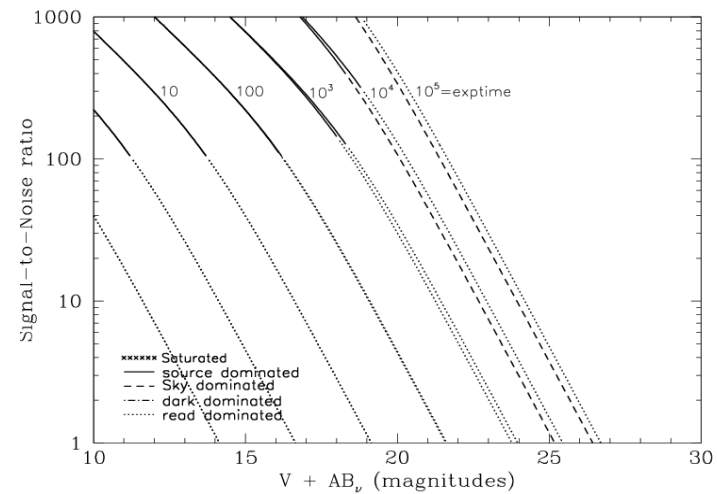


Figure 10.9: Extended Source S/N vs.  $V+AB_v$  for the WFC/F502N filter. Top curves are for low sky and bottom curves are for average sky for a 1 arcsec<sup>2</sup> area.



# WFC/F550M

## Description

Narrow V filter.

Figure 10.10: Integrated System Throughput for WFC/F550M

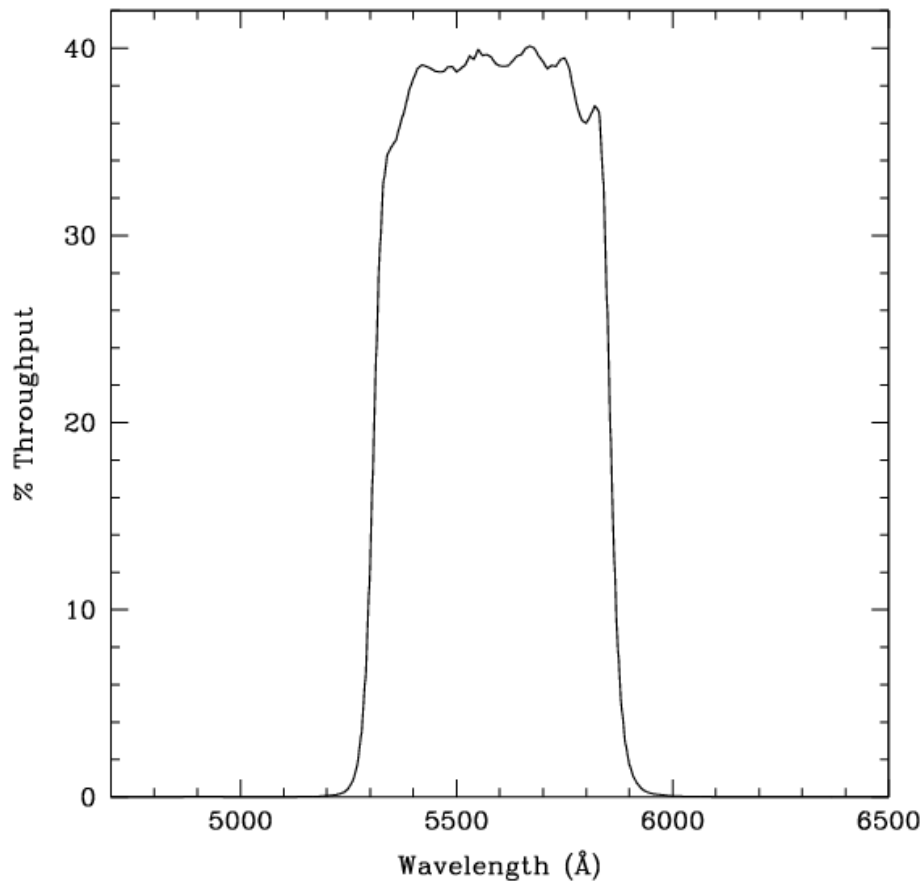


Figure 10.11: Point Source S/N vs.  $V+AB_V$  for the WFC/F550M filter. Top curves are for low sky; bottom curves are for average sky.

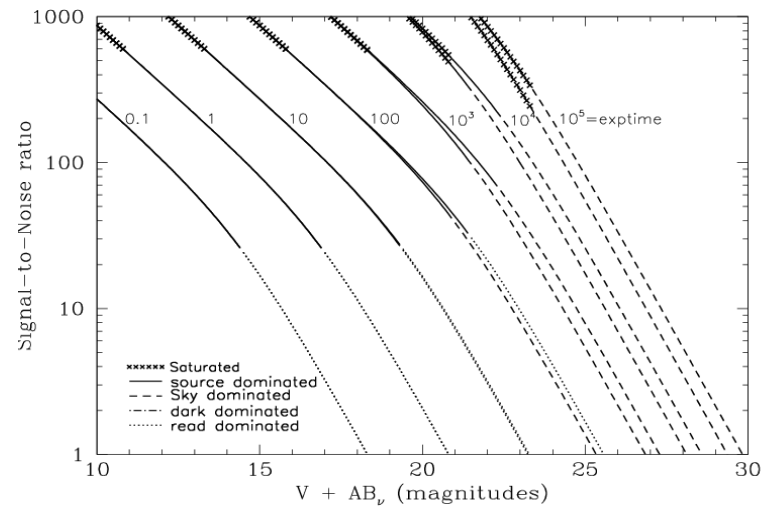
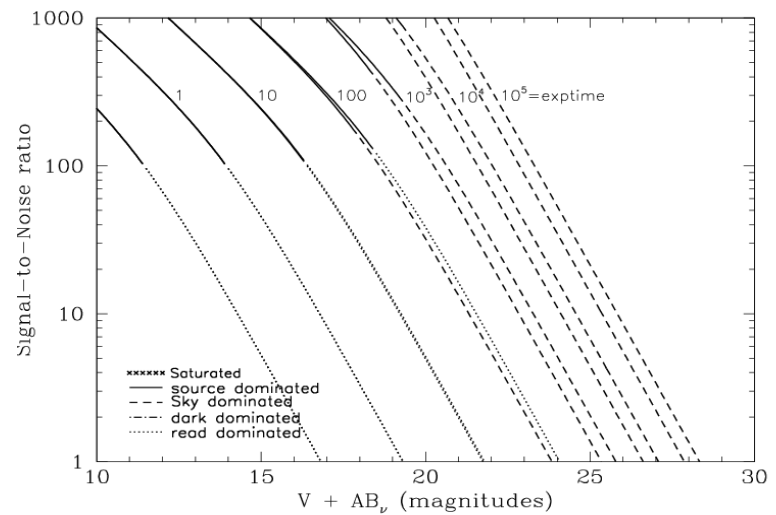


Figure 10.12: Extended Source S/N vs.  $V+AB_V$  for the WFC/F550M filter. Top curves are for low sky and bottom curves are for average sky for a 1 arcsec<sup>2</sup> area.



## WFC/F555W

### Description

Johnson V filter.

Figure 10.13: Integrated System Throughput for WFC/F555W

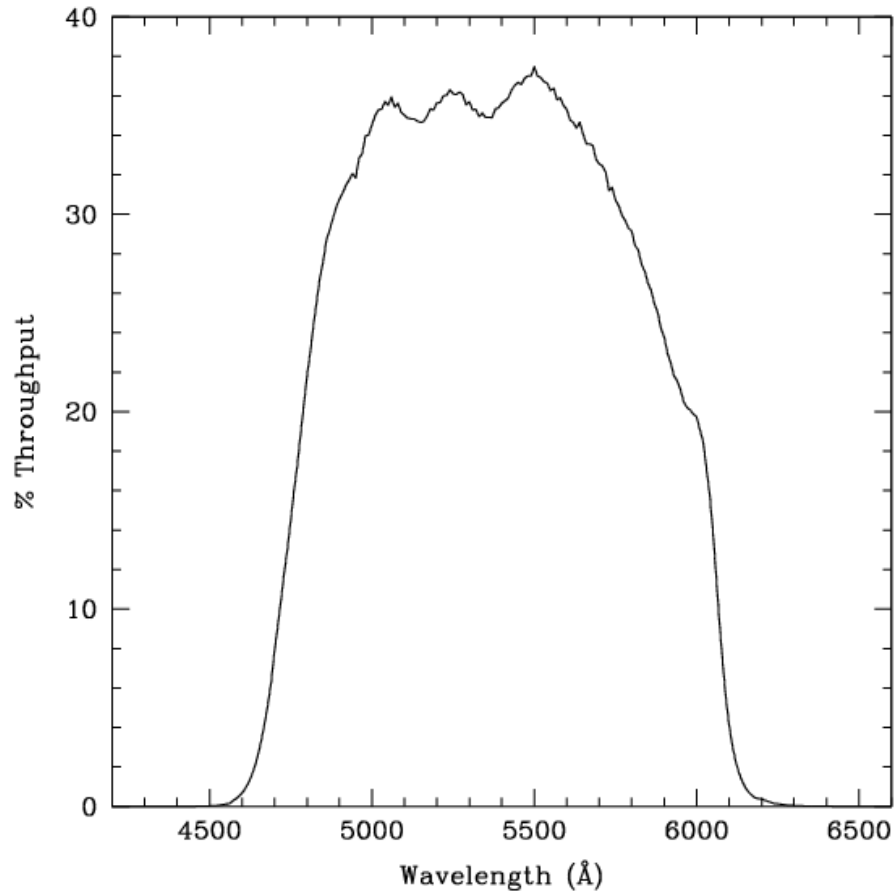


Figure 10.14: Point Source S/N vs.  $V+AB_v$  for the WFC/F555W filter. Top curves are for low sky; bottom curves are for average sky.

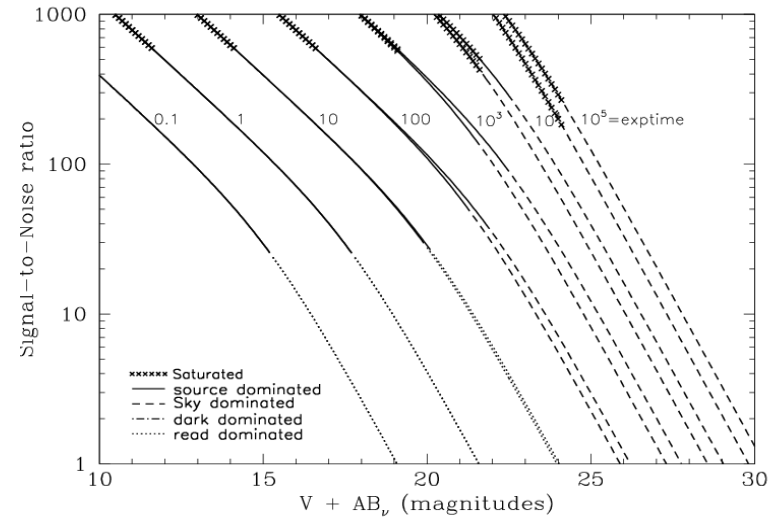
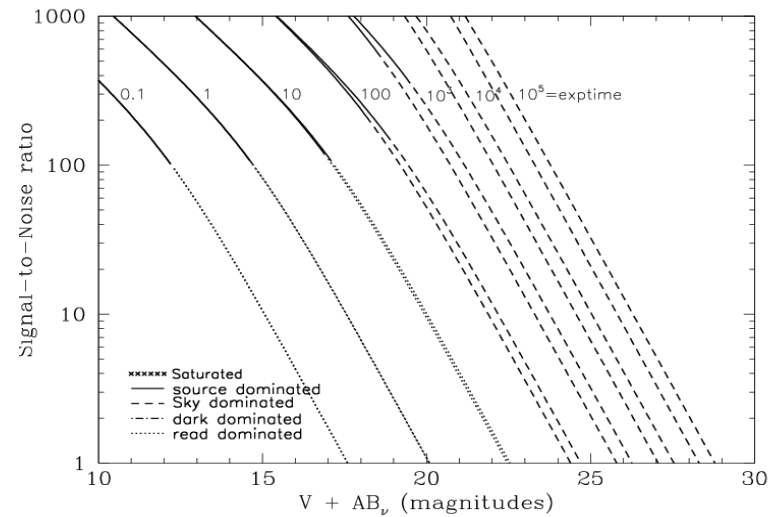


Figure 10.15: Extended Source S/N vs.  $V+AB_v$  for the WFC/F555W filter. Top curves are for low sky and bottom curves are for average sky for a 1 arcsec<sup>2</sup> area.



## WFC/F606W

### Description

Broad V filter.

Figure 10.16: Integrated System Throughput for WFC/F606W

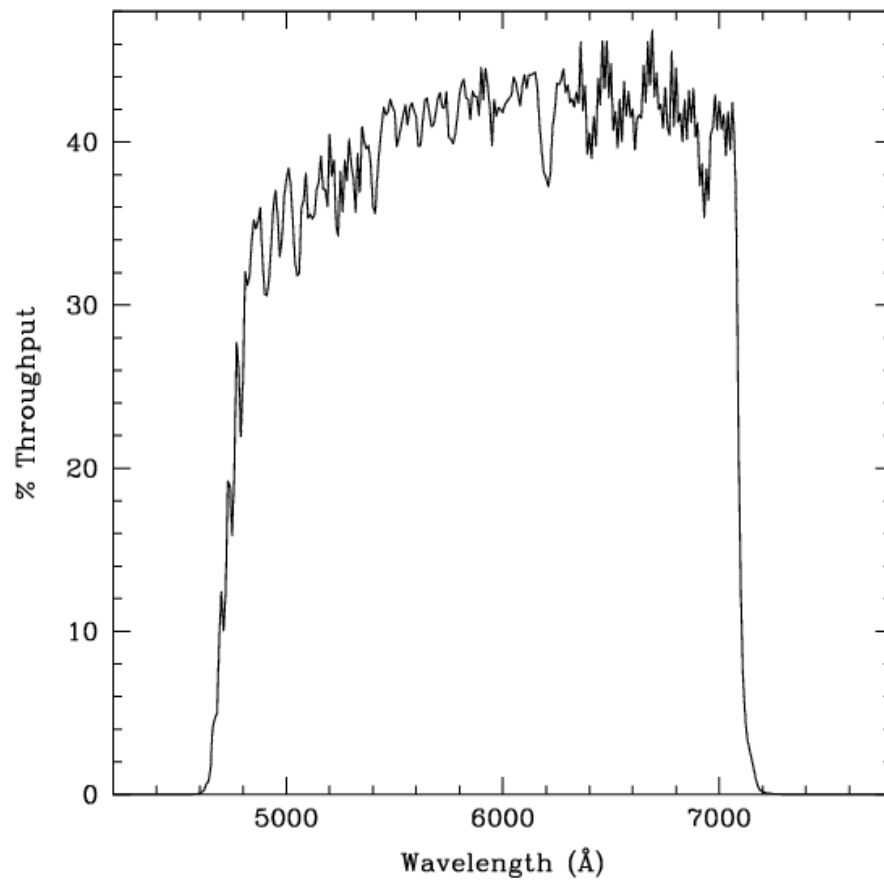


Figure 10.17: Point Source S/N vs.  $V+AB_v$  for the WFC/F606W filter. Top curves are for low sky; bottom curves are for average sky.

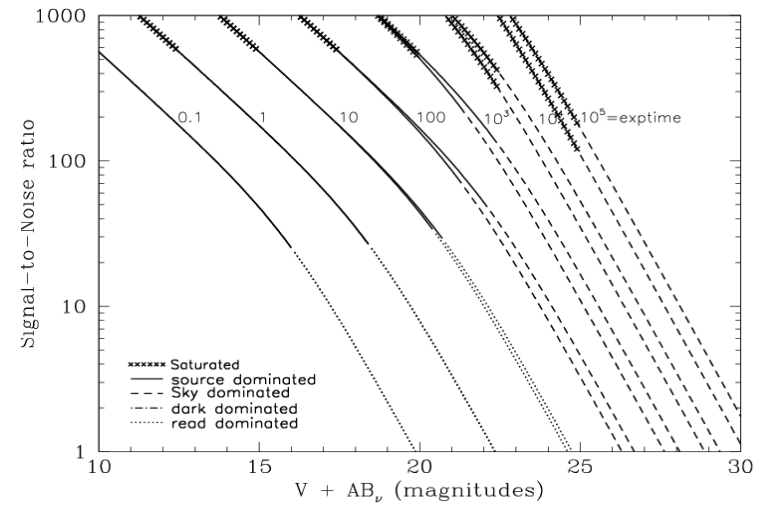
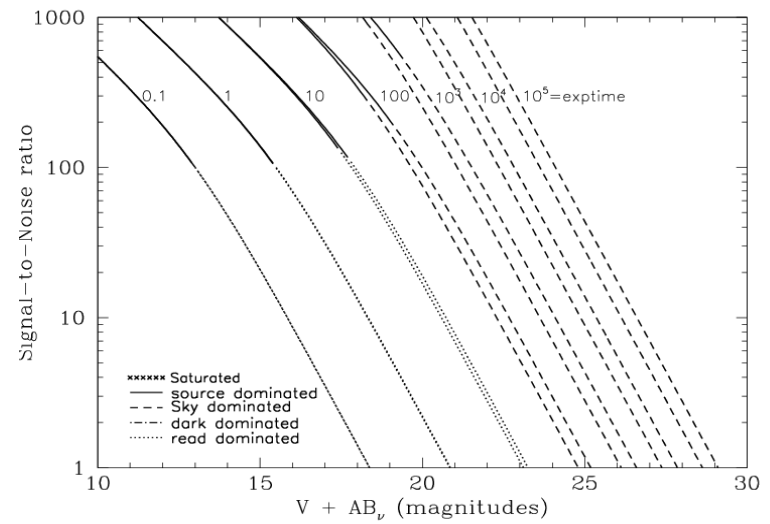


Figure 10.18: Extended Source S/N vs.  $V+AB_v$  for the WFC/F606W. Top curves are for low sky and bottom curves are for average sky for a  $1 \text{ arcsec}^2$  area.



## WFC/F625W

### Description

Sloan Digital Sky Survey r filter.

Figure 10.19: Integrated System Throughput for WFC/F625W

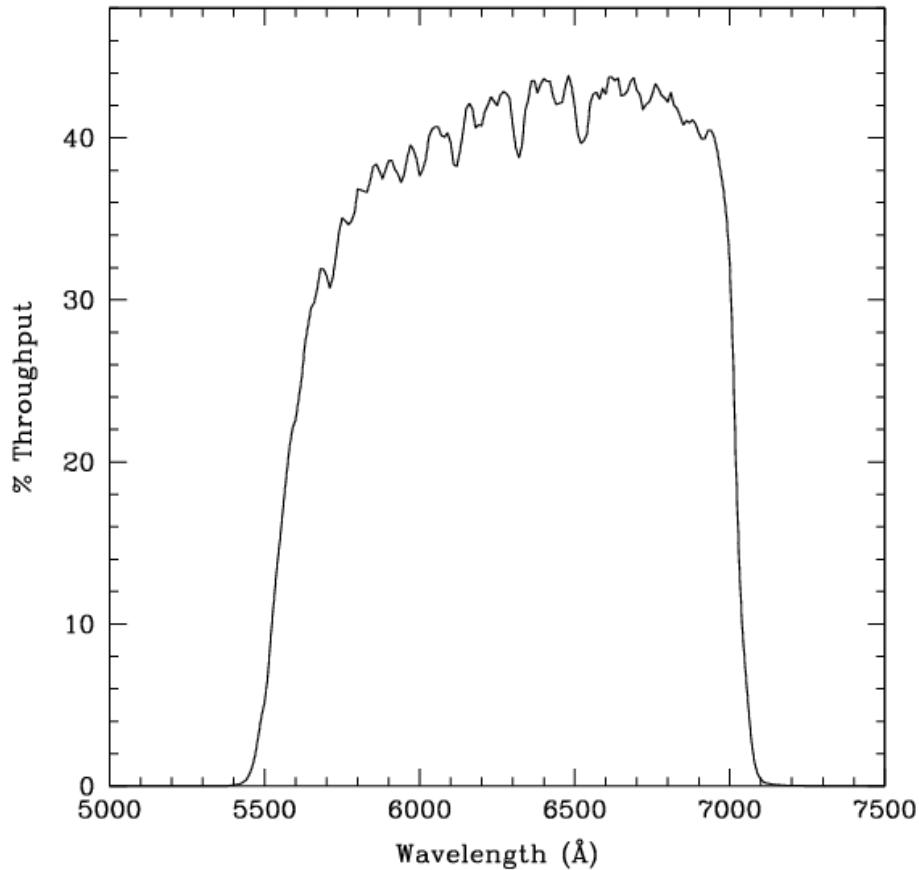


Figure 10.20: Point Source S/N vs.  $V+AB_V$  for the WFC/F625W filter. Top curves are for low sky; bottom curves are for average sky.

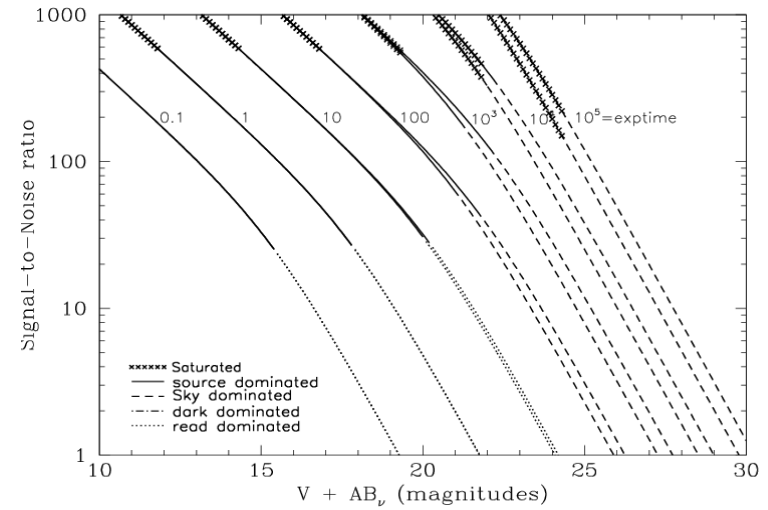
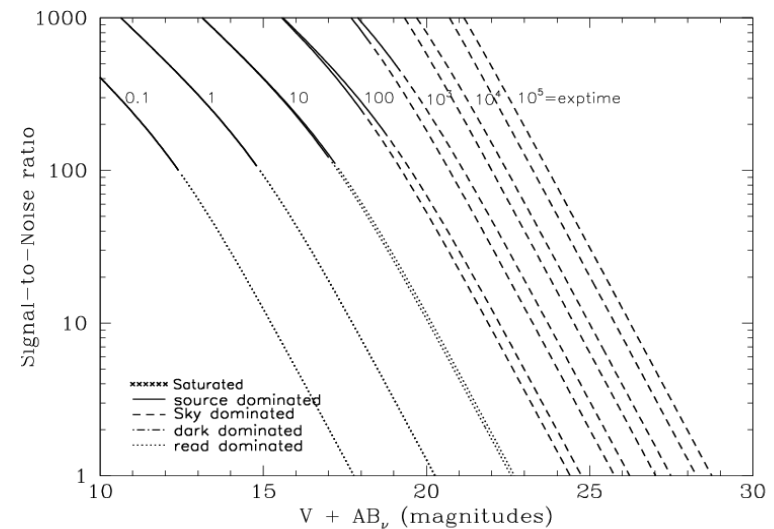


Figure 10.21: Extended Source S/N vs.  $V+AB_V$  for the WFC/F625W filter. Top curves are for low sky and bottom curves are for average sky for a 1 arcsec<sup>2</sup> area.



# WFC/F658N

## Description

H $\alpha$  filter.

Figure 10.22: Integrated System Throughput for WFC/F658N

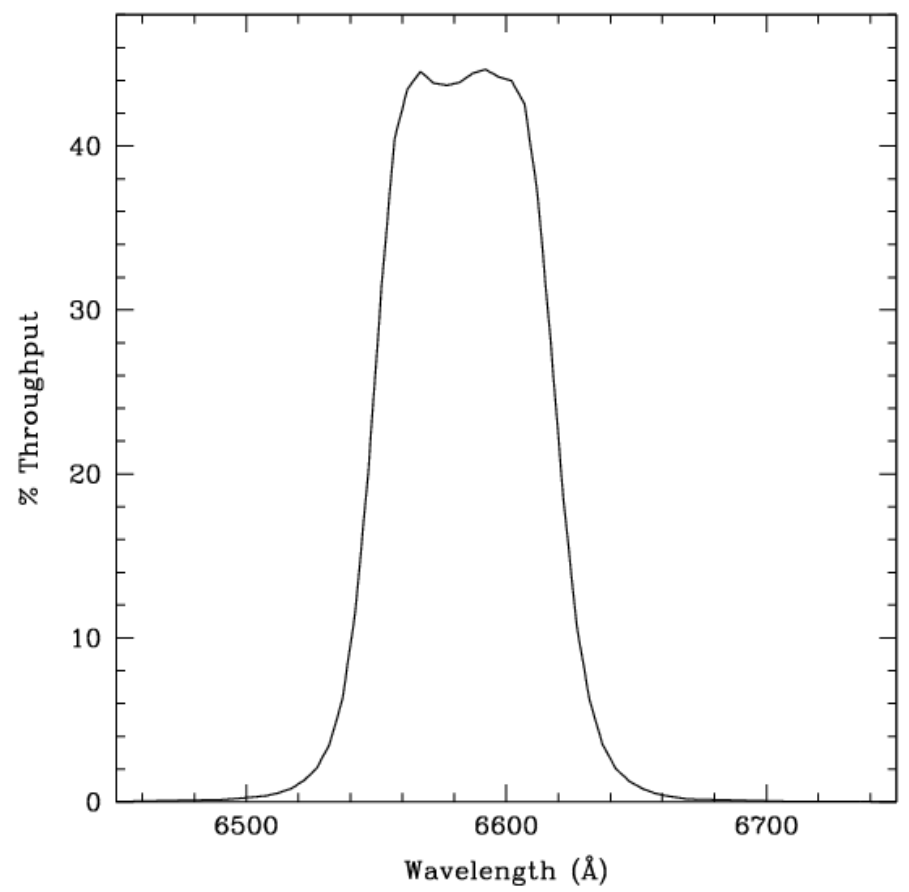


Figure 10.23: Point Source S/N vs.  $V+AB_V$  for the WFC/F658N filter. Top curves are for low sky; bottom curves are for average sky.

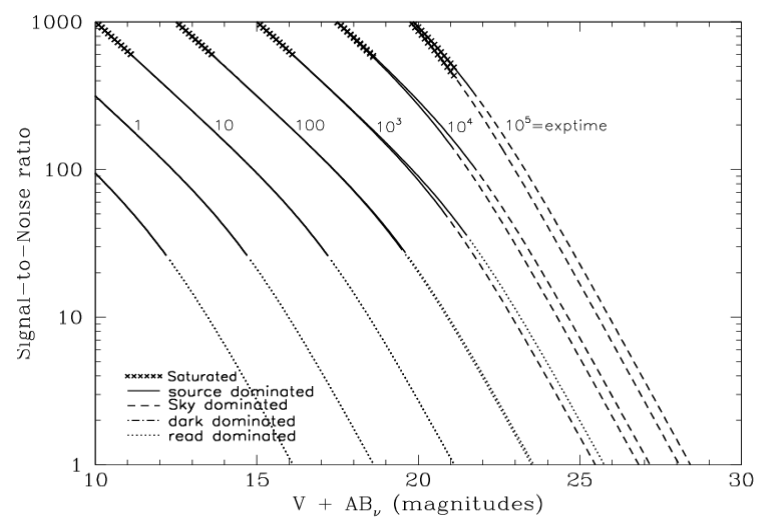
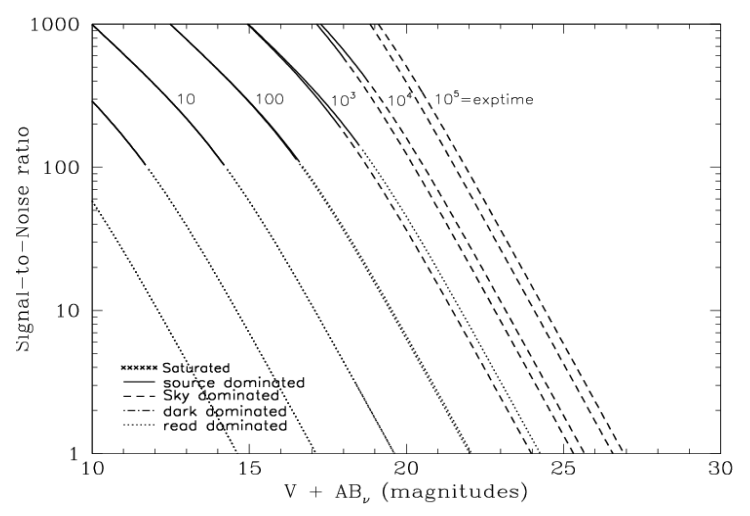


Figure 10.24: Extended Source S/N vs.  $V+AB_V$  for the WFC/F658N filter. Top curves are for low sky and bottom curves are for average sky for 1 arcsec<sup>2</sup> area.





## WFC/F660N

### Description

NII filter.

Figure 10.25: Integrated System Throughput for WFC/F660N

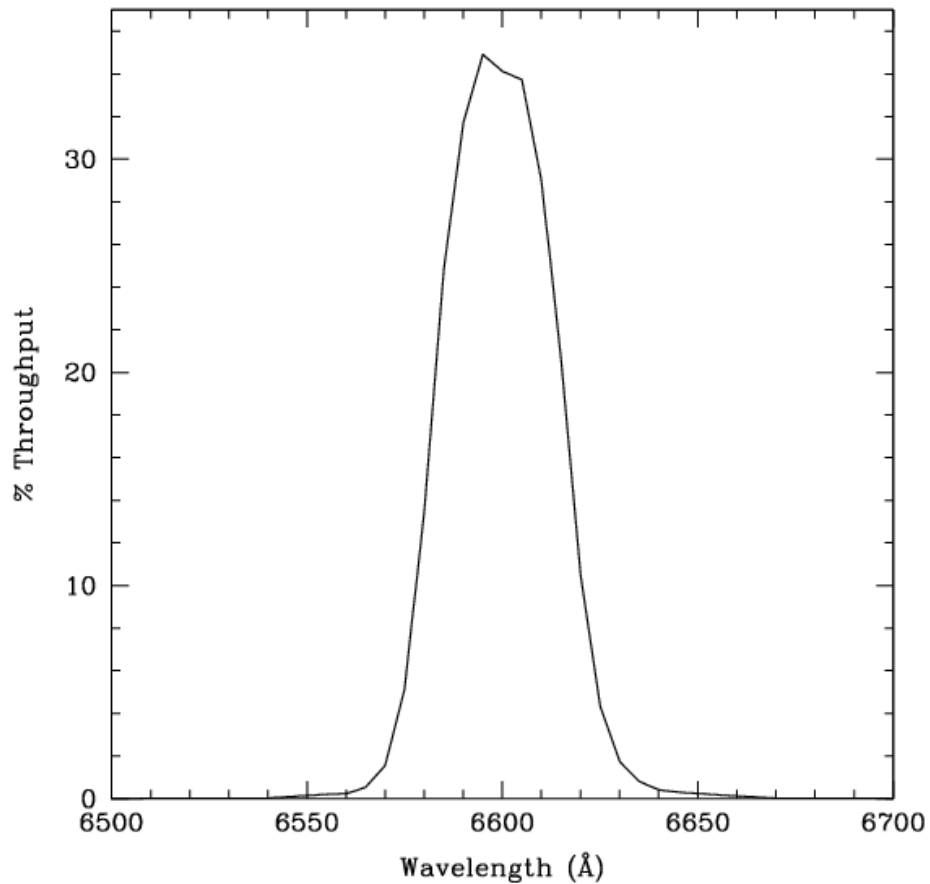


Figure 10.26: Point Source S/N vs.  $V+AB_V$  for the WFC/F660N filter. Top curves are for low sky; bottom curves are for average sky.

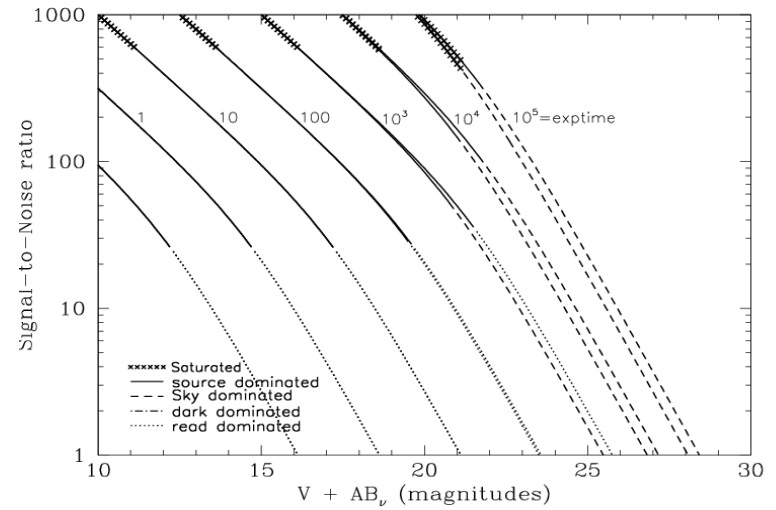
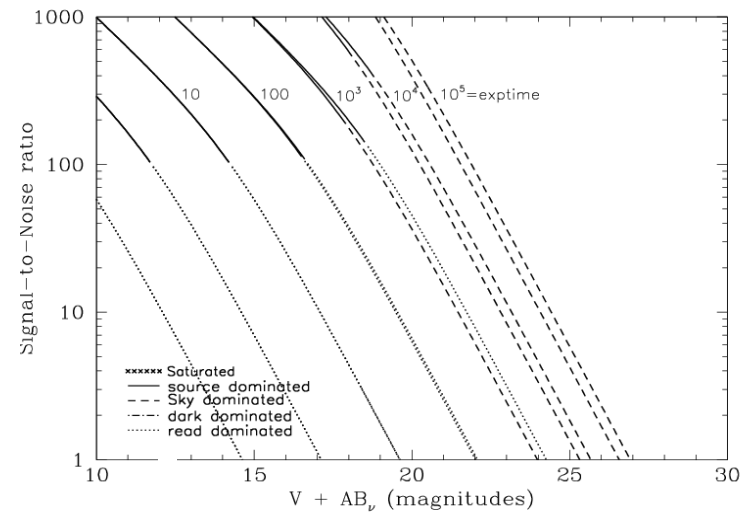


Figure 10.27: Extended Source S/N vs.  $V+AB_V$  for the WFC/F660N filter. Top curves are for low sky and bottom curves are for average sky for a 1 arcsec<sup>2</sup> area.



## WFC/F775W

### Description

Sloan Digital Sky Survey i filter

Figure 10.28: Integrated System Throughput for WFC/F775W

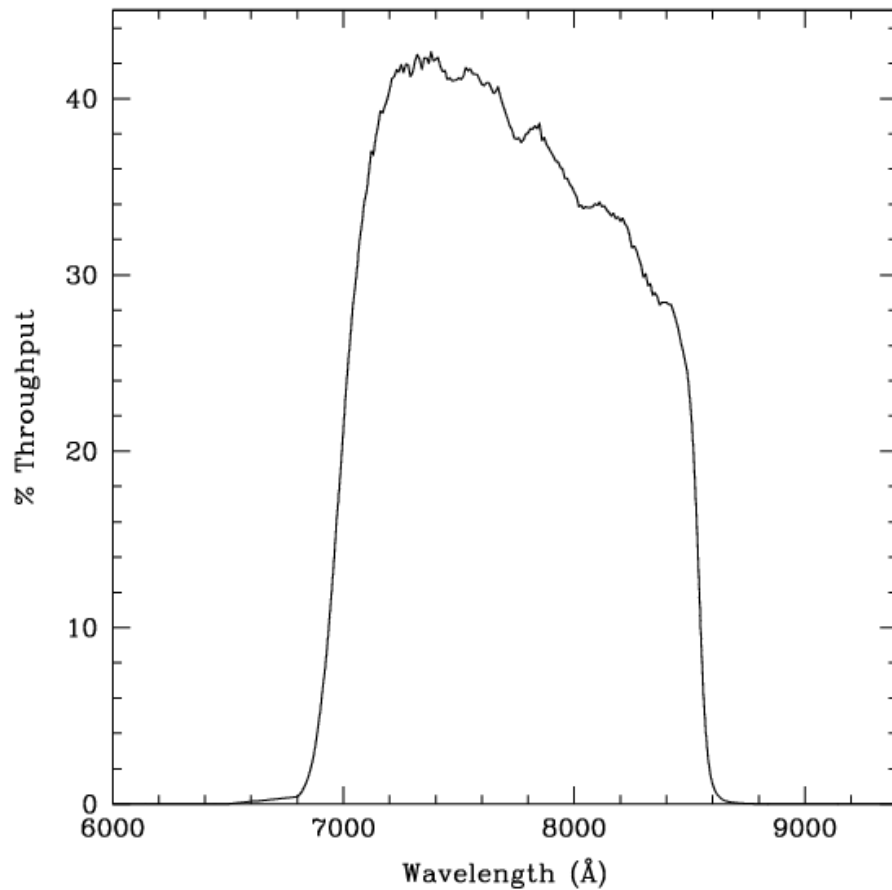


Figure 10.29: Point Source S/N vs.  $V+AB_V$  for the WFC/F775W filter. Top curves are for low sky; bottom curves are for average sky.

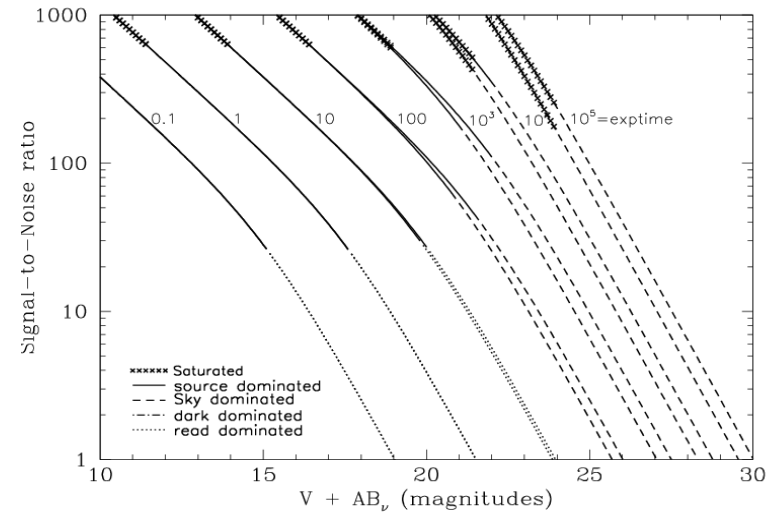
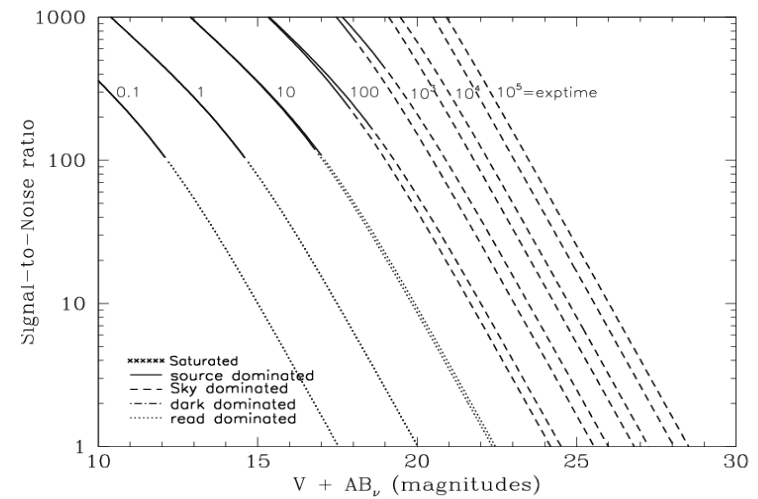


Figure 10.30: Extended Source S/N vs.  $V+AB_V$  for the WFC/F775W filter. Top curves are for low sky and bottom curves are for average sky for a 1 arcsec<sup>2</sup> area.



## WFC/F814W

### Description

Broad I filter.

Figure 10.31: Integrated System Throughput for WFC/F814W

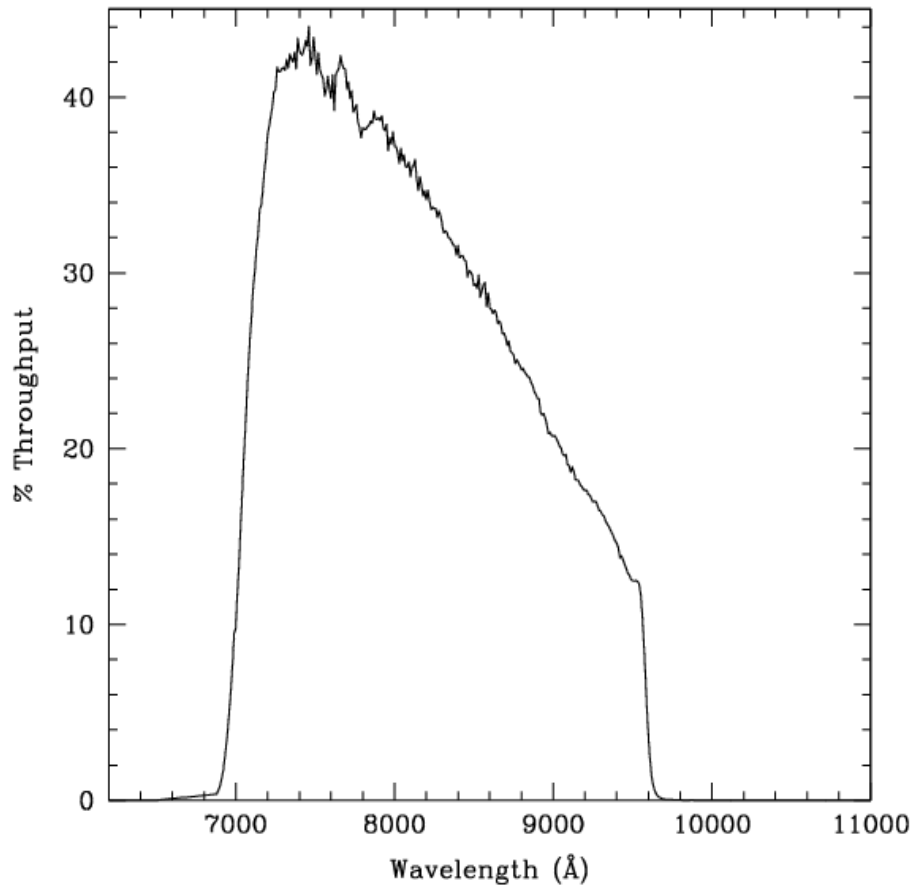


Figure 10.32: Point Source S/N vs.  $V+AB_V$  for the WFC/F814W filter. Top curves are for low sky; bottom curves are for average sky.

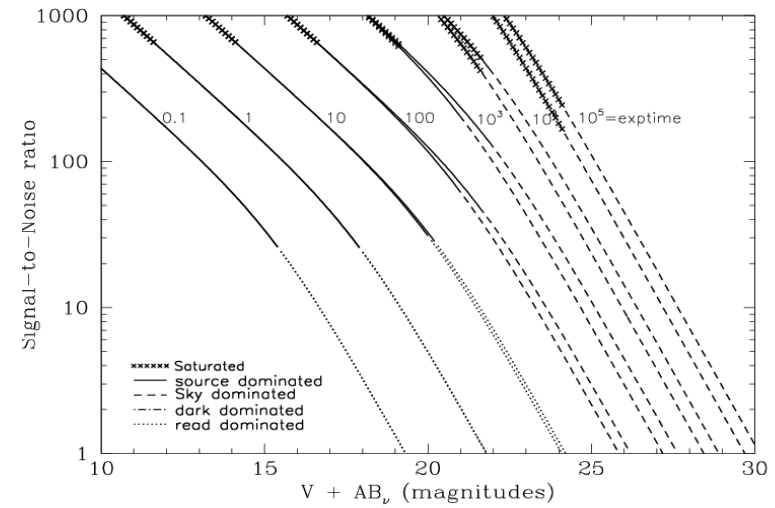
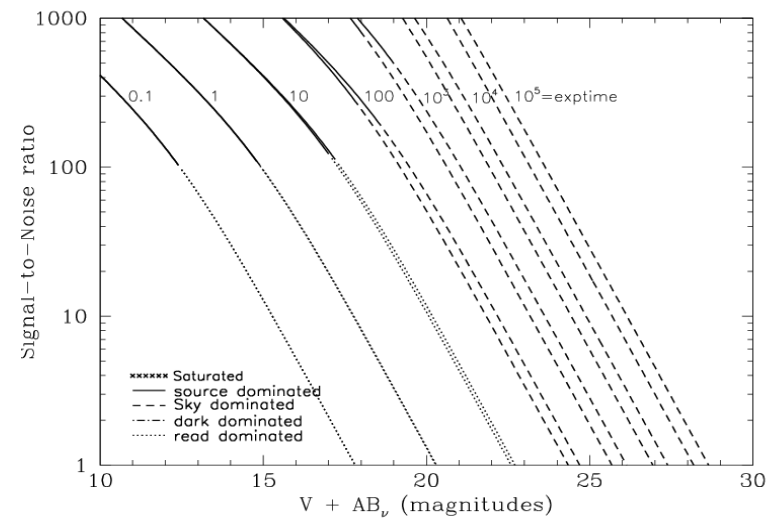


Figure 10.33: Extended Source S/N vs.  $V+AB_V$  for the WFC/F814W filter. Top curves are for low sky and bottom curves are for average sky for a 1 arcsec<sup>2</sup> area.



# WFC/F850LP

## Description

Sloan Digital Sky Survey z filter.

Figure 10.34: Integrated System Throughput for WFC/F850LP

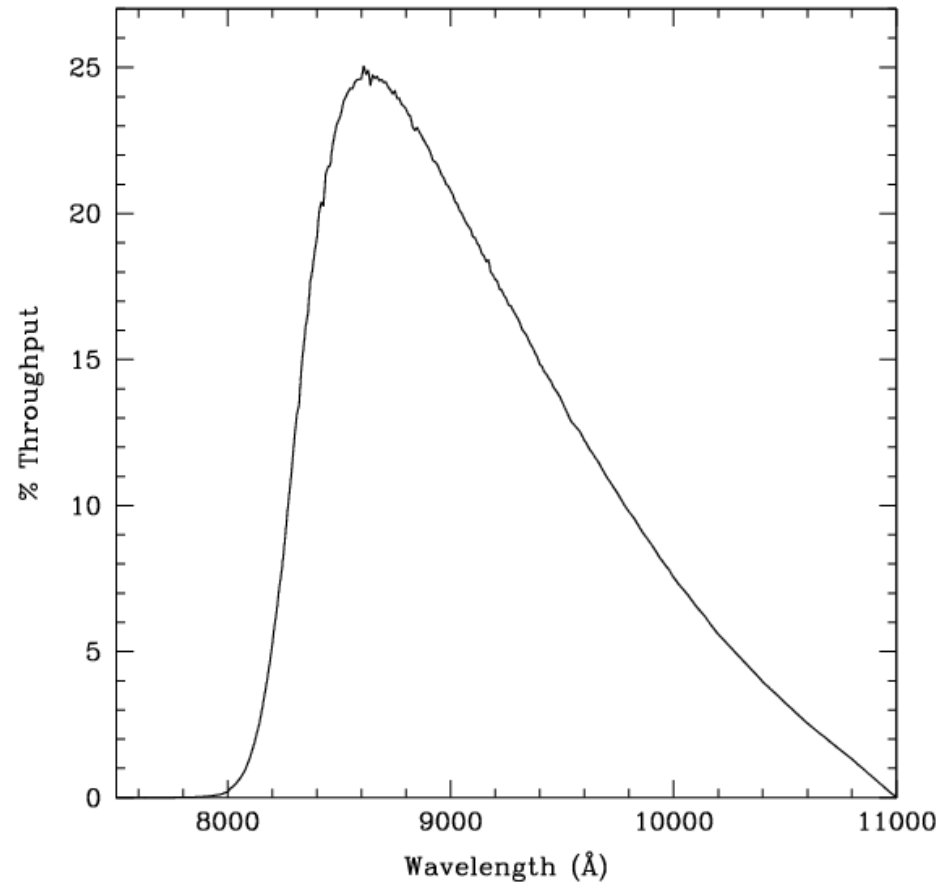


Figure 10.35: Point Source S/N vs.  $V+AB_V$  for the WFC/F850LP filter. Top curves are for low sky; bottom curves are for average sky.

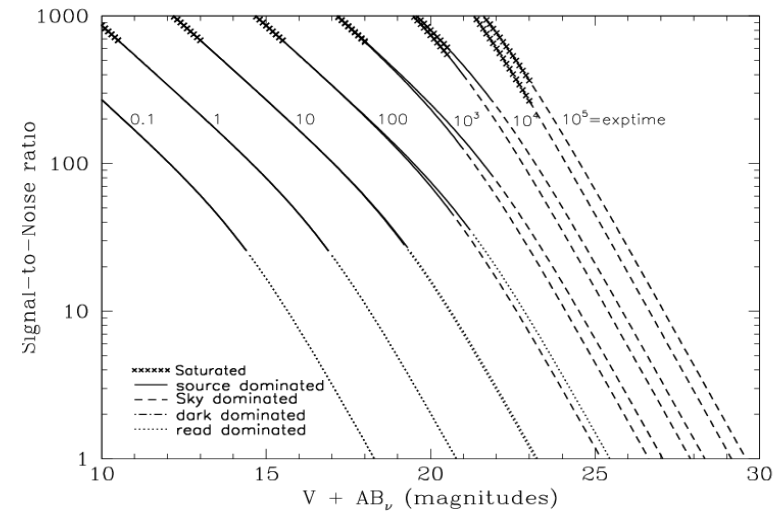
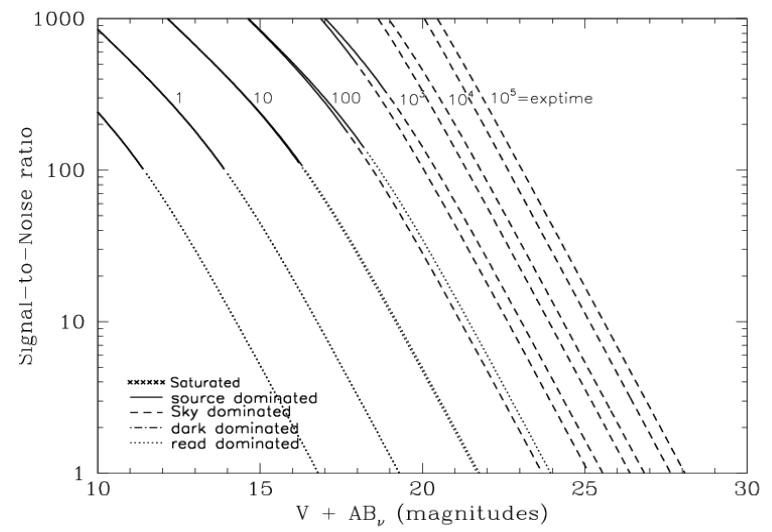


Figure 10.36: Extended Source S/N vs.  $V+AB_V$  for the WFC/F850LP filter. Top curves are for low sky and bottom curves are for average sky for a  $1 \text{ arcsec}^2$  area.



## WFC/G800L

### Description

Grism.

Figure 10.37: Integrated System Throughput for WFC/G800L

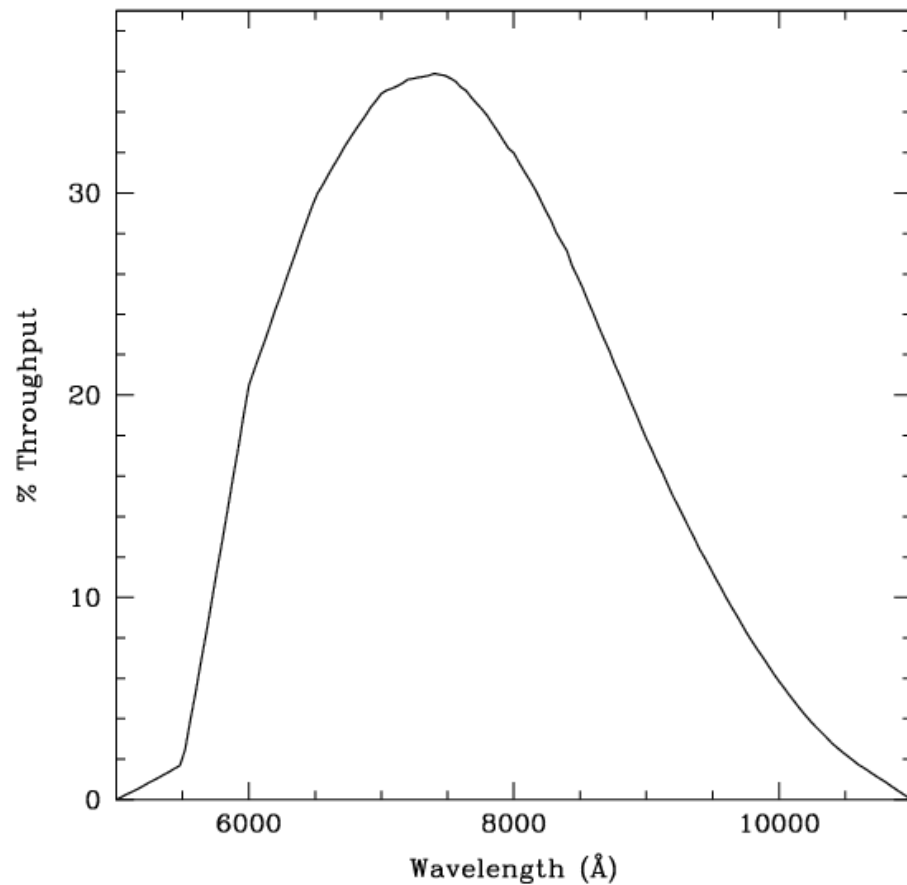


Figure 10.38: Point Source S/N vs.  $V+AB_v$  for the WFC/G800L filter. Top curves are for low sky; bottom curves are for average sky.

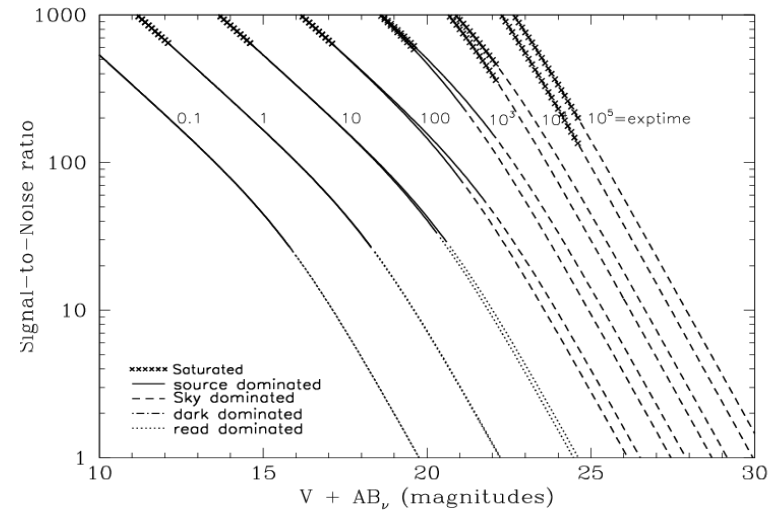
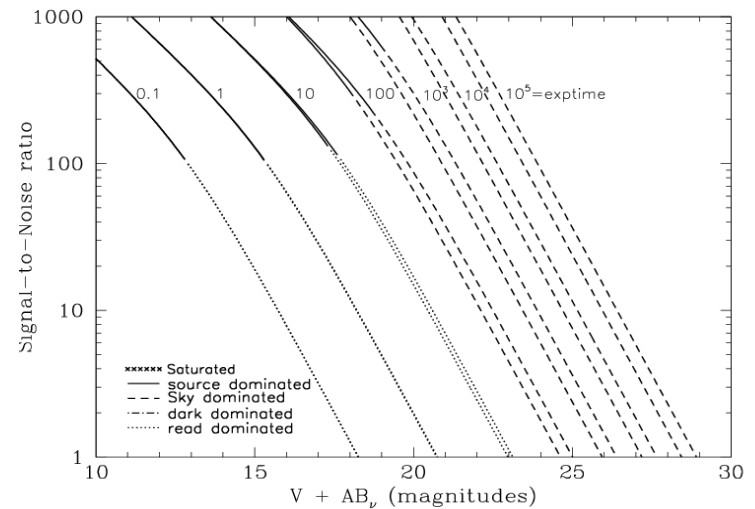


Figure 10.39: Extended Source S/N vs.  $V+AB_v$  for the WFC/G800L filter. Top curves are for low sky and bottom curves are for average sky for a  $1\text{arcsec}^2$  area.



# WFC/CLEAR

## Description

Clear filter.

Figure 10.40: Integrated System Throughput for WFC/Clear

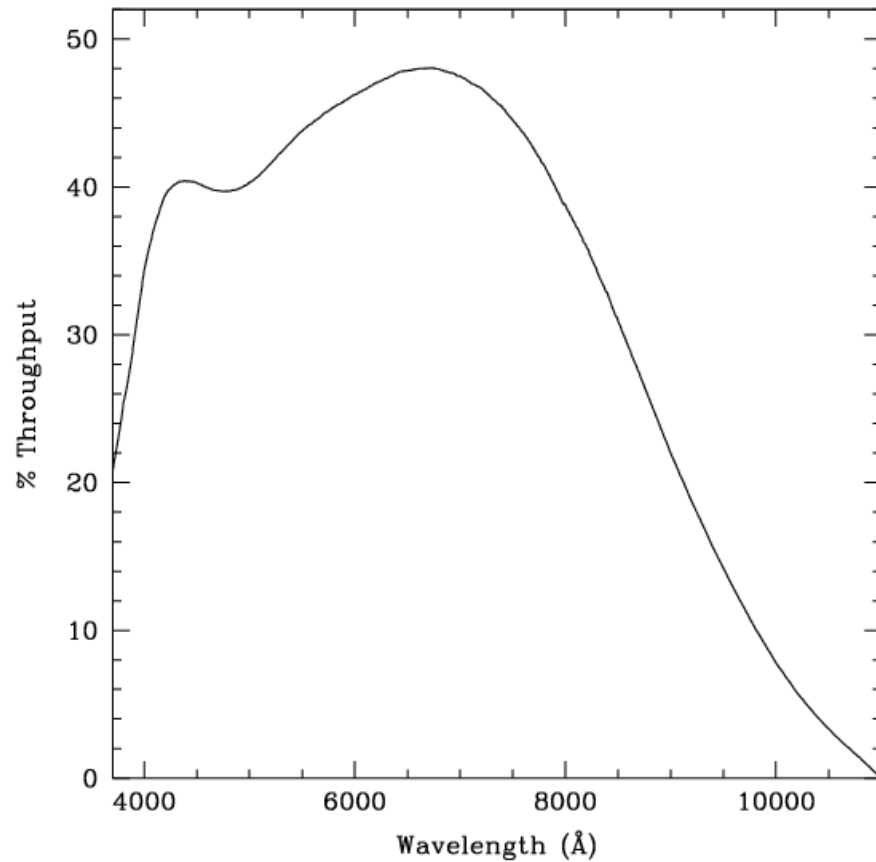


Figure 10.41: Point source S/N vs.  $V+AB_v$  for the WFC/Clear filter. Top curves are for low sky; bottom curves are for average sky.

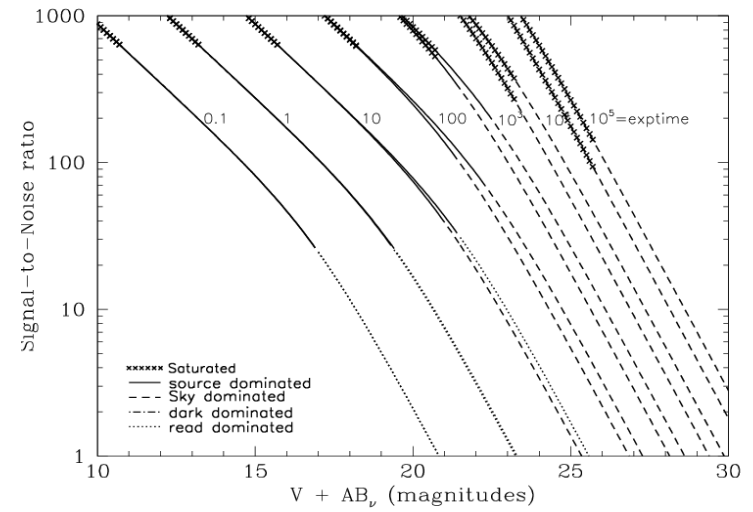
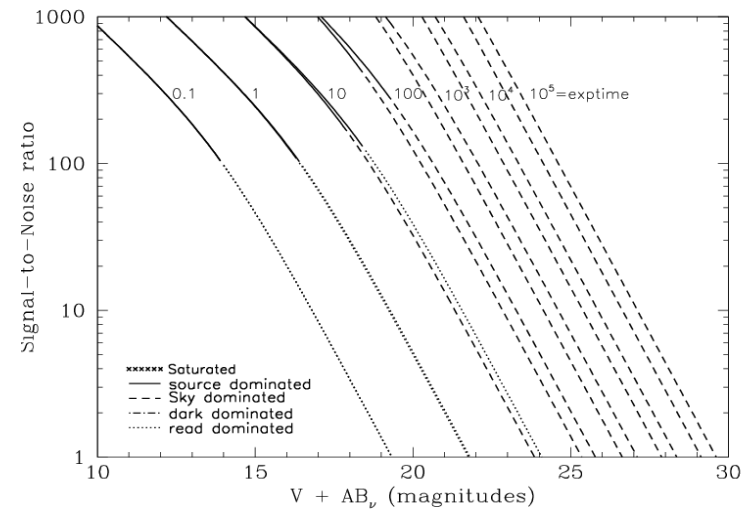


Figure 10.42: Extended source S/N vs.  $V+AB_v$  for the WFC/Clear filter. Top curves are for low sky and bottom curves are for average sky for a 1 arcsec<sup>2</sup> area.



## HRC/F220W

### Description

Near-UV filter.

Figure 10.43: Integrated System Throughput for HRC/F220W

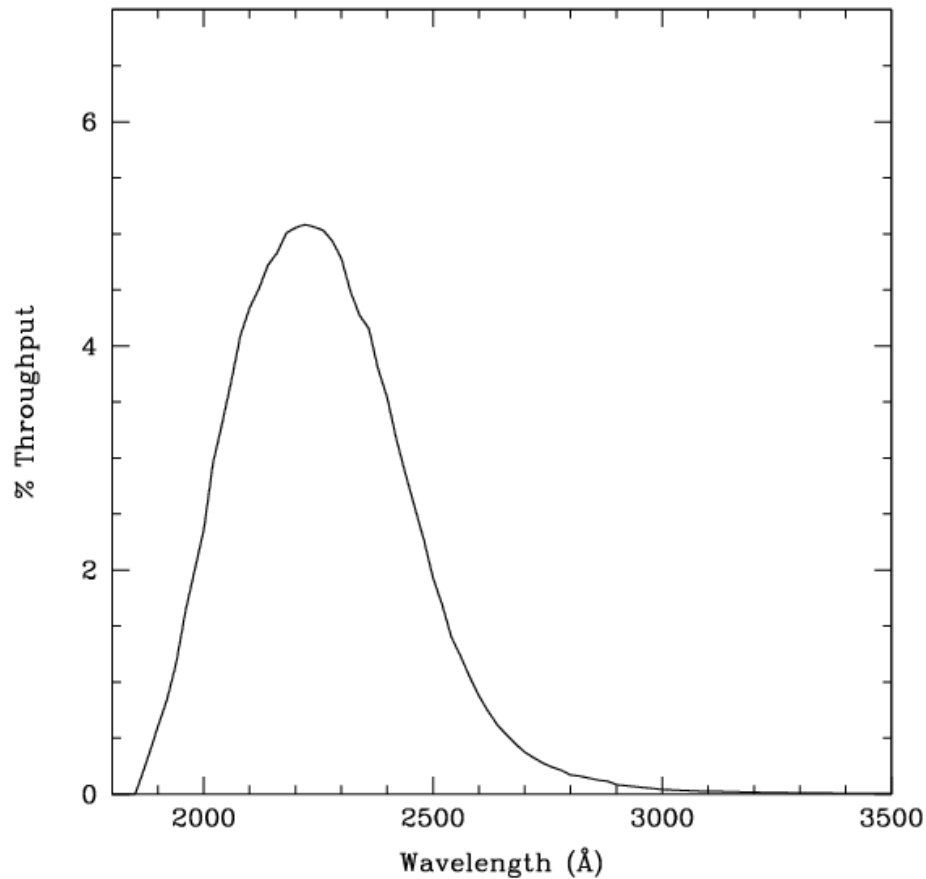


Figure 10.44: Point source S/N vs.  $V+AB_v$  for the HRC/F220W filter. Top curves are for low sky; bottom curves are for average sky.

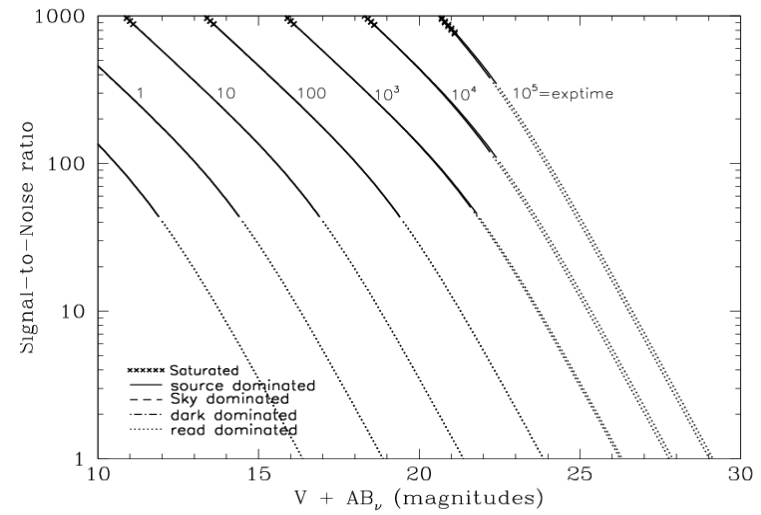
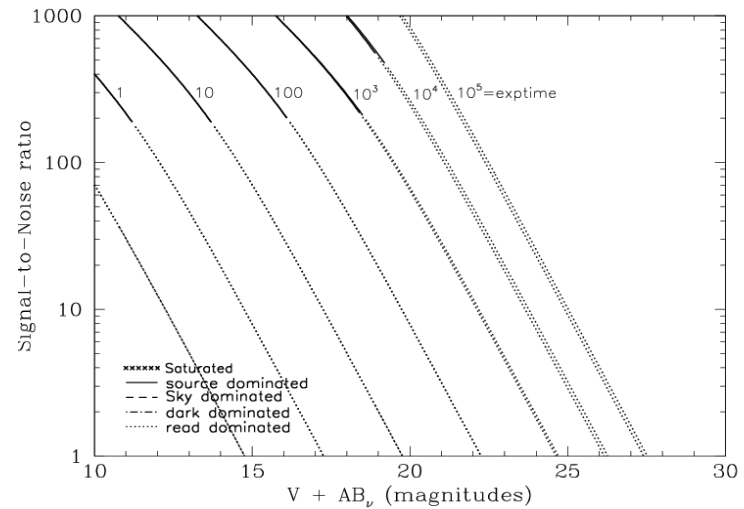


Figure 10.45: Extended source S/N vs.  $V+AB_v$  for the HRC/F220W filter. Top curves are for low sky and bottom curves are for average sky for a 1 arcsec<sup>2</sup> area.



## HRC/F250W

### Description

Near-UV filter.

Figure 10.46: Integrated System Throughput for HRC/F250W

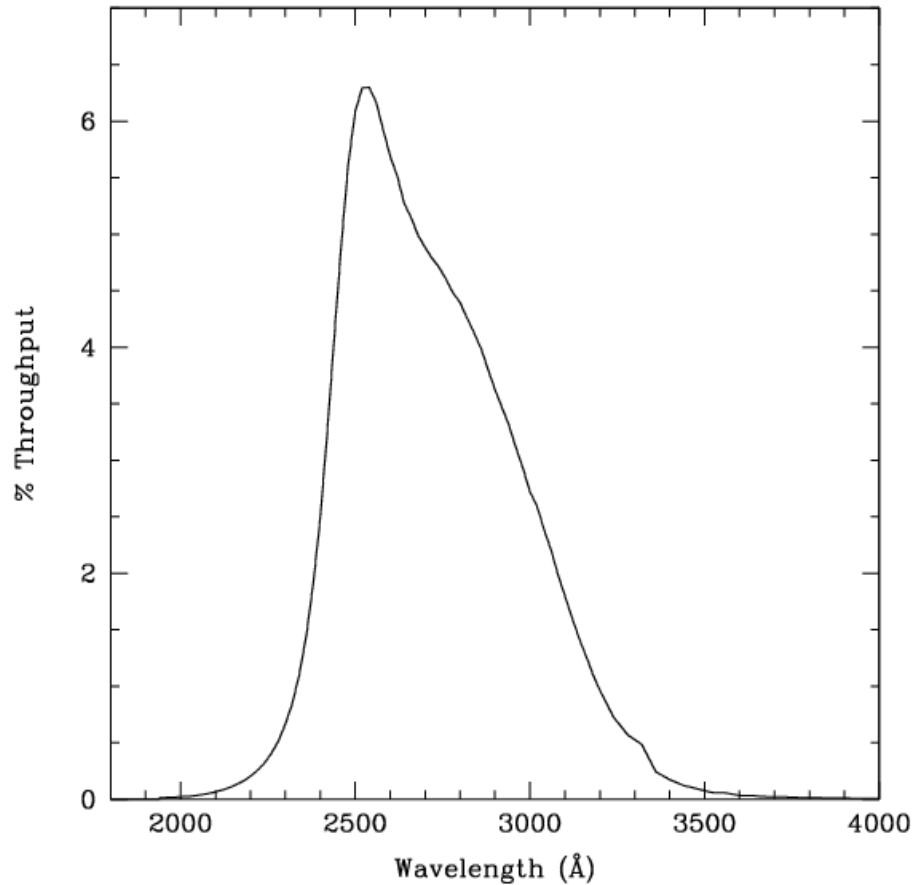


Figure 10.47: Point Source S/N vs.  $V+AB_V$  for the HRC/F250W filter. Top curves are for low sky; bottom curves are for average sky.

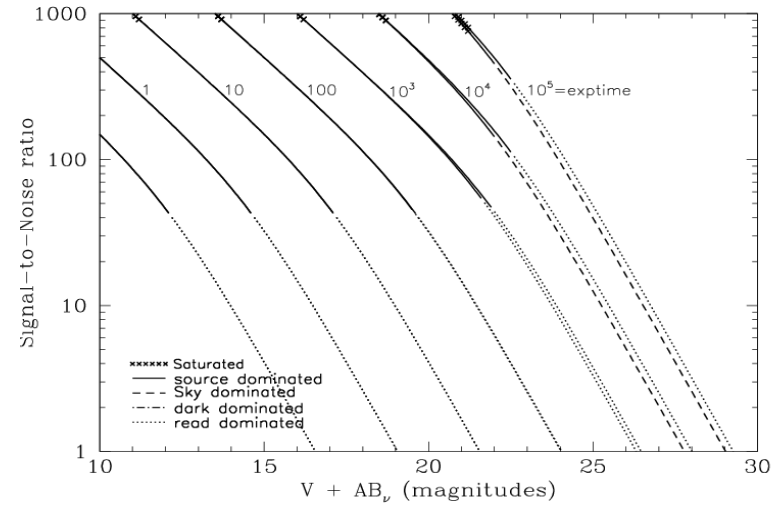
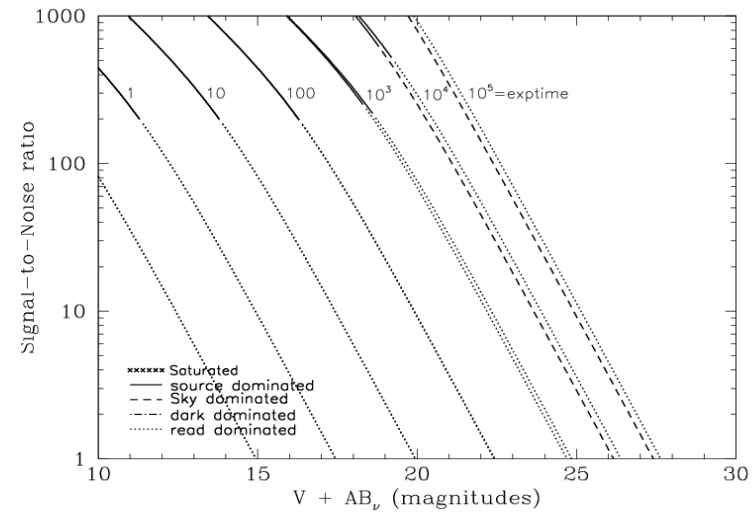


Figure 10.48: Extended Source S/N vs.  $V+AB_V$  for the HRC/F250W filter. Top curves are for low sky and bottom curves are for average sky for a 1 arcsec<sup>2</sup> area.





## HRC/F330W

### Description

HRC u filter.

Figure 10.49: Integrated System Throughput for HRC/F330W

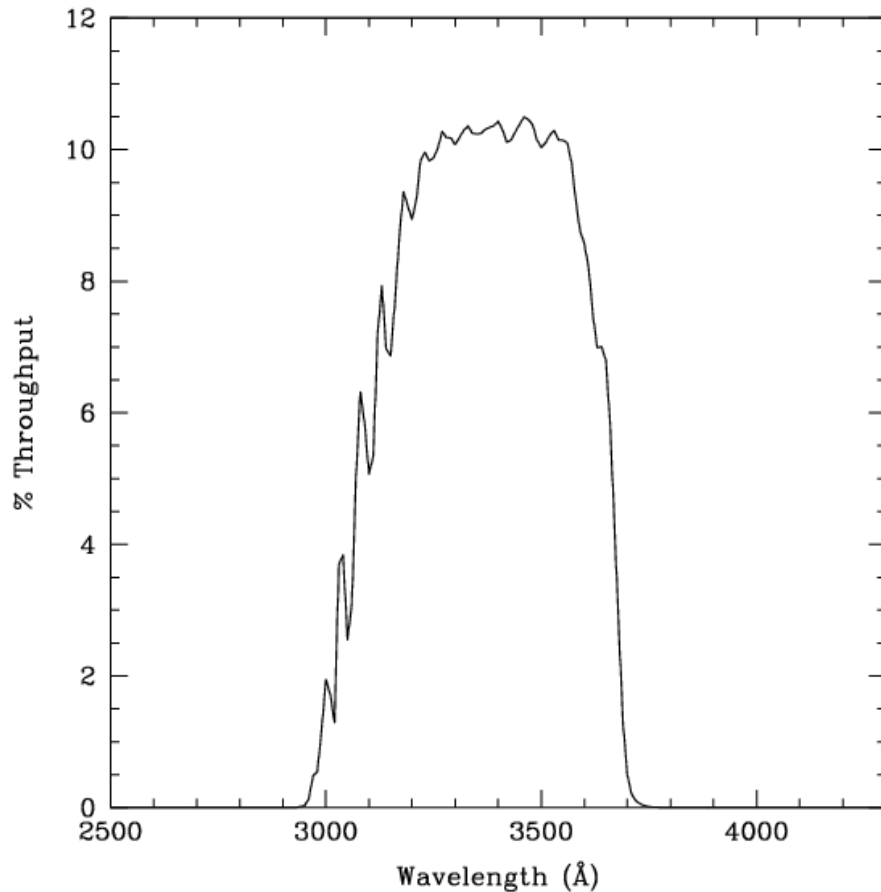


Figure 10.50: Point Source S/N vs.  $V+AB_V$  for the HRC/F330W filter. Top curves are for low sky; bottom curves are for average sky.

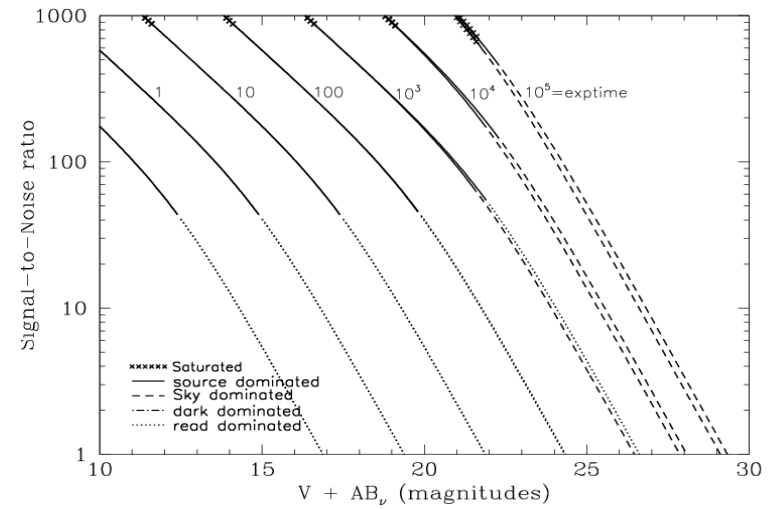
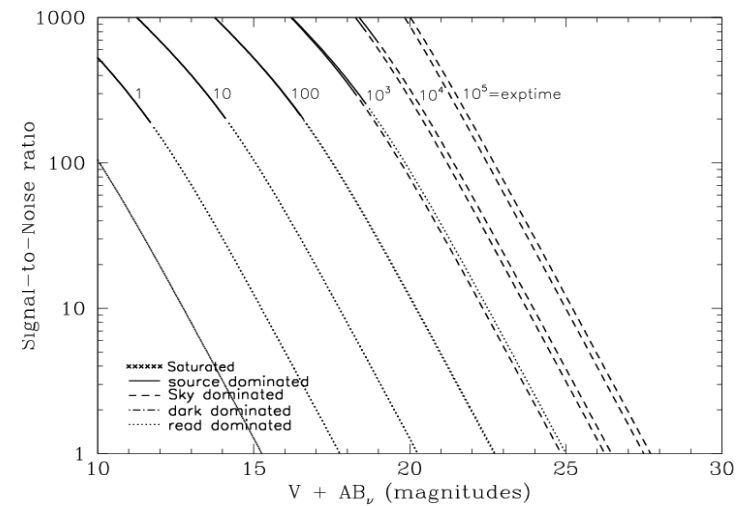


Figure 10.51: Extended Source S/N vs.  $V+AB_V$  for the HRC/F330W filter. Top curves are for low sky and bottom curves are for average sky for a 1 arcsec<sup>2</sup> area.



# HRC/F344N

## Description

NeV filter.

Figure 10.52: Integrated System Throughput for HRC/F344N

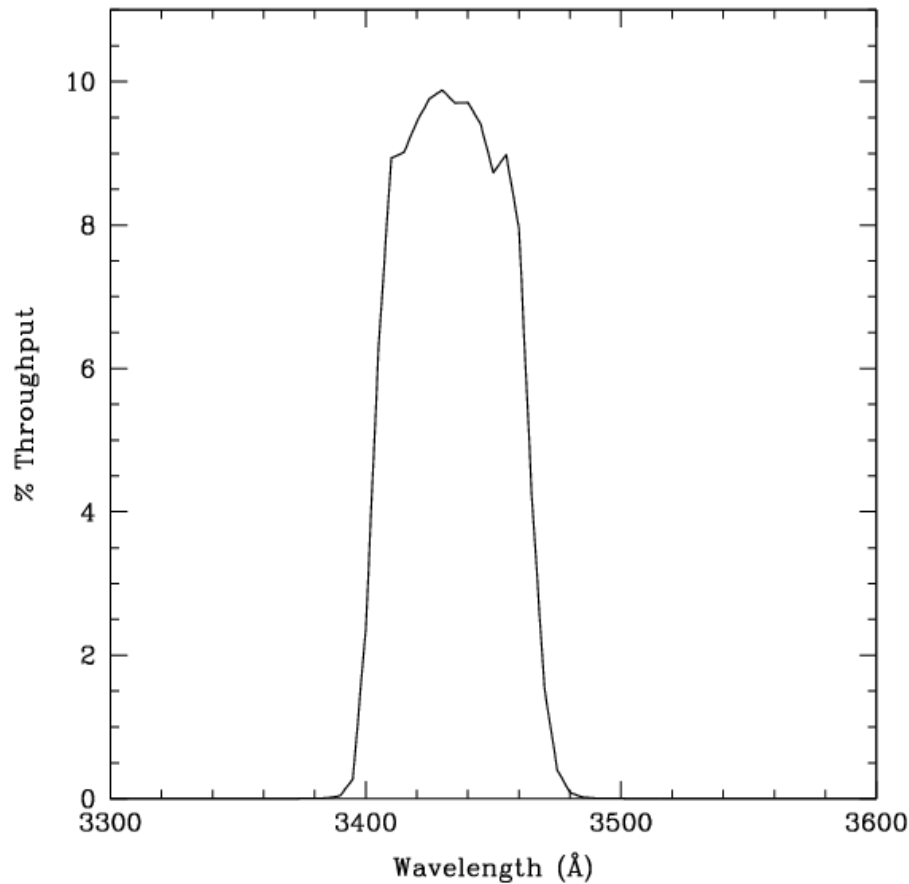


Figure 10.53: Point Source S/N vs.  $V+AB_v$  for the HRC/F344N filter. Top curves are for low sky; bottom curves are for average sky.

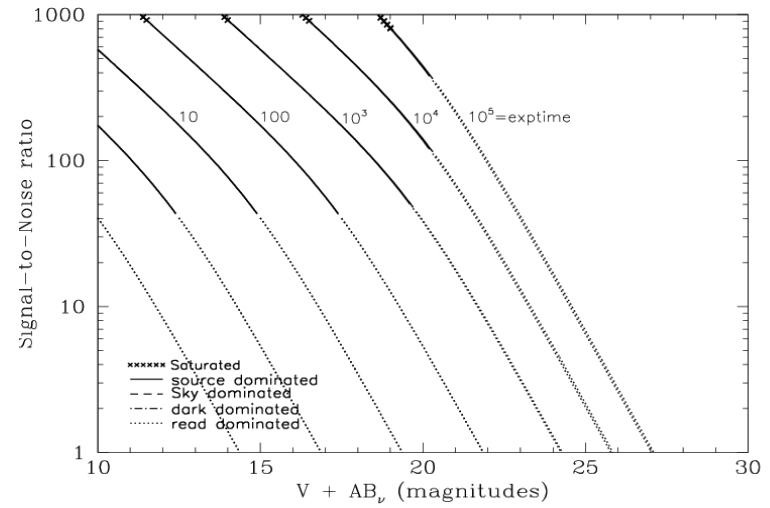
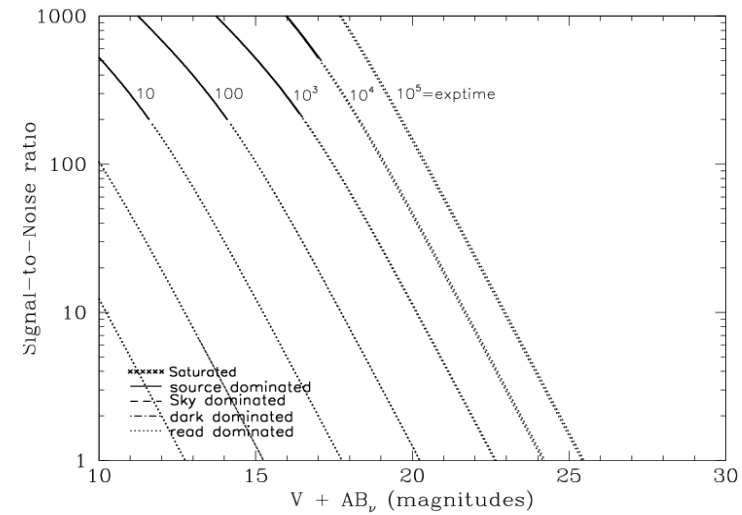


Figure 10.54: Extended Source S/N vs.  $V+AB_v$  for the HRC/F344N filter. Top curves are for low sky and bottom curves are for average sky for a 1 arcsec<sup>2</sup> area.



## HRC/F435W

### Description

Johnson B filter.

Figure 10.55: Integrated System Throughput for HRC/F435W

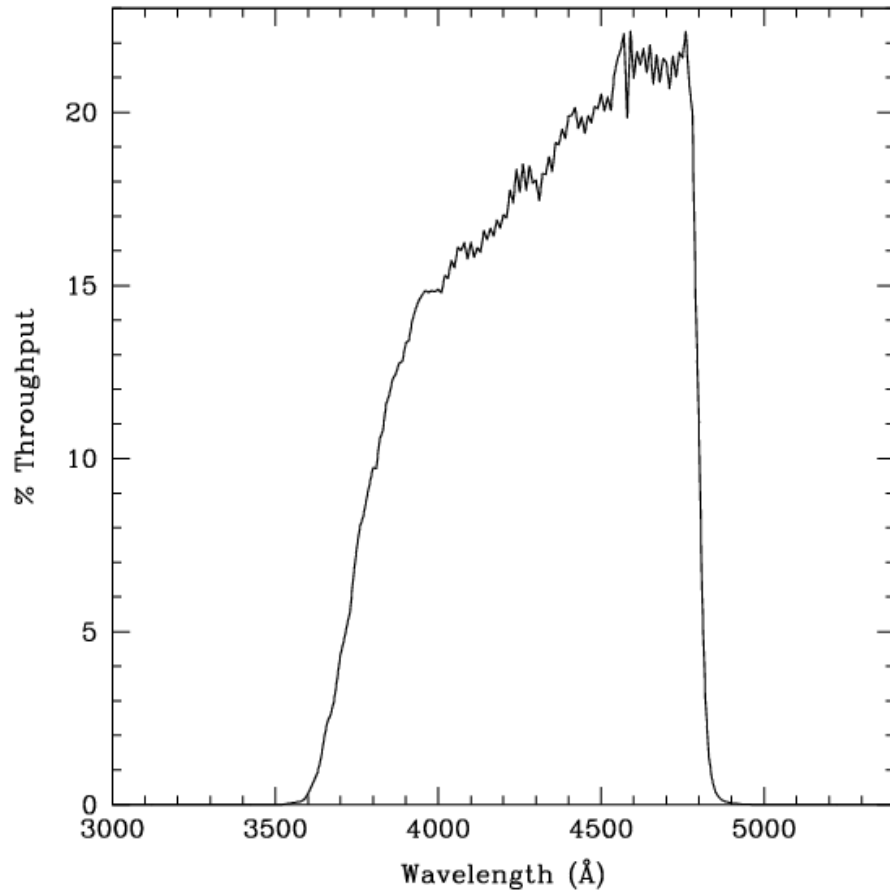


Figure 10.56: Point Source S/N vs.  $V+AB_v$  for the HRC/F435W filter. Top curves are for low sky; bottom curves are for average sky.

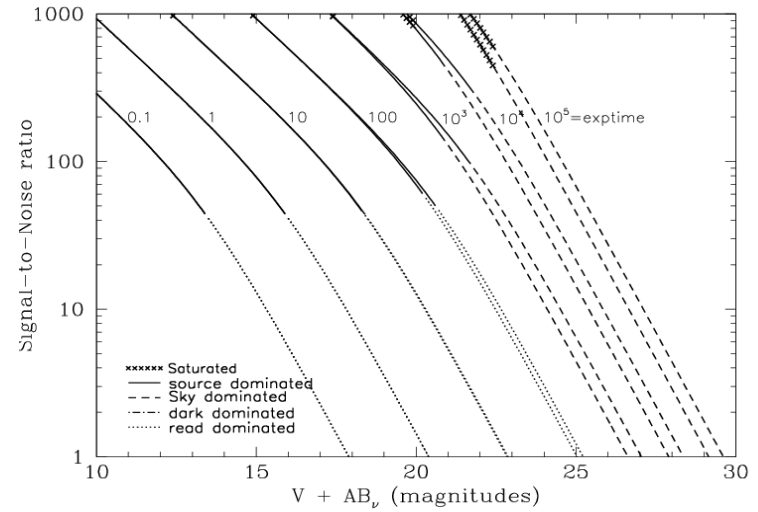
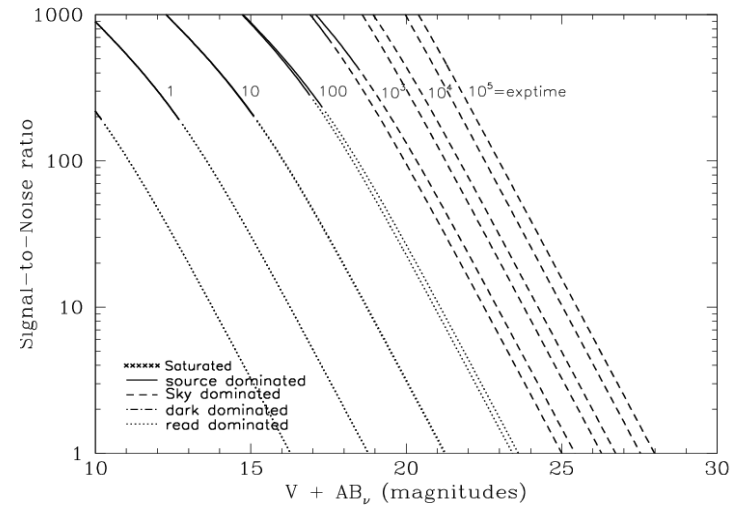


Figure 10.57: Extended Source S/N vs.  $V+AB_v$  for the HRC/F435W filter. Top curves are for low sky and bottom curves are for average sky for a 1 arcsec<sup>2</sup> area.



# HRC/F475W

## Description

Sloan Digital Sky Survey g filter.

Figure 10.58: Integrated System Throughput for HRC/F475W

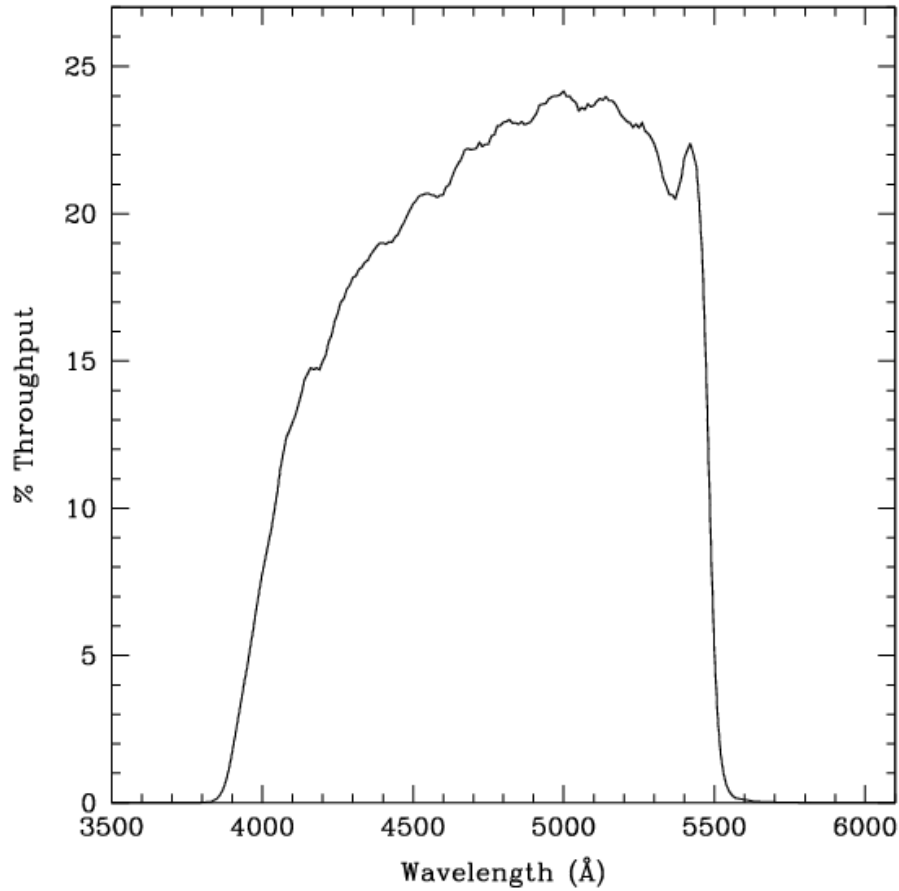


Figure 10.59: Point Source S/N vs.  $V+AB_V$  for the HRC/F475W filter. Top curves are for low sky; bottom curves are for average sky.

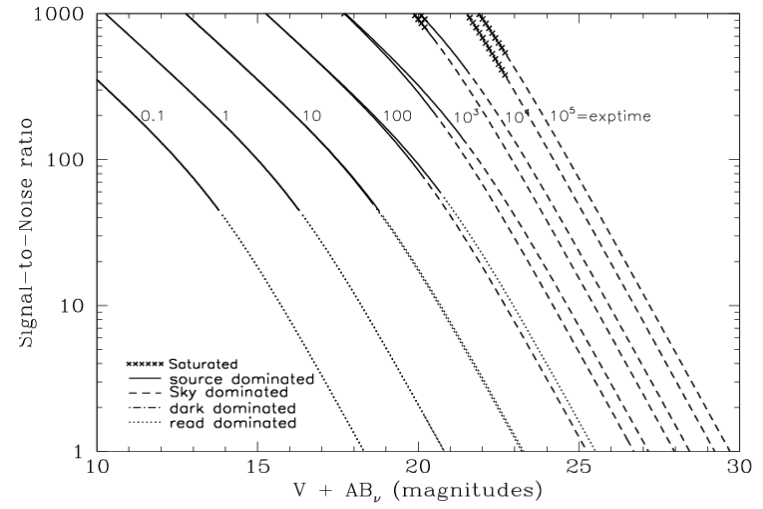
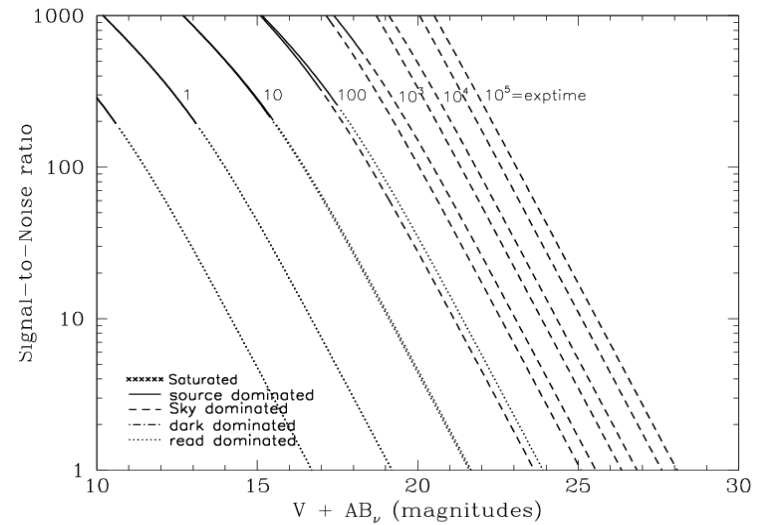


Figure 10.60: Extended Source S/N vs.  $V+AB_V$  for the HRC/F475W filter. Top curves are for low sky and bottom curves are for average sky for a 1 arcsec<sup>2</sup> area.



## HRC/F502N

### Description

OIII filter.

Figure 10.61: Integrated System Throughput for HRC/F502N

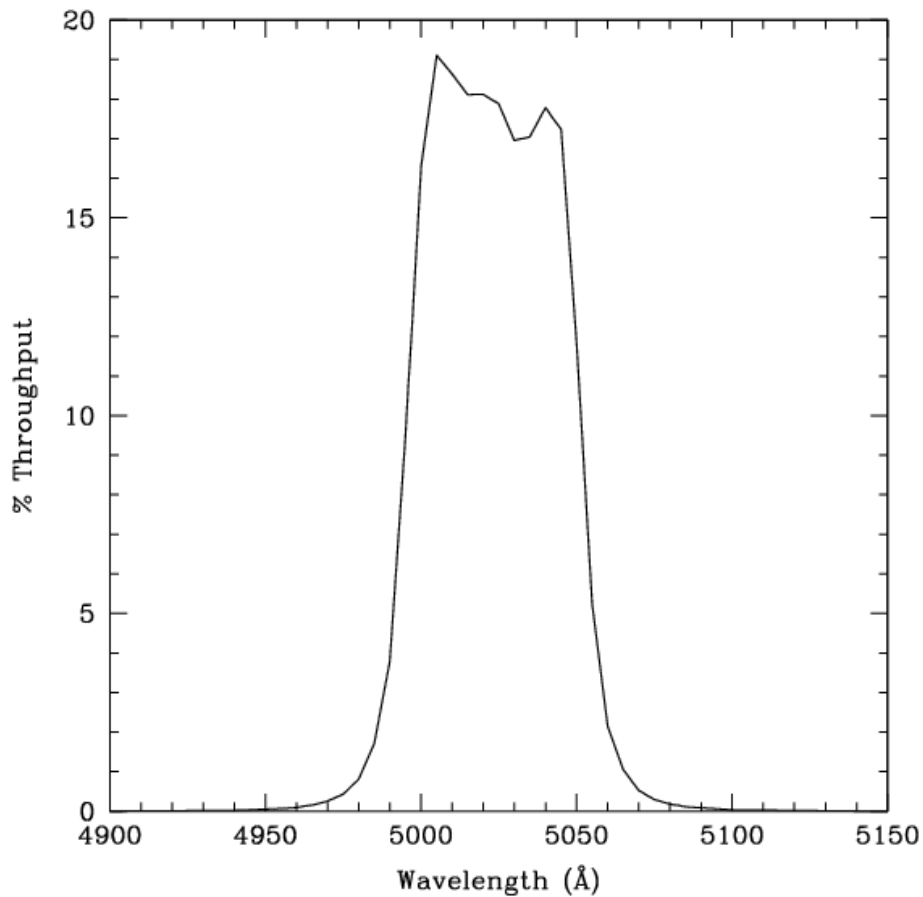


Figure 10.62: Point Source S/N vs.  $V+AB_v$  for the HRC/F502N filter. Top curves are for low sky; bottom curves are for average sky.

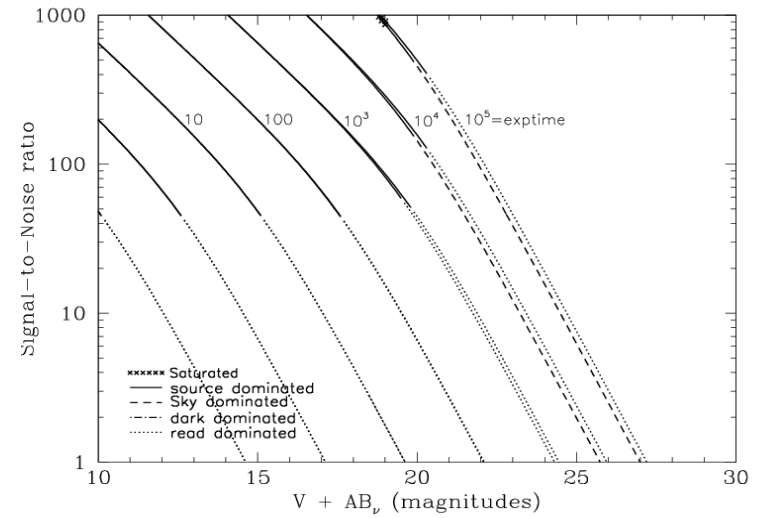
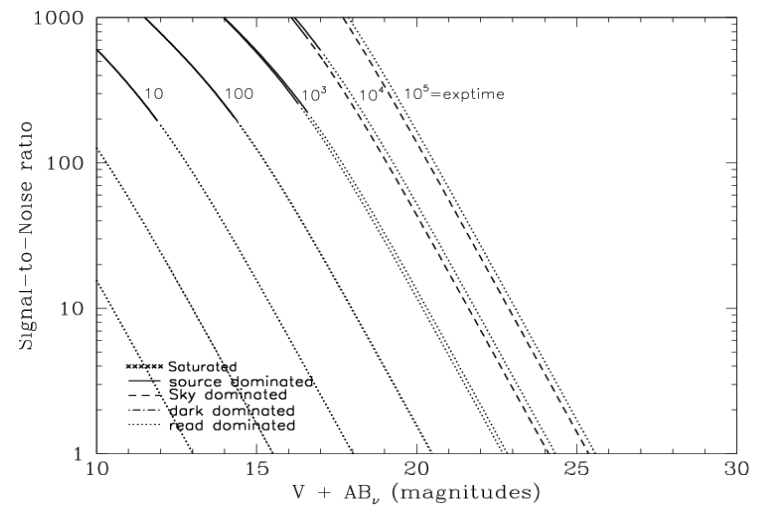


Figure 10.63: Extended Source S/N vs.  $V+AB_v$  for the HRC/F502N filter. Top curves are for low sky and bottom curves are for average sky for a 1 arcsec<sup>2</sup> area.



# HRC/F550M

## Description

Narrow V filter.

Figure 10.64: Integrated System Throughput for HRC/F550M

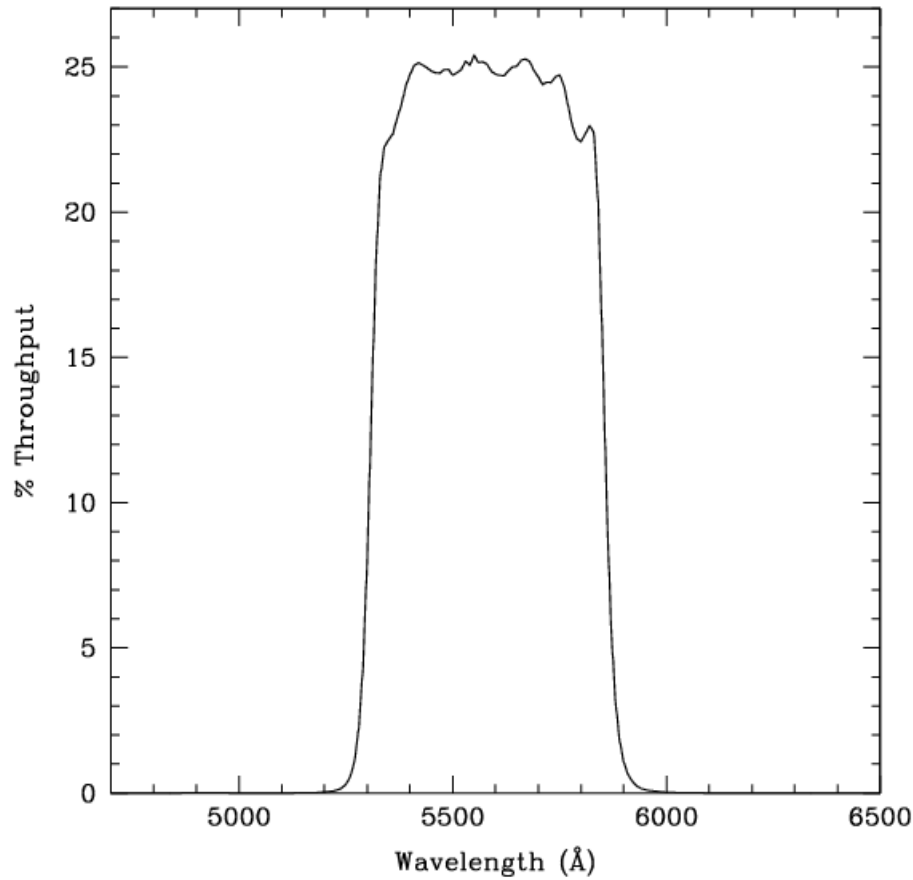


Figure 10.65: Point Source S/N vs.  $V+AB_V$  for the HRC/F550M filter. Top curves are for low sky; bottom curves are for average sky.

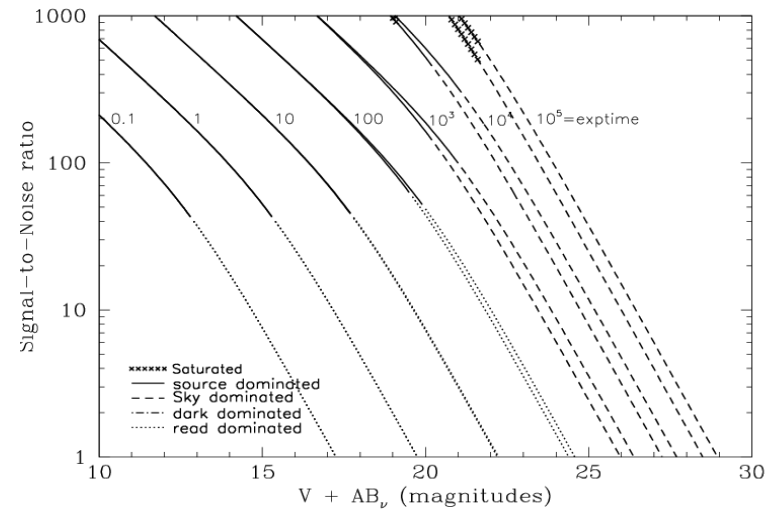
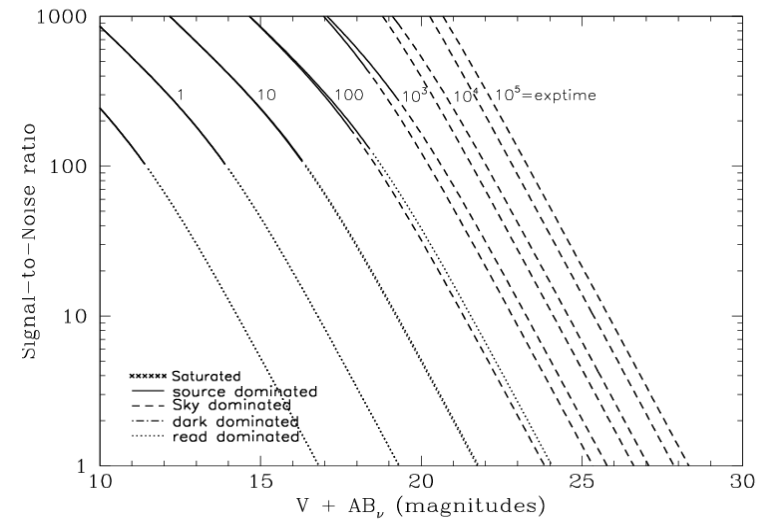


Figure 10.66: Extended Source S/N vs.  $V+AB_V$  for the HRC/F550M filter. Top curves are for low sky and bottom curves are for average sky for a 1 arcsec<sup>2</sup> area.



## HRC/F555W

### Description

Johnson V filter.

Figure 10.67: Integrated System Throughput for HRC/F555W

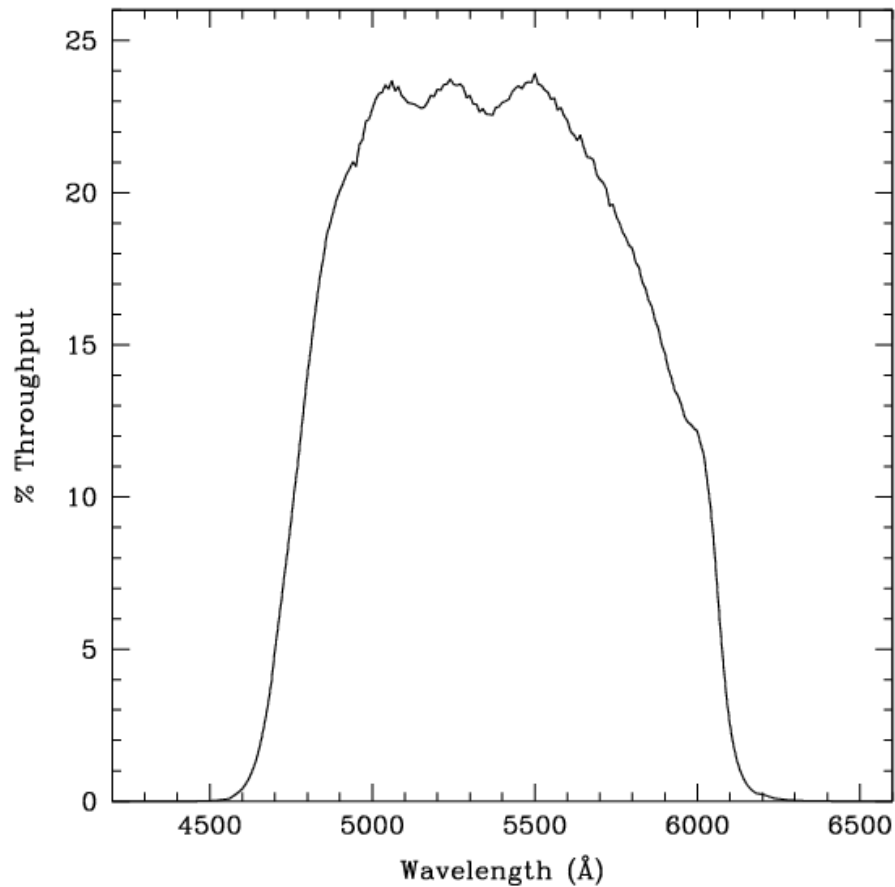


Figure 10.68: Point Source S/N vs.  $V+AB_V$  for the HRC/F555W filter. Top curves are for low sky; bottom curves are for average sky.

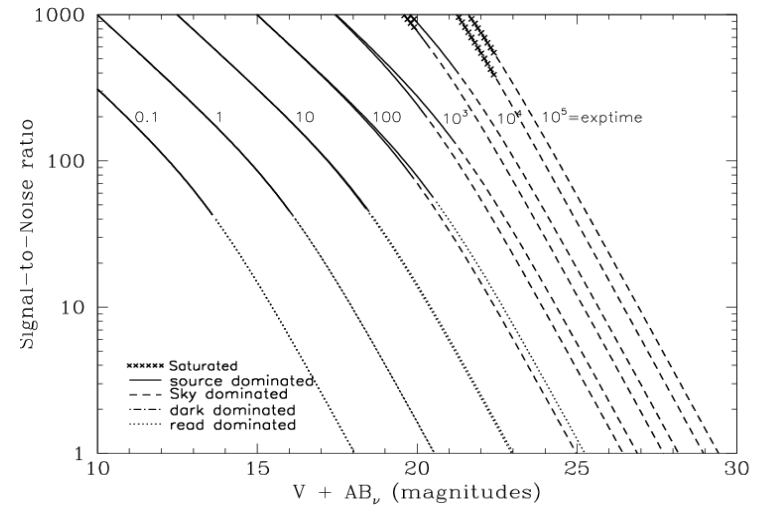
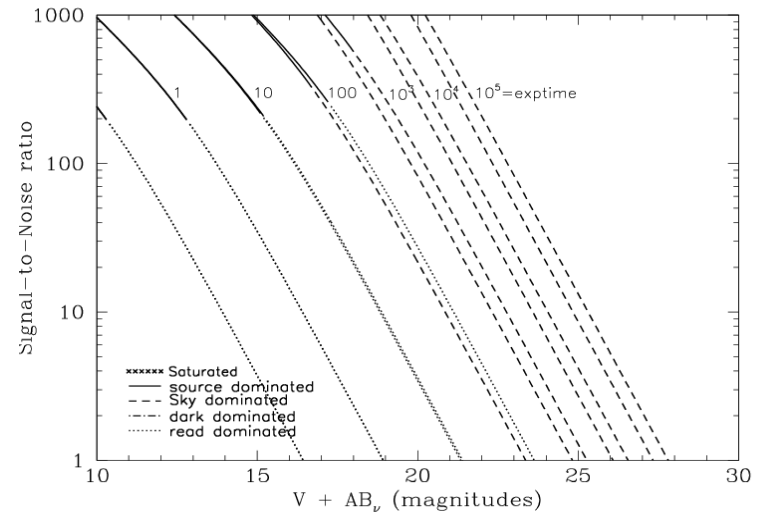


Figure 10.69: Extended Source S/N vs.  $V+AB_V$  for the HRC/F555W filter. Top curves are for low sky and bottom curves are for average sky for a 1 arcsec<sup>2</sup> area.



## HRC/F606W

### Description

Broad V filter.

Figure 10.70: Integrated System Throughput for HRC/F606W

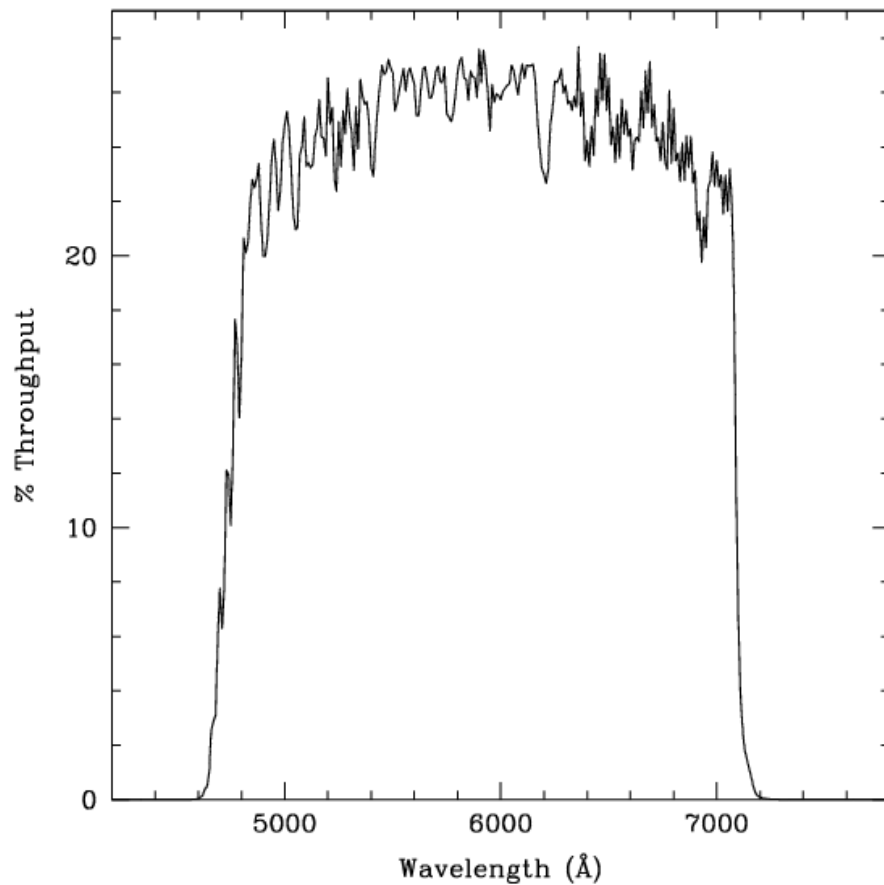


Figure 10.71: Point Source S/N vs.  $V+AB_V$  for the HRC/F606W filter. Top curves are for low sky; bottom curves are for average sky.

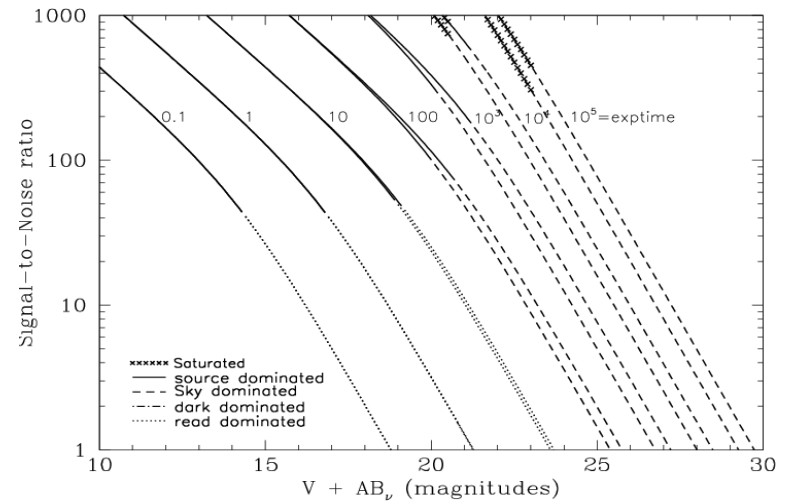
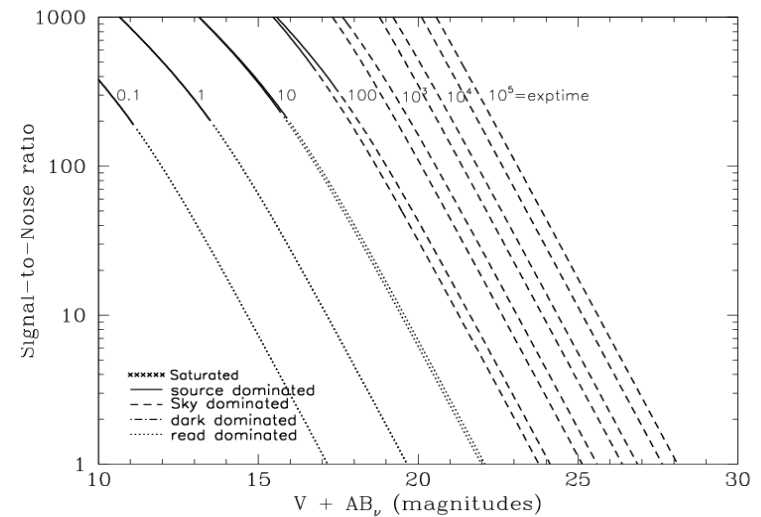


Figure 10.72: Extended Source S/N vs.  $V+AB_V$  for the HRC/F606W filter. Top curves are for low sky and bottom curves are for average sky for a 1 arcsec<sup>2</sup> area.





## HRC/F625W

### Description

Sloan Digital Sky Survey r filter.

Figure 10.73: Integrated System Throughput for HRC/F625W

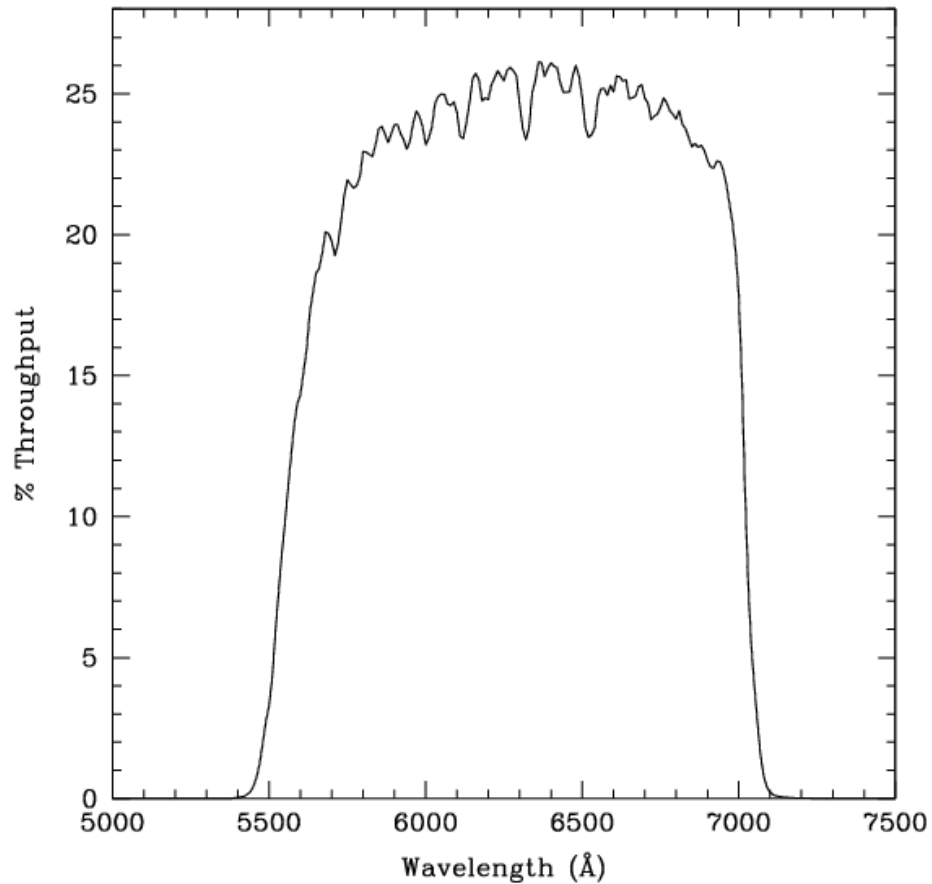


Figure 10.74: Point Source S/N vs.  $V+AB_v$  for the HRC/F625W filter. Top curves are for low sky; bottom curves are for average sky.

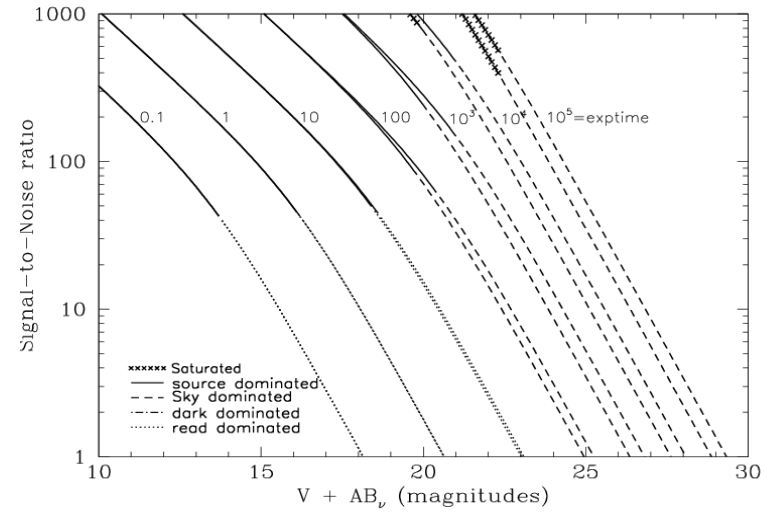
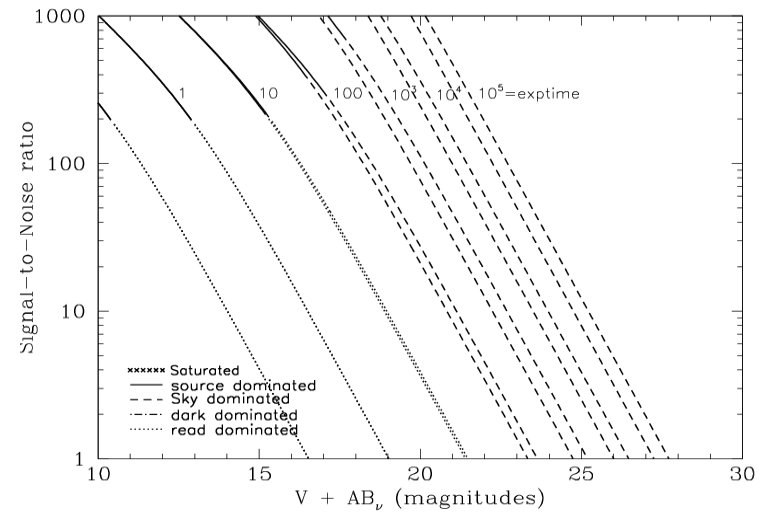


Figure 10.75: Extended Source S/N vs.  $V+AB_v$  for the HRC/F625W filter. Top curves are for low sky and bottom curves are for average sky for a 1 arcsec<sup>2</sup> area.



## HRC/F658N

### Description

H $\alpha$  filter.

Figure 10.76: Integrated System Throughput for HRC/F658N

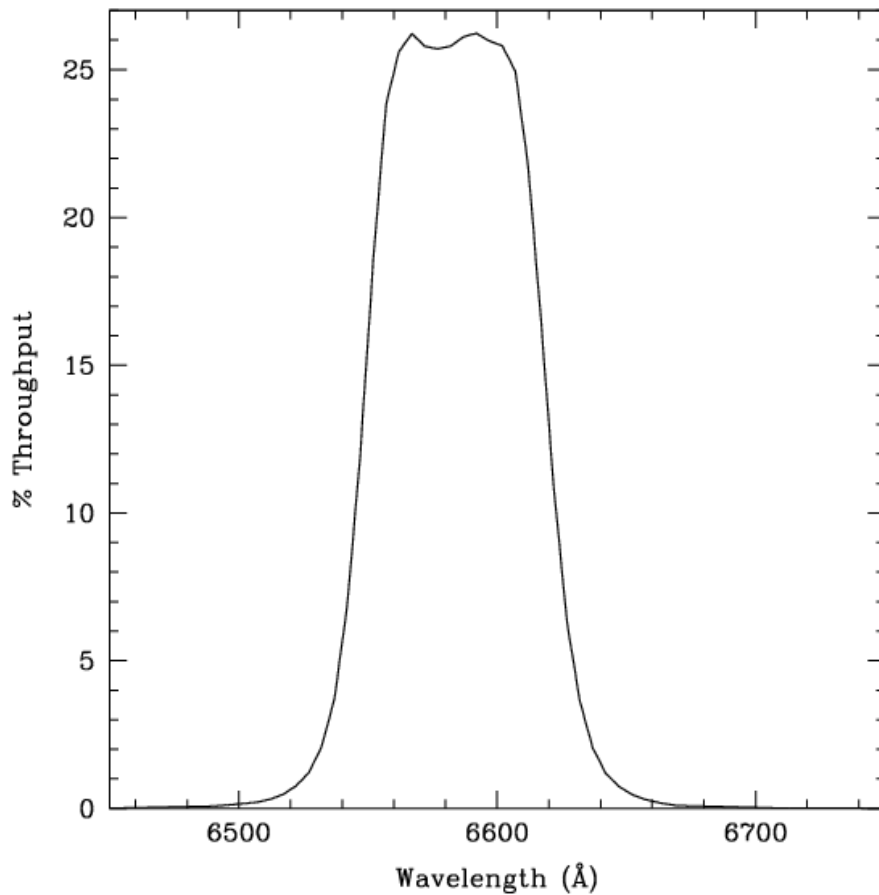


Figure 10.77: Point Source S/N vs.  $V+AB_v$  for the HRC/F658N filter. Top curves are for low sky; bottom curves are for average sky.

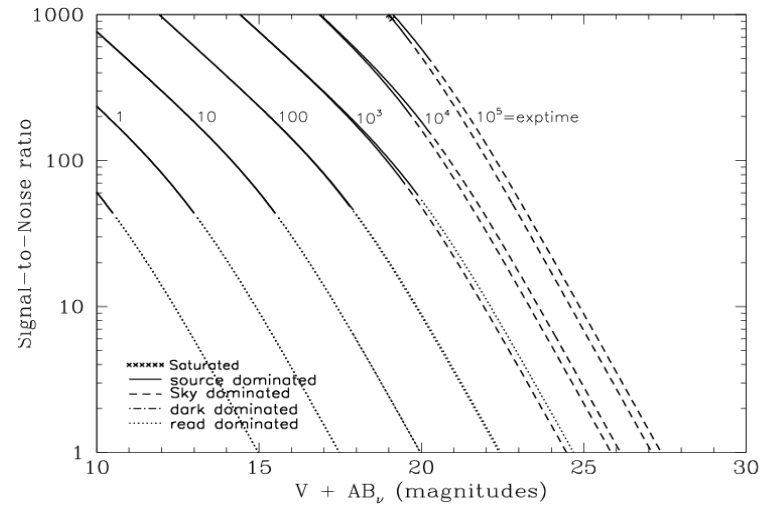
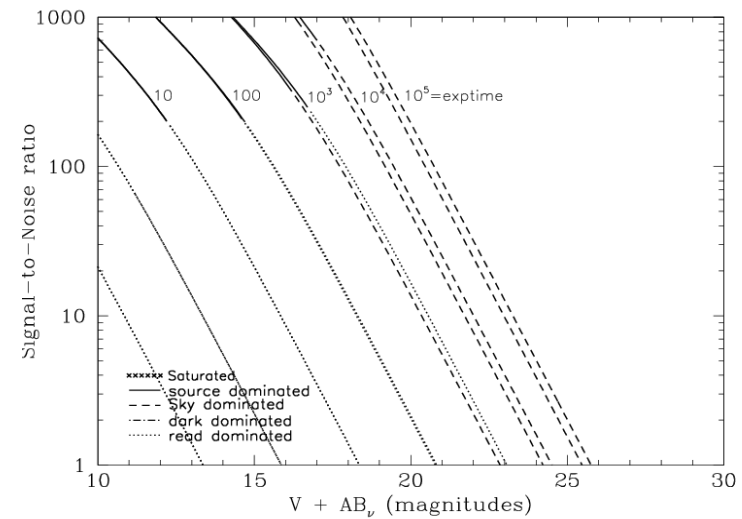


Figure 10.78: Extended Source S/N vs.  $V+AB_v$  for the HRC/F658N filter. Top curves are for low sky and bottom curves are for average sky for a 1 arcsec<sup>2</sup> area.



## HRC/F660N

### Description

NII filter.

Figure 10.79: Integrated System Throughput for HRC/F660N

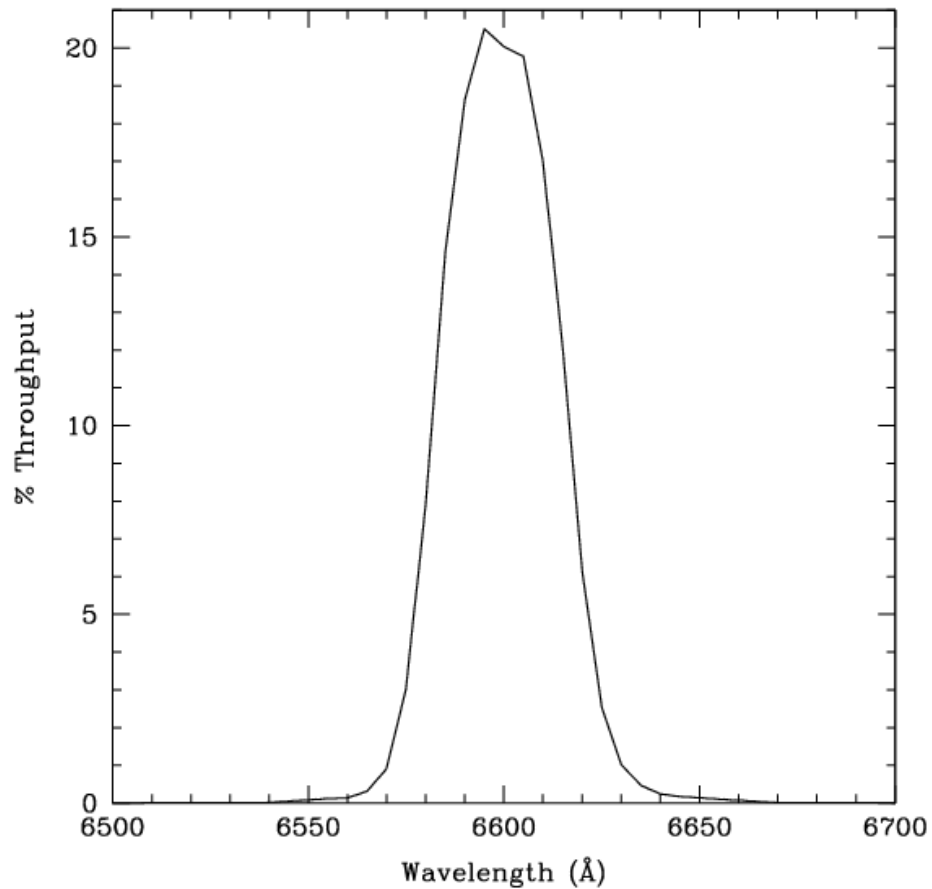


Figure 10.80: Point Source S/N vs.  $V+AB_v$  for the HRC/F660N filter. Top curves are for low sky; bottom curves are for average sky.

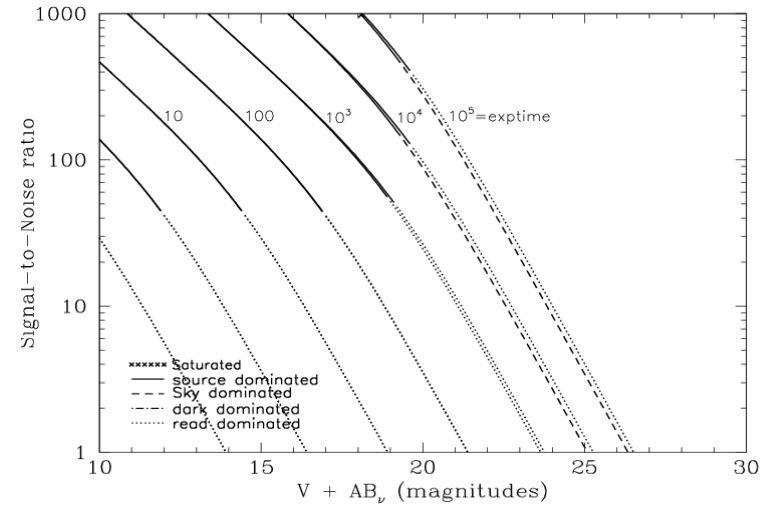
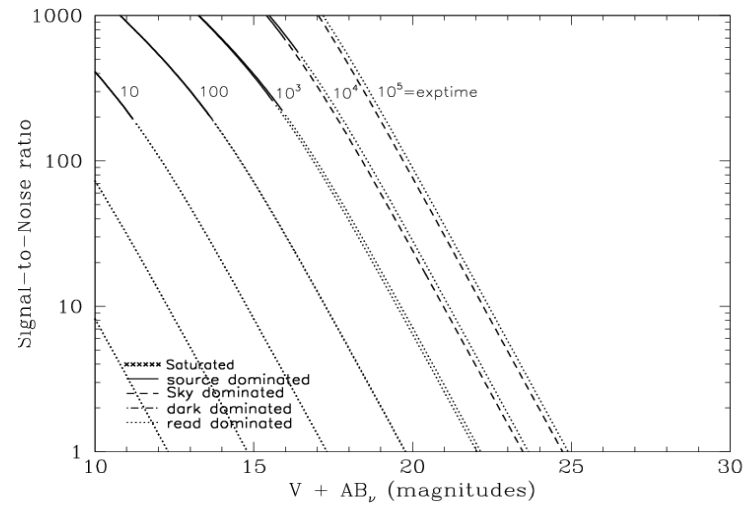


Figure 10.81: Extended Source S/N vs.  $V+AB_v$  for the HRC/F660N filter. Top curves are for low sky and bottom curves are for average sky for a 1 arcsec<sup>2</sup> area.



# HRC/F775W

## Description

Sloan Digital Sky Survey i filter.

Figure 10.82: Integrated System Throughput for HRC/F775W

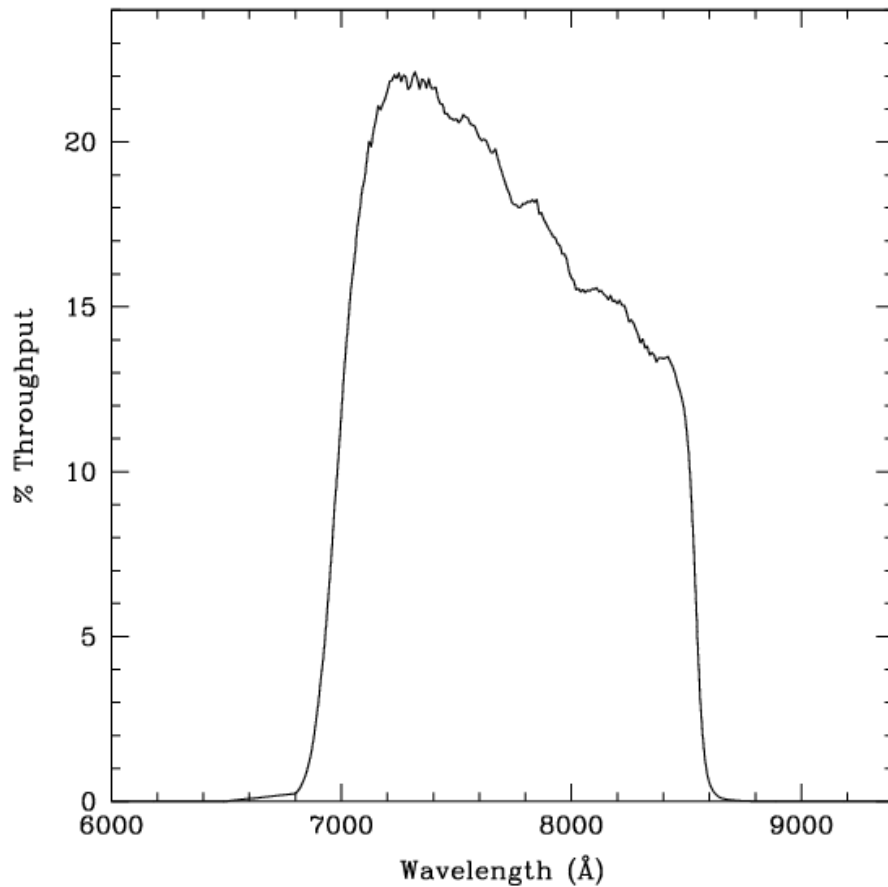


Figure 10.83: Point Source S/N vs.  $V+AB_v$  for the HRC/F775W filter. Top curves are for low sky; bottom curves are for average sky.

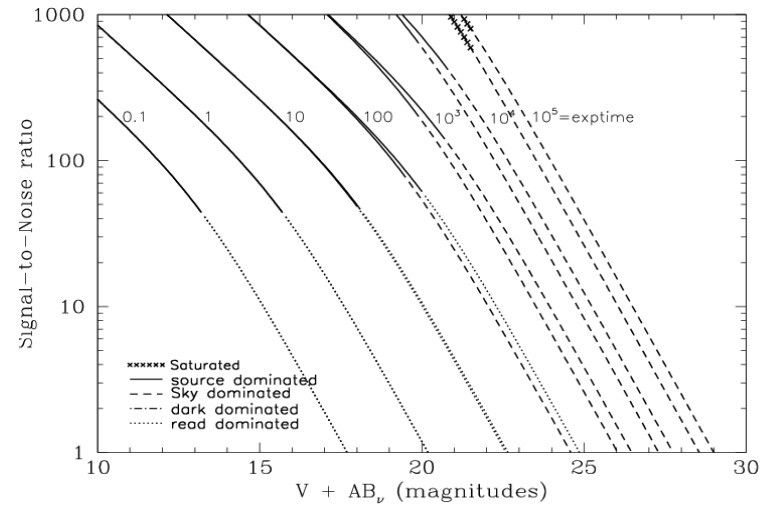
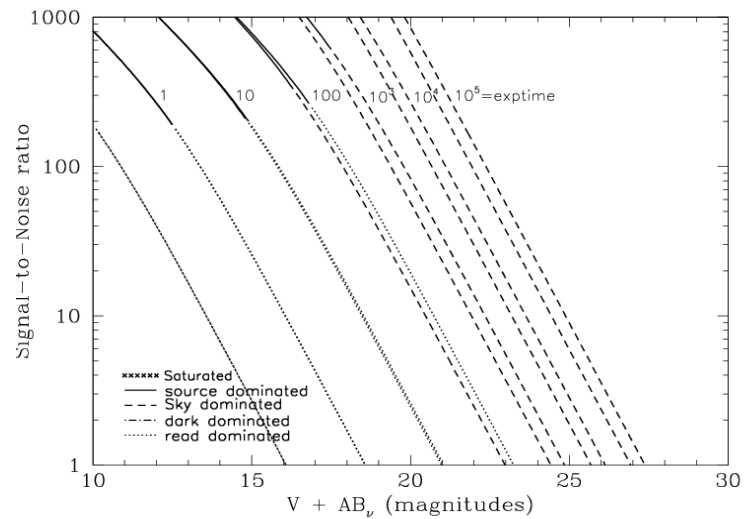


Figure 10.84: Extended Source S/N vs.  $V+AB_v$  for the HRC/F775W filter. Top curves are for low sky and bottom curves are for average sky for a 1 arcsec<sup>2</sup> area.



## HRC/F814W

### Description

Broad I filter.

Figure 10.85: Integrated System Throughput for HRC/F814W

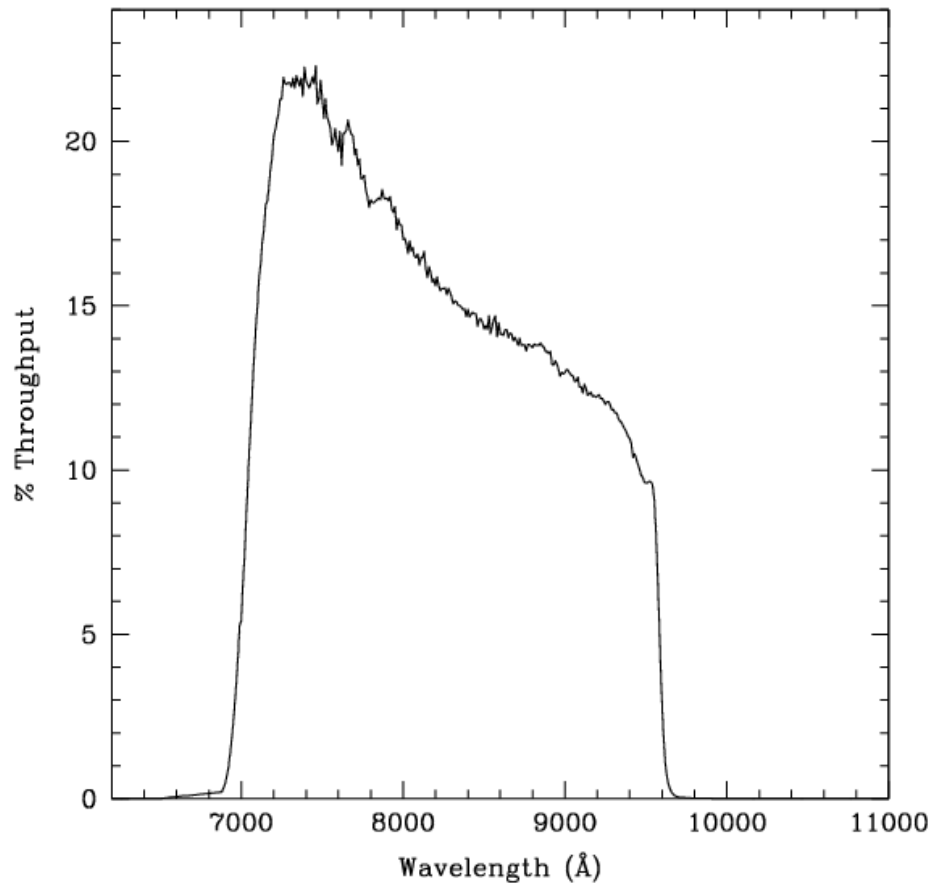


Figure 10.86: Point Source S/N vs.  $V+AB_v$  for the HRC/F814W filter. Top curves are for low sky; bottom curves are for average sky.

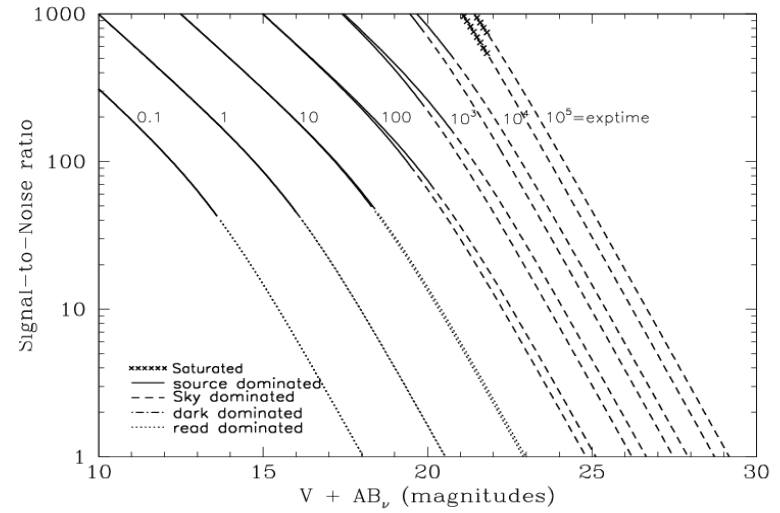
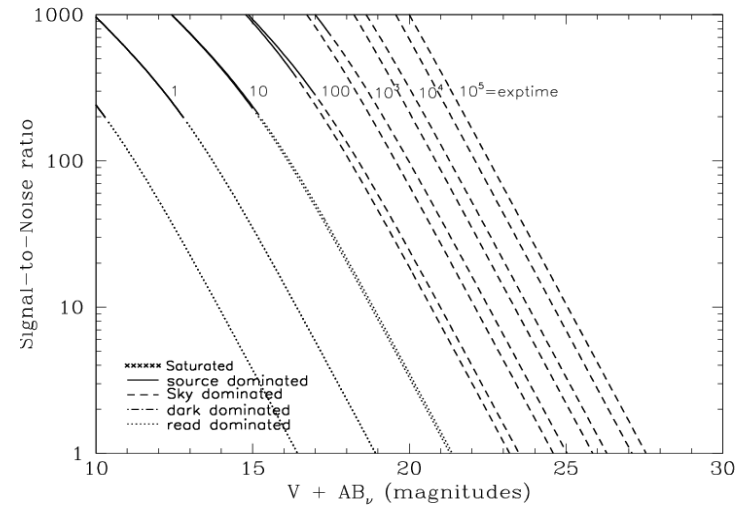


Figure 10.87: Extended Source S/N vs.  $V+AB_v$  for the HRC/F814W filter. Top curves are for low sky and bottom curves are for average sky for a 1 arcsec<sup>2</sup> area.



# HRC/F850LP

## Description

Sloan Digital Sky Survey z filter.

Figure 10.88: Integrated System Throughput for HRC/F850LP

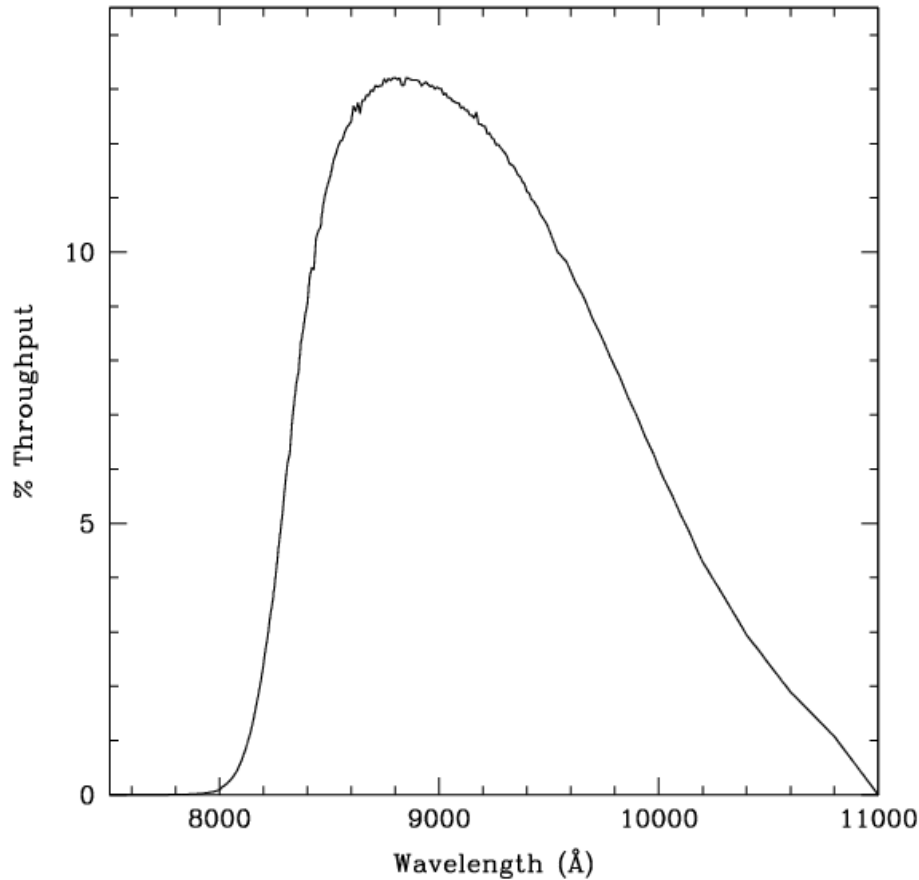


Figure 10.89: Point Source S/N vs.  $V+AB_v$  for the HRC/F850LP filter. Top curves are for low sky; bottom curves are for average sky.

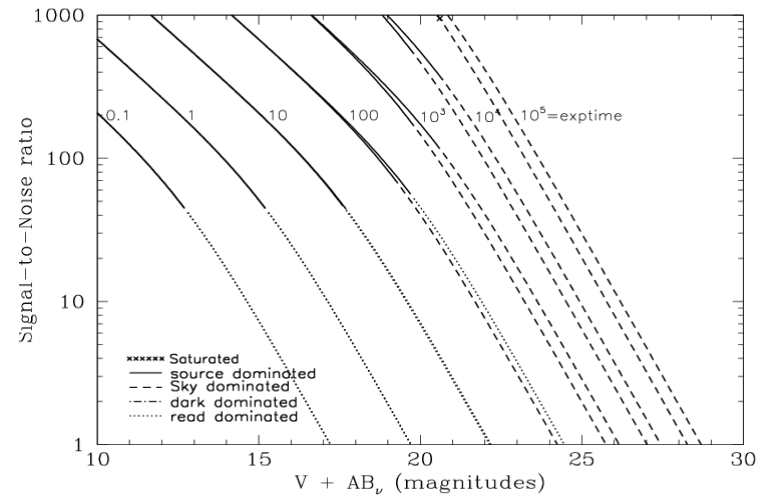
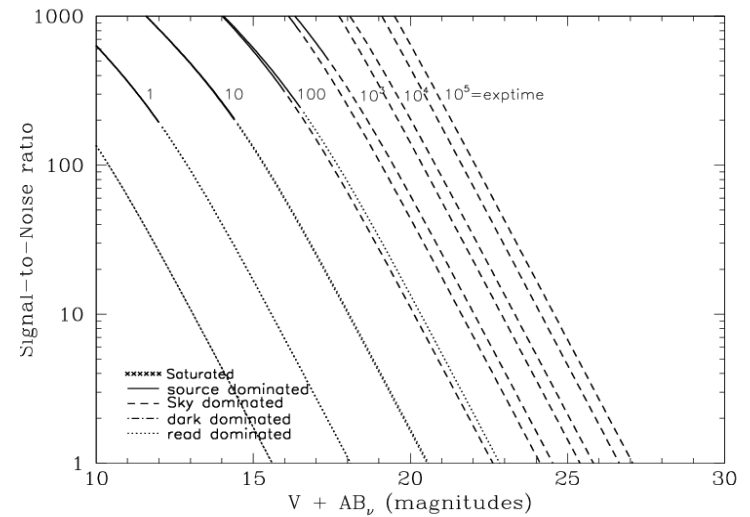


Figure 10.90: Extended Source S/N vs.  $V+AB_v$  for the HRC/F850LP filter. Top curves are for low sky and bottom curves are for average sky for a 1 arcsec<sup>2</sup> area.



## HRC/F892N

### Description

Methane filter.

Figure 10.91: Integrated System Throughput for HRC/F892N

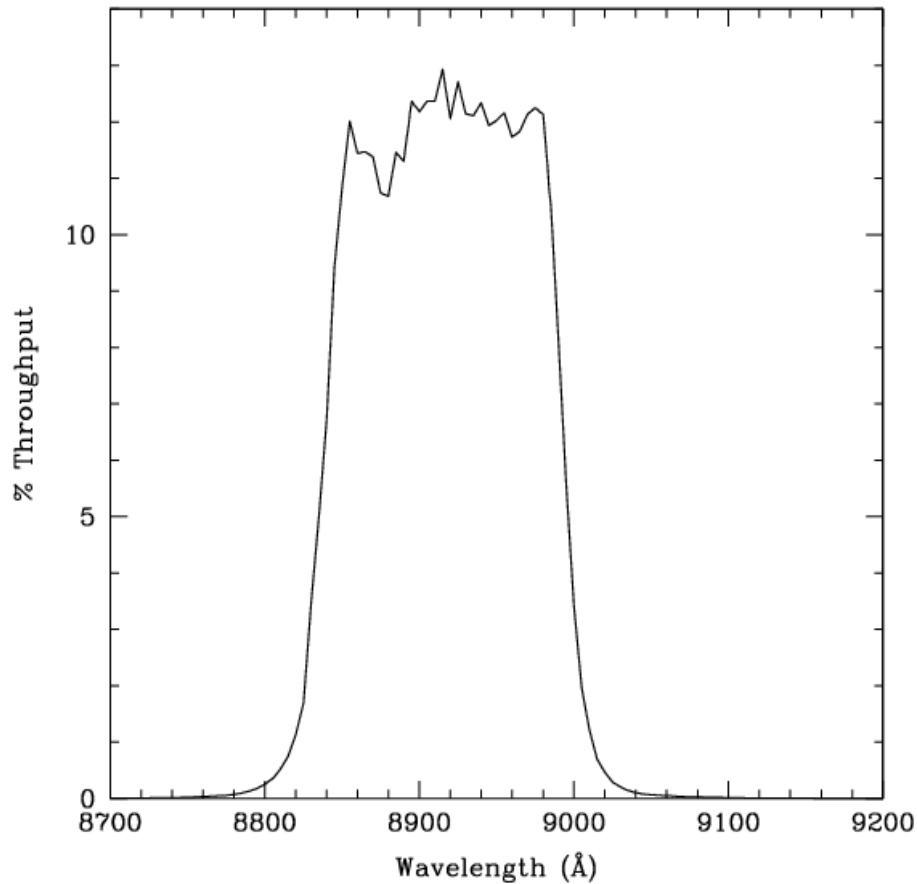


Figure 10.92: Point Source S/N vs.  $V+AB_V$  for the HRC/F892N filter. Top curves are for low sky; bottom curves are for average sky.

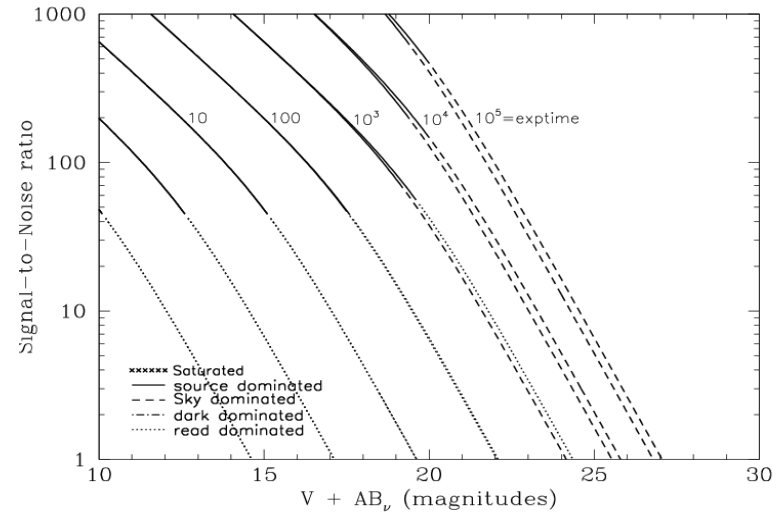
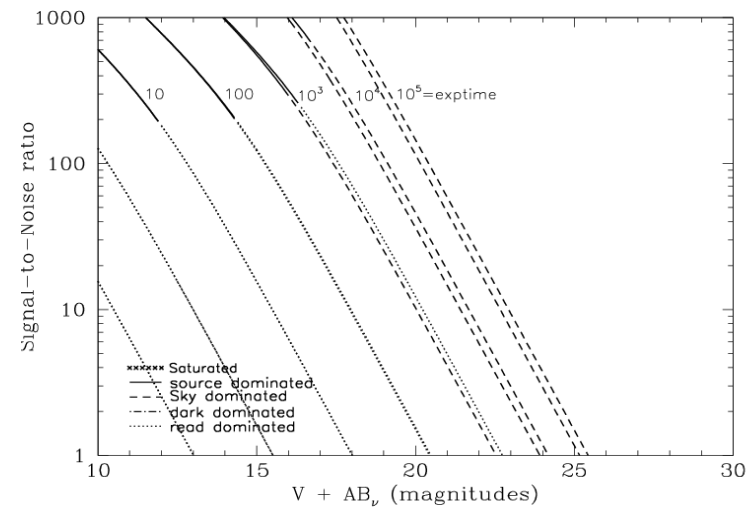


Figure 10.93: Extended Source S/N vs.  $V+AB_V$  for the HRC/F892N filter. Top curves are for low sky and bottom curves are for average sky for a 1 arcsec<sup>2</sup> area.



# HRC/G800L

## Description

Grism.

Figure 10.94: Integrated System Throughput for HRC/G800L

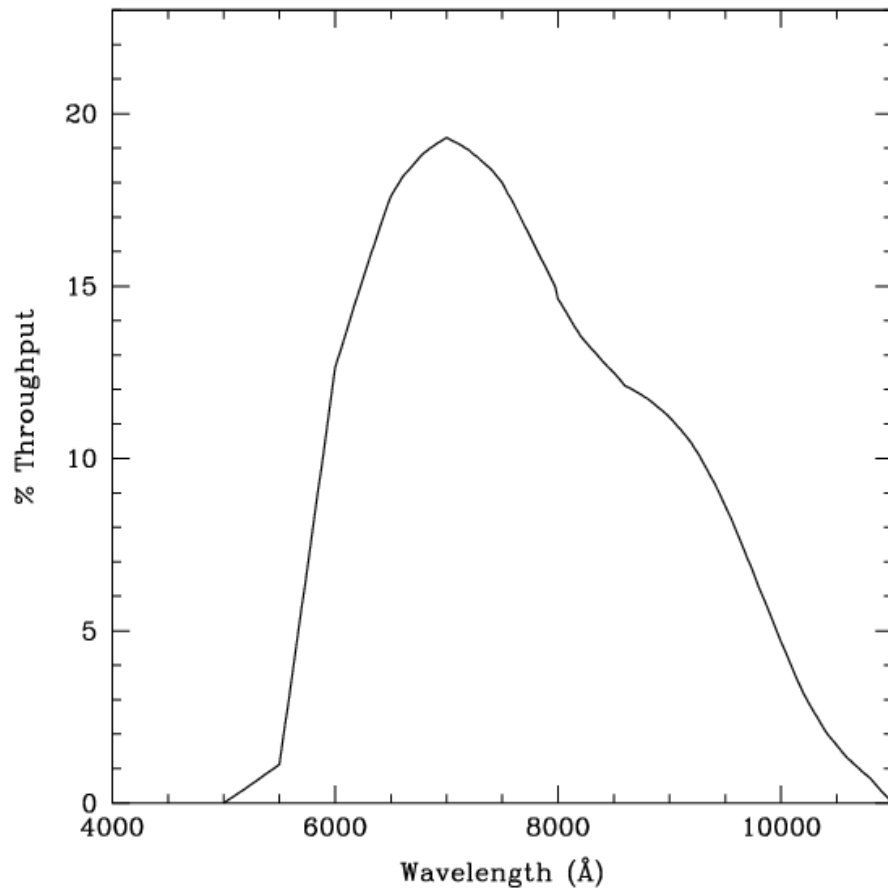


Figure 10.95: Point Source S/N vs.  $V+AB_v$  for the HRC/G800L filter. Top curves are for low sky; bottom curves are for average sky.

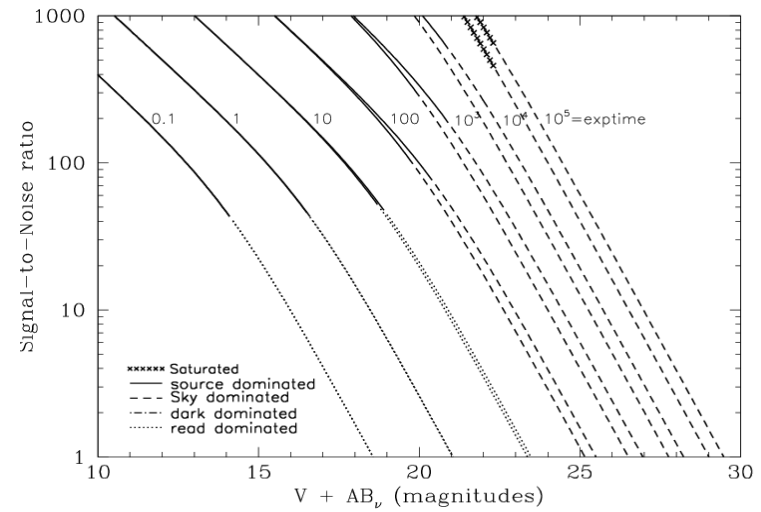
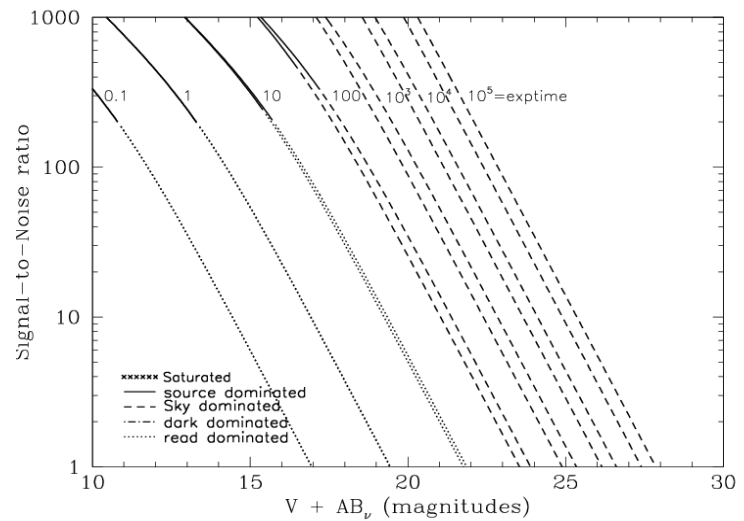


Figure 10.96: Extended Source S/N vs.  $V+AB_v$  for the HRC/G800L filter. Top curves are for low sky and bottom curves are for average sky for a 1 arcsec<sup>2</sup> area.





## HRC/PR200L

### Description

HRC Prism.

Figure 10.97: Integrated System Throughput for HRC/PR200L

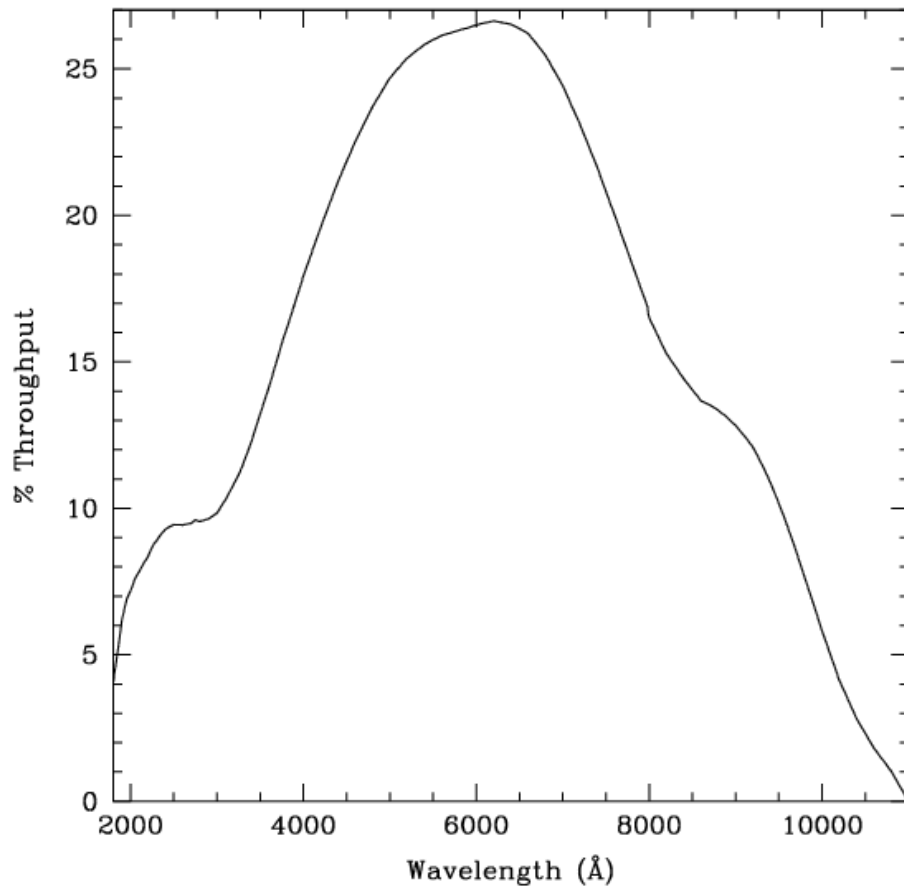


Figure 10.98: Point Source S/N vs.  $V+AB_v$  for the HRC/PR200L filter. Top curves are for low sky; bottom curves are for average sky.

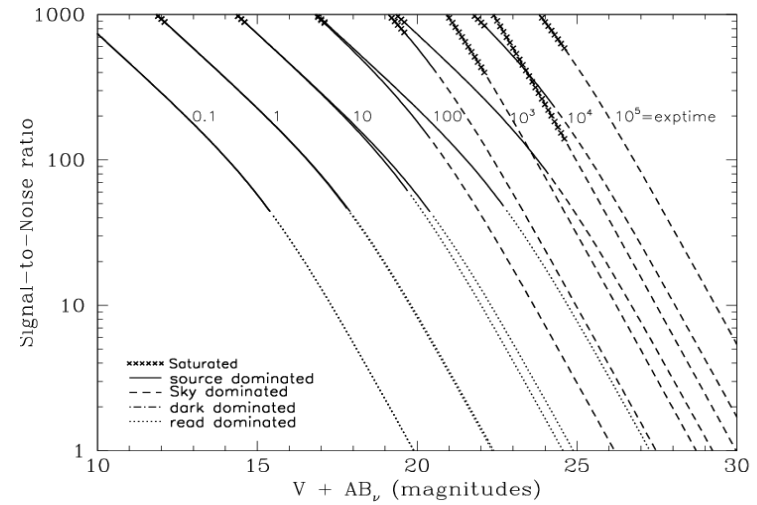
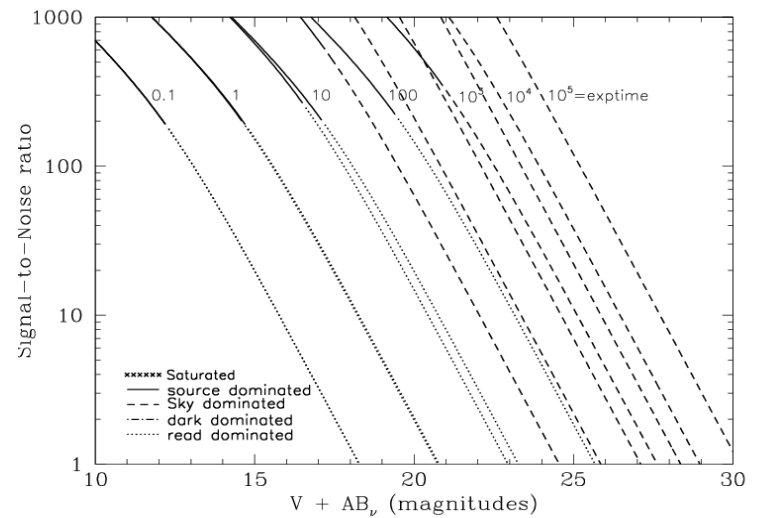


Figure 10.99: Extended Source S/N vs.  $V+AB_v$  for the HRC/PR200L filter. Top curves are for low sky and bottom curves are for average sky for a 1 arcsec<sup>2</sup> area.



# HRC/CLEAR

## Description

HRC Clear Filter.

Figure 10.100: Integrated System Throughput for HRC/Clear

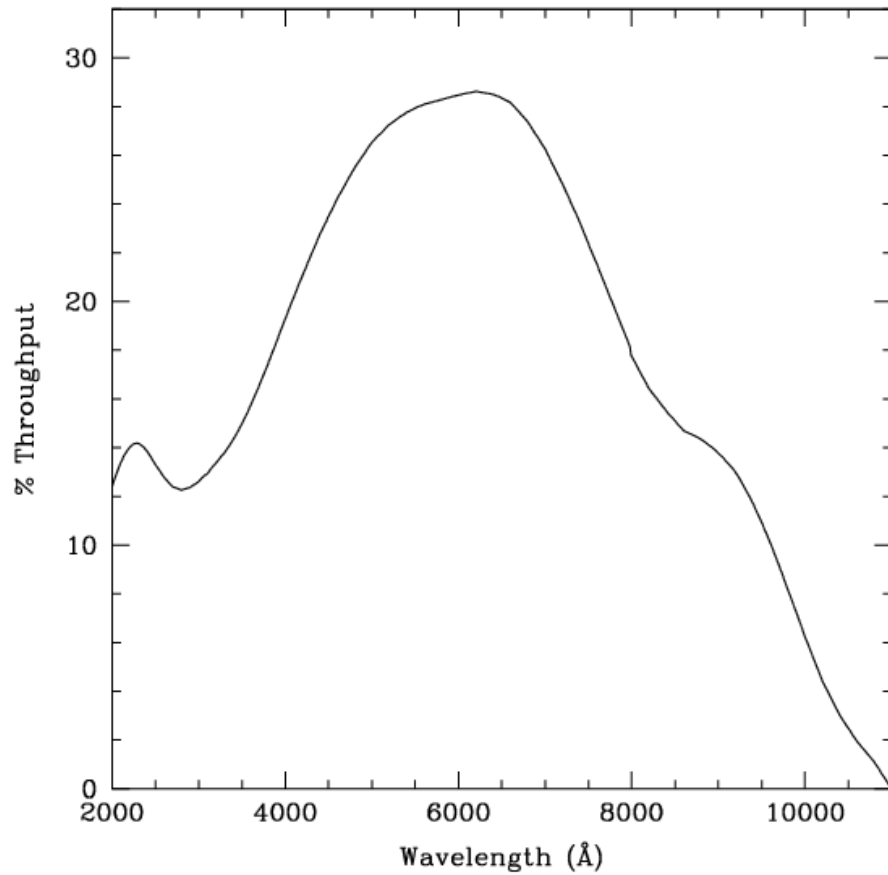


Figure 10.101: Point Source S/N vs.  $V+AB_V$  for the HRC/Clear filter. Top curves are for low sky; bottom curves are for average sky.

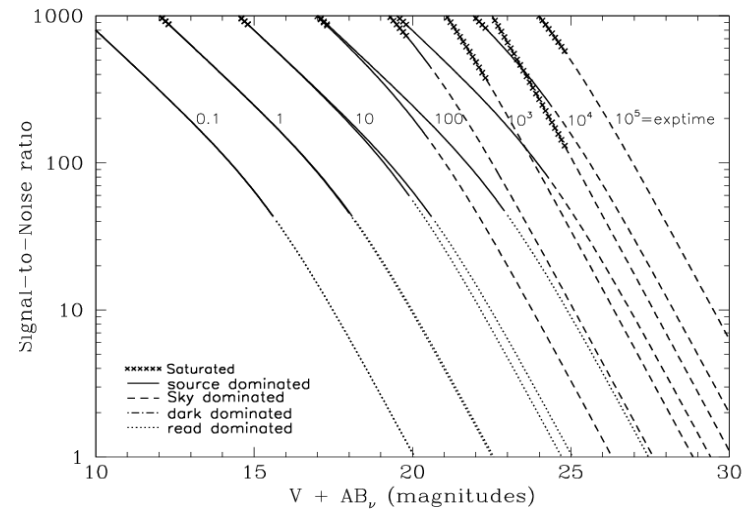
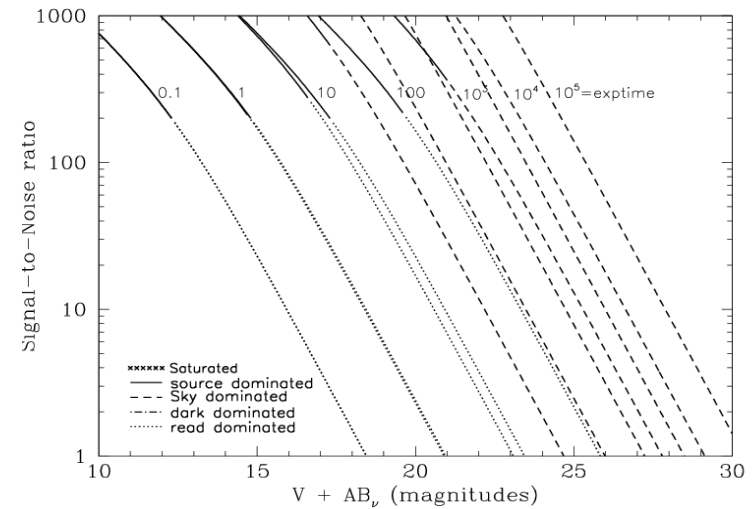


Figure 10.102: Extended Source S/N vs.  $V+AB_V$  for the HRC/Clear filter. Top curves are for low sky and bottom curves are for average sky for a 1 arcsec<sup>2</sup> area.



## SBC/F115LP

### Description

MgF<sub>2</sub> filter.

Figure 10.103: Integrated System Throughput for SBC/F115LP

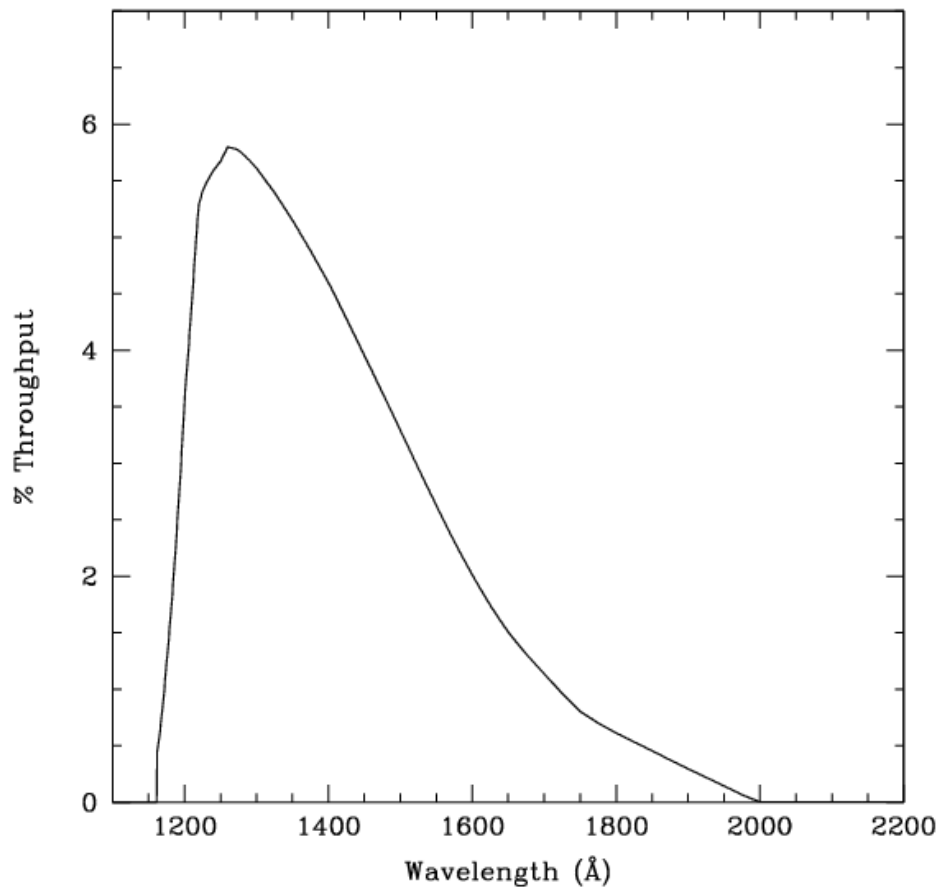


Figure 10.104: Point Source S/N vs.  $V+AB_V$  for the SBC/F115LP filter. Top curves are for low sky; bottom curves are for average sky.

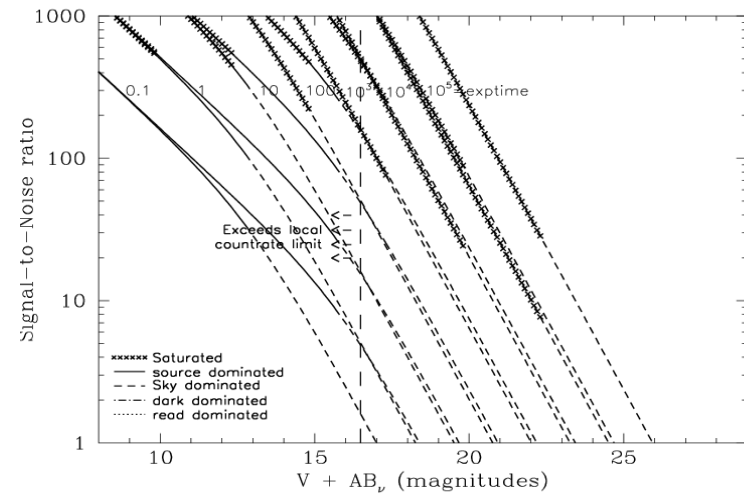
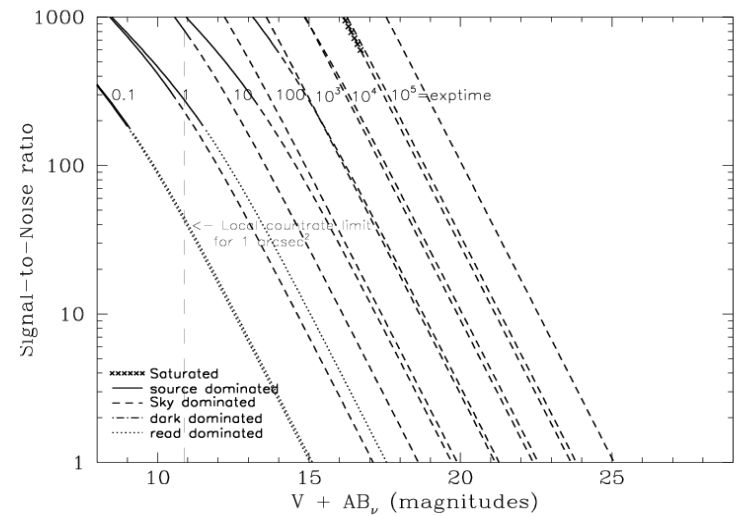


Figure 10.105: Extended Source S/N vs.  $V+AB_V$  for the SBC/F115LP filter. Top curves are for low sky and bottom curves are for average sky for a 1 arcsec<sup>2</sup> area.



## SBC/F122M

### Description

Lyman  $\alpha$  filter.

Figure 10.106: Integrated System Throughput for SBC/F122M

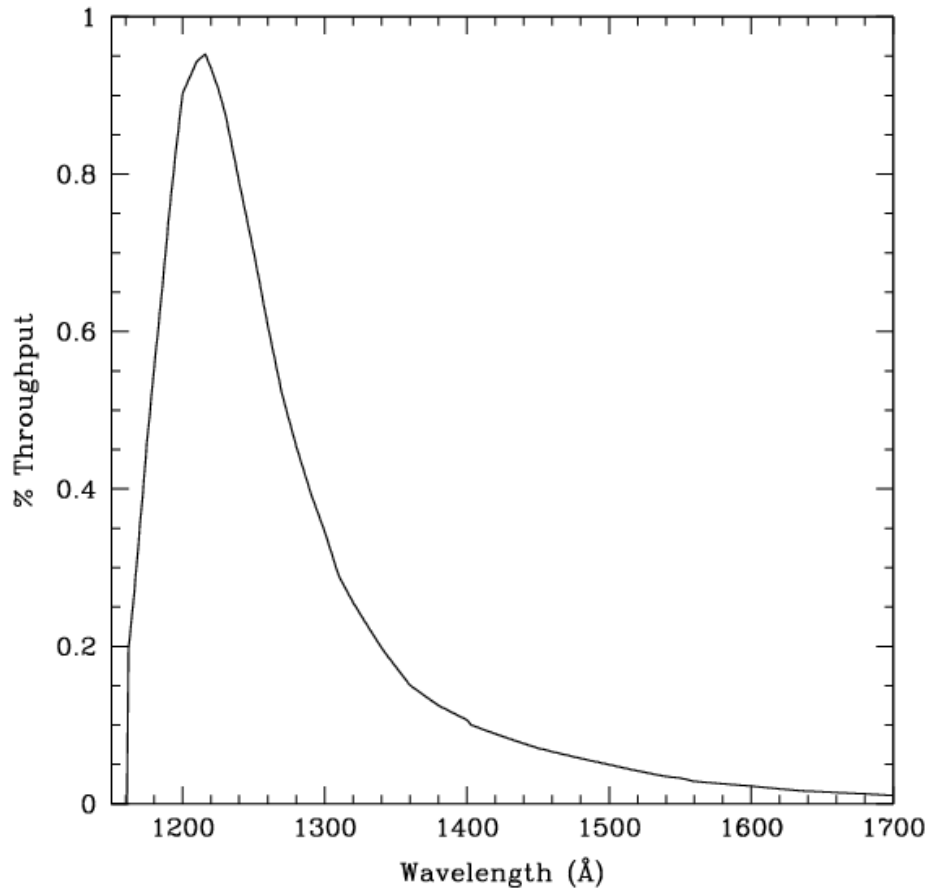


Figure 10.107: Point Source S/N vs.  $V+AB_v$  for the SBC/F122M filter. Top curves are for low sky; bottom curves are for average sky.

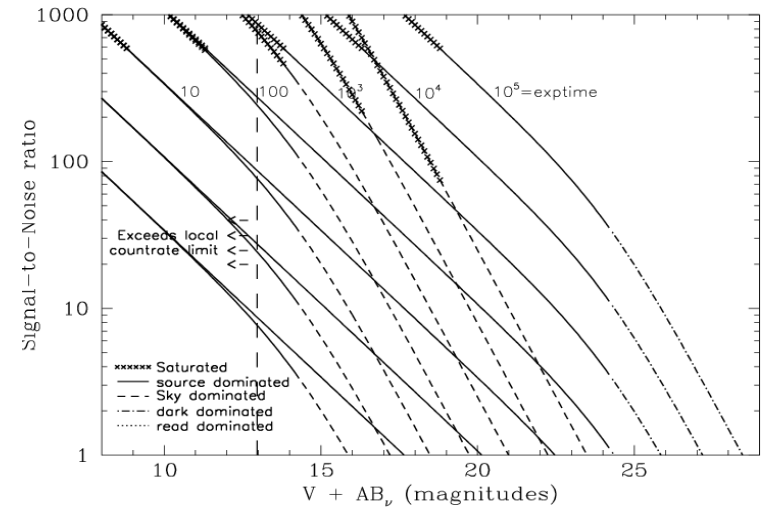
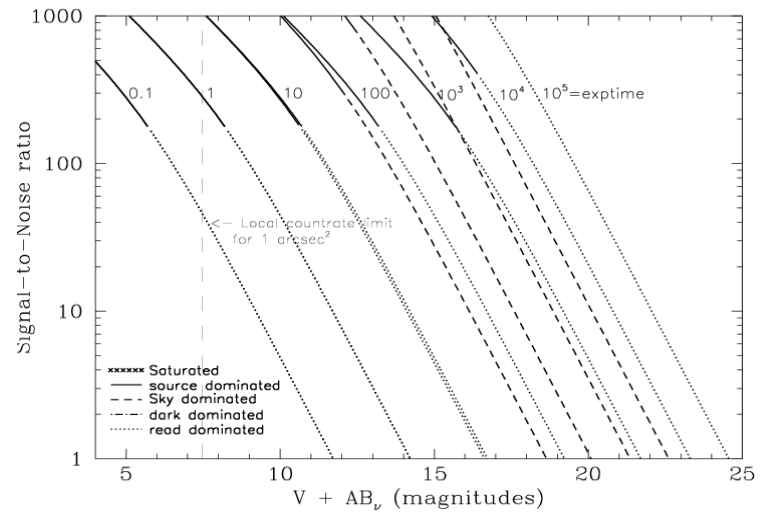


Figure 10.108: Extended Source S/N vs.  $V+AB_v$  for the SBC/F122M filter. Top curves are for low sky and bottom curves are for average sky for a 1 arcsec<sup>2</sup> area.



## SBC/F125LP

### Description

CaF<sub>2</sub> filter.

Figure 10.109: Integrated System Throughput for SBC/F125LP

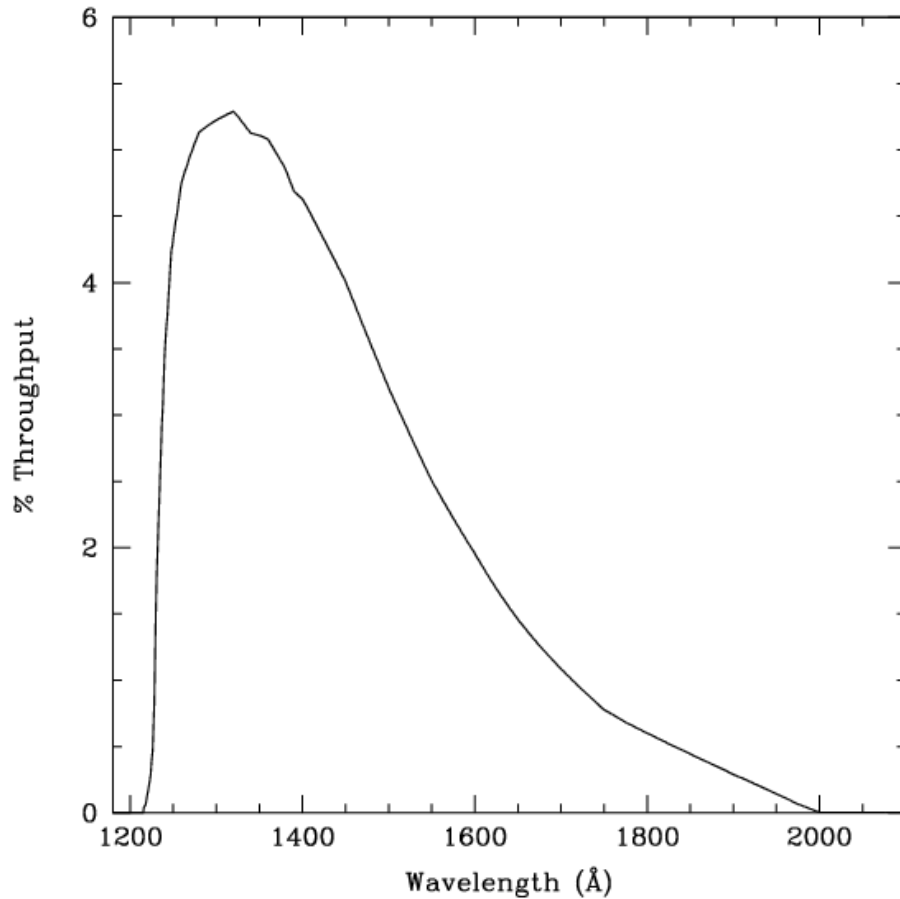


Figure 10.110: Point Source S/N vs.  $V+AB_V$  for the SBC/F125LP filter. Top curves are for low sky; bottom curves are for average sky.

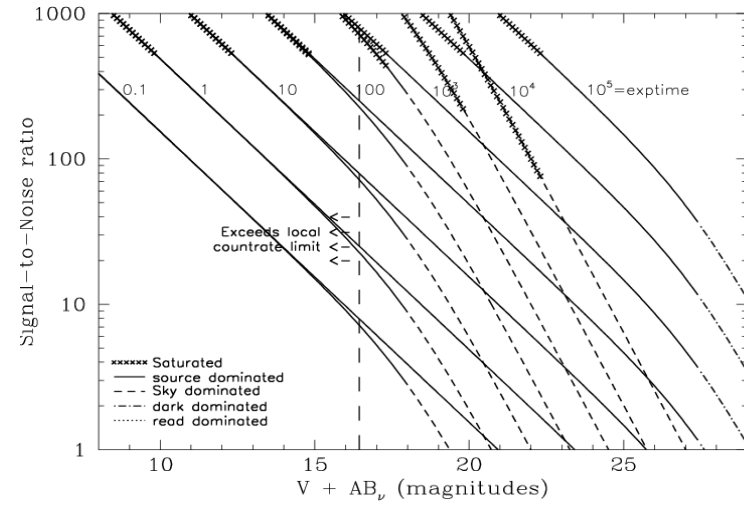
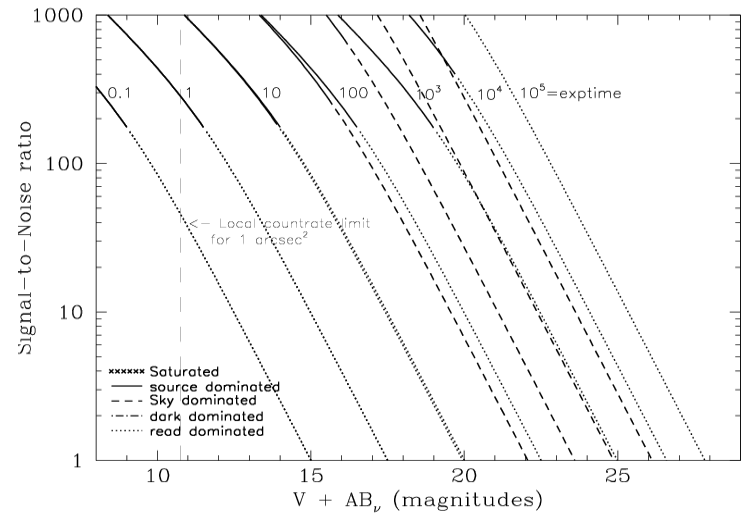


Figure 10.111: Extended Source S/N vs.  $V+AB_V$  for the SBC/F125LP filter. Top curves are for low sky and bottom curves are for average sky for a 1 arcsec<sup>2</sup> area.



# SBC/F140LP

## Description

BaF<sub>2</sub> filter.

Figure 10.112: Integrated System Throughput for SBC/F140LP

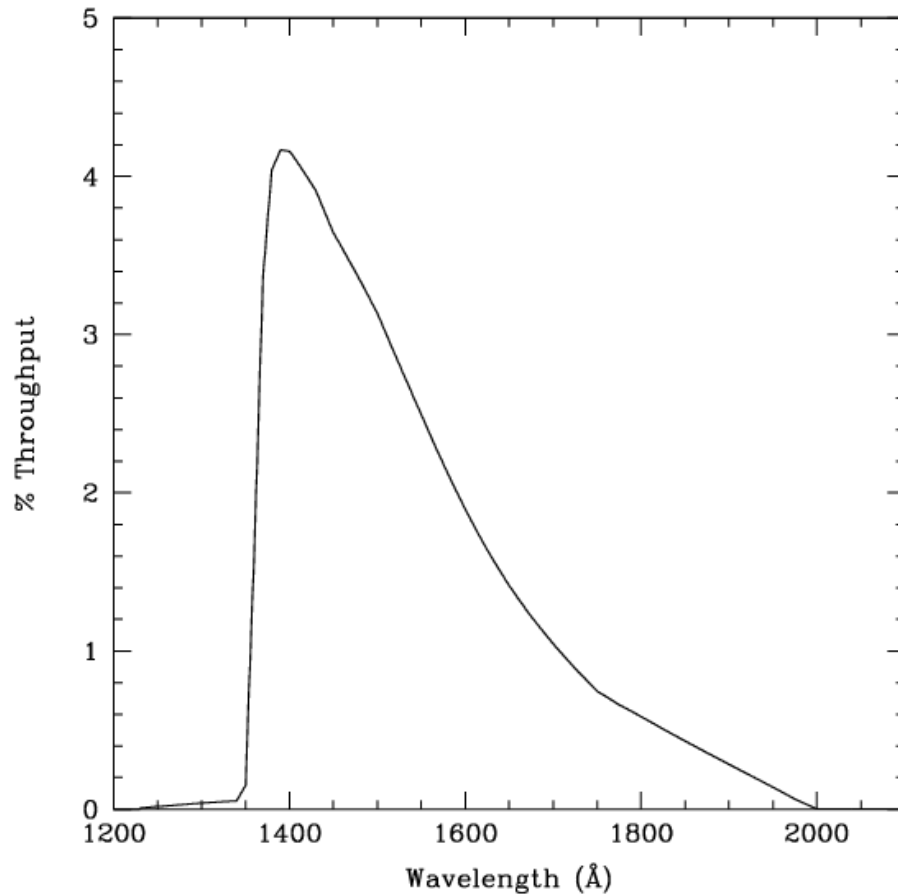


Figure 10.113: Point Source S/N vs.  $V+AB_V$  for the SBC/F140LP filter. Top curves are for low sky; bottom curves are for average sky.

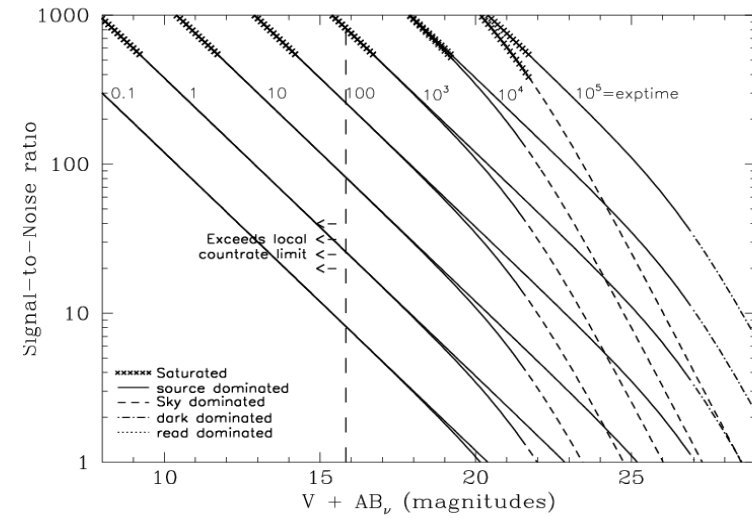
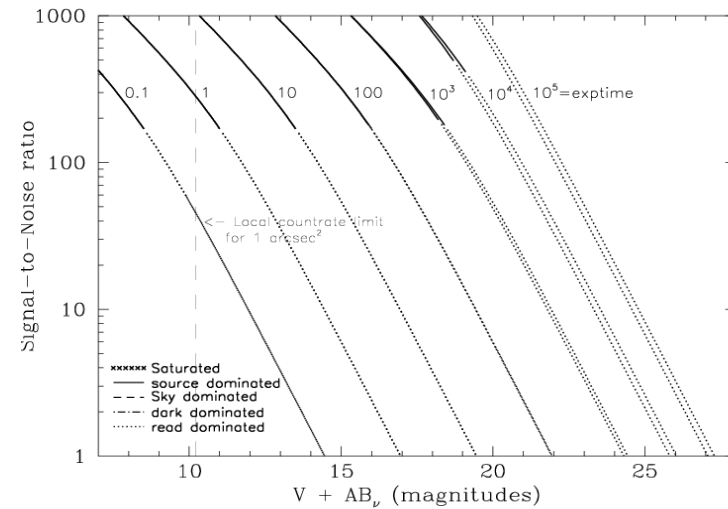


Figure 10.114: Extended Source S/N vs.  $V+AB_V$  for the SBC/F140LP filter. Top curves are for low sky and bottom curves are for average sky for a 1 arcsec<sup>2</sup> area.



## SBC/F150LP

### Description

Crystal Quartz filter.

Figure 10.115: Integrated System Throughput for SBC/F165LP

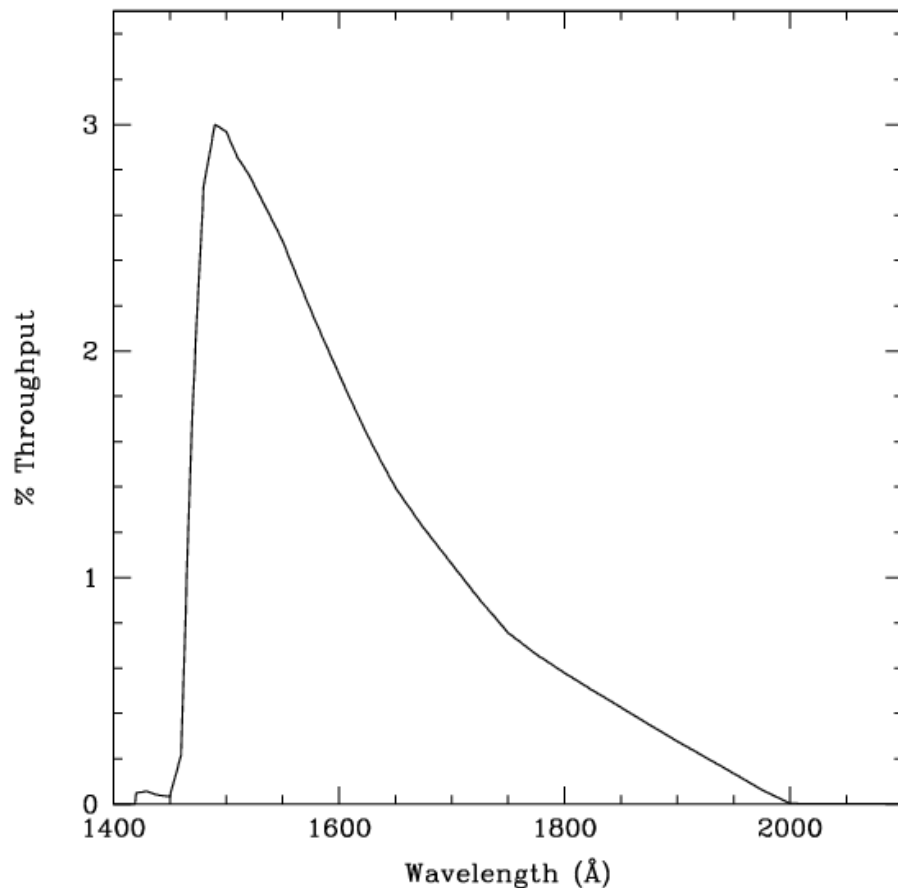


Figure 10.116: Point Source S/N vs.  $V+AB_V$  for the SBC/F150LP filter. Top curves are for low sky; bottom curves are for average sky.

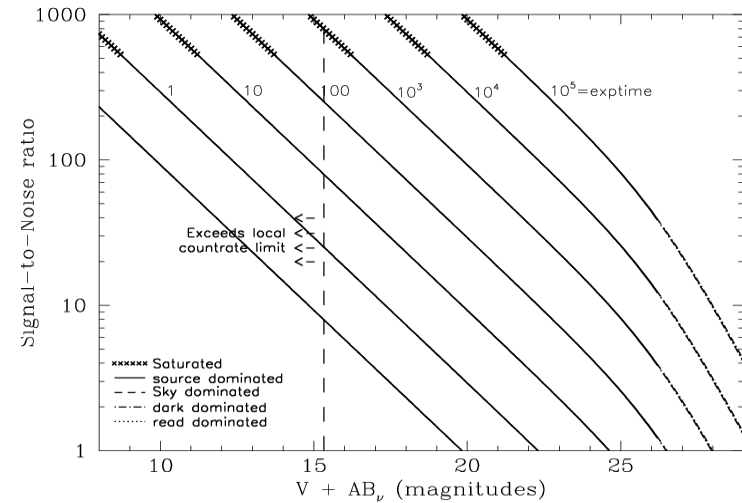
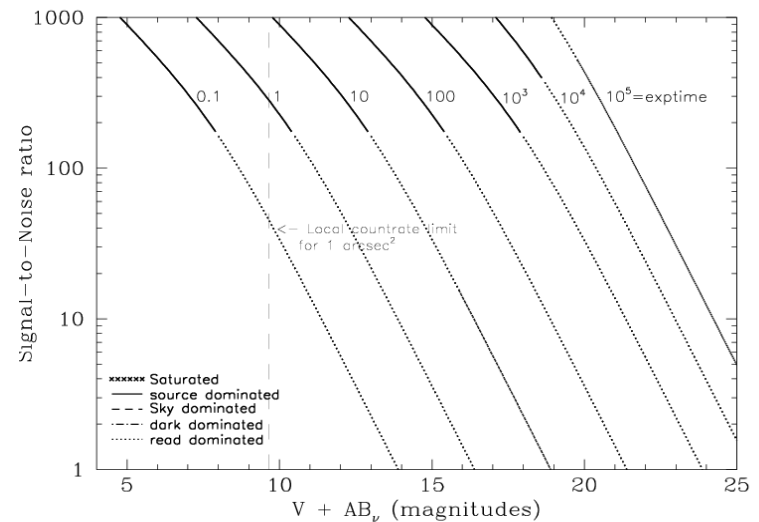


Figure 10.117: Extended Source S/N vs.  $V+AB_V$  for the SBC/F150LP filter. Top curves are for low sky and bottom curves are for average sky for a  $1 \text{ arcsec}^2$  area.



## SBC/F165LP

### Description

Dynasil filter.

Figure 10.118: Integrated System Throughput for SBC/F165LP

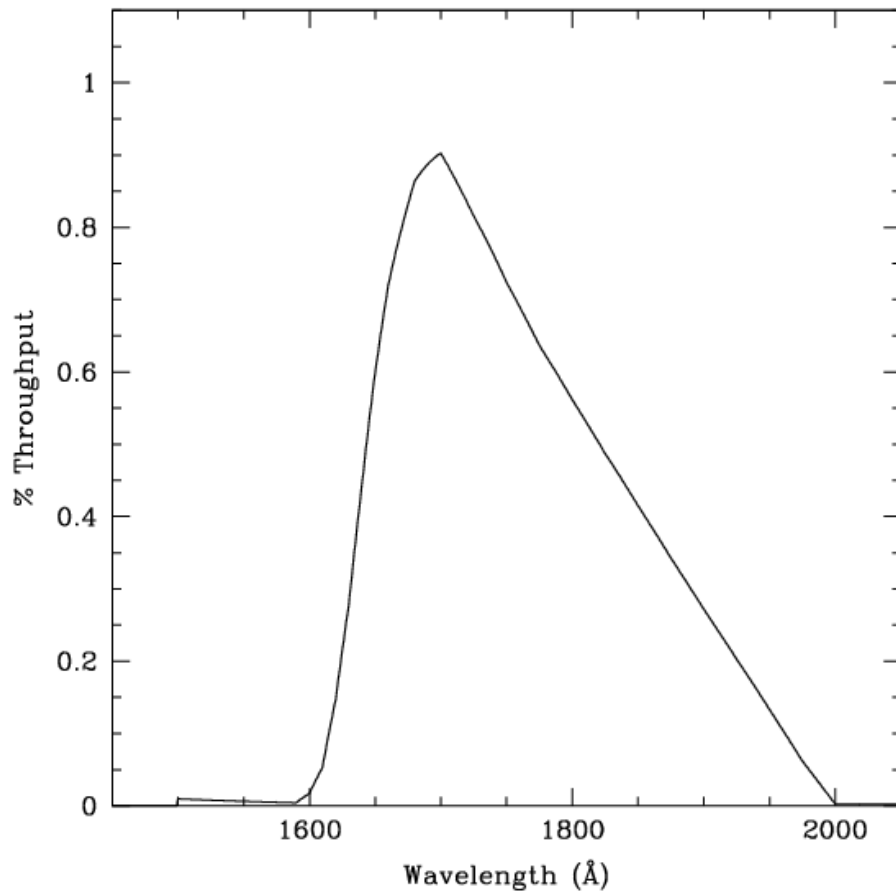


Figure 10.119: Point Source S/N vs.  $V+AB_V$  for the SBC/F165LP filter. Top curves are for low sky; bottom curves are for average sky.

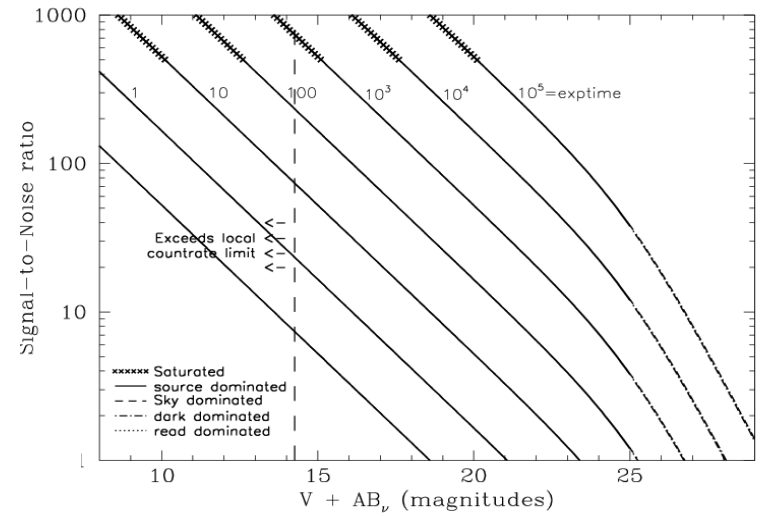
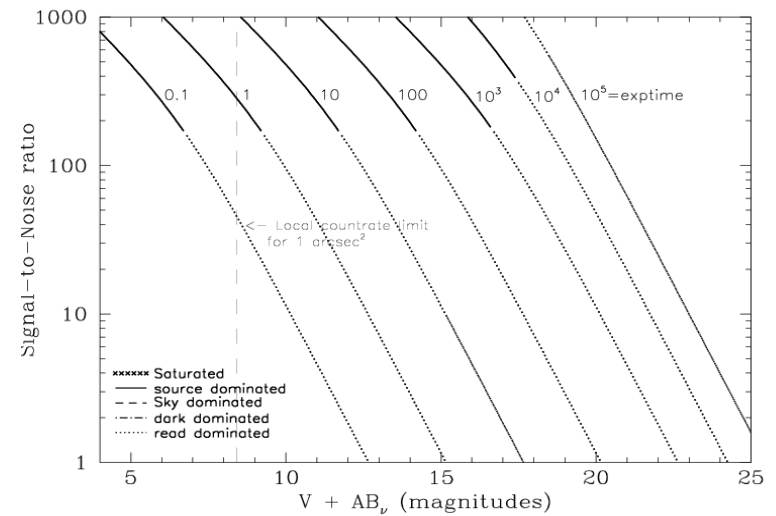


Figure 10.120: Extended Source S/N vs.  $V+AB_V$  for the SBC/F165LP filter. Top curves are for low sky and bottom curves are for average sky for a  $1 \text{ arcsec}^2$  area.





## SBC/PR110L

### Description

LiF<sub>2</sub> Prism.

Figure 10.121: Integrated System Throughput for SBC/PR110LP

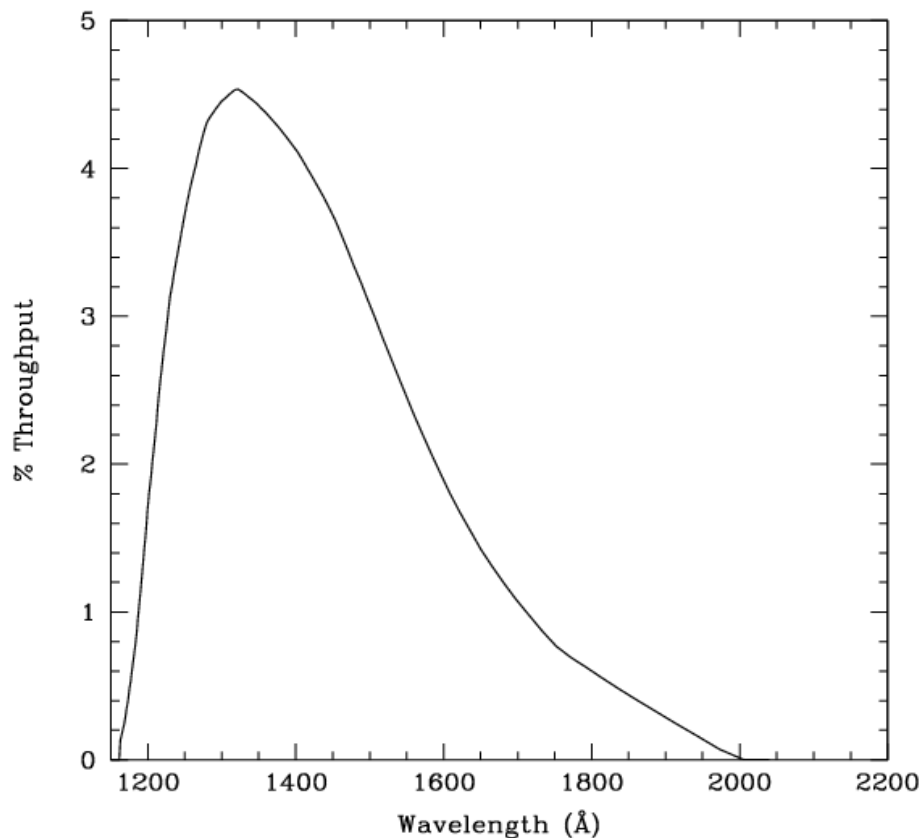


Figure 10.122: Point Source S/N vs.  $V+AB_V$  for the SBC/PR110LP filter. Top curves are for low sky; bottom curves are for average sky.

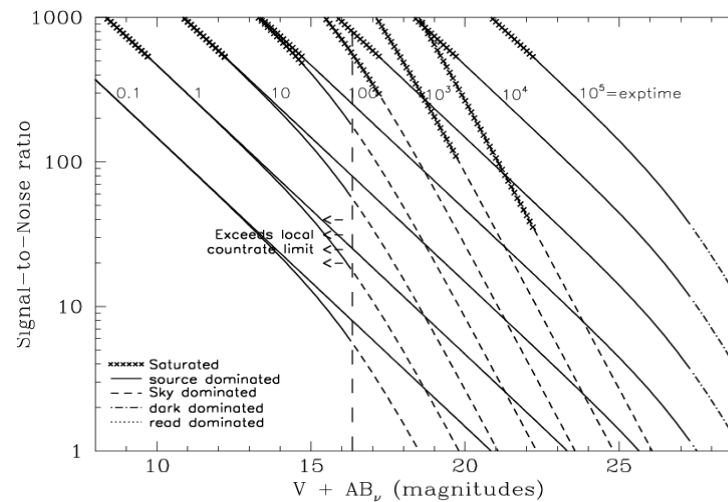
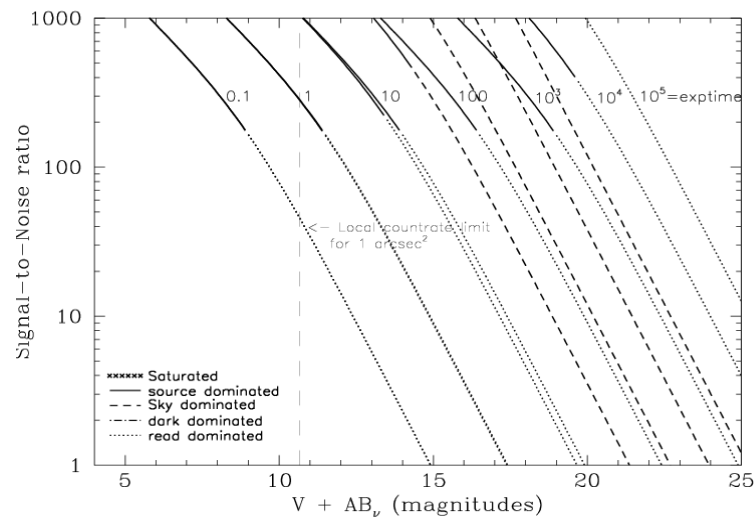


Figure 10.123: Extended Source S/N vs.  $V+AB_V$  for the SBC/PR110LP filter. Top curves are for low sky and bottom curves are for average sky for a 1 arcsec<sup>2</sup> area.



# SBC/PR130L

## Description

CaF<sub>2</sub> Prism.

Figure 10.124: Integrated System Throughput for SBC/PR130LP

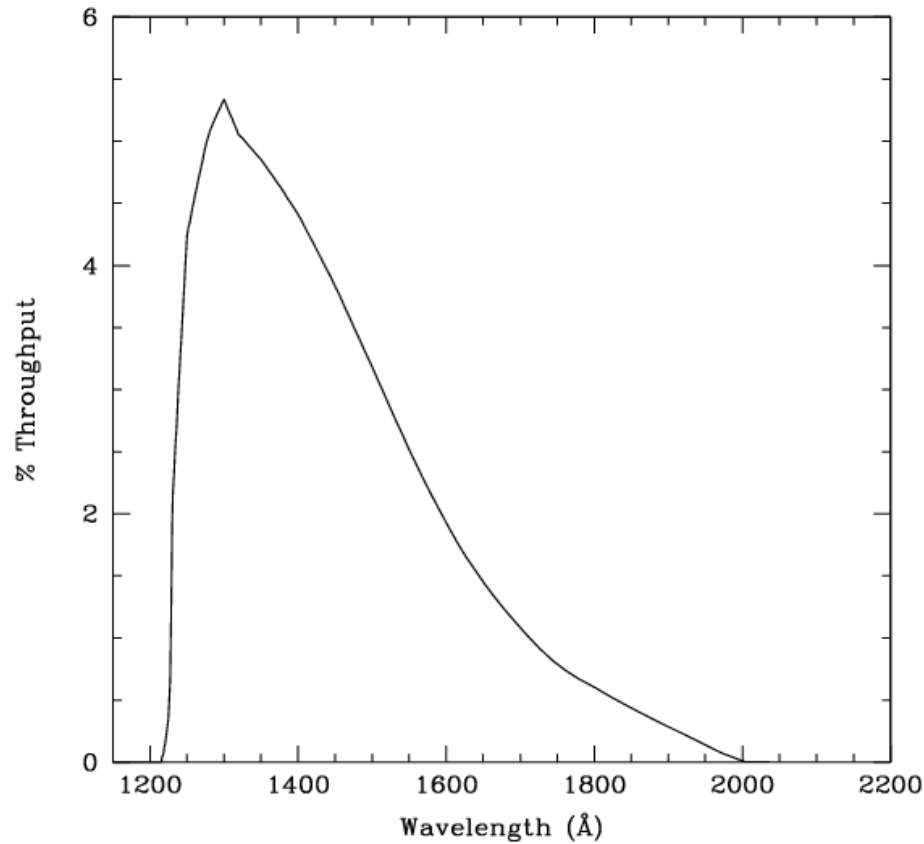


Figure 10.125: Point Source S/N vs.  $V+AB_V$  for the SBC/PR130LP filter. Top curves are for low sky; bottom curves are for average sky.

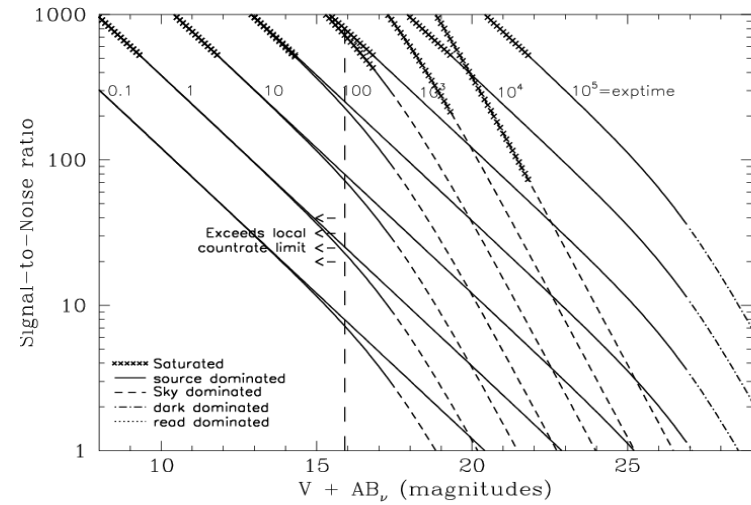


Figure 10.126: Extended Source S/N vs.  $V+AB_V$  for the SBC/PR130LP filter. Top curves are for low sky and bottom curves are for average sky for a 1 arcsec<sup>2</sup> area.

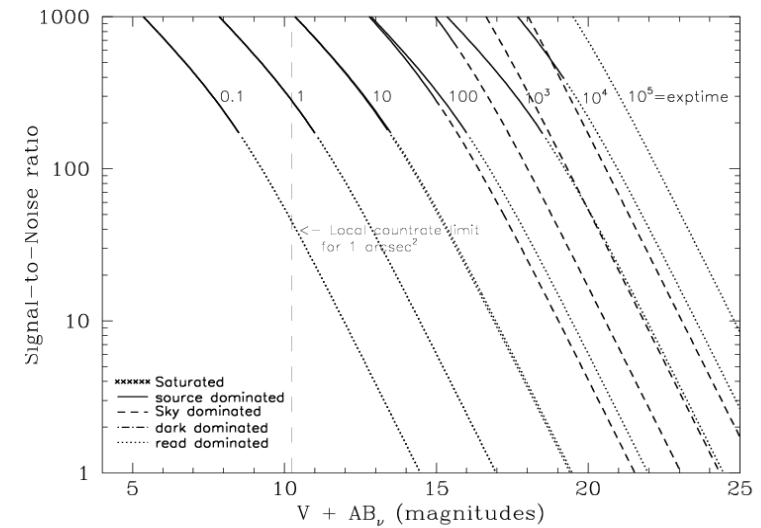


Table 10.1: Color Corrections  $AB_V$  to go from Johnson V Magnitude to AB Magnitude for the WFC

Spectrum	F435W	F475W	F502N	F550M	F555W	F606W	F625W	F658N	F660N	F775W	F814W	F850LP	F892N	G800L	CLEAR
<b>AvgSky</b>	0.64	0.35	0.22	-0.03	0.06	-0.09	-0.21	-0.23	-0.26	-0.39	-0.41	-0.46	-0.46	-0.35	-0.04
<b>Sky (shadow)</b>	0.66	0.37	0.24	-0.03	0.06	-0.10	-0.23	-0.26	-0.29	-0.44	-0.47	-0.54	-0.53	-0.40	-0.07
<b>O5V</b>	-0.43	-0.27	-0.14	0.06	-0.03	0.13	0.29	0.40	0.41	0.69	0.77	1.03	1.00	0.59	0.05
<b>B0V</b>	-0.42	-0.27	-0.16	0.08	-0.03	0.14	0.31	0.42	0.41	0.66	0.73	0.97	0.94	0.57	0.05
<b>A0V</b>	-0.06	-0.07	-0.07	0.04	0.01	0.10	0.17	0.34	0.31	0.37	0.41	0.50	0.50	0.32	0.17
<b>A5V</b>	0.06	-0.002	-0.02	0.02	0.02	0.07	0.12	0.24	0.18	0.25	0.27	0.32	0.31	0.22	0.16
<b>F2V</b>	0.28	0.14	0.06	0.003	0.04	0.007	-0.02	0.02	-0.02	-0.04	-0.04	-0.03	-0.04	-0.03	0.09
<b>G2V</b>	0.56	0.30	0.15	-0.02	0.05	-0.06	-0.15	-0.15	-0.16	-0.29	-0.31	-0.33	-0.33	-0.25	0.01
<b>K0V</b>	0.80	0.42	0.21	-0.05	0.07	-0.11	-0.24	-0.30	-0.30	-0.41	-0.43	-0.46	-0.47	-0.37	-0.03
<b>M0V</b>	1.43	0.81	0.69	-0.14	0.13	-0.32	-0.58	-0.83	-0.83	-1.20	-1.30	-1.55	-1.51	-1.11	-0.53
<b>M6V</b>	1.75	0.90	0.73	-0.17	0.14	-0.39	-0.65	-1.16	-1.14	-2.11	-2.34	-2.80	-2.74	-2.00	-1.28
<b>O7I</b>	-0.39	-0.24	-0.12	0.06	-0.02	0.13	0.27	0.37	0.37	0.65	0.72	0.96	0.94	0.55	-1.28
<b>B0I</b>	-0.33	-0.20	-0.11	0.05	-0.02	0.11	0.24	0.33	0.33	0.54	0.60	0.79	0.77	0.47	0.07
<b>F0III</b>	0.21	0.09	0.02	0.009	0.02	0.03	0.03	0.08	0.05	0.08	0.08	0.09	0.07	0.06	0.12
<b>G0III</b>	0.65	0.34	0.17	-0.02	0.06	-0.08	-0.18	-0.23	-0.24	-0.35	-0.37	-0.42	-0.44	-0.31	-0.01
<b>K2III</b>	1.16	0.59	0.35	-0.06	0.09	-0.18	-0.36	-0.47	-0.47	-0.67	-0.71	-0.82	-0.89	-0.61	-0.16
<b>M0III</b>	1.58	0.82	0.58	-0.11	0.13	-0.32	-0.57	-0.74	-0.74	-1.23	-1.34	-1.59	-1.61	-1.14	-0.54
<b>M6III</b>	1.67	0.94	1.21	-0.12	0.19	-0.63	-0.94	-1.19	-1.14	-2.91	-3.24	-3.91	-3.73	-2.90	-2.13
<b>Elliptical</b>	0.97	0.52	0.36	-0.06	0.09	-0.18	-0.35	-0.47	-0.47	-0.80	-0.91	-1.03	-1.17	-0.72	-0.25
<b>Sa</b>	0.82	0.47	0.32	-0.05	0.09	-0.18	-0.35	-0.53	-0.50	-0.75	-0.83	-0.90	-1.04	-0.66	-0.22
<b>Sb</b>	0.83	0.46	0.29	-0.05	0.08	-0.17	-0.33	-0.50	-0.47	-0.74	-0.84	-0.93	-1.00	-0.67	-0.22
<b>Sc</b>	0.10	0.06	-0.69	0.09	-0.02	-0.16	-0.24	-1.75	-0.83	0.43	-0.80	1.11	-1.06	0.26	0.11
<b>Starburst E(B-V) 0.51-0.60</b>	0.43	0.25	-0.01	0.01	0.05	-0.21	-0.38	-1.37	-0.86	-0.59	-0.66	-0.71	-0.79	-0.56	-0.21
<b>Starburst E(B-V)&lt;0.1</b>	0.24	0.07	-0.95	0.11	-0.02	-0.09	-0.13	-1.15	-0.34	-0.14	-0.18	-0.14	-0.22	-0.15	-0.02
<b>Sun</b>	0.60	0.32	0.18	-0.02	0.06	-0.06	-0.15	-0.16	-0.19	-0.25	-0.26	-0.27	-0.27	-0.22	0.03
<b>Vega</b>	-0.10	-0.10	-0.06	0.04	0.006	0.10	0.18	0.37	0.34	0.41	0.45	0.57	0.51	0.35	0.17

Table 10.2: Color Corrections  $AB_V$  to go from Johnson V Magnitude to AB Magnitude for the HRC

Spectrum	F220W	F250W	F330W	F344N	F435W	F475W	F502N	F550M	F555W	F606W	F625W	F658N	F660N	F775W	F814W	F850LP	F892N	G800L	PR200L	Clear
<b>AvgSky</b>	3.57	2.60	2.03	1.91	0.64	0.34	0.23	-0.03	0.07	-0.08	-0.21	-0.23	-0.25	-0.39	-0.41	-0.47	-0.46	-0.35	0.23	0.32
<b>LowSky</b>	5.33	3.40	1.86	1.74	0.66	0.35	0.24	-0.03	0.07	-0.10	-0.23	-0.26	-0.28	-0.44	-0.47	-0.54	-0.53	-0.39	0.21	0.30
<b>O5V</b>	-1.52	-1.23	-0.86	-0.81	-0.43	-0.26	-0.14	0.06	-0.03	0.12	0.29	0.40	0.38	0.69	0.78	1.04	0.96	0.59	-0.45	-0.59
<b>B0V</b>	-0.15	-0.97	-0.71	-0.68	-0.43	-0.26	-0.16	0.08	-0.03	0.13	0.30	0.41	0.39	0.67	0.74	0.99	0.94	0.57	-0.32	-0.42
<b>A0V</b>	1.77	1.56	1.21	1.18	-0.05	-0.07	-0.07	0.04	0.01	0.09	0.17	0.34	0.31	0.37	0.41	0.51	0.50	0.32	0.36	0.42
<b>A5V</b>	2.62	2.17	1.42	1.37	0.07	-0.002	-0.02	0.02	0.02	0.07	0.11	0.24	0.18	0.25	0.27	0.33	0.31	0.22	0.38	0.46
<b>F2V</b>	3.51	2.54	1.47	1.37	0.29	0.13	0.07	0.003	0.04	0.08	-0.02	0.02	-0.01	-0.04	-0.04	-0.03	-0.04	-0.03	0.33	0.42
<b>G2V</b>	5.67	3.32	1.65	1.65	0.57	0.28	0.16	-0.02	0.06	-0.05	-0.14	-0.15	-0.16	-0.29	-0.31	-0.33	-0.33	-0.25	0.28	0.36
<b>K0V</b>	6.84	4.51	2.41	2.28	0.80	0.40	0.21	-0.05	0.07	-0.10	-0.23	-0.30	-0.29	-0.41	-0.43	-0.46	-0.48	-0.36	0.25	0.34
<b>M0V</b>	7.75	5.96	3.92	3.78	1.42	0.78	0.69	-0.13	0.13	-0.29	-0.57	-0.83	-0.82	-1.19	-1.32	-1.57	-1.51	-1.11	-0.22	-0.13
<b>M6V</b>	7.31	6.34	4.33	4.25	1.73	0.86	0.73	-0.17	0.15	-0.36	-0.63	-1.16	-1.13	-2.09	-2.37	-2.83	-2.74	-2.02	-0.98	-0.89
<b>O7I</b>	-0.32	-0.54	-0.59	-0.55	-0.39	-0.23	-0.13	0.06	-0.02	0.12	0.27	0.37	0.36	0.64	0.73	0.99	0.94	0.55	-0.10	-0.89
<b>B0I</b>	-0.71	-0.68	-0.54	-0.53	-0.33	-0.20	-0.11	0.05	-0.02	0.11	0.23	0.33	0.32	0.53	0.61	0.81	0.77	0.47	-0.15	-0.21
<b>F0III</b>	3.71	2.77	1.60	1.49	0.22	0.08	0.02	0.01	0.02	0.03	0.03	0.08	0.05	0.07	0.08	0.09	0.07	0.06	0.37	0.45
<b>G0III</b>	6.60	4.25	2.26	2.15	0.65	0.32	0.18	-0.02	0.06	-0.07	-0.18	-0.23	-0.23	-0.35	-0.37	-0.42	-0.44	-0.31	0.27	0.36
<b>K2III</b>	8.46	6.61	3.80	3.58	1.15	0.56	0.35	-0.06	0.09	-0.16	-0.35	-0.47	-0.47	-0.67	-0.72	-0.83	-0.88	-0.61	0.14	0.23
<b>M0III</b>	7.73	7.05	5.16	5.02	1.58	0.78	0.58	-0.11	0.13	-0.29	-0.56	-0.73	-0.73	-1.22	-1.36	-1.61	-1.61	-1.14	-0.24	-0.15
<b>M6III</b>	6.26	6.20	4.47	4.29	1.69	0.90	1.21	-0.11	0.20	-0.58	-0.91	-1.19	-1.13	-2.88	-3.29	-3.97	-3.73	-2.94	-1.85	-1.76
<b>Elliptical</b>	5.22	4.66	2.84	2.65	0.97	0.49	0.36	-0.06	0.09	-0.16	-0.35	-0.47	-0.47	-0.79	-0.93	-1.02	-1.17	-0.72	0.05	0.14
<b>Sa</b>	4.36	3.56	2.40	2.36	0.82	0.45	0.32	-0.05	0.09	-0.16	-0.34	-0.53	-0.49	-0.74	-0.84	-0.89	-1.04	-0.65	0.07	0.16
<b>Sb</b>	3.75	3.13	2.13	2.18	0.83	0.44	0.29	-0.05	0.08	-0.15	-0.33	-0.49	-0.47	-0.74	-0.85	-0.92	-1.08	-0.66	0.06	0.15
<b>Sc</b>	2.11	1.17	0.17	-0.06	0.09	0.00	-0.69	0.09	-0.02	-0.16	-0.24	-1.75	-0.83	0.38	0.82	0.54	0.52	0.25	0.25	0.32
<b>Starburst E(B-V) 0.51-0.60</b>	1.84	1.65	1.15	1.16	0.43	0.24	-0.01	0.02	0.06	-0.20	-0.37	-1.37	-0.85	-0.58	-0.67	-0.70	-0.79	-0.56	0.02	0.09
<b>Starburst E(B-V)&lt;0.1</b>	1.00	0.97	0.83	0.82	0.24	0.06	-0.95	0.11	-0.02	-0.09	-0.13	-1.15	-0.34	-0.14	-0.19	-0.12	-0.22	-0.15	0.15	0.19
<b>Sun</b>	5.69	3.58	1.86	1.74	0.60	0.30	0.19	-0.02	0.06	-0.05	-0.15	-0.16	-0.18	-0.25	-0.26	-0.27	-0.27	-0.22	0.30	0.39
<b>Vega</b>	1.67	1.50	1.20	1.16	-0.09	-0.09	-0.06	0.04	0.005	0.09	0.18	0.37	0.34	0.40	0.46	0.58	0.51	0.35	0.35	0.42

Table 10.3: Color Corrections  $AB_V$  to go from Johnson V Magnitude to AB Magnitude for the SBC

Spectrum	F115LP	F122M	F125LP	F140LP	F150LP	F165LP	PR110L	PR130L
<b>AvgSky</b>	-1.84	-2.92	0.32	3.85	10.62	9.27	-1.39	0.29
<b>LowSky</b>	11.82	14.16	11.65	11.06	10.43	9.09	11.64	11.63
<b>O5V</b>	-2.06	-2.16	-2.03	-1.96	-1.90	-1.81	-2.04	-2.03
<b>B0V</b>	-1.63	-1.52	-1.68	-1.66	-1.62	-1.53	-1.65	-1.68
<b>A0V</b>	2.66	3.90	2.48	2.11	1.92	1.84	2.53	2.48
<b>A5V</b>	5.43	7.45	5.26	4.67	4.06	3.16	5.25	5.24
<b>F2V</b>	7.92	10.19	7.75	7.16	6.53	5.20	7.74	7.73
<b>G2V</b>	13.84	16.36	13.66	13.06	12.44	11.06	13.65	13.64
<b>K0V</b>	10.09	10.45	10.01	9.81	9.63	9.33	10.03	10.01
<b>M0V</b>	11.59	11.95	11.52	11.31	11.13	10.82	11.53	11.51
<b>M6V</b>	12.07	12.43	12.00	11.79	11.61	11.31	12.01	11.99
<b>O7I</b>	-0.56	-0.40	-0.60	-0.67	-0.70	-0.70	-0.58	-0.60
<b>B0I</b>	-0.78	-0.59	-0.85	-0.81	-0.77	-0.74	-0.81	-0.85
<b>F0III</b>	7.82	10.10	7.65	6.06	6.43	5.09	7.64	7.63
<b>G0III</b>	9.81	10.17	9.74	9.54	9.36	9.05	9.76	9.74
<b>K2III</b>	13.33	13.70	13.26	13.06	12.88	12.57	13.28	13.26
<b>M0III</b>	11.08	11.44	11.01	10.80	10.62	10.32	11.02	11.00
<b>M6III</b>	10.38	10.74	10.31	10.11	9.93	9.63	10.33	10.31
<b>Elliptical</b>	6.25	6.73	6.12	6.10	6.00	5.92	6.20	6.12
<b>Sa</b>	5.68	6.24	5.54	5.43	5.28	5.08	5.61	5.54
<b>Sb</b>	4.65	5.19	4.51	4.40	4.29	4.26	4.58	4.51
<b>Sc</b>	2.88	3.53	2.73	2.62	2.46	2.34	2.80	2.73
<b>Starburst E(B-V) 0.51-0.60</b>	2.69	3.33	2.54	2.46	2.36	2.15	2.62	2.54
<b>Starburst E(B-V)&lt;0.1</b>	1.34	1.90	1.20	1.15	1.11	1.07	1.27	1.20
<b>Sun</b>	12.00	11.80	12.31	11.80	11.23	10.04	12.04	12.29
<b>Vega</b>	2.76	3.96	2.58	2.22	2.06	1.92	2.63	2.58

## 10.3 Distortion in the ACS

The ACS detectors exhibit more distortion than previous HST instruments. The principal reason for this is that the optics have been designed with a minimum number of components, consistent with correcting for the spherical aberration induced by the OTA, without introducing coma. The result is a high throughput, but focal surfaces far from normal to the principal rays. The WFC detector is tilted at 22 degrees giving an elongation of 8% while the HRC and SBC have a 25 degree tilt leading to an elongation of 12%. In each case, the scales in arcseconds per pixel are smaller along the radial direction of the OTA field of view than along the tangential direction.

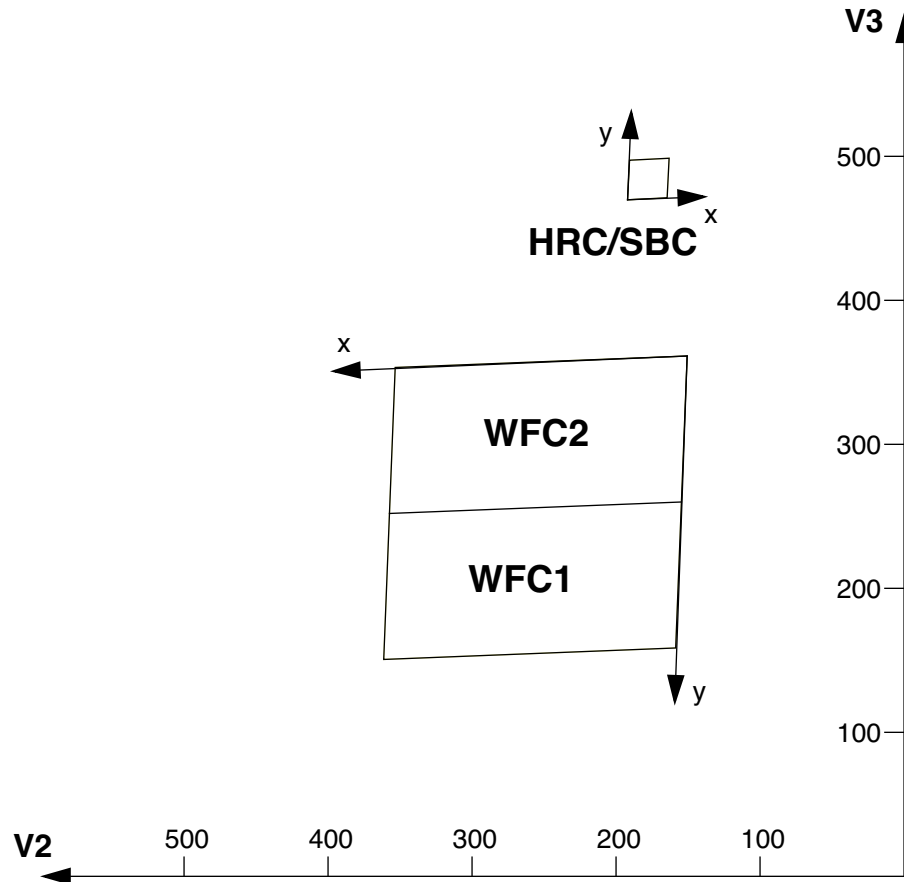
The orientations of the ACS detector edges are approximately in line with the V2 and V3 coordinate axes of the telescope. Consequently, the eigenaxes of the scale transformation are along the diagonals for WFC and the apertures and pixels appear non-rectangular in the sky projection. For the HRC and SBC the situation is even more irregular because the aperture diagonals do not lie along a radius of the HST field of view. Figure 10.127 shows the ACS apertures in the telescope's V2V3 reference frame. For a telescope roll angle of zero this would correspond to an on-sky view with the V3 axis aligned with North and the V2 with East.

If these were the only distortions they would not really present much difficulty. Their impact on photometry and mosaicing or dithering could be simply computed. A more problematic effect is the variation of scale across each detector. For the WFC this amounts to a change of 8% from corner to corner. For the HRC and SBC this variation is only about 1% as they cover much smaller fields of view. The area on the sky covered by a WFC pixel varies by about 20% from corner to corner, allowance for which must be made in photometry of extended objects. Dithering and mosaicing are complicated by the fact that an integral pixel shift near the center of the detector will translate into a non-integral displacement for pixels near the edges. Even this is not a fundamental difficulty, but will imply some computational complexity in registering images and will depend on an accurate measurement of distortions.

The results presented here are derived from on-sky measurements. For WFC and HRC multiple pointings of 47 Tucanae were taken through the F475W filter, resulting in several hundred star location measurements. These were analyzed to express the distortion as quartic polynomials. Additionally, an area of open cluster NGC 188, for which astrometric data are available, was used to establish the exact location and orientation of the aperture in telescope coordinates. At the same time, the scale factors were confirmed. For the SBC, the distortion measurement used the target NGC 6681 and filter F125LP. The alignment was established by observing this

same target with the HRC and SBC consecutively to establish the relative locations. The SBC position was thereby derived from the HRC position.

Figure 10.127: ACS Apertures



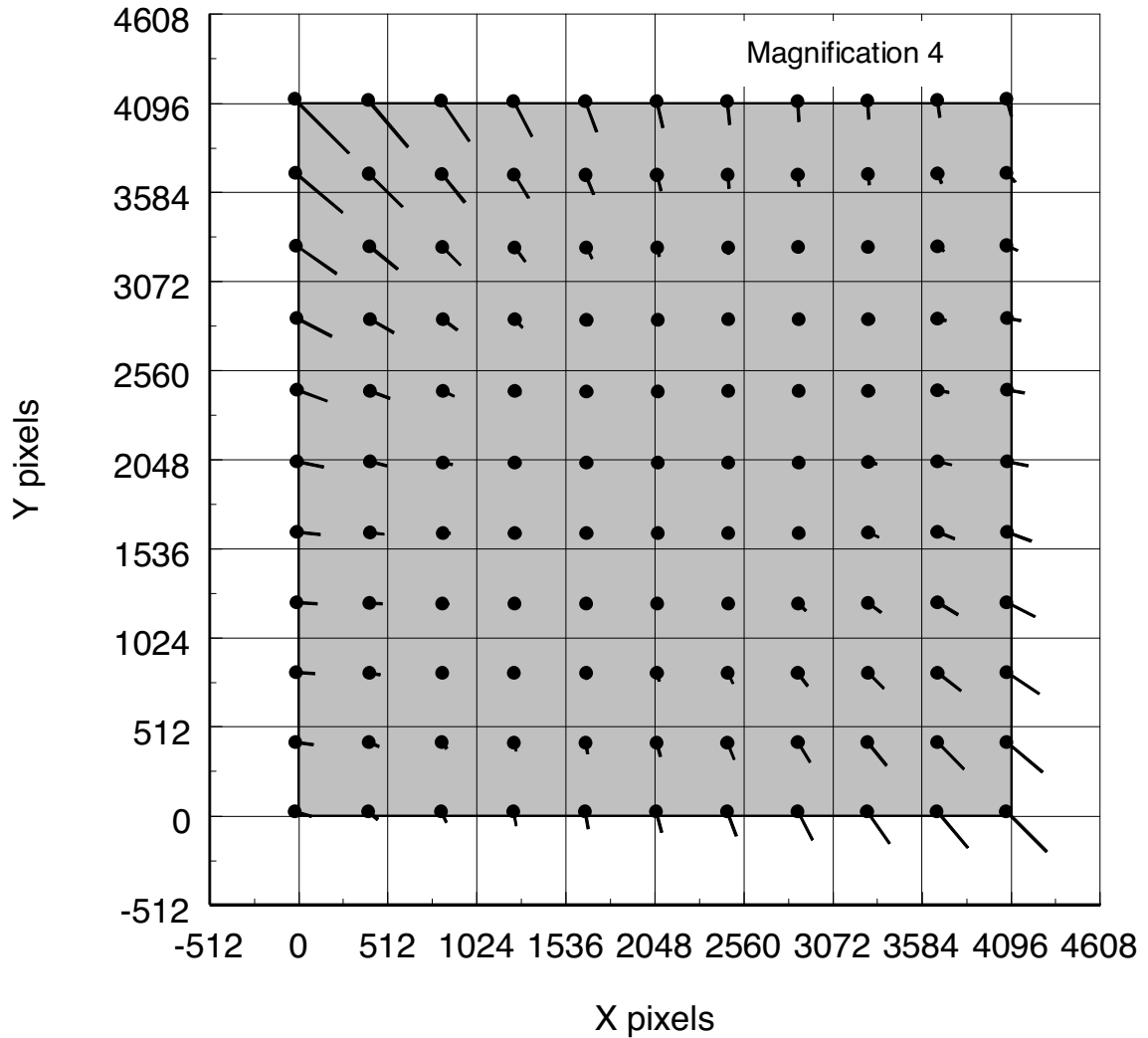
### 10.3.1 WFC

The rhombus shape of the WFC is evident in Figure 10.127. The angle between the x and y axes is about 85 degrees. The WFC1 distortion is illustrated in Figure 10.128, a vector displacement diagram which shows the contribution of the non-linear part of a quadratic fit to the data. The vectors represent the displacements and have been scaled up by a factor of 5 for display. The corner displacements are about 70 pixels. The principal effect is the diagonal variation of scale. A similar result holds for WFC2.

At the center of chip WFC1 the scale in the x direction is 0.0493 arcsec/pixel and 0.0486 in the y direction. For WFC2 these figures are 0.0498 and 0.0503. Between the corner of WFC nearest to the V1 axis and the diagonally opposite corner, the overall scale increases by 9%. WFC1

forms a slightly distorted rectangle 201 by 100 arcseconds in size while WFC2 is 203 by 103 arcseconds. There is a 2.5 arcsecond gap between the two chips.

Figure 10.128: WFC Distortion



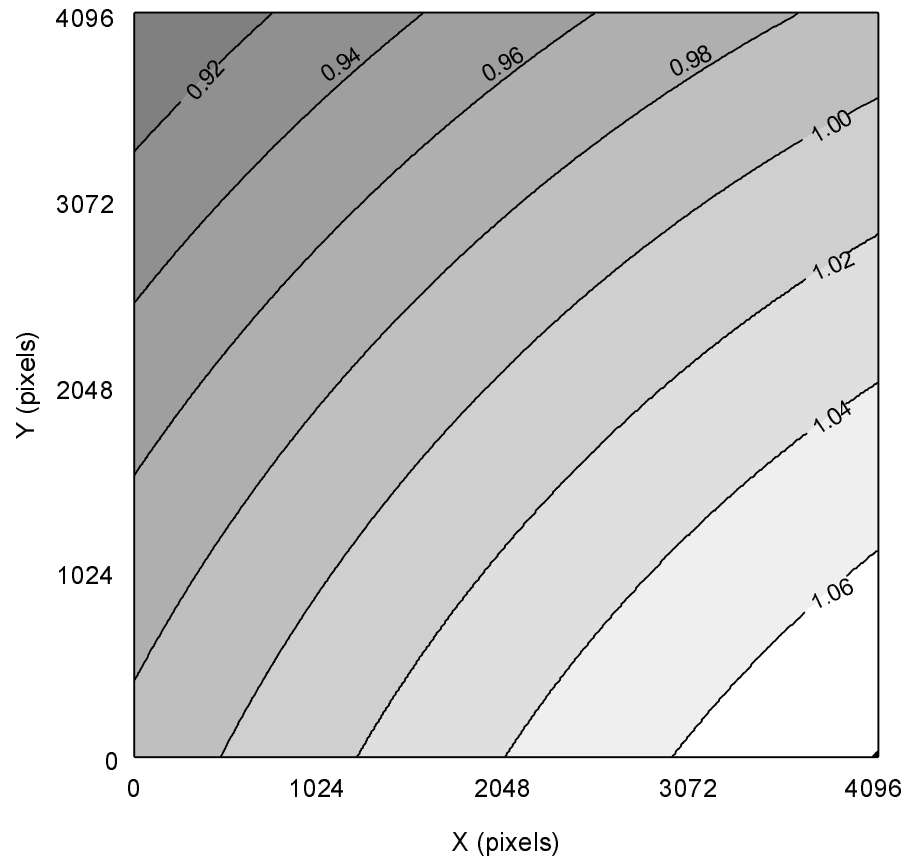
The resulting variation of the projected pixel area on the sky requires corrections to the photometry of point objects. A contour plot of relative pixel size across the WFC normalized to the central pixel, is shown in Figure 10.129. The range of area is from 0.90 to 1.07 times the central value.



### 10.3.2 HRC

The High Resolution Channel has its edges aligned approximately along the V2 and V3 axes. In this case, the center of the aperture lies on a line passing through the V2V3 origin and making an angle of 22 degrees with the V3 axis. The diagonal of the aperture does not correspond to a radius of the HST field of view. So the distortion has no particular symmetry with respect to the detector axes. Again, because the focal plane, and therefore the detector plane is 25 degrees away from the plane normal to the light path, the scales along the axes differ by 14%. However, since the HRC is less than 30 arcsec across, the scale variation is much less than for the WFC, being about 1%. At the center the x and y scales are 0.0284 and 0.0248 arcsec/pixel respectively. The average scales across the middle of the detector are 0.02842 and 0.02485 arcsec/pixel making the x and y widths 29.1 and 25.4 arcsec. The slightly non-square projected aperture shape is evident in Figure 10.127. The angle between the x and y axes on the sky is 84.2 degrees. A vector plot of the deviation from linearity is given in Figure 10.130 in which the deviations have been magnified by a factor of 10 for illustrative purposes. The largest deviation is 4.9 pixels in the top left corner and corresponds to about 0.1 arcsec. The variation of pixel size across the HRC to be used for photometric correction of point sources is shown in Figure 10.131. The maximum deviation from the central value is just over 2%.

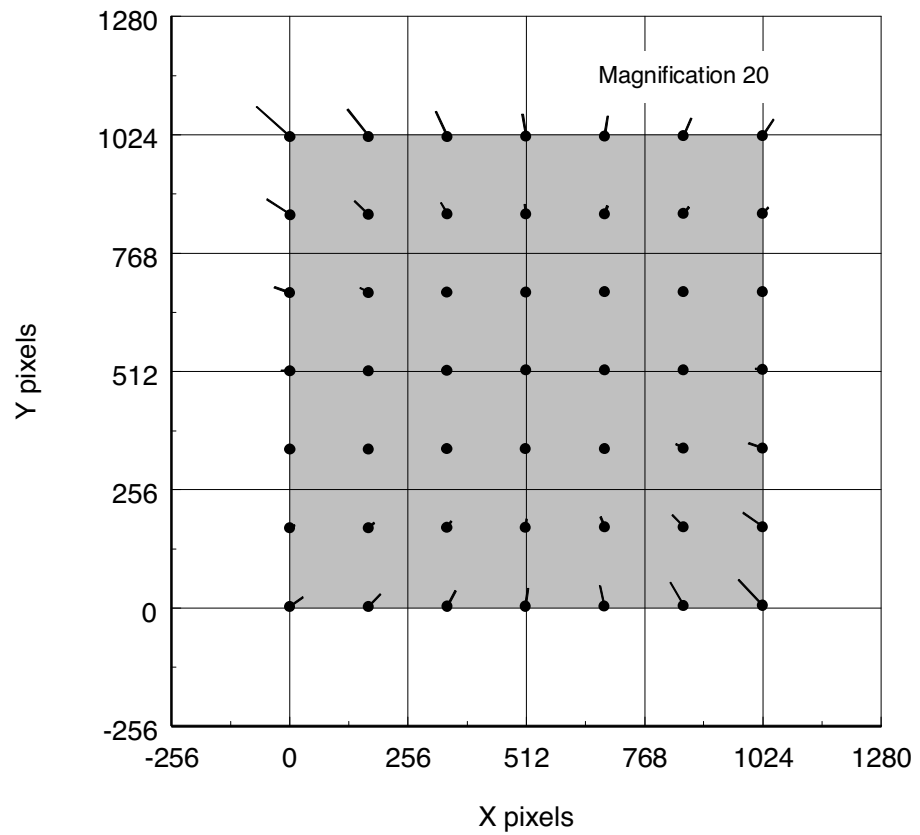
Figure 10.129: Variation of pixel size with position for the WFC  
 Variation of WFC effective pixel area



### 10.3.3 SBC

The Solar Blind Channel contains the MAMA detector. It is centered close to the HRC position in the V2V3 plane and has a slightly larger field of view, about 35 by 31 arcseconds. The scales and distortions have now been measured directly. The maximum distortion displacement is about 2 pixels or 0.06 arcseconds. The HRC and SBC both have much smaller areas than the WFC. In the x direction the scale is 0.0338 arcsec/pixel while in the y direction it is 0.0301. Like the HRC, the SBC exhibits a 13% difference between x and y scales with a variation across the aperture of a little over 2%.

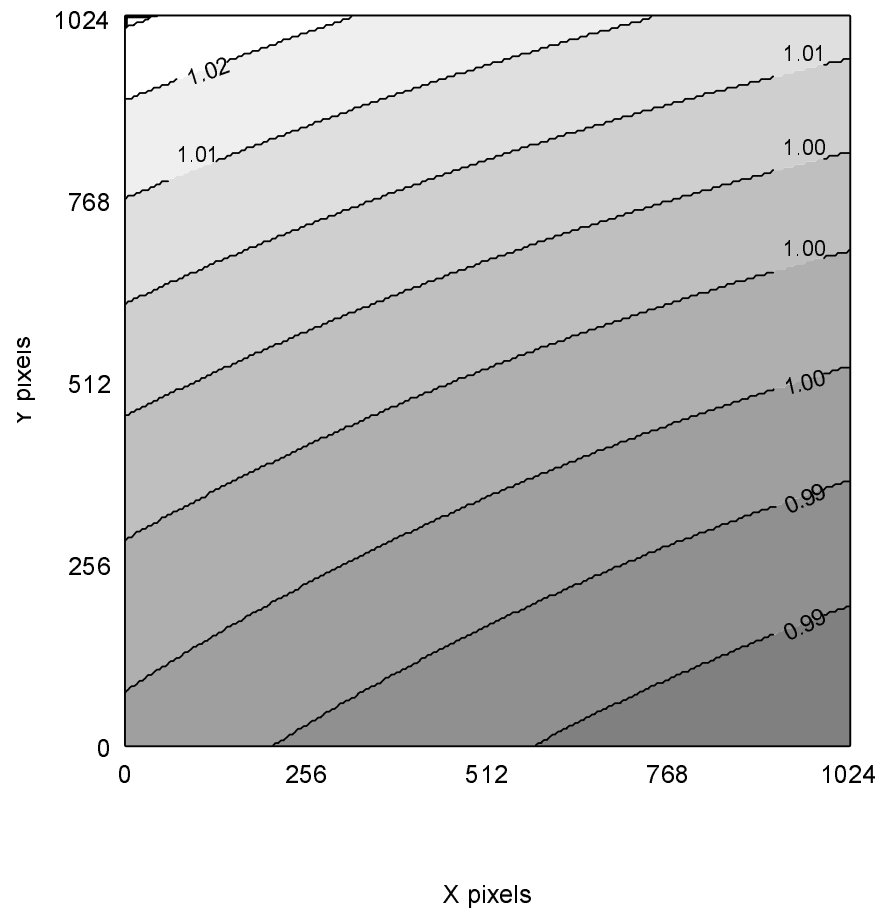
Figure 10.130: HRC Distortion



### 10.3.4 Summary

All values presented in this issue are based on in-flight measurements taken during SMOV. Formerly they were based on the Ball Aerospace optical simulator. The new values are quite close to the previously published numbers in that scale factors have changed by less than 1% and the aperture locations moved by only a few arcseconds.

Figure 10.131: Variation of HRC projected pixel area





PART IV:

# Calibration

---

The Chapters in this Part describe the calibration of ACS. They include an overview of the pipeline calibration process, expected accuracies for data taken in Cycle 12, and plans for calibrating and verifying the instrument's performance.



# Pipeline Calibration

In this chapter . . .

11.1 Overview and New Features / 243
11.2 ACS Pipeline / 248
11.3 ACS Data Products / 251

This Chapter describes the ACS pipeline's calibration software, CALACS. Developed at STScI, CALACS removes various instrumental signatures, combines CR-SPLIT or REPEAT OBS exposures and updates certain header keyword values when calibrating ACS data. This chapter is meant only as a high level overview. The "HST Data Handbook for ACS" version 1.0, January 2002, provides a more thorough discussion of data reduction and analysis issues for ACS.

---

## 11.1 Overview and New Features

### 11.1.1 On The Fly Reprocessing (OTFR)

All data taken by HST are run through STScI's calibration pipeline. This consists of two main software systems, the Operations Pipeline Unified System (OPUS) and the Data Archive and Distribution System (DADS). Raw spacecraft telemetry from Goddard Spaceflight Center (GSFC) is processed by the OPUS step named Generic Conversion into uncalibrated data. CALACS is then run by OPUS to process the uncalibrated data, using specific ACS reference images and tables from the Calibration Data Base System (CDBS), into calibrated data. DADS populates a database from

these data that is accessible to users via StarView. DADS then distributes any data requested for download to the user.

ACS will be the first instrument with the "On The Fly Reprocessing" (OTFR) system in place from the very start of its observing program. OTFR was developed with ACS in mind due to the large file size of the uncalibrated WFC (68.7MB) and calibrated WFC (168MB) images including the data quality array. Previously, the data from OPUS was archived and DADS would distribute that same version of data each time it was requested. Archiving ACS WFC images would have posed a significant storage problem for DADS. OTFR solves this problem by reprocessing the raw spacecraft telemetry files through OPUS "on the fly" for distribution each time any data is requested. Exceptions to this include observations expected to be heavily requested by the community for which the archive will maintain current calibrated versions for quicker access. ACS calibrated data is not required to be archived for later distribution. Only the much smaller raw telemetry files are archived, while the larger uncalibrated and calibrated data is deleted after distribution to the user.

The most current versions of the ACS reference files are used by CALACS each time OTFR is run. Since reference files such as CCD biases and darks are frequently updated, OTFR will use different reference files depending on the date of reprocessing. Previously, the archived data from DADS had to be re-calibrated by manually running the calibration software packages for each instrument with these updated reference files on the user's home workstation. OTFR replaces this step by automatically re-calibrating with the most appropriate, recent reference file data available. The user simply waits until the contemporaneous reference files are in place, and requests the data via StarView. Dark and bias reference files will be updated on an appropriate cadence of weeks to months respectively, while hot pixel lists will be updated daily. The uncalibrated and calibrated data's header keywords are updated with the filenames of the reference files used during that specific OTFR run. The PROCTIME keyword records the pipeline processing time in MJD.

OTFR also enables the user to avoid downloading outdated archived data due to the software changes made for bug fixes, improved algorithms, new capabilities or header keyword changes. Once a code change is made, OTFR will reprocess and distribute the corrected data using the latest software versions available.

Currently OTFR can only distribute all files associated with an ACS observation, including raw and calibrated. Future versions will enable users to select certain parts of the dataset, for example only the fully calibrated image.

Future versions of OTFR could also enable users to set certain calibration parameters for a particular OTFR run. Until then OTFR will process with default values.

The option of re-calibrating aside from OTFR still exists of course.



### *When is OTFR not appropriate?*

- Running CALACS with personal versions of reference files
- Running CALACS with non-default calibration switch values

OTFR will always use the most appropriate ACS calibration reference files by default. In order to use non-default calibration reference files, manual re-calibration is required. The calibration reference file keywords in the uncalibrated data will need to be updated manually with the non-default filenames before running CALACS.

Selection criteria in table 11.1 are used in order to set the values for the calibration switch header keywords in uncalibrated ACS data. In order to use non-default calibration switch values, manual re-calibration is required. The calibration switches in the uncalibrated data will need to be updated manually with the non-default values before running CALACS manually.

Table 11.1: Calibration Switch Selection Criteria

Switch	Description	Criteria
DQICORR	Data Quality Array Initialization	DEFAULT = "PERFORM" If OBSMODE = ACQ then "OMIT"
ATODCORR	Analog to Digital Conversion	DEFAULT = "OMIT"
BLEVCORR	Overscan Region Subtraction	DEFAULT = "PERFORM"
BIASCORR	Bias Subtraction	DEFAULT = "PERFORM"
FLSHCORR	Post Flash Subtraction	DEFAULT = "OMIT"
CRCORR	Cosmic Ray Rejection	If CRSPLIT $\geq$ 2 then "PERFORM" If CRSPLIT < 2 then "OMIT"
DARKCORR	Dark Subtraction	DEFAULT = "PERFORM"
FLATCORR	Flat Field Division	DEFAULT = "PERFORM" If FILTER = G800L then "OMIT"
SHADCORR	Shutter Shading Correction	DEFAULT = "OMIT"
PHOTCORR	Photometric Processing	DEFAULT = "PERFORM"
RPTCORR	Repeat Processing	DEFAULT = "OMIT" If NRPTEXP > 1 then "PERFORM"
EXPSCORR	Full calibration of individual exposures in an association	DEFAULT = "OMIT"
DRIZCORR	Dither processing and distortion correction	DEFAULT = "PERFORM"
GLINCORR	Global Non-Linearity Correction	SBC DEFAULT = "PERFORM"
LFLGCORR	Local and Global Non-Linearity Flagging in DQ Array	SBC DEFAULT = "PERFORM"

The goal of the ACS pipeline is to provide data calibrated to a level suitable for initial evaluation and analysis for all users. Further, observers frequently require a detailed understanding of the calibrations applied to their data and the ability to repeat, often with improved calibration products, the calibration process at their home institution. Therefore, the CALACS and PyDrizzle packages used in this pipeline can also be used to calibrate ACS data off-line and are available within the STSDAS system. In addition, the calibration reference files (e.g. flat fields) are available from the HST Archive via the Archive WWW pages. The most recent version of STSDAS, with CALACS and PyDrizzle can be downloaded from <http://stsdas.stsci.edu/>

### 11.1.2 Post Flash Calibration

CALACS has a post flash calibration step added to its ACSCCD task. Intended to mitigate the reduction of CTE in the later years of the ACS observing program, the proposer can request a post flash via use of the restricted optional parameter FLASHCUR. The ACS post flash operation exposes the WFC or HRC detector to several seconds of illumination from internal LEDs at the end of the normal exposure.

The CALACS calibration switch POSTFLSH controls the function ‘doFlash’ which subtracts a Post Flash reference file, specified by the FLSHFILE header keyword, from the science image. The reference file will have been selected to match the LED level used for the exposure. The status of the Post-Flash exposure will also be verified by checking the keyword FLASHSTA. If there are any problems noted, a comment will be added to the history comments section of the SCI extension header. This reference file will then be read in and scaled it by the duration of the Post-Flash exposure given by the FLASHDUR keyword. After the subtraction has been completed, the mean value of the scaled Post Flash image will be computed, and it will be written to the output SCI extension header as the keyword MEANFLSH.

Figures 11.1 and 11.2 below have been updated to include this new Post Flash calibration step.

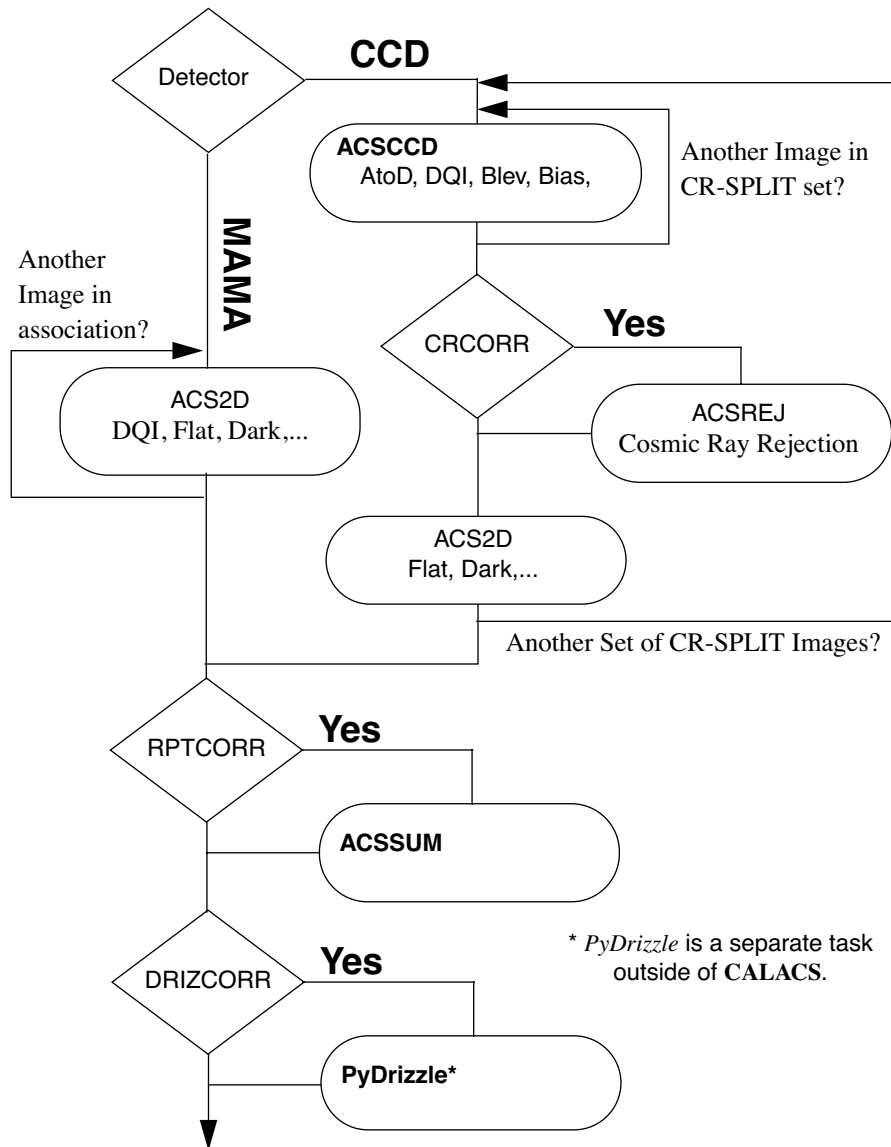
### 11.1.3 Distortion Correction and Dither Combining

All ACS data will automatically be corrected for distortion during standard pipeline processing using a task called PyDrizzle. This task relies on the IDCTAB reference file for the description of the distortion model. It also understands the ACS association tables to allow the pipeline, for the first time ever, to combine dithered observations. Only observation sets which use the dither patterns provided in the proposal instructions will be automatically associated for combining in the pipeline. Programs which

rely on explicit POS TARG commands will NOT be associated in the pipeline, resulting in separately calibrated images for each position. PyDrizzle, though, automatically produces images which are both astrometrically and photometrically accurate regardless of whether they were taken as a single exposure or a set of dithered exposures. The DRIZCORR keyword, by default, will be set to turn on this processing for all ACS observations.

For ACS WFC observations, both WFC chips will be combined into a single field-of-view in the output by PyDrizzle. All ACS distortion-corrected, possibly dither-combined, images will have a single SCI extension, a weight (WHT) extension, and a context (CTX) extension, replacing the standard SCI, ERR and DQ arrays in the CALACS calibrated products. Processing comments are recorded in the trailer file for the DRZ image, including which version of drizzle was used, what parameters were used, and which images were combined (if dithered). The same default parameters, however, are used for all observations in the pipeline. These parameters were chosen to avoid introducing any scale changes, shifts or rotations relative to the original pointing, aside from those corrections incorporated in the distortion model itself. The size of a single, distortion-corrected image can be found in Table 11.3. These products will be properly corrected for distortion, however for dithered observations, the combination may not be ideal and subsequent reprocessing with PyDrizzle offline may be required to obtain the desired scientific value. PyDrizzle can be obtained as part of the most recent release of STSDAS, and also requires the new PyRAF environment to run. Both of these packages can be obtained from the STSDAS WWW pages.

Figure 11.1: Flow Diagram for ACS data shown with CALACS task names.



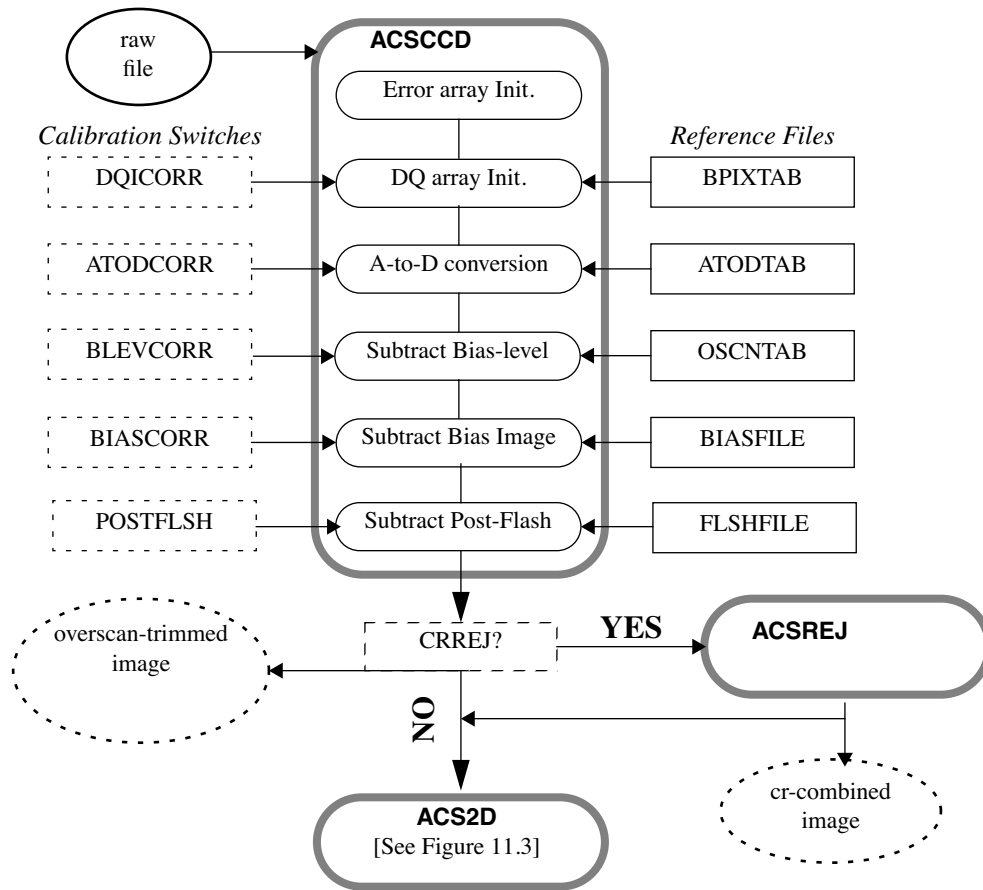
## 11.2 ACS Pipeline

The CALACS package itself consists of 4 calibration tasks which can all be run separately on individual exposures. Since ACS can also produce associated data, such as **CR-SPLIT** or **REPEATOBS** exposures, the task **CALACS** can be used to process these associated exposures, or even individual exposures, automatically by calling the 4 individual tasks in the package as needed. These tasks apply the basic calibrations necessary for ACS data. The flow of data through the ACS pipeline, and what decisions are made while working with associated data, can be seen in Figure 11.1.

Overall, the following calibration steps are performed in order for ACS data:

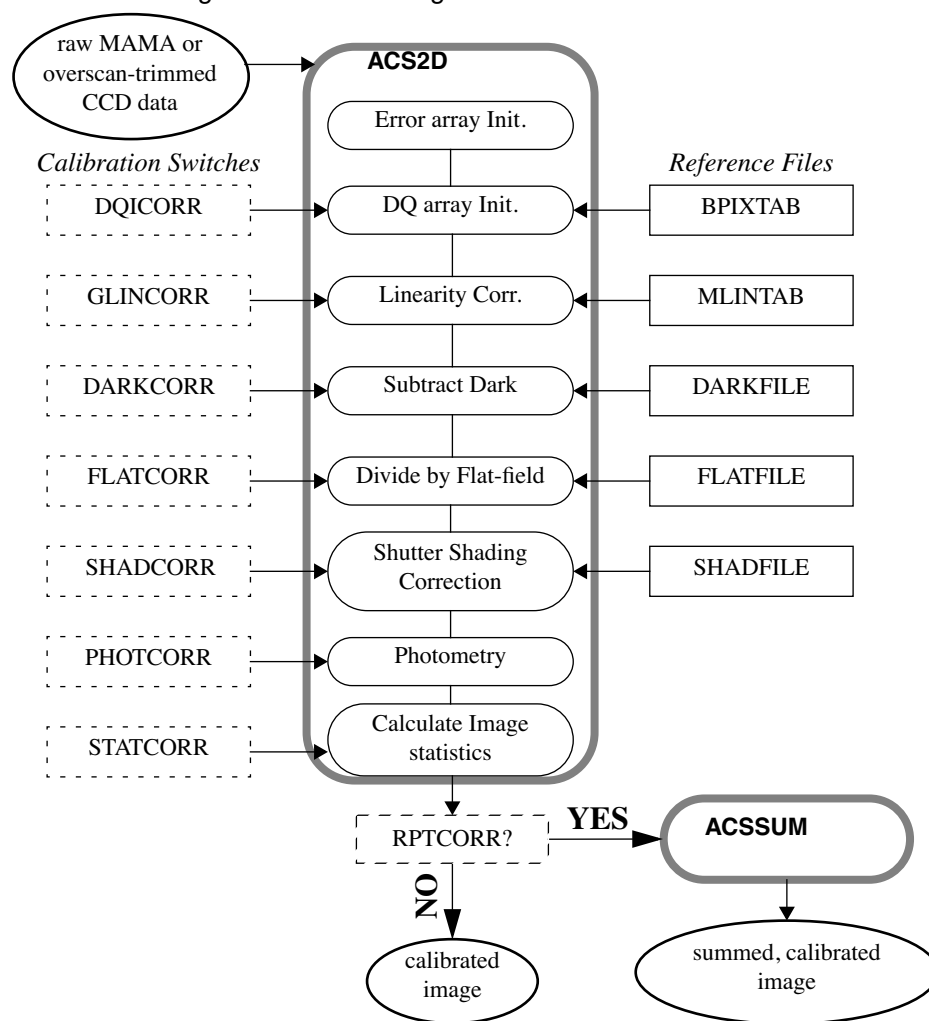
1. Calculate a noise model for each pixel and record in error array
2. Flag known bad pixels and saturated pixels in the data quality array
3. Correct for A-to-D conversion errors, if necessary (CCD data only)
4. Subtract bias-level determined from overscan regions (CCD data only)
5. Subtract bias image (CCD data only)
6. Subtract post flash image (CCD data only)
7. Perform cosmic-ray rejection and combining of CR-SPLIT data (CCD data only)
8. Perform global linearity corrections (MAMA data only)
9. Scale and subtract dark image and calculate mean dark value
10. Perform flat-fielding
11. Perform Shutter-shading correction (if not done in cosmic-ray rejection)
12. Calculate values for photometry keywords
13. Calculate image statistics

Figure 11.2: Flow diagram for CCD data in CALACS



From Figure 11.1, it can also be seen that the calibration tasks have been split to handle CCD-specific calibrations separate from those steps which can be applied to any ACS data. The MAMA data obtained from the SBC does not have the overscan regions found in CCD data, and therefore those steps pertaining to the use of the overscan regions were split into a separate task. The initial processing performed on CCD data alone is shown in Figure 11.2, with the result being processed like the rest of the ACS data through the processing steps shown in Figure 11.3.

Figure 11.3: Flow diagram for MAMA and CCD data in CALACS.

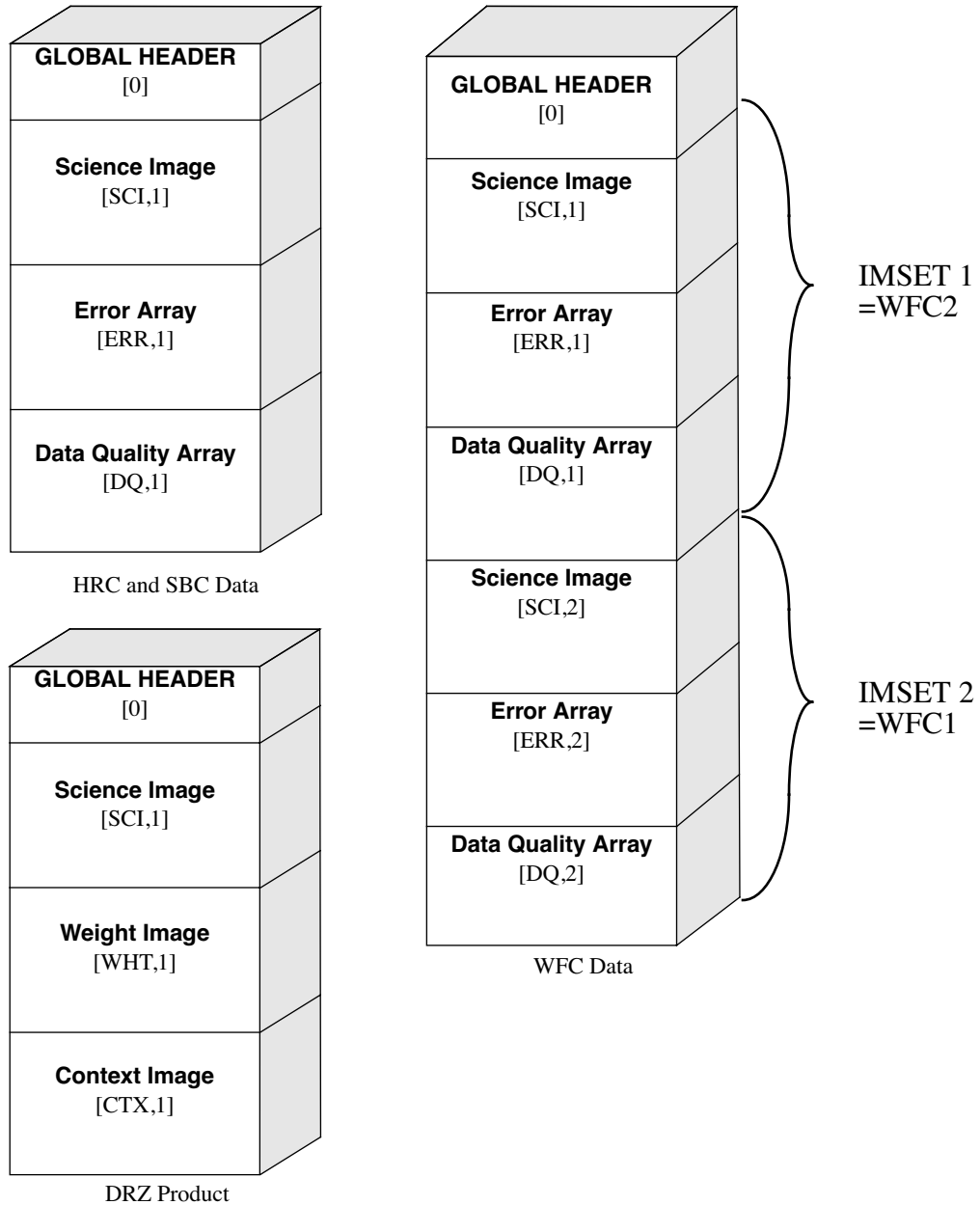


## 11.3 ACS Data Products

The inputs for pipeline processing are:

- raw exposure - FITS formatted, integer data
- association table (only for associated data)
- trailer file from Generic Conversion (optional for reprocessing)

Figure 11.4: Data format for ACS Modes



Processing single exposures will result in the creation of a single fully calibrated ACS exposure stored in the FITS format shown in Figure 11.4. The current baseline version of CALACS will also recognize and correctly process **CR-SPLIT** or **REPEAT-OBS** exposures by interpreting the association table and determining which exposures should be combined during calibration. Processing an association usually results in a single calibrated product created from combining the individual exposures in the association.



The only exception for the current baseline version of the pipeline would be for dithered observations. Since combining dithered observations is not performed by CALACS has not been included in the pipeline yet, processing the association table for these observations would result in a single calibrated exposure for EACH position in the dither pattern, not just one single product. The separate products for each dither position then would be combined in the pipeline by PyDrizzle to produce a single, distortion corrected, combined product. More details on this can be found in Chapter 4 of the "HST Data Handbook for ACS".

### 11.3.1 Storage Requirements for ACS Data

The large size of ACS WFC exposures presents another unique problem for observers using ACS, especially when dealing with data that requires associations. Raw ACS exposures which serve as input to the pipeline have the sizes given in Table 11.2.

Table 11.2: Size of raw ACS data for each detector.

Detector	Size of FITS file ( $S_{\text{raw}}$ )	X Pixels	Y pixels/array
WFC (2 Chips)	68.7 MB	4144	2068
HRC (1 Chip)	4.4 MB	1062	1044
SBC (1 detector)	4.2MB	1024	1024

The total size of the WFC image includes both the SCI arrays, while the HRC and SBC detectors only have one chip/array. The file sizes given in Table 11.2 presume that both the SCI array and DQ array are populated with short integer values, but that the ERR array is NULL with all pixels having a value of zero. During processing, the SCI arrays get converted to floating point data from the input integer data. The ERR array also gets populated with floating point values. As a result, the final size of the calibrated images are much larger and they will become even larger once the distortion corrections is applied, as given in Table 11.3.

Table 11.3: Final sizes of calibrated ACS exposures for each detector.

Detector	Size of FITS file ( $S_{\text{final}}$ )	X Pixels	Y pixels/array	Size of DRZ file ( $S_{\text{DRZ}}$ ) <sup>1</sup>
WFC (2 Chips)	168 MB	4096	2048	215MB
HRC (1 Chip)	10.5 MB	1024	1024	16MB
SBC (1 detector)	10.5 MB	1024	1024	16MB

1. This size assumes no dither offset or scale change.

While the size of the final calibrated HRC or SBC exposures are comparable to those of STIS or WFPC2, the ACS WFC exposures are over 16 times as large. In addition, the following equation should be used to estimate the minimum amount of free storage that should be available during processing of associated ACS data:

$$D_{min} = (1 + n) \cdot S_{final} + n \cdot S_{raw} + (2.1 + p^2) \cdot S_{DRZ}$$

where:

- $D_{min}$  is the minimum free disk space required for processing,
- $S_{final}$  is the size of the calibrated exposure (from Table 11.3),
- $S_{raw}$  is the size of the raw exposure (from Table 11.2), and
- $n$  is the number of exposures in each CR-SPLIT set or REPEATOBS set.
- $S_{DRZ}$  is the size of the distortion corrected, dither combined (if needed) exposure (from Table 11.3).
- $p$  is the percentage shift (in pixels) across all dither positions.

### Size of Reference Files for Re-Processing

Another additional concern when processing ACS observations would be the amount of storage taken for reference files. For ACS WFC observations, a complete set of reference files could exceed 520MB by themselves! HRC and SBC reference files, in comparison, only require about 45MB of disk space.

## 11.3.2 Speed of Pipeline Processing

Some observers will eventually want to re-calibrate their ACS data locally. This will require the following to be available on the observers system:

- CALACS pipeline software within STSDAS
- PyDrizzle software within STSDAS (also requires PyRAF)
- the latest reference files obtained from the STScI WWW pages
- the uncalibrated exposures (\*\_raw.fits) from OTFR via StarView
- any association table for the observation

Starview is available for users to download from:

*<http://starview.stsci.edu/html/>*

In addition to information on how to install and use Starview, the pages also include instructions on how to become a registered archive user.

ACS ISR 99-03 "CALACS Operation and Implementation" (Hack) is available on the ACS web site and should be consulted before manually re-processing ACS data.

Re-processing ACS HRC or SBC data will not put a serious burden on most computing systems since the data sizes are relatively small, both for the science data and the reference files. Processing ACS WFC observations, on the other hand, severely tests most computing platforms available. Great care has been taken to minimize the memory requirements of the pipeline software to accommodate most computing configurations. Even so, CALACS requires up to 130MB memory to process WFC data. Unfortunately, this places an extra burden on the I/O capabilities of the computer, since the reference files are all applied one line at a time to the ACS data with each WFC reference image being 170MB in size.

Benchmarks of pipeline processing of ACS WFC datasets are given in Table 11.4. The tests were run with all the ACS data, relevant reference data and executables on a hard disk local to the CPU, and no other processes were active during the test. The CPU usage given in Table 11.4 reports the amount of time the CPU was active, reflecting the amount of time spent waiting for disk I/O. From this table, it becomes obvious that a great deal of thought must go into the computing platform used for processing these very large datasets, and that suitable computing resources should be secured by ACS observers for processing ACS data. This same reasoning can be extended to running analysis tools on ACS data as well, again requiring not only fast computers with reasonable amounts of memory, but also fast I/O, in order to efficiently analyze ACS data.

Table 11.4: Timing Tests of CALACS without running PyDrizzle

Dataset	Run-time	CPU Usage
<b>Ultra-10: 300Mhz CPU, 256Mb memory, Ultra-SCSI HD</b>		
WFC Assoc. CR-SPLIT=2	12m 54s	71%
Single WFC	4m 34s	79%
Single HRC	0m 19s	67%
HRC Assoc. CR-SPLIT=2	0m 42s	90%
<b>Sparc-4: 110Mhz CPU, 96Mb memory, SCSI-2 HD</b>		
WFC Assoc. CR-SPLIT=2	1h 26m 40s	34%
Single WFC	35m 16s	37%
Single HRC	0m 50s	84%
HRC Assoc. CR-SPLIT=2	3m 33s	69%



# Calibration Accuracies

In this chapter . . .

12.1 Summary of Accuracies / 257
----------------------------------

In this Chapter we describe the accuracies that can be expected from ACS observations.

---

## 12.1 Summary of Accuracies

In these Tables we list the accuracy that we expect to achieve from the planned calibration program. These estimates reflect the current understanding on the instrument and may need to be updated once on orbit data have been thoroughly analyzed. Updates will be available on the ACS web pages (under “Calibration”). Although data will be analyzed according to our list of calibration priorities all calibration data are immediately public and accessible through the HST archive so that users in need of extremely accurate or urgent results will be able to carry out their own calibration.

Users should realize that some of these numbers represent only a guess based on our experience with WFPC2 and STIS. As our understanding of the instrument capabilities and limitations grows, so will the reliability of these accuracy estimates. The values quoted here remain at pre-launch values; inflight data suggests these values are reasonable.

The extensiveness of our calibrations will also depend, in part, on the science programs selected by the proposers and the TAC. Clearly, we will spend little or no time calibrating filters or capabilities that are not requested by observers. We have selected a subset of the filters as those that we expect to receive heavy use, which we designate as supported

filters. The accuracy numbers quoted here for photometric measurements are for supported filters only. The supported filters are WFC/F435W, WFC/F555W, WFC/F606W, WFC/F625W, WFC/F775W, WFC/F814W, WFC/F850LP, HRC/F330W, HRC/F435W, HRC/F555W, HRC/F606W, HRC/F625W, HRC/F775W, HRC/F814W and HRC/F850LP.

The accuracies tabulated are assuming that the Poisson noise in the data is negligible. Clearly, low-S/N data will have accuracies dominated by this unavoidable noise source.

Table 12.1: WFC Accuracies

Attribute	Accuracy	Limiting factor
Relative Astrometry within a chip	0.25 pixel	Calibration & stability of geometric distortion
Relative astrometry between chips	0.5 pixel	Stability
Absolute astrometry	1"	Guide Star, Catalog uncertainties
Absolute Photometry	3%	Absolute Calibration, standards
Relative Photometry within an image	1%	Flat-field characterization or characterization of geometric distortion.
Repeated photometry of same star	0.3%	Stability of Flatfield
Transformation to Standard Magnitude Systems	0.02mag SDSS 0.025mag WFPC2 0.03mag BVRI	DQE curve determination
Polarimetry	2% $3\sigma$	
Wavelength Calibration	20Å grism	Accuracy of dispersion solution
Grism Spectrophotometry	10%	

Table 12.2: HRC Accuracies

Attribute	Accuracy	Limiting factor
Relative Astrometry within the field	0.1 pixel	Calibration & stability of geometric distortion
Absolute astrometry	1"	Guide Star, Catalog uncertainties
Absolute Photometry	2%	Absolute Calibration, standards
Relative Photometry within an image	1%	Flat-field characterization or characterization of geometric distortion.
Repeated photometry of same star	0.3%	Stability of Flatfield
Transformation to Standard Magnitude Systems	0.02mag SDSS 0.025mag WFPC2 0.03mag BVRI	DQE curve determination
Polarimetry	2% $3\sigma$	
Wavelength Calibration	20Å grism	Accuracy of dispersion solution
Grism Spectrophotometry	10%	

Table 12.3: SBC Accuracies

Attribute	Accuracy	Limiting factor
Relative Astrometry within the field	0.25 pixel	Calibration & stability of geometric distortion
Absolute astrometry	1"	Guide Star, Catalog uncertainties
Absolute Photometry	5%	Absolute Calibration, standards
Relative Photometry within an image	1%	Flat-field characterization or characterization of geometric distortion.
Repeated photometry of same star	1%	Stability of Flatfield
Wavelength Calibration	1 pixel prisms	Accuracy of dispersion solution
Prism Spectrophotometry	20%	





# Calibration Plans

## In this chapter . . .

13.1 Ground Testing and Calibration / 262
13.2 SMOV Testing and Calibration / 262
13.3 Cycle 11 Calibration / 264
13.4 Cycle 12 Calibration / 266

In this Chapter we describe the current status of ACS calibrations as well as solid plans for the first year of operations and tentative plans for the Cycle 12 period of primary interest in this Handbook. At the time this is being written SMOV observations are (just) complete, and while analyses are well underway, closure is not available from even this less than fully comprehensive characterization of the instrument. However, the broad outline of instrument capability and expectations for calibrations has been established with in-flight data, with excellent outcomes in most regards. The calibration program supporting the first year of science observations has been developed and is only just starting to return data. For further information please access the STScI web page for ACS, and/or consult the Helpdesk for staff input to specific questions.

---

## 13.1 Ground Testing and Calibration

Ground calibration and testing was a prime responsibility of the ACS Investigation Definition Team (Principal Investigator Holland Ford, JHU) and was carried out at Ball Aerospace in Colorado. Thermal vacuum (and supplemental dry-nitrogen environment) testing in which orbital conditions were simulated was conducted pre-launch at Goddard Space Flight Center. Filter transmission curves, and detector quantum efficiency curves, were derived at GSFC and JHU. These tests characterized the basic properties of the optics, the detectors, and the mechanisms. During ground calibration the highest priority was given to those measurements essential to establish that instrument design specs were being met, and to those measurements that could not be obtained on-orbit. Most of the non-unique ground test data are being superseded by on-orbit measurements as analyses of these become available.

---

## 13.2 SMOV Testing and Calibration

The primary goal of the SMOV3B is a timely commissioning of the HST observatory for normal science operations. For ACS this has included basic testing of the instrument functionality as well as testing/setting of the focus (internal and external), measuring the sensitivity in all filters, establishing the geometric distortion and plate scale, quantifying the point spread function for each camera, and adjusting flat fields to properly capture low-frequency variations for which ground calibrations are always difficult. Data from SMOV proposals are non proprietary and fully accessible through the HST archive. We list below the program IDs and proposal titles. Details of the Phase II programs may be found via: <http://presto.stsci.edu/public/propinfo.html>. Some programs are of very limited technical interest (e.g. Science data buffer check), while others (e.g. WFC flat field stability) collected large amounts of data in standard filters on objects of potential archival science interest.

Table 13.1: ACS SMOV Proposals

Proposal ID	Titles
8947	CCD Daily Monitoring
8948	CCD CTE Test
8992	ACS ERO Program
9002	ACS Dump Test & Verification of Memory Loads
9003	ACS Science Data Buffer Check
9004	ACS Calibration Lamp Checkout Contingency
9005	CCD Functional
9006	CCD Temperature Set Point Determination
9008	ACS MAMA Initial Turnon & Anomalous Recovery Procedure
9009	ACS MAMA Fold Analysis
9010	SMOV Contamination Plan
9011	ACS to FGS Fine Alignment
9012	HRC Coronagraphic Acquisition
9013	ACS Coarse Corrector Alignment
9014	ACS Fine Corrector Alignment
9015	ACS Image Quality Verification
9016	HRC Coronagraph Repeatability
9017	ACS Image Stability Verification
9018	WFC Flat Field Stability
9019	HRC Flat Field Stability
9020	Preliminary ACS Sensitivity
9022	SBC Dark Current Measurement
9023	ACS SBC Image Quality Verification
9024	SBC Flat Field uniformity
9025	Scattered Light in Coronagraphic Obs
9026	ACS Ramp Filter Test
9027	ACS SBC Geometric Distortion Calibration
9028	CCD Geometric Distortion
9029	ACS Grism/Prism Performance Check
9031	ACS CCD hot pixel annealing
9032	ACS CCD Flash calibration
9574	Focus Monitor

## 13.3 Cycle 11 Calibration

The SMOV calibration and testing period extended for roughly two months taking routine monitoring of ACS performance through April 2002. With the nominal start of Cycle 11 at July 1, 2002 and with a desire not to define the final calibration program for Cycle 11 until some flight experience from SMOV could be obtained, a decision was made to break the Cycle 11 calibration into two parts: (1) an interim program continuing routine monitoring (darks, biases) and extending characterization in areas not well covered by SMOV, and (2) the standard full program expected to start in July 2002 and run for one year. Tables 13.2 and 13.3 will list program IDs and titles for the interim and standard Cycle 11 calibrations respectively.

### 13.3.1 Calibration Priorities

As for any instrument the ACS calibration plan represents a compromise between the desire to calibrate the instrument as well as possible and the availability of finite resources both in terms of primary HST orbits and in terms of human resources at STScI. The list of priorities that guided the Cycle 11 calibration planning is:

1. *Monitor the Health and Safety of the Instrument.* This includes obtaining all data necessary to verify that the instrument is performing as planned and to insure a useful lifetime as extended as possible.
1. *Update and Maintain Pipeline Reference Files.* Dark, biases, flat fields and sensitivities used in the pipeline calibration need to be accurate and current. Information on newly released reference files is announced via the Space Telescope Analysis Newsletter and posted on the STScI WWW pages. The updated list of recommended reference files to be used with each data set is available through the HST Archive, and will be automatically applied when calibrated data are requested from the Archive.
2. *Characterization of Optical Performance.* The point spread function and its variation across the field of view needs to be carefully determined as a function of wavelength.
3. *Characterization of detectors.* This includes charge transfer effects, long wavelength fringing.

Table 13.2: Cycle 11 ACS Interim Calibrations

Proposal ID	Proposal Title
9558	CCD Monitor
9559	Focus Monitor
9560	CCD Linearity Check
9561	Internal CTE Monitor
9562	Internal Flat Field Stability
9563	Photometric Stability
9564	UV Earth Flats
9565	Contamination Monitor
9566	CCD Hot Pixel Annealing
9567	SBC Dark Current
9568	Grism/Prism Calibration

Table 13.3: Cycle 11 ACS Standard Calibrations

Proposal ID	Proposal Title
9647	CCD Daily Monitor Part I
9648	External CTE Monitor
9649	ACS internal CTE monitor
9650	CCD Hot Pixel Annealing
9651	ACS CCD Flash Calibration
9652	SBC Dark Current
9653	ACS MAMA Initial Turn-on and Anomalous Recovery Procedure
9654	ACS photometric Stability
9655	ACS Post-SMOV UV Contamination Monitor
9656	Stability of the ACS CCD: geometry, flat fielding, photometry
9657	ACS Internal Flat Field Stability
9658	UV Earth Flats
9659	Gain Dependence of Biases
9660	Earth Bright Limb Calibration
9661	ACS Polarization Calibration
9662	HRC+WFC Shutter Stability Test
9663	Focus Monitoring

Proposal ID	Proposal Title
9664	SDSS Primary Standards
9665	Extreme Red Stars
9666	Photometric Transformations
9667	ACS PSF Characterization
9668	ACS Coronagraph Wavelength Dependence
9669	ACS Coronagraph stability and vignetting
9670	UV and Narrow Band Filter Red Leak Check
9671	ACS Ramp Filter Check
9672	Grism/Prism Calibration
9673	CCD Daily Monitor (9674 & 9675 continue this)

The Cycle 11 calibration program is intended to most effectively balance the needs of the community for obtaining excellent science results from the instrument with the limited resources available (e.g., a nominal limit of 10% time available for calibration). Common uses of the instrument will be fully calibrated.

## 13.4 Cycle 12 Calibration

The Cycle 12 calibration program will be developed in detail during the spring of 2003 at which time: (1) Instrument performance will have been tracked for one year on-orbit. (2) The results of SMOV and many of the Cycle 11 calibration programs will be fully known with documented results. (3) Feedback will be available from the community on the effectiveness of ACS calibrations to date. (4) The approved Cycle 12 science program and implied instrument use will be known.

The goal of the Cycle 12 calibration program will again be to optimally support science results from the community while balancing the program with available resources (HST orbits and staff analysis time). Routine calibrations such as darks will be carried forward at the proper cadence. Resources will also be allocated to further characterization of capabilities and calibration of science observations as required in response to evolution of either performance or needs reflected in the science program as a whole.

In special circumstances proposers may wish to request additional orbits for the purpose of calibration. These can be proposed in two ways and should be for calibrations that are not likely to be in the core calibration programs. An example of a non-core calibration would be one that needs to

reach precision levels well in excess of those outlined in Tables Table 12.1, Table 12.2 or Table 12.3.

At the time of writing this Handbook the entries in the Cycle 12 performance tables have been left at the pre-launch values. Early results from SMOV and Cycle 11 calibrations suggest that these were reasonable goals, but changes of detail may be expected as more calibration results are obtained.

The first type of special calibration would simply request additional orbits within a GO program for the purpose of calibrating the science data to be obtained (see section 4.3 of the CP). In this case the extra calibration would only need to be justified on the basis of the expected science return of the GO's program.

The second type of special calibration would be performed as a general service to the community via Calibration Proposals (section 3.6 of CP). In this case the calibration observations should again be outside the core responsibilities of the ACS group to perform, and furthermore should be directed at supporting general enhancement of ACS capabilities with the expectation of separately negotiated deliverables if time is granted.

Proposers interested in obtaining either type of special calibration should consult with Instrument Scientists from the ACS Group via questions to the Help Desk at least 14 days before the proposal deadline in order to ascertain if the proposed calibrations would be done at STScI in the default program.

Observations obtained for calibration programs will generally be flagged as non-proprietary.





# Glossary

The following terms and acronyms are used in this Handbook.

**A-D:** Analog to digital

**ABMAG:**  $-2.5 \log (F_{\nu}) - 48.60$  where  $F_{\nu}$  is the flux from the source in  $\text{erg cm}^{-2} \text{sec}^{-1} \text{hz}^{-1}$

**$AB_{\nu}$ :** Correction to ABMAG to account for the fact that the source spectrum is not constant in  $F_{\nu}$

**ABC:** Aberrated Beam Coronagraph

**ACS:** Advanced Camera for Surveys

**BOP:** *Bright-Object Protection*

**calacs:** *ACS calibration pipeline software*

**CCD:** Charge Coupled Device. Solid-state, light detecting device

**CDBS:** Calibration Data Base System for maintaining reference files and tables used to calibrate HST observational datasets.

**CP:** Call for Proposals

**CR:** Cosmic ray

**CR-SPLIT:** *Division of a CCD exposure into shorter exposures to be used for cosmic ray rejection*

**CS:** *Contact Scientist*

**CTE:** *Charge transfer efficiency*

**CVZ:** Continuous viewing zone

**DQ:** Data quality

**DN:** Data number

**ETC:** Exposure Time Calculator. ETCs are web-based tools which can be accessed through the ACS web pages.

**ERO:** *Early release observations*

**FAQ:** Frequently asked questions

**FGS:** Fine Guidance Sensors

**FITS:** Flexible Image Transport System. A generic IEEE and NASA defined standard file format used for storing image data.

**FOC:** Faint Object Camera

**FOS:** Faint Object Spectrograph

**FOV:** Field of view

**FSW:** Flight software

**FTP:** File Transfer Protocol. Basic tool used to retrieve files from a remote system. Ask your system manager for information about using FTP.

**FUV:** Far ultraviolet (~912-2000 Å)

**FWHM:** Full width at half maximum

**GEIS:** Generic Edited Information Set. Multigroup format used by STS-DAS for storing some HST image data.

**GHRS:** Goddard High-Resolution Spectrograph

**GO:** General Observer

**GSC:** *Guide Star Catalog*

**GTO:** Guaranteed Time Observer

**HDA:** *Hubble Data Archive*

**Help Desk:** *Facility for getting help on HST related topics via email. help@stsci.edu.*

**HRC:** High Resolution Channel

**HSP:** High-Speed Photometer

**HST:** Hubble Space Telescope

**HUT:** *Hopkins Ultraviolet Telescope*

**ICD:** Interface control document. Defines data structures used between software or systems to ensure compatibility.

**IDT:** Investigation Definition Team

**IHB:** *Instrument Handbook*

**IR:** Infrared

**IRAF:** Image Reduction and Analysis System. The environment in which STSDAS operates.

**IS:** Instrument Scientist

**ISR:** Instrument Science Report

**IUE:** International Ultraviolet Explorer

**K:** Degree Kelvin

**LMC:** Large Magellanic Cloud

**MAMA:** Multi-Anode Microchannel Array

**MCP:** Microchannel Plate

**ND:** Neutral density

**NICMOS:** Near-Infrared Camera and Multi-Object Spectrograph

**NUV:** Near ultraviolet (~2000-4000 Å)

**OSS:** Observation Support System

**OTA:** Optical Telescope Assembly

**OTFC:** *On-the-Fly Calibration*

**PC:** Program Coordinator

**Phase I:** *A proposal for observing time on HST*

**Phase II:** An approved HST proposal; includes precise detail of how program is to be executed

**PI:** Principal investigator

**PSF:** Point-spread function.

**QE:** Quantum efficiency

**QEH:** Quantum efficiency hysteresis

**QSO:** Quasi-stellar object

**RA:** Right ascension

**reference file:** *data file containing ACS parameters or calibration information which is used by the calibration pipeline*

**rms:** Root mean square

**RPS2:** *Remote Proposal Submission-2; proposal submission software*

**SAA:** *South Atlantic anomaly*

**SBC:** Solar-Blind Channel

**SITe:** Scientific Image Technologies; company that designed the ACS CCDs

**SMOV:** Servicing Mission Observatory Verification

**S/N:** Signal-to-noise ratio

**ST-ECF:** Space Telescope European Coordinating Facility

**STAN:** *Space Telescope Analysis Newsletter*

**STIS:** Space Telescope Imaging Spectrograph

**STMAG:** STScI magnitude system;  $-2.5 \log (F_{\lambda}) - 21.10$  where  $F_{\lambda}$  is the flux from the source in  $\text{erg cm}^{-2} \text{sec}^{-1} \text{\AA}^{-1}$

**STScI:** Space Telescope Science Institute

**STSDAS:** Space Telescope Science Data Analysis System. The complete suite of IRAF data analysis and calibration routines used to process HST data.

**SV:** Science verification. Process of taking observations that can be used for HST instrument calibration.

**synphot:** *STSDAS synthetic photometry (IRAF) software package*

**TAC:** Telescope Allocation Committee

**TIR:** Technical Instrument Report

**URL:** Uniform resource locator. Address for WWW.

**UV:** Ultraviolet

**WFC:** Wide-Field Channel

**WF/PC:** Wide Field/Planetary Camera

**WFPC2:** Wide Field Planetary Camera-2. Replacement for WF/PC installed during first servicing mission of December 1993.

**WWW:** World Wide Web. Hypertext-oriented method for finding and retrieving information over the Internet.

# Index

## A

- AB(nu) 102, 187, 231
- Aberrated Beam Coronagraph 69
- Aberration Correction 24
- ABMAG 98, 187
- ACCUM mode
  - HRC 148
  - SBC 148
  - WFC 146
- Accuracies
  - HRC 259
  - SBC 259
  - WFC 258
- ACQ mode
  - effective neutral density filters 149
  - HRC 149
- Analysis 271
- Annealing
  - HRC 130
  - WFC 130
- Apertures
  - HRC 148, 161
  - SBC 161
  - WFC 146, 156
- A-to-D Converter
  - HRC 126, 148
  - WFC 126, 146
- Auto-Parallels 168

## B

- Bandpass 39, 98, 189
- Blooming 126
- BOP

- exceeding bright object limits 143
  - screening 141, 143
  - solar system objects 143
- Bright Object Protection 138
  - global limit 139
  - limiting V magnitudes 140
  - local limit 139
- Buffer
  - compression 146
  - HRC 148
  - internal memory 28
  - overheads 146
  - SBC 149

## C

- CALACS
  - flow diagram CCD 250
  - flow diagram MAMA 251
  - Switches 245
- Calibration
  - accuracies 257
  - cycle 12 264
  - ground testing 262
  - lamps 27
  - non-science exposures 34
  - outsourcing 267
  - pipeline 243, 255
  - polarizers 64
  - SMOV3B 262
- Call for Proposals(CP) 8
- Capabilities
  - coronagraphy 22
  - imaging 21
  - polarimetry 22

- spectroscopy 22
- CCDs
  - HRC. See HRC
  - WFC. See WFC
- CDBS 243
- Charge Transfer Efficiency 17, 130
- Comparison of Instruments 43
- Coordinated Parallels 167
- Coronagraph
  - design 69
- Coronagraphy
  - exposure time calculation 83
  - Lyot stop 69
  - occulting finger 70
  - occulting masks 69
  - PSF 81
  - target acquisition 148, 149
- Cosmic Rays
  - HRC 126
  - WFC 126
- Cosmic rays 126
- Countrate Limits
  - SBC 133, 138
- CR-SPLIT 150, 152, 168, 176
- CTE 16, 130
- Cycle 12
  - calibration 264
  - scheduling policies 12

## D

- Dark Current
  - HRC 120
  - SBC 133
  - WFC 120
- Data 270, 271
- Data Number(DN) 122, 146, 148
- Data Quality(DQ) 253
- Data Storage
  - buffer size 28
- Data Transfer 28
- Data Volume 16, 253
- Detectors
  - HRC. See HRC
  - SBC. See SBC
  - WFC. see WFC

- Dithering
  - goals 149
  - strategy 150
  - STSDAS dither package 151
- Documentation
  - FAQs 8
  - requesting 8
  - world wide web 9
- Drizzle 154
- Dynamic Range 155

## E

- Earthshine 108, 116
- Encircled Energy
  - measured 122
  - models 58
- Exposure Time Calculator(ETC) 97
  - bright object limits 141
  - examples 112
  - sky backgrounds 116
- Exposures
  - calibration 34
  - overheads 176
  - target-acquisition 34
- Extinction 111

## F

- FAQs 8
- Field of View(FOV)
  - HST 30
- Field of View(FOV)
  - HRC 22, 43, 161
  - SBC 22, 43, 161
  - WFC 21, 43, 156
- Filter Wheel
  - SBC 26
  - WFC/HRC 26
- Filters 27, 39, 98
  - HRC/F220W 202, 203
  - HRC/F250W 204
  - HRC/F330W 205
  - HRC/F344N 206
  - HRC/F435W 207
  - HRC/F475W 208

- HRC/F502N 209
- HRC/F550M 210
- HRC/F555W 211
- HRC/F606W 212
- HRC/F625W 213
- HRC/F658N 214
- HRC/F660N 215
- HRC/F775W 216
- HRC/F814W 217
- HRC/F850LP 218
- HRC/F892N 219
- HRC/G800L 220
- HRC/PR200L 221
- Johnson-Cousins 51
- narrow-band 52
- Ramp Filters
  - HRC 53
  - WFC 52
- SBC Summary Table 40
- SBC/F115LP 223
- SBC/F122M 224
- SBC/F125LP 225
- SBC/F140LP 226
- SBC/F150LP 227
- SBC/F165LP 228
- SBC/PR110LP 229
- SBC/PR130LP 230
- Sloan Digital Sky Survey 51
- WFC/F435W 189
- WFC/F475W 190
- WFC/F502N 191
- WFC/F550M 192
- WFC/F555W 193
- WFC/F606W 194
- WFC/F625W 195
- WFC/F658N 196
- WFC/F660N 197
- WFC/F775W 198
- WFC/F814W 199
- WFC/F850LP 200
- WFC/G800L 201
- WFC/HRC Summary Table 39
- Flat Field
  - general 245
  - HRC 125
  - SBC 137
  - WFC 123
- Fringing 121
- Full Well 43, 126
- Full Width Half Maximum(FWHM)
  - HRC 53
  - WFC 51
- G**
- Gain
  - HRC 123, 148
  - WFC 123
- Geocoronal emission 110
- Geometric Distortion
  - HRC 237
  - PSF 60
  - temporal changes 150
  - WFC 51
- Ground Testing 262
- H**
- Help Desk 8
- Hot Pixels 128
- HRC
  - ACCUM 148
  - accuracies 259
  - ACQ mode 149
  - apertures 148, 161
  - A-to-D converter 148
  - buffer 148
  - characteristics 53, 120
  - coating 120
  - cosmic rays 126
  - dark current 120
  - description 23
  - flat field 125
  - fringing 121
  - full well 126
  - full width half maximum(FWHM) 53
  - gain 148
  - hot pixels 128
  - multiple electron events 54, 131
  - occulting masks 162
  - physical overscan 122
  - point spread function 57
  - QEH 121

- ramp filters 147
- read noise 120
- readout 122
- red leaks 54
- saturation 126
- spectral response 121
- subarrays 148
- virtual overscan 122

**I****Imaging**

- caveats 48
- filters 38, 53, 55
- HRC detector 53
- limiting magnitude 50
- saturation 50
- SBC detector 55
- signal-to-noise 50
- throughput 49
- WFC detector 51

Instrument 271

Integrated System Throughput 49

**L****Lamps**

- deuterium 27
- tungsten 27

Light Paths 25, 26

Limiting Magnitudes 50

**Linearity**

- CCDs 156
- SBC 138

LOW-SKY 110

Lyot Stop 69

**M**

Magnitude 271

MAMA. See SBC

Memory. See Buffer

**N****NICMOS**

- characteristics 43

- comparison 45

**Non-linearity**

- SBC 138

**O****Observing Considerations**

- coronagraph 28
- dithering 28
- pattern 28

Observing Strategy 152

**Observing Techniques**

- coronagraphy 83

On-The-Fly-Reprocessing(OTFR) 243

**Optical Path**

- HRC/SBC 26
- WFC 25

**Optics**

- coronagraph 24
- corrective optics 24
- fold mirror 24
- HRC/SBC 24
- spherical aberration 24
- WFC 24

Orbit-Time Determination 175

ORIENT 163

**Orientation**

- computing 163
- ORIENTAT 163
- PA\_APER 164

**Overheads**

- buffer size 176
- examples 177
- types 173

**P****Parallel Observations**

- coordinated parallels 167
- pointing 166
- pure parallels 171
- visual target tuner 167

Parallel Observing 29

Patterns 149

**Phase I**

- bright object limits 141



- preparation 6, 29, 145
- Phase II
  - bright object limits 141
  - preparation 8
- Photometry
  - accuracy 258
  - encircled energy 58, 98
  - zero point 98
- Pipeline
  - calibration 255
  - data products 251
  - reprocessing 254
  - see calacs 271
  - storage requirements 253
- Pivot Wavelength 98
- Pixel Response Function (PRF) 56
- Point Spread Function (PSF)
  - HRC 57
  - SBC 58
  - WFC 57
- Pointing Stability 152
- Polarimetry
  - Calibration 64
  - filters 66, 67
  - FOV 67
  - throughput 64
- Policy
  - CCD
    - auto-parallel 14
  - SBC
    - bright-object protection 13
    - coronagraph 24
    - parallel observing 13
- Post-flash 27
- Precision 257
- Proposal 271
  - BOP 138
  - exposure time 33
  - feasibility 33
  - Phase I 8
  - Phase II 8
  - subarrays 34
  - submission 271
  - tradeoffs 32
- Proposals
  - calibration exposures 34
- PSF

- coronagraphy 81
- encircled energy 58
- geometric distortion 60
- HRC halo 53, 58
- models 57
- PRF 56
- residual aberrations 61
- SBC halo 55, 58
- TinyTIM 56, 57
- WFC halo 52, 58
- Pure Parallels
  - pure parallel program 171

## Q

- Quantum Efficiency Hysteresis 121

## R

- Ramp Filters
  - aperture location 147
  - apertures 158
  - See Filters
- Read Noise 43, 126
- Readout Time 23, 176
- Red Leaks
  - HRC 54
  - SBC 55

## S

- Saturation
  - CCDs 126
  - SBC 134
- SBC
  - ACCUM mode 131, 148
  - Accuracies 259
  - accuracies 259
  - apertures 161
  - BOP 144
  - buffer 149
  - characteristics 55, 133
  - description 23
  - flat field 137
  - global countrate 138
  - limiting countrates 139
  - local countrate 138
  - microchannel plate 132

- point spread function 58
- PSF 55, 134
- red leaks 55
- repeller wire 55, 132
- signal-to-noise ratio 136
- spectral response 133
- Scheduling
  - SBC considerations 12
- Sensitivity
  - HRC/G800L 90, 91
  - HRC/PR 200L 92
  - WFC/G800L 88, 89, 90
- Shutter 126
- Signal-to-Noise 104
- sky background 116
- SMOV3B
  - proposals 262
- Solar System Objects 143
- South Atlantic Anomaly 12
- Spectral Response. *See* Imaging throughput 49
- Spectroscopy
  - HRC 88
  - SBC 90
  - WFC 87
- ST-ECF
  - help desk 9
- STIS 12
  - characteristics 43
  - comparison 46
  - filter curves 47
- Subarrays
  - amplifier 147
  - coronagraph 148
  - CTE 147
  - data volume 147
  - HRC 148
  - overscan 147
- Synphot 98
- T**
  - Target ACQ
    - accuracy 28
    - aperture 28
    - coronagraph 28
    - ramp filters 28
- Terms used in this manual 269
- TinyTIM 56, 57, 58
- Tools 269
- Transmission Curves
  - broad-band filters 41
  - medium-band filters 41
  - narrow-band filters 42
  - SBC filters 42
  - SDSS filters 41
- U**
  - Undersampling 51, 53
  - User Support
    - help desk 8
- W**
  - WFC
    - ACCUM 146
    - accuracies 258
    - apertures 146, 156
    - characteristics 51, 120
    - cosmic rays 126
    - dark current 120
    - description 23
    - flat field 123
    - fringing 121
    - full well 126
    - full width half maximum(FWHM) 51
    - hot pixels 128
    - physical overscan 122
    - point spread function 57
    - QEH 121
    - ramp filters 147
    - read noise 120
    - readout 122
    - saturation 126
    - spectral response 121
    - virtual overscan 122
  - WFC/HRC Summary Table 98
  - WFPC2
    - characteristics 43
    - comparison 44
    - filter curves 45
  - WWW pages 9
- Z**
  - Zodiacal Light 110, 116



